AD-769 285

DEVELOPMENT AND EVALUATION OF PG/SIC CODEPOSITED COATINGS FOR ROCKET NOZZLE INSERTS. VOLUME I. THERMAL AND MECHANICAL PROPERTIES OF PYROLYTIC GRAPHITE/ SILICON CARBIDE CODEPOSIT

Richard H. Singleton

Atlantic Research Corporation

Prepared for:

Air Force Rocket Propulsion Laboratory

October 1973

DISTRIBUTED BY:

NTIS

National Technical Information Service
U. S. DEPARTMENT OF COMMERCE
5285 Port Royal Road, Springfield Va. 22151

UNCLASSIFIED

AD-769 285

SECURITY CLASSIFICATION OF THIS PAGE (When Data Entered)

REPORT DOCUMENTATION PAGE

READ INSTRUCTIONS BEFORE COMPLETING FORM

1. REPORT NUMBER
AFRPL-TR-73-70 Vol. I

2. GOVT ACCESSION NO.

3. RECIPIENT'S CATALOG NUMBER

4. TITLE (and Subtitle) Development and Evaluation of PG/Sic Codeposited Coatings for Rocket Nozzle Inserts

Volume I – Thermal and Mechanical Properties of Pyrolytic Graphite/Silicon Carbide Codeposit

5. TYPE OF REPORT & PERIOD COVERED
Special - Jan. 1972 to July 1973

6. PERFORMING ORG. REPORT NUMBER
46-5544-I3

7. AUTHOR(s)
Richard H. Singleton

8. CONTRACT OR GRANT NUMBER(s)
F04611-72-C-0047

9. PERFORMING ORGANIZATION NAME AND ADDRESS
Atlantic Research Corporation
5390 Cherokee Avenue
Alexandria, Virginia 22314

10. PROGRAM ELEMENT, PROJECT, TASK AREA & WORK UNIT NUMBERS
Project No: 3148
BPSN: 623148

11. CONTROLLING OFFICE NAME AND ADDRESS
Air Force Rocket Propulsion Laboratory
Director of Laboratories
Edwards, CA 93523
Air Force Systems Command, United States Air Force

12. REPORT DATE
Oct. 1973

13. NUMBER OF PAGES
243

14. MONITORING AGENCY NAME & ADDRESS(if different from Controlling Office)
Commander, DCASD Baltimore
Building 22, Fort Holabird
Baltimore, Maryland 21219

15. SECURITY CLASS. (of this report)
Unclassified

15a. DECLASSIFICATION/DOWNGRADING SCHEDULE
N/A

16. DISTRIBUTION STATEMENT (of this Report)

17. DISTRIBUTION STATEMENT (of the abstract entered in Block 20, if different from Report)

18. SUPPLEMENTARY NOTES

19. KEY WORDS (Continue on reverse side if necessary and identify by block number)
Pyrolytic Graphite
Rocket Nozzles
Silicon Carbide
Properties

20. ABSTRACT (Continue on reverse side if necessary and identify by block number)

Phase I - Task 3. The thermal and mechanical properties of PG/SiC were determined as functions of temperature, 4500°F, SiC concentration, to approximately 25 percent, and crystal orientation, a and c directions, of the PG phase. The material was found to be unique in that it is nearly isotropic with respect to thermal expansion and elastic modulus but still quite anisotropic with respect to thermal conductivity. The room temperature tensile strength was much greater than PG in the c direction, as expected as a result of the SiC crystal reinforcement. Tensile strength and elastic modulus were also greater than PG in the ab direction to up 4000°F. The data must be considered to be preliminary and nonstatistical.

DD FORM 1 JAN 73 1473 EDITION OF 1 NOV 65 IS OBSOLETE

UNCLASSIFIED

ABSTRACT

This three-volume document describes the fabrication development and evaluation of codeposited pyrolytic graphite-silicon carbide coatings on graphite substrates for a rocket nozzle application. The general purposes of the program were to establish a reproducible coating technique and to evaluate the coating by determination of its thermal and mechanical properties and by 1.0-inch throat diameter subscale rocket motor test firings. The study was preliminary to the fabrication and testing of 1.7-inch throat diameter PG/SiC lined nozzles in the High Pressure Solid Propellant Test Facility in the Rocket Propulsion Laboratory at Edwards Air Force Base. The work was done under the overall technical cognizance of the RPL Project Engineer, Mr. William F. Payne. The results obtained in these studies are presented in three separately bound volumes as follows:

Volume I – Thermal and Mechanical Properties of PG/SiC Codeposit

By determination of its thermal and mechanical properties, it was found that the PG/SiC coating is unique in that it is nearly isotropic with respect to thermal expansion and elastic modulus but quite anisotropic with respect to thermal conductivity. The tensile strength was much greater than pyrographite in the c direction, as expected as a result of the SiC crystal reinforcement. Mechanical properties in the ab direction were equal to or better than pyrographite.

Volume II – Vapor Deposition of Pyrolytic Graphite/Silicon Carbide Codeposited Coatings

Parameters were established to vapor deposit PG/SiC coatings on components for nozzles with throat diameters up to 1.7 inches.

Volume III – Subscale Solid Rocket Motor Testing of PG/SiC Lined Throat Inserts

Six ATJ graphite 1.0-inch throat diameter nozzle throat inserts and four entrance approach sections were coated with PG/SiC and test fired with a low oxidizing 21 percent aluminum 5600°F propellant. A preliminary throat erosion rate for PG/SiC of 4 mils per second at 2000 psia and 7 mils per second at 2500 psia average chamber pressure was established. Use of a graded coating in which the last third of the deposit was pure pyrographite approximately halved the erosion rate. The inserts appeared to be less prone to cracking when the ATJ substrates had been heat treated at 5400°F prior to coating.

The Tables of Contents for Volumes II and III are included here for completeness and cross-reference.

VOLUME I

TABLE OF CONTENTS

VOLUME II

TABLE OF CONTENTS

VOLUME III

TABLE OF CONTENTS

LIST OF ILLUSTRATIONS

LIST OF ILLUSTRATIONS (continued)

SECTION I

INTRODUCTION

It was known that pyrolytic graphite (PG)/silicon carbide (SiC) was less anisotropic than PG and that this was due to the fact that the SiC reinforcing needles were perpendicular to the PG plane in the microstructure. Thus, the coefficient of thermal expansion (CTE) was decreased in the c direction, and the tensile strength was increased in the c direction. The present work was undertaken to measure the thermal (CTE, thermal conductivity) and mechanical properties (in both tension and compression) up to 4500 or 5000°F. The objective was to procure engineering data for use in structural analysis for the design of the 1.7-inch throat diameter HIPPO nozzle.

Although (a) a separate individual run had to be made to fabricate each specimen, (b) only single point data was obtained in most cases, and (c) process control (especially SiC content) was less than desired, it is felt that a good set of preliminary data was procured.

At this writing, new data has been obtained under the SCALE UP program on the CTE of PG/SiC in the ab direction which is 10 to 20 percent higher than the data reported in this report. Since CTE is the most important single property with respect to structural analysis, the reader should be cautioned not to use this CTE data before consulting with Atlantic Research Corporation.

SECTION II

OBJECTIVE

Procure a preliminary nonstatistical data package on CTE and thermal conductivity, and generate stress-strain curves in both the compressive and tensile modes, as functions of material orientation; i.e., a and c direction.

SECTION III

DATA HIGHLIGHTS

The work that was completed at Southern Research Institute (SoRI) is summarized in Table I.

1. THERMAL PROPERTIES

The CTE was determined over the temperature range 70 to 5000°F in both the a and c directions for PG/SiC compositions ranging, nominally, from 0 to 25 weight percent SiC. The thermal expansion data is

Table I. Test Matrix for PG and PG/SiC Properties by SoRI.

	PG	8% SiC	15% SiC	20% SiC	25% SiC	PG STOCK	PG/SiC STOCK
THERMAL CONDUCTIVITY							
ab DIRECTION <1500°F	2	–	–	2	2	PLATE	TUBE AND PLATE
c DIRECTION <1500°F	2	–	–	2	2	PLATE	TUBE AND PLATE
c DIRECTION >2000°F	–	–	–	3	3	–	TUBE
THERMAL EXPANSION (70 to 5000°F)							
ab DIRECTION	3	2	2	2	2	TUBE	TUBE AND PLATE
c DIRECTION	2	2	2	2	2	PLATE	TUBE AND PLATE
TENSION (σ/ϵ)							
ab DIRECTION 70°F	1	–	2	2	1	PLATE	TUBE
ab DIRECTION 3000°	–	–	2	2	1	–	TUBE
ab DIRECTION 4000°F	–	–	2	2	1	–	TUBE
ab DIRECTION 4500°F	1	–	2	3	2	PLATE	TUBE
c DIRECTION 70°F	3	–	3	–	4	TUBE	TUBE
COMPRESSION (σ/ϵ)							
ab DIRECTION 70°F	2	–	5	1	2	TUBE	TUBE
ab DIRECTION 3000°F	–	–	1	–	2	–	TUBE
ab DIRECTION 4500°F	–	–	2	–	1	–	TUBE
c DIRECTION 70°F	–	–	–	3	–	–	TUBE

NOTE: NUMBERS REPRESENT NUMBER OF TEST REPLICATES

summarized in Figure 1. It has recently been discovered that the SiC contents are higher than formerly supposed and Figure 1 contains the corrected compositions. It may be observed in Figure 1 that this first cycle data shows that the addition of 18 percent or more SiC to PG renders it nearly isotropic. It also appears to improve the thermal stability of the PG, since the rapid rise in the ab direction PG curve above 4000°F is eliminated. These CTE data are preliminary and should not be used for engineering purposes without consultation with Atlantic Research. The data is plotted on smaller coordinates in the Southern Research Institute Report 73-031 which is attached to this report as Appendix I. For comparative purposes, the Δ/L of the ATJ graphite coating substrate has recently been determined to be 1.01 percent in the with grain direction, between 70 and 4000°F. A good match between the CTE of ATJ and that of PG/SiC in the ab direction is evident.

The coatings were made on graphite substrates in either 2-inch-diameter cylindrical or plate form using a thin PG layer predeposit to facilitate separation from the substrate. Pure PG was laid down at 4000°F on AGSR graphite; whereas, PG/SiC was deposited at 3200°F on ATJ graphite. The microstructures consisted of fine acicular fairly well dispersed particles generally aligned perpendicular to the substrate surface and 0.5 to 1.0 micron in thickness with an L/D ratio greater than 3. The coatings were made during the spring of 1972.

Specimens 3 inches long were machined with their lengths in the coating gas flow direction from plate, or cylinders, for the ab plane CTE measurements. The c direction CTE specimens were fabricated by cutting disks from plate, or similar round shapes from cylinders, and stacking them to form a pile 1 inch high. All measurements were made at SoRI using a graphite dilatometer with a dial gauge.

The thermal conductivity of PG was determined between room temperature and 1700°F in both the ab plane and the c direction. The thermal conductivities of PG/20% SiC and PG/35% SiC were determined to 1700°F in the ab plane and to 4300°F in the c direction. The data are summarized in Figure 2, along with similar data for the ATJ graphite substrate taken from the literature. It may be observed that, although the addition of SiC to PG lowers the anisotropy to a considerable extent, PG/SiC is still quite anisotropic with respect to thermal conductivity. The data is plotted on smaller coordinates in Appendix I.

The ab plane and c direction comparative rod thermal conductivity specimens for measurement from room temperature to 1500°F were made from either plate or cylindrical stock. The ab specimens were fabricated by fitting accurately machined layers together to form a cylinder, 0.6 to 1.0 inch long by 0.75 inch in diameter, with the c axis of the material perpendicular to the specimen axis. The c direction comparative rod specimen was a single layer flat disk or an arc-disk cut from a cylinder. The method utilizes a common heat flux flowing in series through the unknown specimen and one or more specimens of known thermal conductivity. Measurement of the ΔT through each unit allows a simple calculation of the unknown thermal conductivity. Above 1500°F, excessive heat losses make this method inaccurate and the radial in-flow method is used.

In their radial heat flow method, a known heat flux was passed through the PG/SiC cylindrical specimen in the c direction and the ΔT across the specimen was measured by optical pyrometry. The heat flux was measured by water flow calorimetry. Measurements were made from 2300 to 4300°F. The data appeared to blend well[1] with the comparative rod data. The PG/SiC specimens were 2 inches in O.D. X 2 inches long by approximately 150 mils thick.

---

[1] See Figures 18 and 20 of Appendix A.

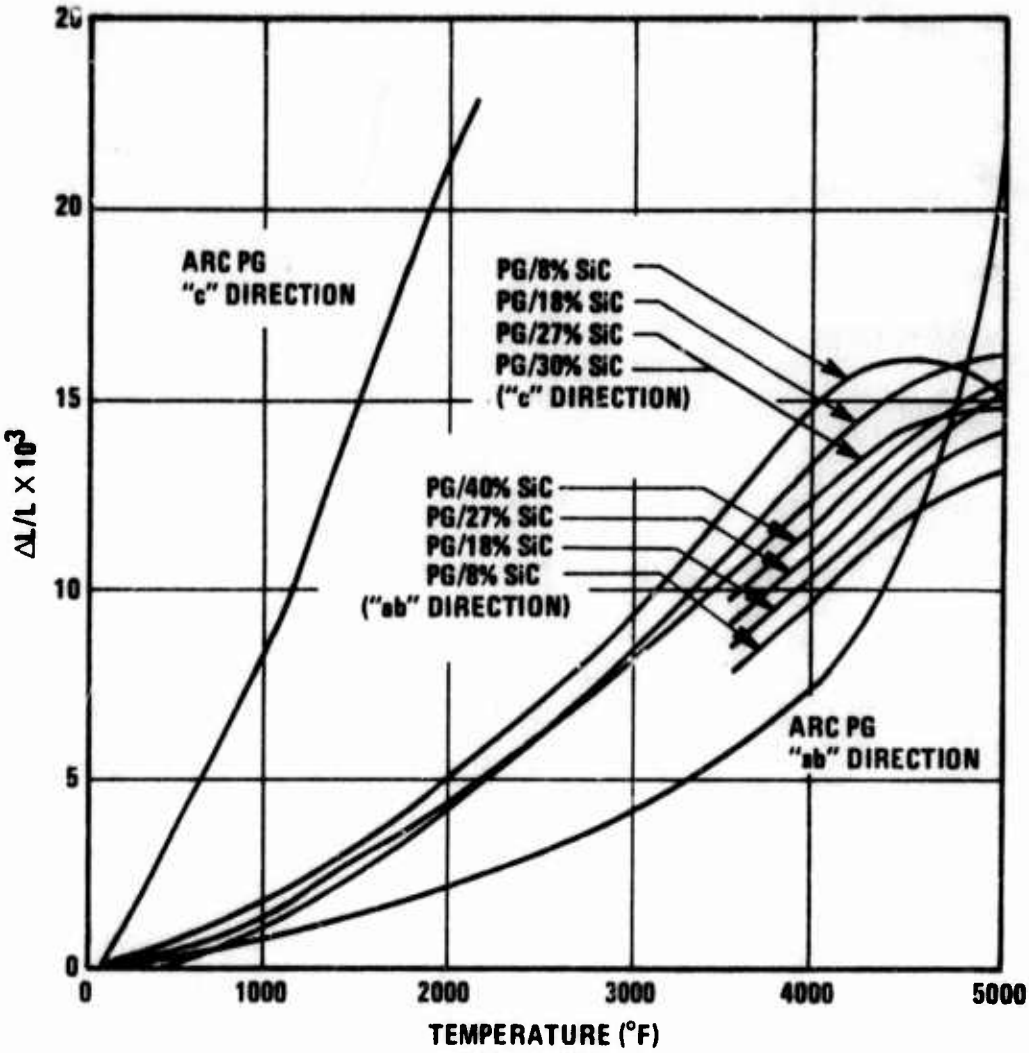

Figure 1. Thermal Expansion of PG and PG/SiC Codeposit.

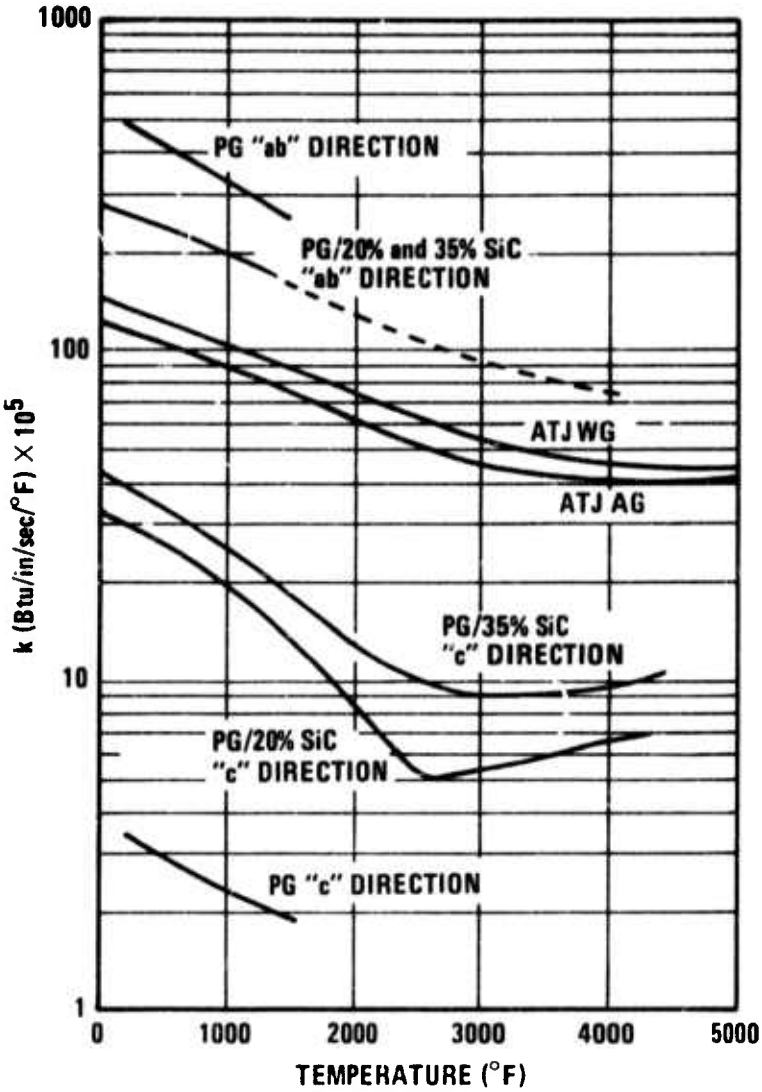

References

PG	ab	Appendix B	Figure 15
PG	c	Appendix B	Figure 16
PC/20% SiC	ab	Appendix B	Figure 17
PG/20% SiC	c	Appendix B	Figure 18
PG/35% SiC	ab	Appendix B	Figure 19
PG/35% SiC	c	Appendix B	Figure 20

ATJ WG&AG Private communication 1972
from SRI

Figure 2. Thermal Conductivity of PG and PG/SiC Codeposit.

During the coating material fabrication for thermal conductivity specimens, the pure PG was deposited at 4000°F, to a depth of 90 to 200 mils; whereas the PG/SiC was deposited at 3200°F to a depth of 110 to 180 mils. The microstructure of the PG/SiC generally consisted of fine acicular fairly well dispersed particles aligned perpendicular to the substrate surface and with an L/D ratio greater than 3. The thermal conductivity coatings were made in May through August 1972, except that the PG plate was fabricated in October 1972.

2. MECHANICAL PROPERTIES

Two-inch-I.D. by 9-inch-long graphite cylinders coated on their inside diameters with PG/SiC to a depth of 100 to 150 mils in the gauge section were submitted to SoRI for tensile meeasurements. Similar tubes 5 inches long were submitted for compression testing. This latter shipment included some pine PG 40 to 60 miles thick. Some PG plate 50 mils thick was also submitted for tensile testing. The PG was laid down at 4000°F on AGSR cylinders and the PG/SiC was deposited at 3200°F on ATJ graphite cylinders. The microstructure of the PG/SiC generally consisted of fine, acicular, well dispersed SiC in a crack-free PG matrix. The coatings were made during the summer of 1972. The SiC content was determined at SoRI by ashing of material taken from the gauge area of broken room temperature specimens. Compositions varied considerably from nominal and, consequently, data was obtained at more compositions than originally planned. Although the number of replicates and temperatures were small, some fairly definite trends were established.

The results showed that the addition of SiC to PG increased the tensile strength almost linearly over the temperature range 70 to 3000°F. Above 3000°F, the strengthening effect of the SiC began to decrease and was significantly diminished, but still present, at 4500°F. The tensile elastic modulus and strain-to-failure both increased with SiC content over the entire temperature range, 70 to 4500°F. The compressive elastic modulus similarly increased with SiC content up to 3000°F, but the effect was much less pronounced at 4500°F.

The complete mechanical properties data and techniques used in their determination at SoRI are contained in their Report SoRI-EAS-73-183 which is attached to this report as Appendix II.

a. Tensile Properties

Typical ab plane stress-strain curves in tension are shown in Figures 13 and 14 of Appendix II for PG/16% SiC and PG/20% SiC, respectively, as a function of temperature. It may be observed that the curves show a nearly linear elastic bahavior up to and including 3000°F; whereas above this temperature the curves are bilinear showing some plastic deformation. The ultimate tensile strengths are plotted as functions of SiC content and temperature in Figure 3. It may be seen that the strength peaks at approximately 3000°F and then drops, at 4500°F, to near the room temperature values for the lower SiC contents and to below the room temperature values for the high SiC contents. The tensile modulus of elasticity is plotted as a function of SiC content and of temperature in Figure 4. Again, the modulus values peak at near 3000°F.

The original ab plane specimens were fabricated at SoRI by machining away the substrate and some of the coating in the gauge section. However, breakage occurred in room temperature testing in the specimen heads prior to breakage in the gauge section. Consequently, arc-of-cylinder specimens were fabricated with conforming grips. These were used successfully throughout the program, and stress-strain curves made with full cylinders coincided fairly well with these arc coupons at room temperature. The PG coupon specimens were made from plate.

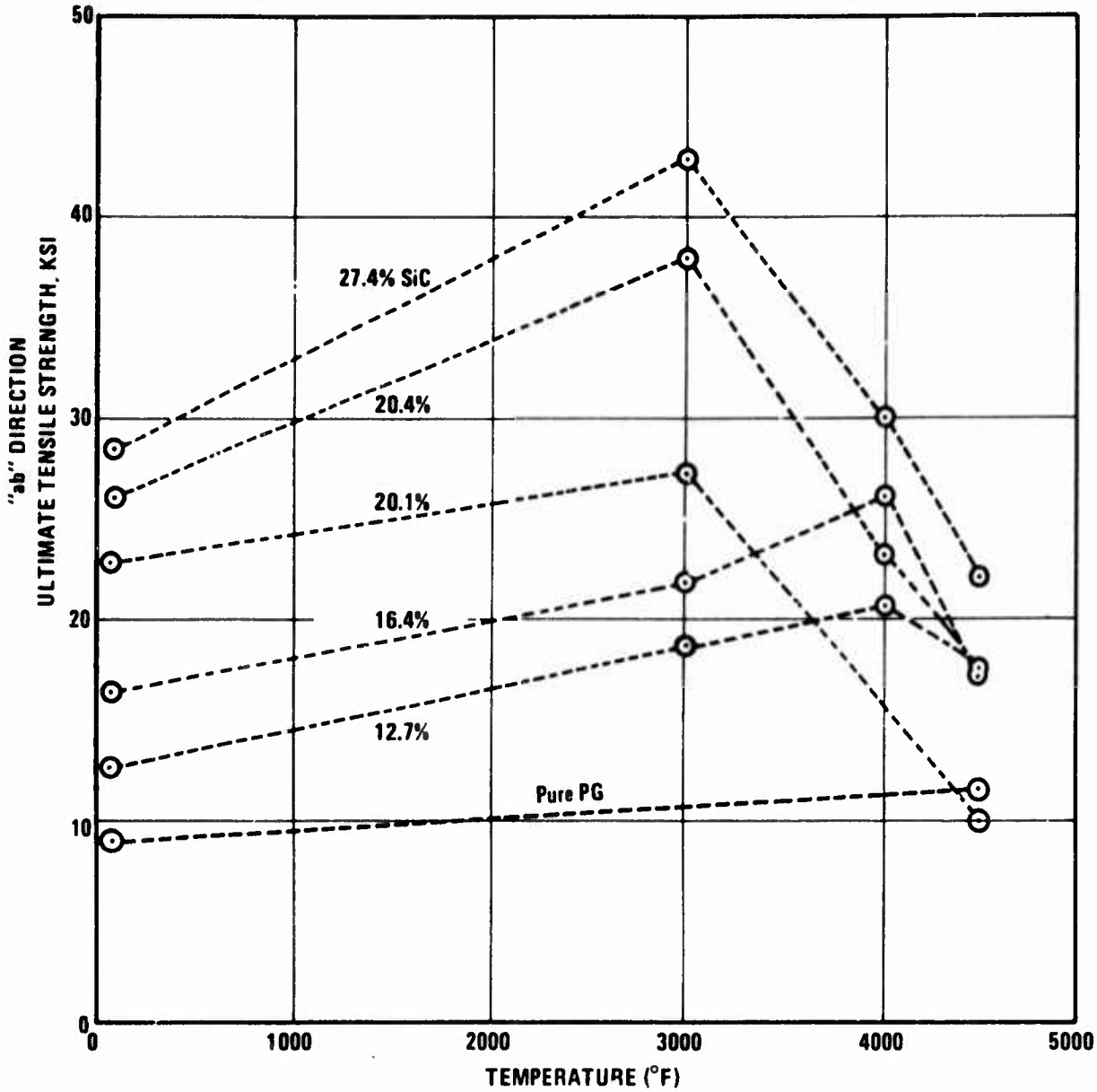

Figure 3. Strengths of PG/SiC Codeposit in the "ab" Plane.

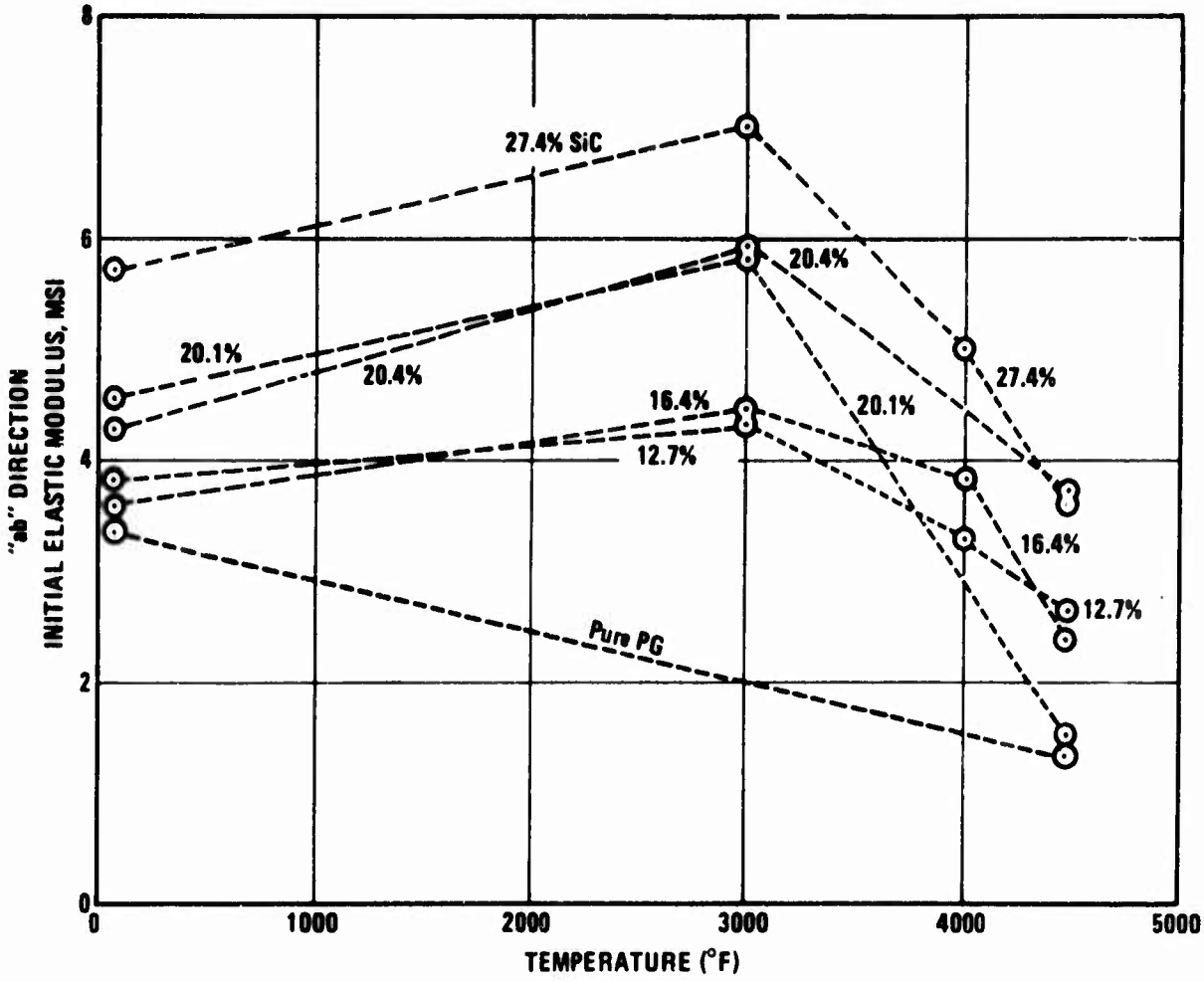

Figure 4. Moduli of Elasticity in Tension of PG/SiC Codeposit in the "ab" Plane.

For the c direction tensile tests, conforming grips were epoxy bonded to arc-disk specimens cut from cylinders. The pure Atlantic Research PG tensile strength averaged 792 psi; whereas, the epoxy bond broke at 3,000+ psi in the case of the PG/SiC specimens at room temperature. Previous privately communicated measurements in the c direction at SoRI had indicated strengths near 8,000 psi for PG/SiC at room temperature. Insufficient length was available in the c direction for the use of strain gauges so that the elastic modulus and stress-strain curves were not obtained.

Poisson's ratio in tension was determined to be 0.14 for PG/20% SiC at room temperature in the a/b mode.

b. Compressive Properties

The compressive strength specimens were fabricated by machining off the graphite substrate and some of the coating in the gauge section, using Atlantic Research supplied cylinders shorter than those used for tensile testing. In addition, arc coupon specimens were fabricated similar to but shorter than those used for tensile testing. The coupon specimens were used at temperature. Room temperature testing with arc and full cylinder specimens indicated good agreement in data. The specimens buckled in testing above a certain strain level. SoRI did not report the data beyond this point and consequently ultimate strength and strain-to-failure were not obtained. However, SoRI claims that the stress-strain curves are accurate up to the point of buckling.

The compressive stress-strain curves are fairly similar to the tensile curves for the first 0.5 percent strain. However, they are bilinear at all temperatures. As can be seen in Figure 16 of Appendix II, the elastic modulus in compression is quite similar to, although slightly less than, that in tension, peaking at approximately 3000°F.

Room temperature stress-strain curves were obtained in compression in the c direction on 160-mil-thick disks taken from Atlantic Research plate Run 001-47. This PG/SiC material contained approximately 20 percent SiC. The stress-strain curves are shown in Figure 5. The data was not reported in Appendix II.

Poisson's ratio in compression was determined to be -0.9 for PG and 0.14 for PG/16% SiC at room temperature in the a/b mode.

c. Room Temperature Properties Summary

The room temperature mechanical properties data obtained in this investigation on PG and PG/SiC are summarized and compared in Table II. It is apparent that the SiC addition significantly reduces the anisotropy of PG and greatly strengthens it in the c direction. No shear measurements were made. However, it appears certain that the SiC addition increases the shear strength in the ab plane.

d. Flexural Strength Data

Some limited room temperature flexural strength and elastic modulus data were obtained in August 1972 at Atlantic Research on PG/SiC ring segments cut from the ends of materials properties specimens intended to be submitted to SoRI and or plate. The PG/SiC microstructure of those specimens examined showed a fine dispersion of SiC needles in a PG matrix. All specimens were broken with the substrate side in tension. The details

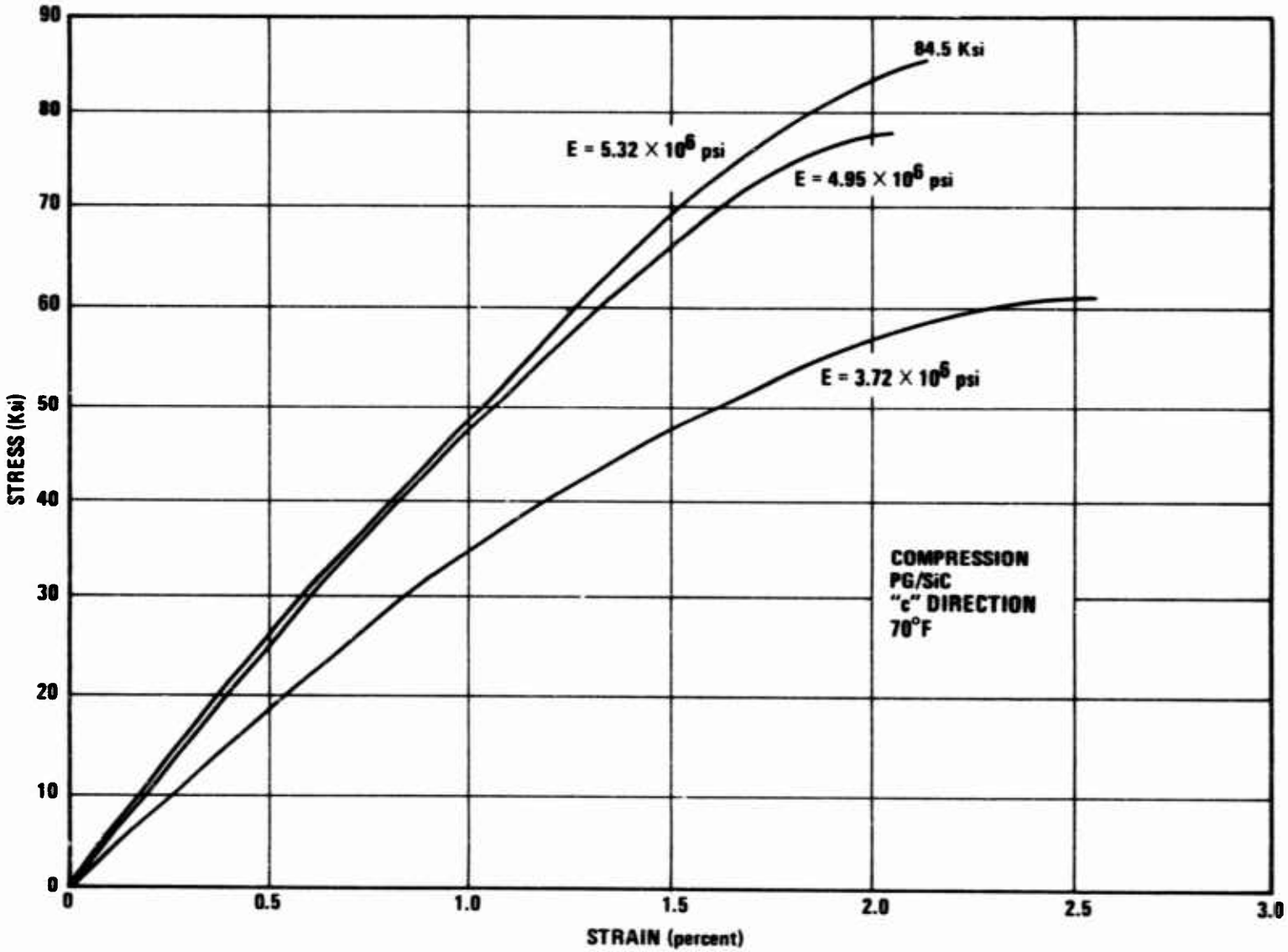

Figure 5. Stress-Strain Curve of PG/27 percent SiC in Compression in the "c" Direction at Room Temperature.

Table II. Room Temperature Mechanical Properties.

		PG	PG 20% SiC	RATIO
ab	ELASTIC MODULUS, TENSION, psi X 10^6	3.6	4.6*	1.3
c	ELASTIC MODULUS, COMPRESSIVE, psi X 10^6	1.5**	4.7	3
	RATIO ab/c	2.4	1.0	
ab	TENSILE STRENGTH, psi	9000	25,000	3
c	TENSILE STRENGTH, psi	800	8000**	10
	RATIO ab/c	11	3	
	POISSON'S RATIO ab/ab	0.12	0.14*	1
ab	TENSILE STRAIN TO FAILURE, percent	0.25	0.5	2

*BOTH TENSION AND COMPRESSION

**PRIVATE COMMUNICATION FROM SRI

are contained in Appendix III. A small correction was made for the 1 inch radius of curvature. The flexural strengths are plotted in Figure 6 as a function of SiC content. As expected, the data is somewhat higher than the room temperature tensile strength data (see Figure 3). There appears to be a slight trend toward higher strengths at higher SiC content. However, the slope of the dotted line was influenced by the tensile data trend.

The room temperature modulus of elasticity was also calculated using the deflection measurement at failure. The data is plotted in Figure 7 along with similar data from the tensile tests. The similarity of data in the flexural and tensile modes is quite good.

A number of NOL ring tests were also made at room temperature on PG/SiC. However, this approach was abandoned when it was determined that the strengths were only 20 to 40 percent of that obtained in the flexural tests.

SECTION IV

DATA SUMMARY

Thermal Expansion	Figure 1
Thermal Conductivity	Figure 2
Tensile Strength – a direction	Figure 3
Tensile Elastic Modulus – a direction	Figure 4
Tensile σ-ϵ Curves - a direction (typical)	Appendix B - Figures 13 and 14
Compressive Elastic Modulus - a direction	Appendix B - Figure 16
Compressive σ-ϵ Curve - a direction (typical)	Appendix B - Figure 18
Compressive σ-ϵ Curve – c direction	Figure 5
Comparison of Room Temperature Properties of PG and PG/SiC	Table II

SECTION V

CONCLUSIONS

1. The addition of 20 weight percent SiC to PG renders the material nearly isotropic with respect to thermal expansion (first cycle) and modulus of elasticity.

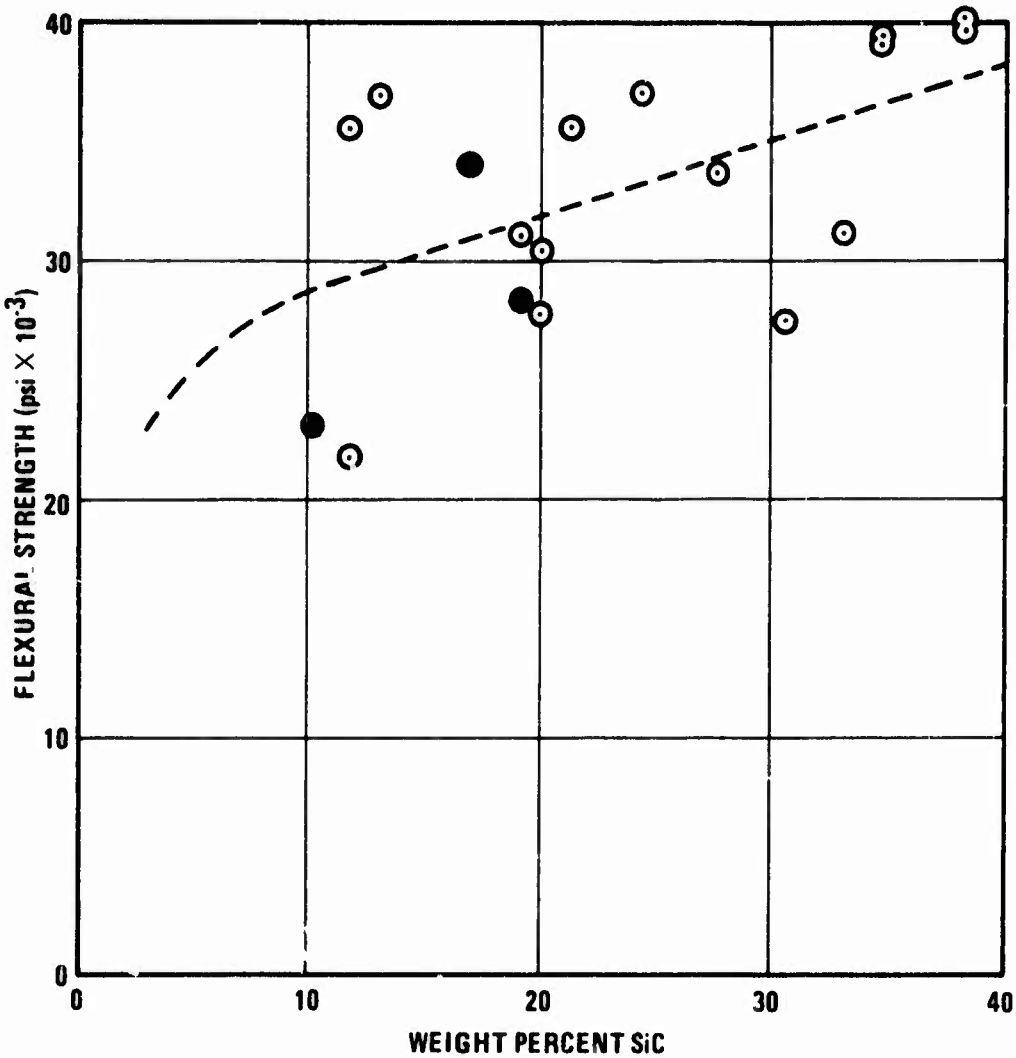

Figure 6. Flexural Strength of PG/SiC in the "ab" Plane at Room Temperature.

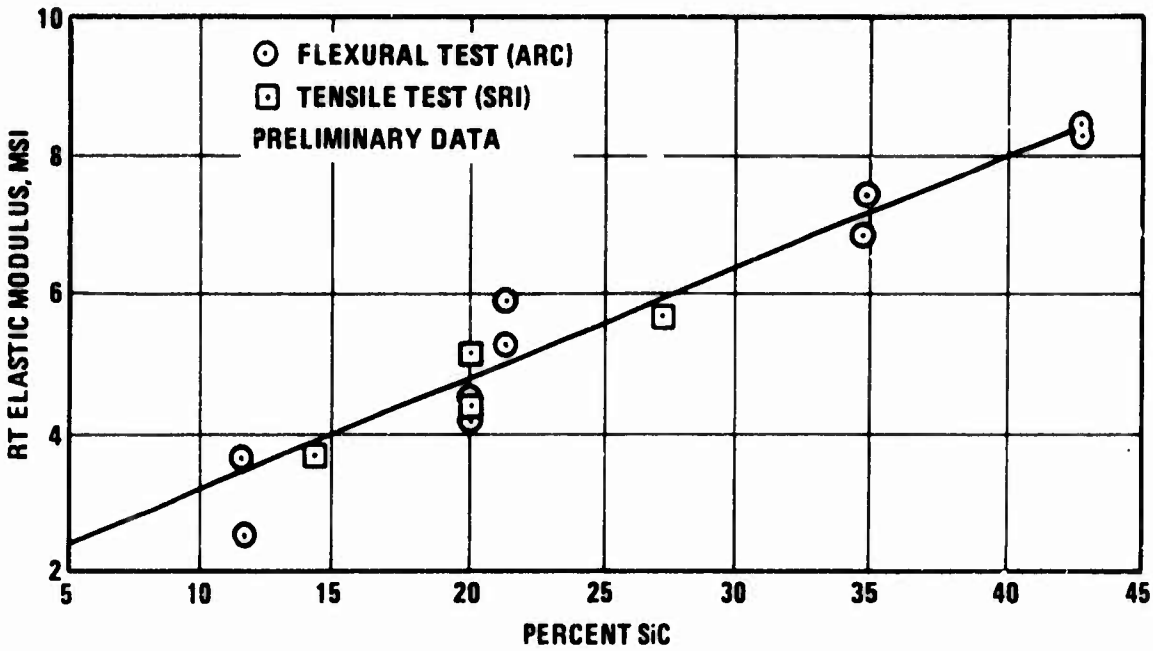

Figure 7. Modulus of Elasticity in Flexure and in Tension of PG/SIC at Room Temperature.

2. The addition of 20 weight percent SiC to PG renders it less anistropic with respect to thermal conductivity. However, the material must still be considered anisotropic with respect to this property.

3. The addition of SiC to pyrographite increases its strength and modulus of elasticity in the ab plane up to 4000°F.

SECTION VI

RECOMMENDATION

A much more detailed and comprehensive set of property data should be procured using PG/SiC codeposit material fabricated in large lots so that replicate specimens can be fabricated that are identical with respect to SiC concentration and morphology.

SECTION VII

MATERIAL FABRICATION

A system was established so that all coated parts could be catalogued. Each specimen carries two series of numbers. The first identifies the specimen use, in this case, characterization. The second series denotes the deposition run log book number. An example of this system as used in this report is as follows:

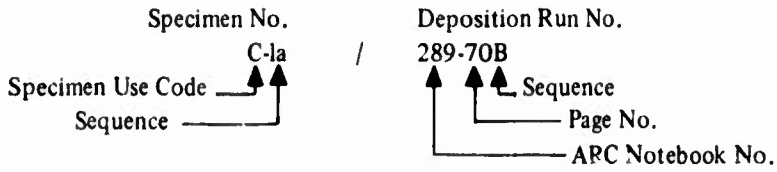

This fabrication description covers only those coating materials which were actually used for testing at SoRI.

1. THERMAL PROPERTY MATERIAL

All thermal property coating materials were fabricated as free standing bodies. To achieve this, the following procedure was used: For the PG/SiC parts, a precoat of unalloyed PG, 5 to 10 mils thick, is deposited on ATJ substrate at 3700°F. Deposition is then stopped for one-half hour and the temperature is reduced to 3200°F. At this time the deposition gas mixture is introduced and the desired coating thickness is applied. After cooling and disassembly, the substrate is machined longitudinally in four places to the coating. The substrate can then be readily separated from the coating, as no bonding takes place between the PG and the PG/SiC.

The unalloyed free-standing PG parts are fabricated in a similar manner; the precoat and the final coat are both applied at 4000°F and the substrate is AGSR graphite. The substrate is slotted longitudinally before deposition leaving a substrate thickness of 30 to 50 mils in four places, 90 degrees apart. This allows the substrate to break apart during cooldown and aids in the prevention of cracking of the PG coating.

The coatings were deposited in both cylindrical and plate form. The cylindrical substrates were 2 inches I.D. by 3.75 inches O.D. by 3.5 inches long. Three of these graphite cylinders were placed in series inside of a 4-inch I.D. tubular resistance heated Pereney furnace as shown in Figure 8. Only the central unit was used for SoRI property specimens except, on occasion, a shorter length was used from the downstream section. The plates were made in a similar manner, as shown in Figure 9, except that the inside surface of the substrate was broached to form a square, instead of circular, cross section. The saw cuts were all made in the corners. The aft plates, 2 1/4 inches wide, were submitted to SoRI for property measurement.

The fabrication parameters are listed in Table III. The reactants were introduced in quite low concentrations in nitrogen carrier gas. For PG/SiC, the total flow rate was 140 scfh, giving a velocity at coating temperature of 150 and 90 ft/sec for the circular and square cross-sections, respectively. For PG, the velocities were 60 percent greater.

The methyl trichlorosilane, MTS, flow rate was controlled by bubbling metered nitrogen through a container of liquid MTS held at 90°F. Using the calculation method described in Phase I, Task 1, and assuming saturation of the bubbler gas with MTS, the MTS concentration was varied, as shown in Table III, from 0.45 to 0.98 percent. The methane CH_4 concentration was maintained at near 2.9 percent for PG/SiC and 2.0 percent for PG. Hydrogen H_2 was used at a near 6 percent level in most of these PG/SiC runs. It was later abandoned. It appeared to be ineffective. The water-cooled copper injector contained one single influent hole, through which all of the reactant gases were introduced, and which was maintained approximately 4 inches from the fore end of the substrate section being coated for properties measurement. The coating densities (by sink-float), the SiC contents (by ashing), and the thicknesses (by microscopic filar measurement of polished end pieces) were all measured at Atlantic Research immediately after coating and prior to shipment to SoRI. In addition, the morphology was determined by microexamination of polished specimens.

A number of densities were measured at Atlantic Research on some of the tested specimens in June 1973 after they were returned. These results are compared with the original 1972 data in Table IV. The close checks are gratifying.

The characteristics of the coating specimen material used at SoRI are summarized in Table V. The last column lists the composition as determined from the density-composition curve developed in Phase I, Task 1. These last column figures are more reliable than the %Sic by ashing data. The low results by ashing are likely caused by incomplete conversion of SiC to SiO_2.

The microstructures of the coating material are summarized in Table VI. Although no microstructure code existed in 1972, some of the specimens were coded in June 1973. The majority of the material showed a fine, evenly dispersed, Code 20, microstructure. A typical Code 20 microstructure, as determined in 1972, is shown in Figure 10. The meaning of the code is given at the bottom of Table VI.

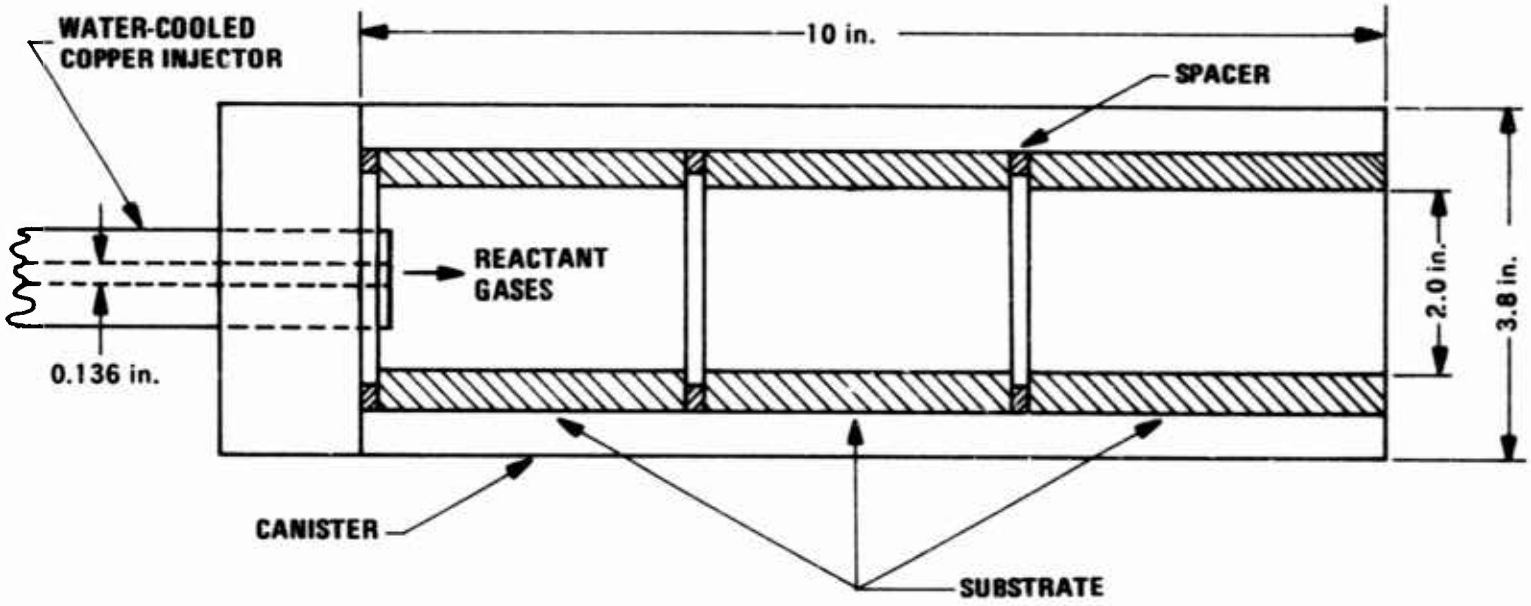

Figure 8. Deposition Assembly for Cylindrical Thermal Property Specimen Fabrication in a 4-inch I.D. Resistance Furnace.

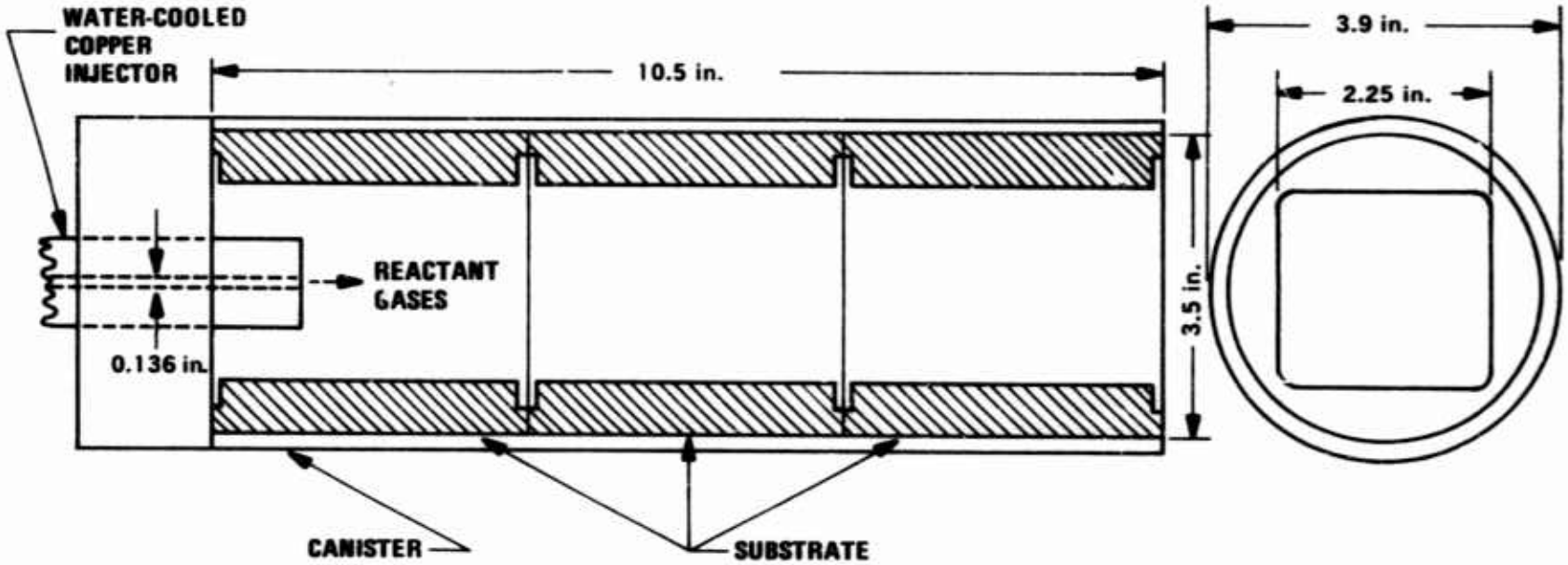

Figure 9. Deposition Assembly for Plate Thermal Property Specimen Fabrication in a 4-inch I.D. Resistance Furnace.

Table III. Thermal Property Materials Fabrication Parameters and Characteristics.

NOMINAL % SiC	RAW MATERIAL NO.	LOG RUN NO.	RAW MATERIAL SHAPE	RAW MATERIAL LENGTH TO SRI (in)	PERCENT			INJECTOR TO SUBSTRATE (in)	DENSITY (g/cc)			% SiC BY ASHING			THICKNESS (mil)		
					CH_4	MTS	H_2		ENTR.	MID.	EXIT	ENTR.	MID.	EXIT	ENTR.	MID.	EXIT
THERMAL EXPANSION																	
0	C2	162-18	TUBE	4.75	2.0	0	0	3.75	2.20	–	2.19	–	–	–	67	–	58
0	C14	162-30	PLATE	3.5	2.0	0	0	4.5	2.20	2.20	2.20	–	–	–	53	–	77
8	C19	289-71B	PLATE	3.5	2.9	0.45	6.0	3.5	2.25	2.25	2.25	8.3	9.3	8.3	58	78	76
15	C7	289-76	PLATE	3.5	2.9	0.45	6.0	4.5	2.28	2.28	2.3	14.7	18.6	14.4	110	112	100
20	C17	162-11	TUBE	3.25	2.9	0.45	6.0	3.5	2.35	–	2.4	20.9	–	24.2	94	–	126
20	C25	162-26	PLATE	3.5	2.9	0.60	5.9	4.5	2.4^-	2.38	2.35^+	22.9	22.0	19.8	–	–	114
25	C13	162-12	TUBE	3.25	2.8	0.75	5.8	3.5	2.52	–	2.5	30.9	–	29.1	77	–	110
25	C15	162-12[a]	TUBE	3.25	2.8	0.75	5.8	3.5	2.4	–	–	27.4	–	–	114	–	–
THERMAL CONDUCTIVITY																	
0	C38	033-25	PLATE	13	2.1	0	0	–	2.18	2.18	2.18	–	–	–	180	125	100
20	C11	162-7	TUBE	3.25	2.9	0.45	6.0	3.5	2.3^+	–	2.35^-	20.6	–	18.7	110	–	176
20	C56	162-2	TUBE	3.25	2.8	0.45	5.9	3.5	2.3^-	–	2.35^-	17.3	–	19.8	134	–	150
25	C29	162-42	PLATE	3.5	2.8	0.98	5.8	4.5	2.48	2.45	2.4^-	27.8	24.9	22.1	160	152	134
25	C47	162-50	TUBE	4.5	3.0	0.77	0	3.75	2.42	–	–	27.6	–	–	141	165	167
ELECTRICAL RESISTIVITY																	
15	C7	289-76	PLATE	3.5	2.9	0.45	6.0	4.5	2.28	2.28	2.3^-	14.7	18.6	14.4	110	112	190
25	C31	162-42	PLATE	3.5	2.8	0.98	5.8	4.5	2.48	2.45^-	2.4	27.8	24.9	22.1	160	152	134

[a]USED FOR HALF OF AFT SECTION, INSTEAD OF USUAL MIDDLE SECTION.

Table IV. Density Rechecks — Thermal Properties.

NOMINAL %SiC	RAW MATERIAL NO.	OLD DENSITIES			NEW RECHECK DENSITIES			PROPERTY	
		ENTR.	MID.	EXIT	ENTR.	MID.	EXIT		
20	C17	2.35	–	2.4	2.35	–	2.4	CTE	ab
25	C13	2.52	–	2.5	2.48	–	2.48	CTE	ab
25	C15	2.4	–	–	2.38	–	–	CTE	c
20	C11	2.3^{+}	–	2.35^{-}	–	2.31[a]	–	k	ab
20	C11	2.3^{+}	–	2.35^{-}	–	2.31[b]	–	k	c
25	C29	2.48	2.45^{-}	2.40^{-}	FIVE PLATES: 2.42, 2.48, 2.48, 2.42, 2.48 AVG. 2.46			k	ab

[a]CENTER OF SRI SPECIMEN CR-2AB-C-11

[b]CENTER OF SRI SPECIMEN CR-1C-C11

[c]SPECIMEN CONSITED OF FIVE PARALLEL PLATES – USED SPECIMEN

Table V. Thermal Properties — Specimen Characterization Summary.

NOMINAL % SiC	RAW MATERIAL NO.	RAW MATERIAL SHAPE	RAW MATERIAL LENGTH TO SRI (in)	MEASUREMENT DIRECTION	AVERAGE THICKNESS (mil)	AVERAGE % SiC BY ASHING	AVERAGE DENSITY (g/cc)	AVERAGE % SiC FROM DENSITY	TOTAL RUN TIME (hr)	DEPOSITION RATE (mil/hr)
THERMAL EXPANSION										
0	C2	TUBE	3	ab	65	0	2.20	–	5.0	13
0	C14	PLATE	2	c	70	0	2.29	–	6.0	12
8	C19	PLATE	3.25	ab & c	70	8.6	2.24	(13)[b]	5.0	14
15	C7	PLATE	3.25	ab & c	110	15.9	2.28	18	11.0	10
20	C17	TUBE	1.5	ab	110	23.3	2.35	27	7.7	14
20	C25	PLATE	3	c	115	21.6	2.35	27	8.0	14
25	C13	TUBE	3	ab	95	30.4	2.48	(41)	5.7	17
25	C15	TUBE[a]	1.5	c	110	27.4	2.38	30	5.7	19
THERMAL CONDUCTIVITY										
0	C38	PLATE	6	ab	170	0	–	–	14.0	12
20	C11	TUBE	3	ab & c	140	19.7	2.31	22	8.6	16
20	C56	TUBE	3	c	145	18.5	2.3	21	8.2	18
25	C29	PLATE	3	ab	150	25.3	2.45	(37)	12.0	13
25	C47	TUBE	2	c	160	27.6	2.42	(34)	6.0	27
ELECTRICAL RESISTIVITY										
15	C7	PLATE	4	ab	110	15.9	2.28	18	11.0	10
25	C31	PLATE	2	ab	150	24.9	2.42	(34)	12.0	13

[a]USE FRONT HALF OF AFT SECTION, INSTEAD OF USUAL MIDDLE SECTION.

[b]BRACKETED VALUES LESS ACCURATE SINCE OUTSIDE OF COMPOSITION WHERE DENSITY-COMPOSITION RELATIONSHIP ESTABLISHED.

Table VI. Microstructure of Thermal Property Specimens.

RAW MATERIAL NO.	NOMINAL % SiC	SiC NEEDLES	DISPERSION
THERMAL EXPANSION			
C2	0	FAIRLY GOOD. SOME LARGE CONES WITH STRAIN LINES	
C14	0	NO RECORD	
C19	8	FINE. CODE 21[a] PER JUNE, 1973	GRAIN BOUNDARY CONCENTRATIONS
C7	15	FINE	EVEN
C17	20	FINE. CODE 20	EVEN
C25	20	NO RECORD. CODE 30[a] (somewhat coarse) PER JUNE, 1973	EVEN (per June, 1973)
C13	25	FINE. CODE 20	EVEN
C15	25	FINE. CODE 20	EVEN EXCEPT GRAIN BOUNDARY CONCENTRATIONS NEAR EXIT END
THERMAL CONDUCTIVITY			
C38	0	NO RECORD	
C11	20	FINE. CODE 20 PER JUNE, 1973	EVEN
C56	20	FINE	EVEN
C29	25	NO RECORD. CODE 30[a] (somewhat coarse) PER JUNE, 1973	EVEN (per June, 1973)
C47	25	NO RECORD. CODE 30/60[a] ENTRANCE END AND CODE 11/21[a] EXIT END PER JUNE, 1973	EVEN ENTRANCE END GRAIN BOUNDARY CONCENTRATIONS AT EXIT END

[a] CODE 10 - SiC NEEDLES $<0.9\,\mu$ dia. AND L/D >3. GOOD DISPERSION

CODE 11 - SiC NEEDLES $<0.9\,\mu$ dia. ANS L/D >3. POOR DISPERSION - COLLECTS IN GRAIN BOUNDARIES

CODE 20 - SiC NEEDLES 0.9 TO 2.6 μ dia. AND L/D >3. EVEN DISPERSION

CODE 21 - SiC NEEDLES 0.9 TO 2.6 μ dia. AND L/D >3. POOR DISPERSION COLLECTS IN GRAIN BOUNDARIES

CODE 30 - SiC NEEDLES $>2.6\,\mu$ dia. AND L/D >3. EVEN DISPERSION

CODE 60 - SiC NEEDLES $>2.6\,\mu$ dia. AND L/D >3. POOR DISPERSION PG STRAIN LINES

Old 1972 (SiC is dark)

150X

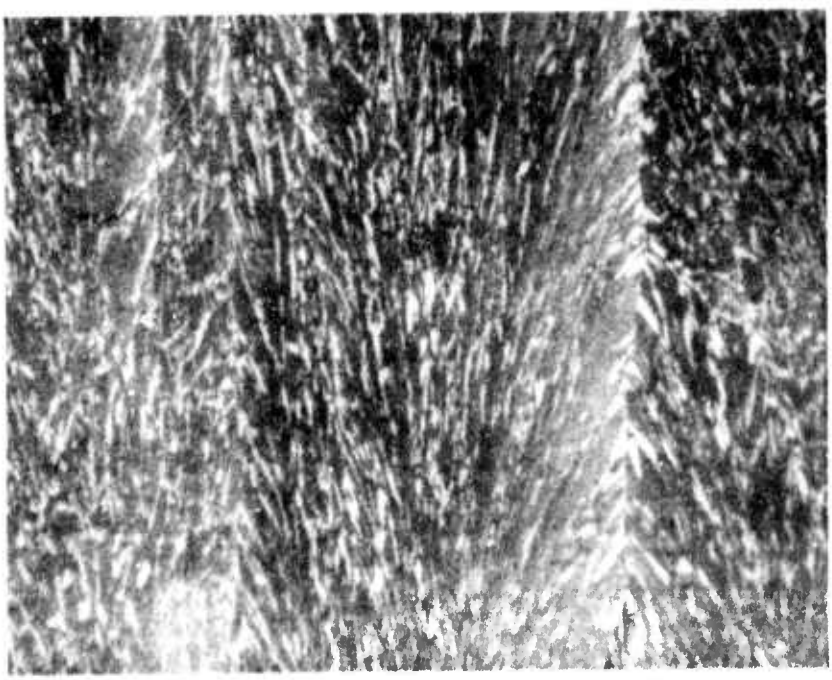

New 1973 (SiC is light)

160X

Figure 10. Microsturcture of PG/20 percent SiC Thermal Conductivity Specimen from C11 Material Code 20.

2. MECHANICAL PROPERTY MATERIAL

The tensile and compressive specimens were fabricated by coating the inside diameters of 2 inch I.D. graphite cylinders using techniques similar to those described under the thermal property material. Schematics of the coating apparati are shown in Figures 11 and 12. Only the aft compressive tes. specimen was sent to SoRI. The coating fabrication parameters are shown in Table VII. The pure pyrographite was deposited using 2 percent methane in nitrogen carrier gas at 4000°F. The PG/SiC was deposited using approximately 3 percent methane and 0.2 percent MTS, for the nominally 8 percent SiC composition, and 0.5 percent MTS for the nominally 20 percent SiC composition at 3200°F. The coating thickness profiles are shown in Table VIII. It should be noted that the coating thickness does not become appreciable until a point approximately 5 inches downstream from the injector. The original intention at SoRI was to fabricate the specimens by thinning down the central portions so as to expose the coating but leave the substrate on the ends for mechanical support during testing. However, because of difficulties already discussed in this report, SoRI finally turned to the fabrication of arc coupon specimens per Figure 3 of Appendix II for the tensile specimens (5 inches long) and per Figure 5 for the compression specimens (2.4 inches long). The centers of the specimens were near the center of the tubes supplied to SoRI. No characterization work was done at Atlantic Research prior to shipment to SoRI.

The silicon carbide contents of the specimens were determined at SoRI by ashing using material circumferentially adjacent to the central parts of the specimens. After return of the material, densities and the microstructures adjacent to the fracture were determined at Atlantic Research. The results are shown in Table IX.

The percent silicon carbide was determined at Atlantic Research indirectly from the density, using a density to SiC content relationship developed at Atlantic Research and as described in Phase II, Task 1. As can be seen from the table, these indirect values check the %/SiC by ashing at SoRI quite well. The greatest anomaly appears to be with specimen C45 which analyzed 16 percent at SoRI and 22 percent at Atlantic Research by density. It may be observed in Figure 16 of Appendix II that Specimen C45 had a higher room temperature modulus of elasticity than expected for its composition. The density values shown in Table IX, as determined by SoRI, appear to be inaccurate. The morphology of the material appears to be, on the average, Codes 20 and 21 which is fine silicon carbide needles, 1 to 2 microns in diameter either well dispersed or somewhat concentrated in the grain boundaries.

The pure PG plate used for ab direction tensile specimens was fabricated in the familiar square cross-section using plates 2 1/4 inches wide on their inside surfaces by 4 1/2 inches long. This coating was done in the 6-inch Pereny furnace which is also resistance heated. Certain of the coating parameters and the material characteristics of this material are shown in Table VII and IX, respectively.

The raw material for the compressive testing of PG/SiC in the c direction, which testing was not reported in Appendix II although the testing was done at SoRI, was especially thick plate fabricated in the induction heated 12-inch-diameter furnace under the Scale-up Program. Fabrication parameters, and the material characteristics, are listed in Tables VII and IX, respectively.

The microstructure of PG/SiC material C33 is shown at various magnifications in Figure 13. The microstructure of pure PG material C38 is shown in Figure 14.

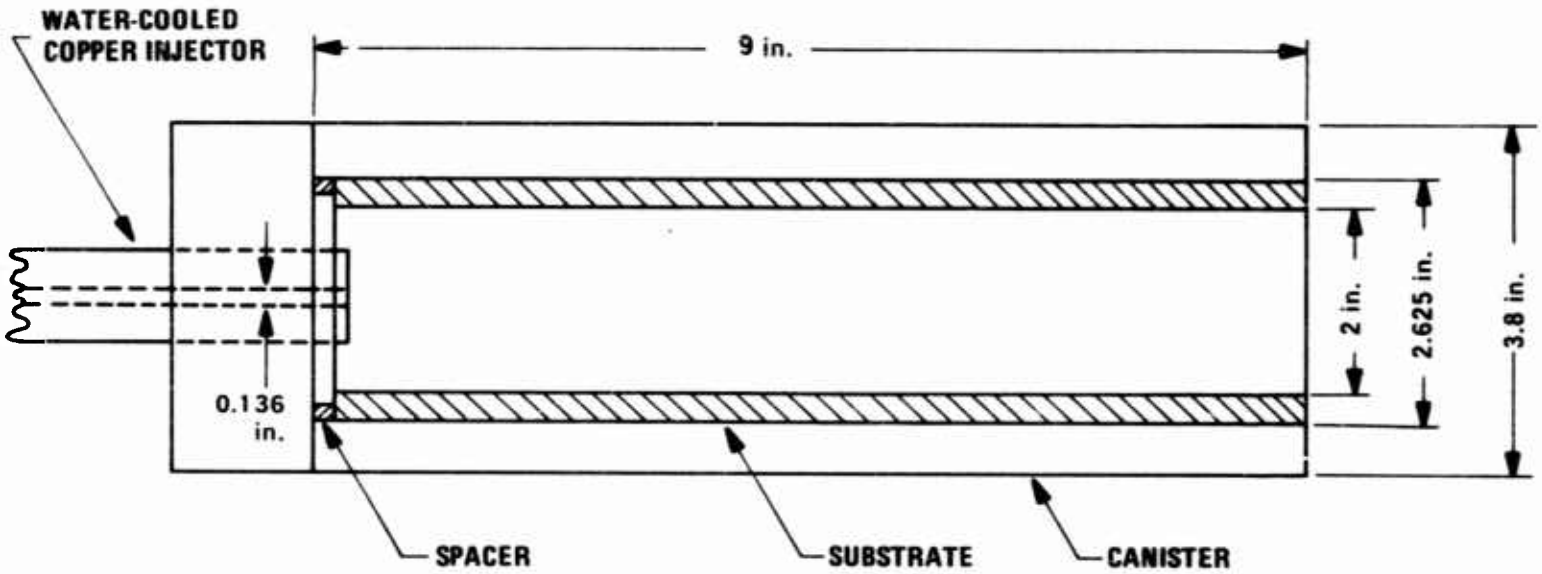

Figure 11. Deposition Assembly for Cylindrical Tesnile Test Specimen Fabrication in a 4-inch I.D. Resistance Furnace.

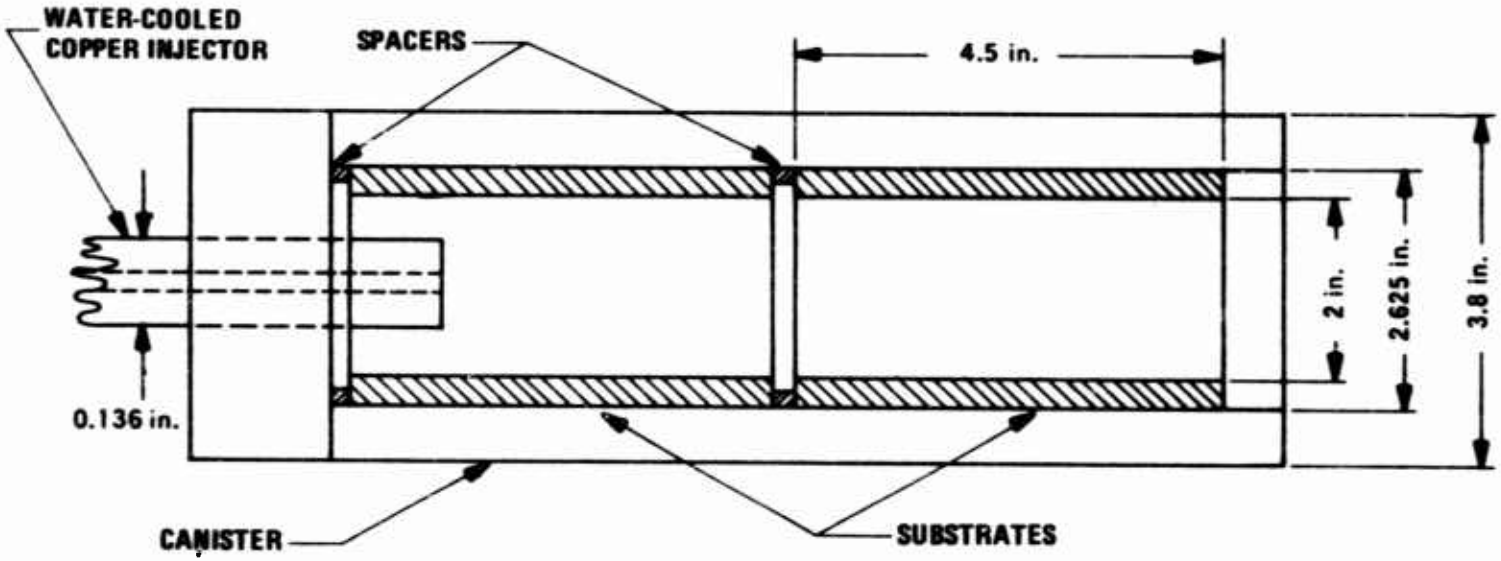

Figure 12. Deposition Assembly for Cylindrical Compressive Test Specimen Fabrication in a 4-inch I.D. Resistance Furnace.

Table VII. Mechanical Property Materials Fabrication Parameters (Cylinders).

NOMINAL % SiC	RAW MATERIAL NO.	LOG RUN NO.	PERCENT CH_4	PERCENT MTS	PERCENT H_2	INJECTOR TO SUBSTRATE (in)	TOTAL RUN TIME (hr)	MAXIMUM THICKNESS (near center) (mil)	MAXIMUM COATING RATE (mil/hr)
TENSILE ab									
0[a]	C38	033-25	2.0	–	0	NOT RECORDED	14.0	140	10
8	C53	162-69	2.9	0.19	0	0.5	8.5	168	20
8	C55	162-70	2.9	0.19	0	NOT RECORDED	8.2	162	20
20	C35	162-37	2.9	0.47	6.0	0.5	8.0	168	21
20	C43	162-64	2.9	0.47	6.0	0	9.1	146	16
20	C39	162-59	2.9	0.47	6.0	0	5.0	128	26
COMPRESSIVE ab									
0	C16	162.46	2.1	–	0	3.75	4.2	59	14
	C18	162-47	2.1	–	0	3.75	4.2	56	13
8	C51	162-68	2.9	0.19	0	0.5	8.0	164	20
	C59	162-72	2.9	0.19	0	3.75	8.2	166	20
20	C33	162-38	2.9	0.47	6.0	4.0	8.0	179	22
	C45	162-65	2.9	0.46	6.0	4.5	6.25	110	18
	C23	162-16	2.9	0.61	6.0	3.75	7.0	177	25
	C21	162-15	2.9	0.46	6.0	3.75	7.8	176	23
	C49	162-67	2.9	0.46	6.0	4.5	6.4	113	18
TENSILE c									
0	C30	162-76	2.1	–	0	0	3.2	56	17
8	C53		SEE ABOVE UNDER TENSILE ab						
20	C39		SEE ABOVE UNDER TENSILE ab						
COMPRESSIVE c									
20	–	001-47	2.8	0.34	0	–	17.8	261	15

[a]PG PLATE

Table VIII. Thickness Profiles (mil) Mechanical Property Specimen.

RAW MATERIAL NO.	ENTRANCE	1"	2"	3"	4"	5"	6"	7"	8"	EXIT
TENSILE ab										
C38[a]	160/200	–	110/145	–	90/110	–	–	–	–	–
C53	53	62	93	148	168	167	144	120	–	90
C55	63	89	125	155	162	152	123	–	–	85
C35	56	71	102	141	168	173	152	132	105	87
C43	18	30	47	70	106	134	146	133	114	88
C39	5	15	29	51	95	116	128	125	108	86

COMPRESSIVE ab

RAW MATERIAL NO.	ENTRANCE	1"	2"	3"	4"	EXIT	5"	6"	EXIT (C51 only)
C16	44	50	57	59	–	49	–	–	–
C18	34	46	53	56	–	54	–	–	–
C51[b]	67	86	138	155	164	–	140	118	81
C59	161	169	166	141	104	82	–	–	–
C33	87	149	178	179	154	140	–	–	–
C45	106	115	110	95	–	72	–	–	–
C23	167	177	173	150	121	90	–	–	–
C21	170	182	176	159	129	107	–	–	–
C49	107	116	113	94	–	71	–	–	–

[a]PLATE 2 1/4 in. X 4 in. LONG

[b]ORIGNIALLY FABRICATED AS A TENSILE SPECIMEN

Table IX. Mechanical Properties - Specimen Characterization Summary.

NOMINAL % SiC	RAW MATERIAL NO.	% SiC BY ASHING	DENSITY (g/cc) SRI	DENSITY (g/cc) ARC	% SiC FROM ARC DENSITY	MORPHOLOGY[a]
TENSILE ab						
0	C38	0	2.19	2.18	–	–
8	C53	13	2.37	2.21	12	CODE 21
8	C55	16	2.37	2.21	12	CODE 10 EXCEPT L/D <3
20	C35	20	2.44	2.31	22	GROUP 20
20	C43	20	2.41	–	–	–
20	C39	27	2.48	–	–	–
COMPRESSIVE ab						
0	C16	0	–	–	–	–
	C18	0	–	–	–	–
8	C51	16	–	2.24	15	CODE 11
	C59	16	2.34	2.24	13	CODE 10/20
20	C33	13	2.34	2.21	10	CODE 20
	C45	16	–	2.31	22	CODE 21
	C23	20	–	2.30	21	CODE 30
	C21	25	2.43	2.34	26	CODE 20
	C49	25	–	2.325	24	CODE 21
TENSILE c						
0	C30	0	–	–	–	–
8	C53	13	–	–	–	–
20	C39	27	–	–	–	–
COMPRESSIVE c						
20	–	26	–	2.35	27	CODE 30/21

[a]SEE TABLE V FOR CODE.

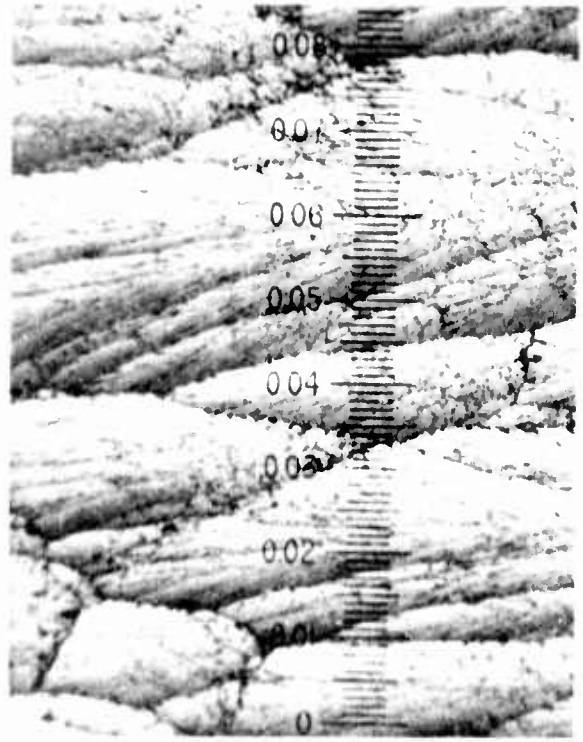

80X

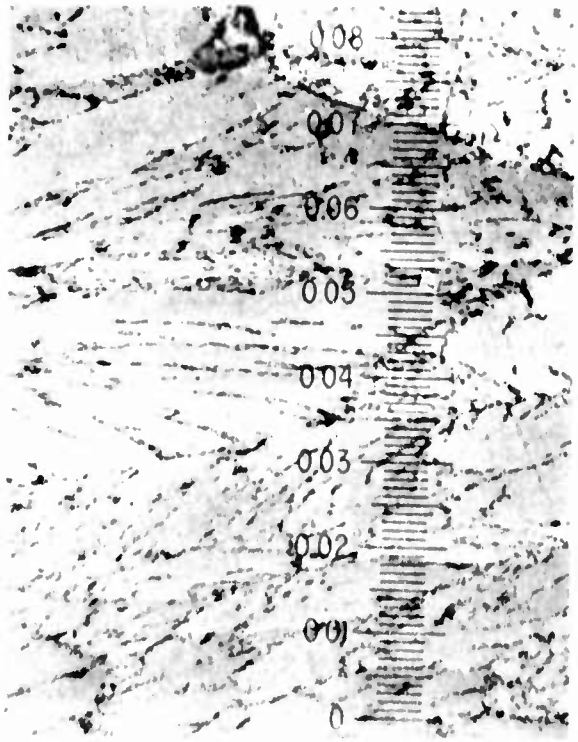

200X

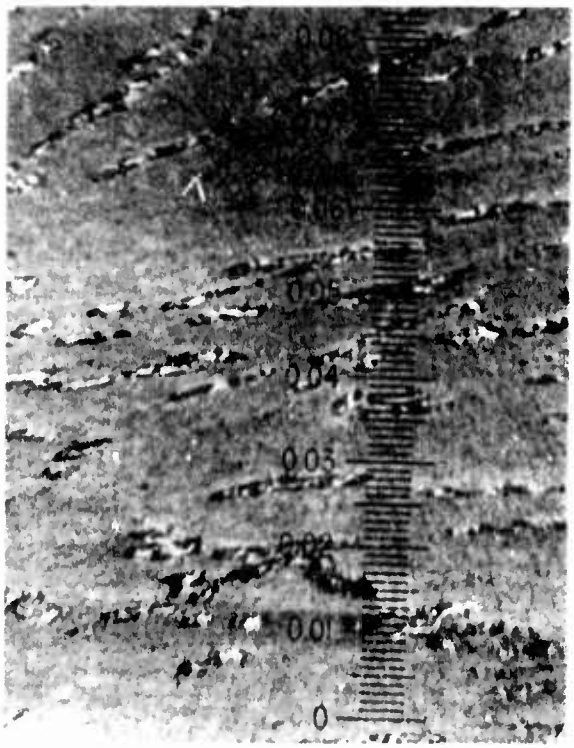

800X

1200X

Figure 13. Microstructure of PG/13 percent SiC Compressive Specimen from C33 Material Code 20.

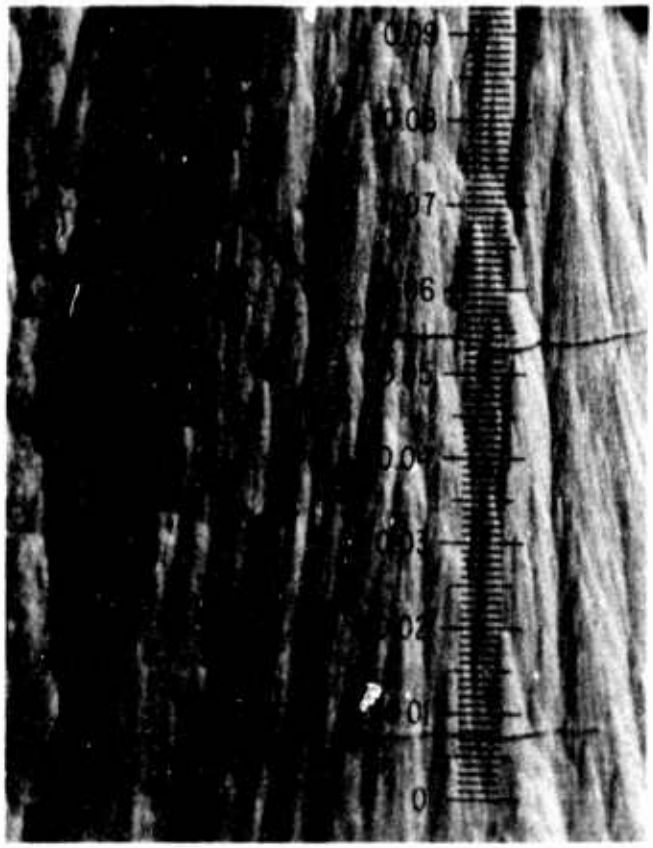

80X

Figure 14. Microstructure of Pure Pyrographite Tensile Specimen from C38 Material.

SECTION VIII

DISCUSSION

Thermal expansion measurements are generally made over fairly long periods of time. The specimens are heated slowly between temperature increments, and the strain is measured optically or with the use of a dilatometer. However, in the nozzle application, short-time thermal expansion data is required. It is now well known that PG/SiC is unstable above 4000°C. Note the permanent deformation in Figures 3 through 12 in Appendix I. The permanent deformation, or instability, is probably caused by an ordering of the pyrographite phase and possibly by a conversion of the cubic beta silicon carbide into hexagonal alpha silicon carbide. The ordering of the PG causes a growth in the ab plane and a shrinkage in the c direction.

The permanent deformations in the thermal expansion measurements made at SoRI are summarized in Table X. A more realistic picture of the true short-time expansion above 4000°F might be obtained by subtracting these deformations from the first cycle $\Delta L/L$ data, as shown in the corrected column at 5000°F. After application of the permanent deformation correction, the $\Delta L/L$ versus temperature anisotropy is considerably increased, as seen in Table XI. This is as expected in view of the pyrographite ordering phenomenon.

It is important to note that this thermal ordering in the pyrographite phase phenomenon masks the true shape of the thermal expansion curve. A second cycle slow thermal expansion curve might, in fact, more closely simulate a first cycle rapid heatup thermal expansion cu.ve. A second cycle curve was obtained for pure pyrographite at SoRI, as shown in Figure 3 of Appendix I. This could have been predicted in at least an approximate way by subtracting the permanent deformation, which was approximately 1.5 percent from the first cycle data, from the first cycle curve.

It may then be somewhat realistic with respect to a thermal stress calculation during a nozzle firing to consider that the thermal expansion anisotropy of pyrographite silicon carbide is really very close to that shown in Table XI after the permanent deformation correction has been applied. The material then may be considerably more anisotropic than originally thought It is likely, however, that the first cycle data applies quite well when cooldown stresses in the coating furnace are being considered. The psuedo second-cycle data should possibly be considered only for test firing structural analyses.

Extrapolation of the elastic modulus versus the percent silicon carbide in Figure 7 to 0 percent SiC indicates an elastic modulus for the pyrographite phase of approximately 2.5 million psi. The Phase I, Task 1 results indicated a density for the PG phase of 1.14 gm/cc It would seem very desirable to be able to improve the density and quality of the pyrographite phase. It would appear unlikely that the SiC phase could be significantly improved unless its activity could be tied up chemically, and its dissociation pressure reduced thereby, by addition of another metal carbide so as to form a compound or a solid solution.

Some loss of SiC occurred in the 4500°F mechanical property tests. The strength and elastic modulus data at 4500°F are conservative, i.e., if anything the values should be higher. It is doubtful that PG or PG/SiC would exhibit a strong strain rate effect, although it has been observed that the strength of PG is decreased somewhat by increasing strain rate, e.g., a 20 percent reduction caused by a 100-fold increase in strain rate.

Table X. Permanent Deformation in Thermal Expansion Testing of PG/SiC.

PERCENT SiC	PERMANENT DEFORMATION PERCENT 5000°F PD	PERCENT ΔL/L 4000°F	PERCENT ΔL/L 5000°F Δ	PERCENT CORRECTED ΔL/L 5000°F Δ - PD
ab DIRECTION				
0	1.5	0.75	2.25	0.75
8	0.32	0.98	1.34	1.02
18	0.36	1.05	1.42	1.06
27	0.35	1.11	1.51	1.16
40	0.20	1.16	1.54	1.34
c DIRECTION				
0	-2.8	5.0	3.5	6.3
8	-1.0	1.5	1.5	2.5
18	-0.35	1.32	1.62	1.94
27	-0.30	1.24	1.50	1.80
30	-0.42	1.25	1.45	1.87

Table XI. Thermal Expansion Anisotropy of PG/SiC.

PERCENT SiC	FIRST CYCLE ANISOTROPY 5000°F	FIRST CYCLE ANISOTROPY 5000°F CORRECTED FOR PERMANENT DEFORMATION[a]
0	1.55	8.4
8	1.12	2.5
18	1.14	1.8
27	0.99	1.55

[a]CORRECTED ANISOTROPY = $\frac{\Delta L/L \text{ - PERMANENT DEFORMATION ("c" direction)}}{\Delta L/L \text{ - PERMANENT DEFORMATION ("ab" direction)}}$

All of the data given in this report should be redetermined. A technique should be developed such that a large quantity of PG/SiC of uniform concentration, thickness and morphology could be produced. This would represent a tremendous saving in coating run time and coating evaluation time and would yield a more reliable set of properties data. Specifically, large plates or large cylinders should be produced. A minimum length of 5 inches, with a uniform 3-inch center section, is desirable because of the tensile specimen requirement.

APPENDIX I

THERMAL PROPERTIES SoRI

THERMAL PROPERTIES OF PYROLYTIC GRAPHITE AND CODEPOSITED SIC/PG WITH VARIOUS WEIGHT PERCENTAGES OF SILICON-CARBIDE

Final Report

to

ATLANTIC RESEARCH CORPORATION
Alexandria, Virginia

Purchase Order 78119

Southern Research Institute
Birmingham, Alabama
January, 1973

SoRI-EAS-73-031
Project 2931-F

THERMAL PROPERTIES OF PYROLYTIC GRAPHITE AND CODEPOSITED SIC/PG WITH VARIOUS WEIGHT PERCENTAGES OF SILICON-CARBIDE

INTRODUCTION

This is the final report to Atlantic Research Corporation covering thermal property evaluations on Pyrolytic Graphite and Codeposited SiC/PG with various weight percentages of silicon-carbide. The evaluations were performed under Purchase Order 78119.

MATERIAL

The material was furnished by Atlantic Research Corporation. We received Pyrolytic Graphite and Codeposited SiC/PG with 8%, 15%, 20% and 25% by weight percentage silicon-carbide.

The test matrix is shown in Table 1.

The specimen were identified at SoRI as follows:

CR - 1 - AB - C - 11

- 11 — ARC material identification
- AB — 'A-B' direction or 'C' direction
- 1 — Specimen number
- CR — Type of Specimen:

CR - Comparative Rod
RI - Radial Inflow
ER - Electrical Resistivity
TE - Thermal Expansion

X-ray diffraction analysis gave the following values for ARC-PG:

$d_{002} = 3.438 \times 10^{-8}$ cm

ℓ_c (crystallite height in the 'C' Direction) $= 94 \times 10^{-8}$ cm

$\rho = 2.205$ gm/cm^3

APPARATUSES AND PROCEDURES

Several apparatuses were used in this program to evaluate thermal expansion, thermal conductivity and electrical resistivity on Pyrolytic Graphite and Codeposited SiC/PG with various weight percentages of silicon-carbide. Each apparatus is briefly described under proper headings, and detailed descriptions of these apparatuses are included in the appendices.

THERMAL EXPANSION

Quartz Dilatometer

Thermal expansion was measured from 70F to 1700F in a quartz tube dilatometer. The dilatometer consists of a hollow quartz cylinder which contains the specimen and a quartz push rod. The bottom of the push rod rested on the top of the specimen and the top of the push rod was flush with the top of the outer cylinder. A dial gage with its styles resting on the top of the push rod was used to measure the relative motion between the specimen and the dilatometer tube. Thermal expansion measurements in the 'A-B' direction were made using a 3-inch long specimen. However, for the 'C' direction (due to small material thickness) several pieces were stacked together to form a specimen. We have used this stacked specimen configuration for the measurements under other several programs conducted here. This method does not add any additional uncertainty in the measurements than the usual ±3 percent.

Graphite Dilatometer

Thermal expansion measurements are made from 70F to 5500F utilizing graphite dilatometer with a dial gage. The basic principle of operation is the same as the quartz dilatometer. The specimen is radiantly heated in a graphite tube furnace.

The uncertainties in measurements of the quartz and graphite dilatometers, based on error analyses, are estimated at ±3 percent and ±5 percent, respectively.

THERMAL CONDUCTIVITY

Comparative Rod Apparatus

The thermal conductivity measurements in the 'A-B' direction were made using a cylindrical specimen. However, to determine thermal conductivity in the 'C' direction, a "bare wire" technique described in the following paragraph was employed.

The method of measuring specimen temperature is illustrated in Figure 1. Chromel/alumel thermocouple wires, 0.005 inch in diameter, were placed through a grooved disc of boron nitride. A double bore alumina tube was placed in this groove to carry the Chromel/alumel wires to the center of the specimen. These wires were flattened at the end to a thickness of about 0.002 inch and positioned on a Grafoil disc which was in contact with the specimen surface. The Grafoil disc served the electrical path to form the thermocouple. The specimen temperature gradient was corrected by substracting the temperature gradient across the Grafoil disc which was obtained from the in-house thermal conductivity data.

Radial Inflow Apparatus

To measure thermal conductivity of SiC/PG sleeve in the 'C' direction, an optical method and the water calorimeter was employed. The configuration for this method is shown in Figure 2. The technique involves measuring inside and outside specimen surface temperatures with an optical pyrometer. The sleeve was centered on a calorimeter by means of ATJ graphite specimens support cylinder fitted into the top and bottom CS graphite guards. In order to view the inner walls of the specimen, no packing was used in the annulus. The calorimeter was painted with a flat black enamel. Heat transfer takes place from the specimen to the calorimeter by gas conduction and radiation. A 0.100 inch diameter hole was drilled in a surrounding cylinder to measure the face temperature of the specimen. This hole provided a blackbody cavity with a length to diameter ratio of about 3:1. A similar hole 0.100 inch in diameter was drilled through both the specimen support cylinder and the specimen. This hole was offset 0.130 inch from the centerline so that the view of the inner wall was not obstructed by the calorimeter.

Electrical Resistivity

Electrical resistivity from 70°F to 1800°F was measured using our electrical resistivity apparatus. The equipment consists of a split furnace, d.c. power supply, d.c. ammeter, k-3 potentiometer and specimen electrodes. The heated zone of the furnace is about 12 inches long which easily allows maintaince of a uniform specimen temperature over 1-1/2 inch specimen gage length.

The uncertainty in measurements of the electrical resistivity with this apparatus is about ±2 percent. This is based on an error analysis of the system as well as comparison runs on materials which gave agreement within about ±2 percent to the values reported in the literature.

DATA AND RESULTS

Thermal Expansion

Thermal expansion data to 5000F in the 'A-B' and in the 'C' directions of PG and codeposited SiC/PG at four different silicon carbide contents (8%, 15%, 20% and 25% by weight) are presented in Figures 3 through 12 and in Tables 2 through 17. Composite plots for two directions are shown in Figures 13 and 14. Included for a comparison are the across grain expansion data on AGSR graphite which ARC used for the substrate, for the pyrolytic graphite and the with grain data on ATJ graphite (not the same material used by ARC) which was used for the substrate, for the codeposited SiC/PG.

It can be observed from Figures 13 and 14, that with increase in the silicon carbide contents, the thermal expansion in the 'A-B' direction increased while it decreased in the 'C' direction, compared to pyrolytic graphite. Thus, silicon carbide contents reduced the anisotropy. The 20 percent level silicon carbide material was essentially isotropic.

The data indicated that the materials were unstable above about 4200F (approximate temperature of the deposition). At the specimen temperature of about 4200F, the silicon carbide (β-form) dissociates from the pyrolytic graphite. After completion of the runs in graphite dilatometers, we found crystals of silicon carbide deposited on the graphite push rods. (Similar deposition was noticed during the thermal conductivity measurements). This deposition was varified by x-ray diffraction analysis as β-silicon carbide.

One of the specimens from pyrolytic graphite was exposed twice to 5000F. The material shows stability up to 5000F during the second run (see Figure 3).

The ARC-PG did not show negative expansion in the 'A-B' direction from 70F to about 1000F. The negative expansion (rather negative coefficient of expansion) on conventional pyrolytic graphite is explained in terms of Poission contraction of the layer planes (basal) associated with large expansion perpendicular to the layer planes (C-axis) as explained by Riley.[1] Above about 1000F, this effect is assumed to be counteracted by a true therma expansion of the layer planes to produce a small positive thermal expansion coefficient.

---

[1]Riley, D. P., Phys. Soc. 57. 487 (1945).

Why this negative expansion behaviour was not shown by ARC-PG was probably due to the material structure.

It was thought initially that ARC-PG may contain SiC as an impurity. However, x-ray diffraction data indicated that if the impurity of SiC were present, it was less than 1 percent by weight.

The x-ray diffraction study gave 'd' spacing (3.438 Å) which indicated that ARC-PG was turbostratic in structure. (By turbostratic structure we mean that the adjacent basal planes are randomly rotated with respect to one another, and thus, do not display an evidence of three-dimensional ordering. This does not mean that the distance between the layer planes is variable. All the layer planes are at a distance given by 'd' spacing of the x-ray diffraction analysis).

Bacon[2] and Franklin[3] have shown that the increase in the unit cell height 'C' (=2d) above the perfect graphite value of 6.708 Å is a quantitative measure of the amount of turbostratic structure. Their relationship is approximated by a parabolic expression:

$$C = 6.880 - 0.172\ (1-p) - 0.128\ p\ (1-p)$$

where

p = the probability of stacking disorder (basal planes)

Using the value of the 'd' spacing given by the x-ray diffraction, the value of 'p' for ARC-PG was 99 percent. This indicated that the ARC-PG was almost turbostratic in structure. This conclusion is also supported by the value of the crystallite height (ℓ_c). Typical values of 'p' for ATJ-S graphite is 30 percent.

In PG, structure can range from a material where the growth cone develops from the deposition surface (substrate necleated) to a material where the growth cones are regenerated continuously throughout the thickness of the deposition (continuously nucleated). Substrate nucleated structure exhibits maximum crystal orientation and therefore highest anisotropy. Thus, turbostratic structure of ARC-PG indicated a possibility of continuously nucleated structure. Microstructure analysis will varify this observation.

---

[2]Bacon, E. E., Acta Crystallite, 4, 558 (1951).

[3]Franklin, R. E., Acta. Crystallite, 4, 253 (1951).

The high expansion of pyrolytic graphite in the 'C' direction is as expected. As the planes (basal) becomes further apart with temperature, the frequency of vibration is lower (out of plane acoustic modes) due to a decrease in the interplanar interaction. This decrease in the interplanar interaction is due to an increase in the 'd' spacing with temperature.

On an atomic basis, thermal expansion corresponds to an increase in the average interatomic distance. Therefore, comparing microscopic and macroscopic properties one can write:

$$\left(\frac{d_1 - d}{d}\right)_T = \left(\frac{l_1 - l}{l}\right)_T = \left(\frac{\Delta \ell}{\ell}\right)_T$$

where

d = equilibrium distance between two basal planes (3.438 Å)

d_1 = above distance at temperature, T

$\frac{\Delta \ell}{\ell}$ = unit thermal expansion at temperature, T

At 4000F, $\frac{\Delta \ell}{\ell}$ was = 5×10^{-3} in./in. or equal to 5 percent in the 'C' direction. Thus at 4000F, the increased in the basal plane distance was about 5 percent. This increase in the distance between the layer planes resulted in a decrease in the interplanar interaction which caused decreased in the frequency of vibration or an increase in the thermal expansion in the 'C' direction.

More attention was given in explaining the thermal expansion behaviour of ARC-PG, since future improvements in the properties of codeposited material will largely depend upon the properties of this pyrolytic graphite.

Thermal Conductivity

Thermal conductivity data on ARC-PG and Codeposited SiC/PG with 20% and 25% silicon carbide, in the 'A-B' and in the 'C' directions are presented in Figures 15 through 20 and in Tables 18 through 25.

For ARC-PG the anisotropy ratio of conductivity at 200F was 150. The data on ARC-PG for both orientations compares favorably with other SoRI data.

At elevated temperatures the thermal conductivity of the undelaminated pyrolytic graphite in the 'C' direction is affected by a prior heat treatment (~3000C or above) but that in the 'A-B' direction, remains at about the same level. Due to a heat treatment, turbostratic structure is modified so as to exhibit a more 3-dimensional stacking order of the basal planes. Since ordering the crystal structure corresponds to ordering the basal planes, this ordering will increase the interaction energy between the basal planes and therefore will increase the phonon energy. The increase in the phonon energy will result in an increase in the group velocity and therefore, a decrease in the phonon density (population per unit volume), which will lead to a decrease in the thermal resistivity or an increase in the thermal conductivity. However, the structure of each basal plane is not much influenced by a heat treatment. Therefore, at high temperatures, the thermal conduction in pyrolytic graphite in the 'C' direction is generally affected by a heat treatment while that in the 'A-B' direction remain much the same.

Other important factors which will influence the thermal conductivity of pyrolytic graphite such as (1) delaminations and their locations, (2) conduction of gases in the delaminations, and (3) radiation, are discussed elsewhere.[4]

Higher silicon carbide contents have reduced the anisotropy, compared to pyrolytic graphite. The anisotropy ratio of conductivity for 20 percent silicon carbide at 200F was about 10 compared to about 150 for pyrolytic graphite at 200F. A composite plot for two directions are shown in Figures 21 and 22.

Electrical Resistivity

The electrical resistivity data in the 'A-B' direction to 1800F for the codeposited SiC/PG with 15% and 20% silicon carbide are presented in Figure 23 and in Table 26. The data are compared with other pyrolytic graphite. The decrease in the electrical resistivity with temperature is explained in terms of a decrease in the scattering at the crystallite boundary with temperature. In this temperature region (70 to 1800F), the thermal scattering is not that predominant. By increasing the silicon carbide from 15% to 25%, an increase in the resistivity near room temperature by four-fold (4 times) was observed. The electrical resistivity

[4] "Thermal conductivity of pyrolytic graphite cylinders in various gas environments." The Ninth Thermal Conductivity Conference, 1969.

of a single crystal silicon carbide near room temperature is about 1,000,000 μohm-cm, which explains why an increase in the resistivity occurred with a slight increase in the silicon carbide contents.

Submitted by:

S. G. Bapat
Associate Engineer

Approved by:

C. D. Pears, Head
Mechanical Engineering Division

SoRI-EAS-73-031
Project 2931-F

(5:12)
dcb

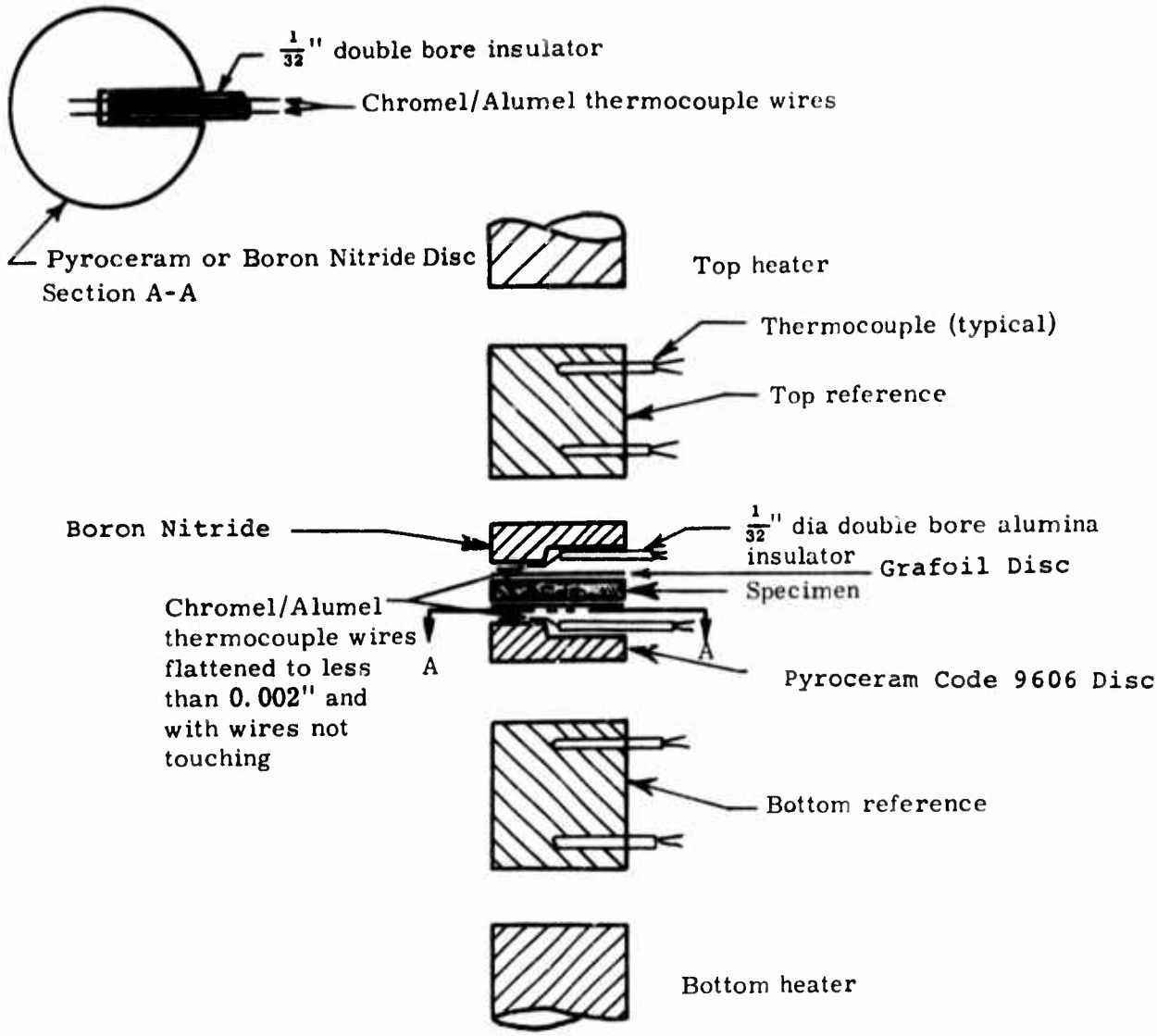

Figure 1. Expanded Schematic of References and Specimen Configuration for Thin Materials Using the Comparative Rod Apparatus and the Bare Wire Method of Measuring Specimen Surface Temperature

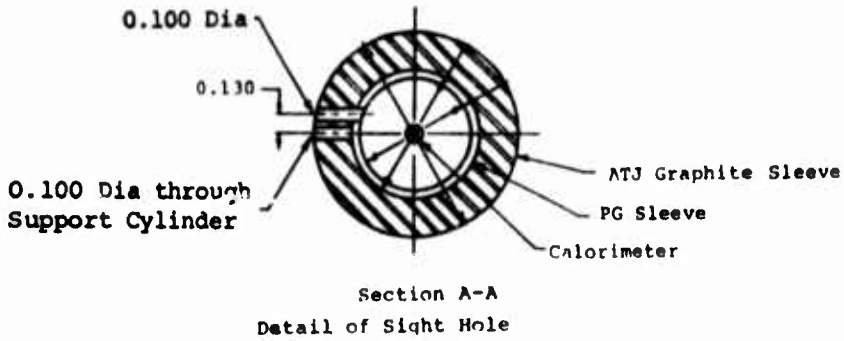

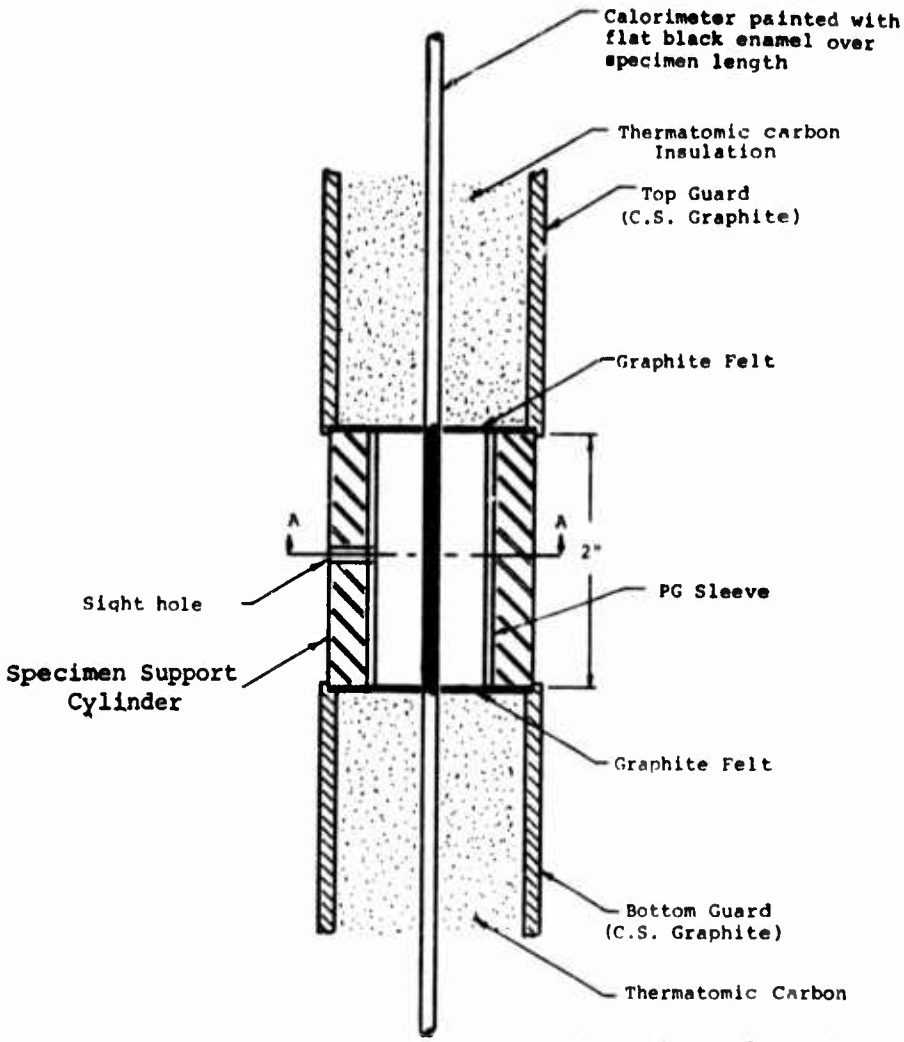

Figure 2. Buildup for Optical Measurements of Inside Surface Temperature of a PG Sleeve during thermal conductivity measurements in the 'C' Direction using the Radial Inflow Apparatus

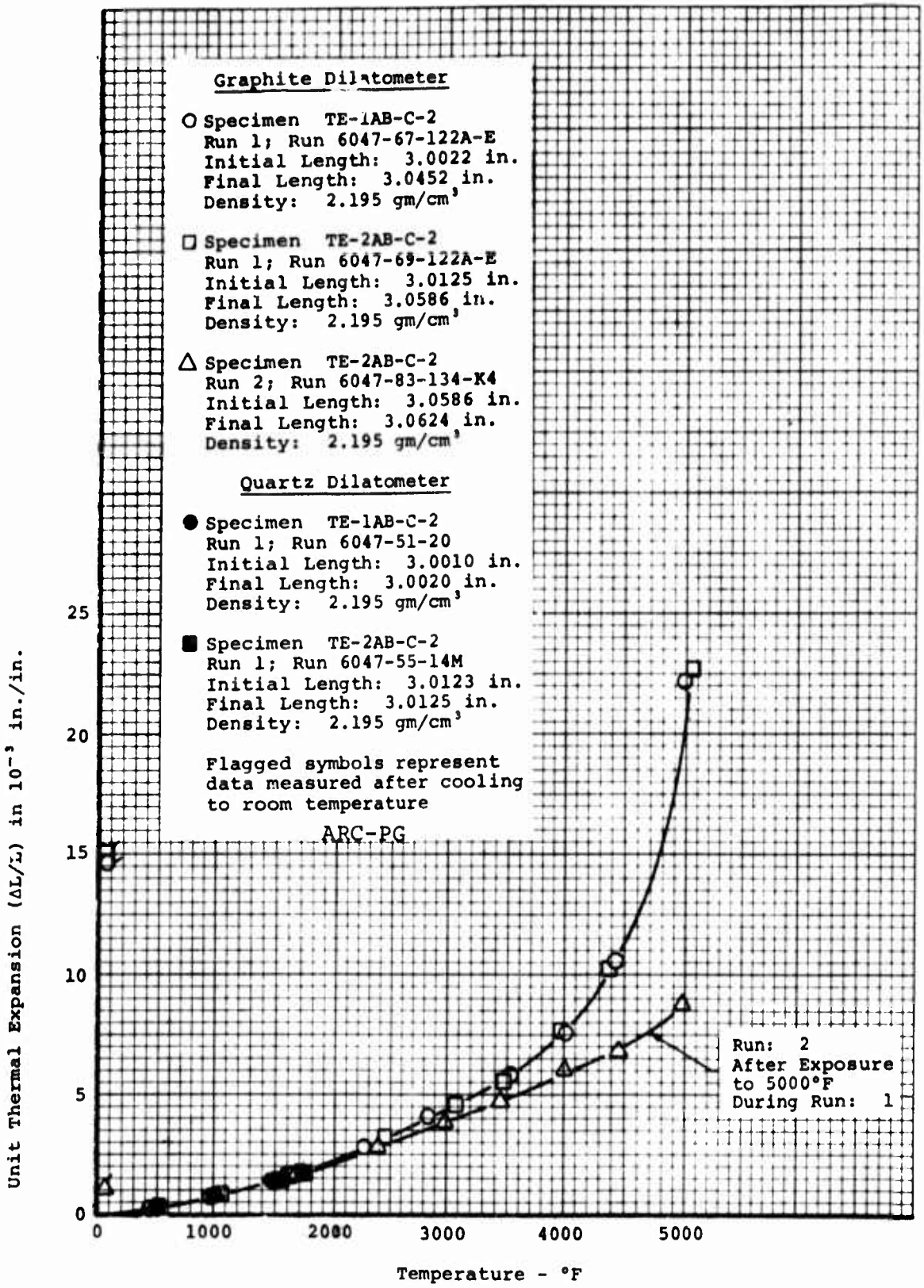

Figure 3. Thermal Expansion of Pyrolytic Graphite in the 'A-B' Direction

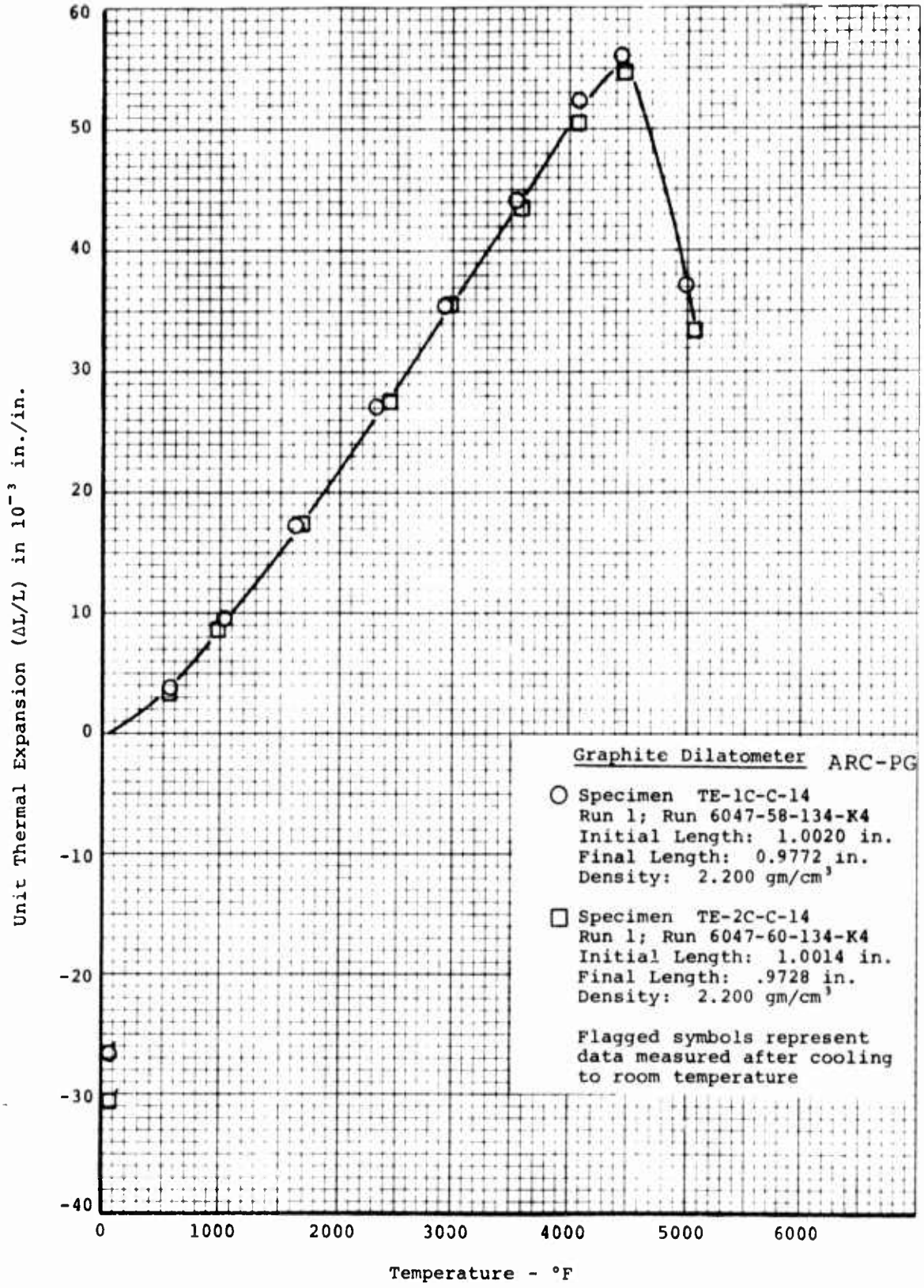

Figure 4. Thermal Expansion of Pyrolytic Graphite in the 'C' Direction

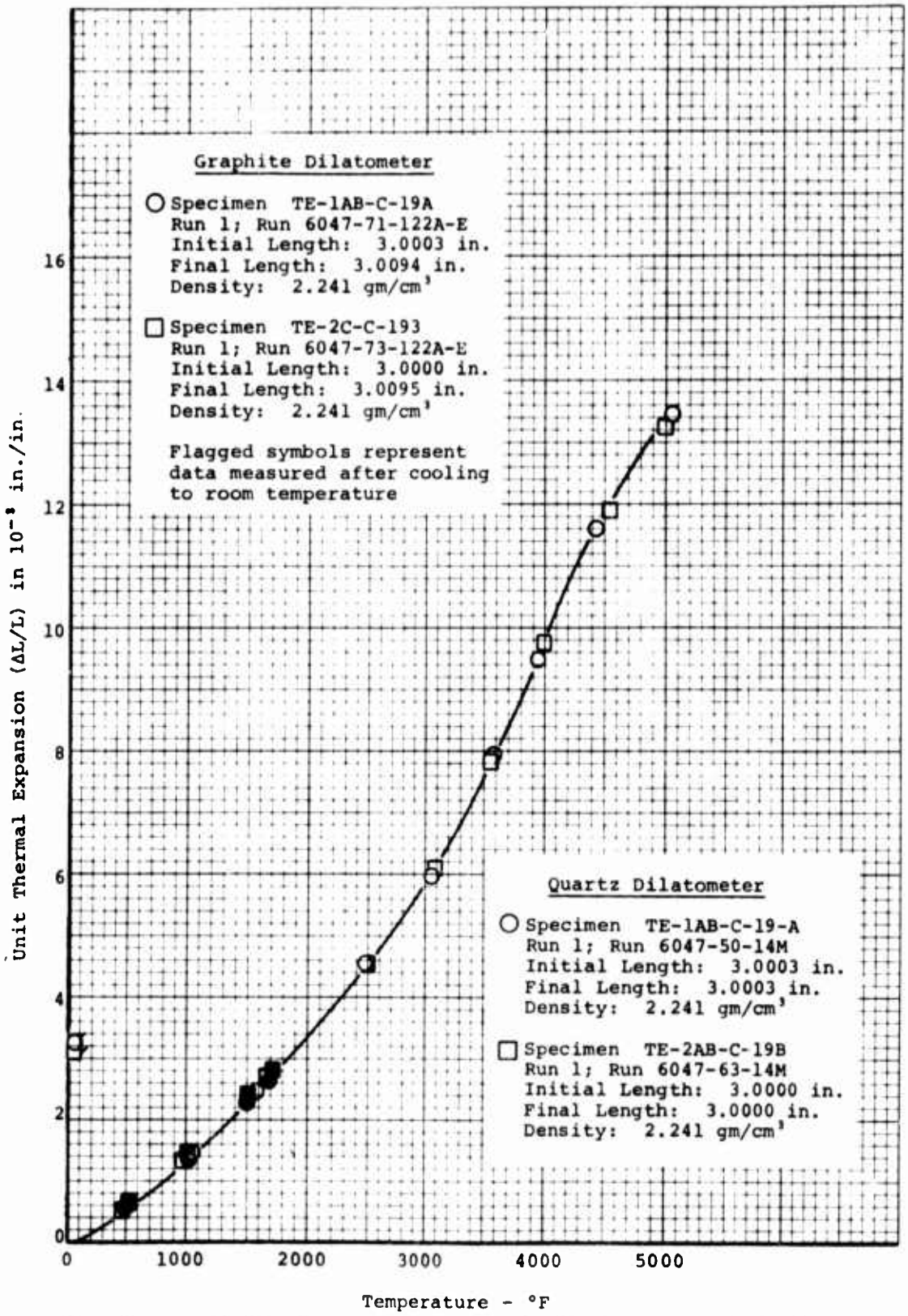

Figure 5. Thermal Expansion of Codeposited Pyrolytic Graphite Plate with 13 Percent SiC in the 'A-B' Direction

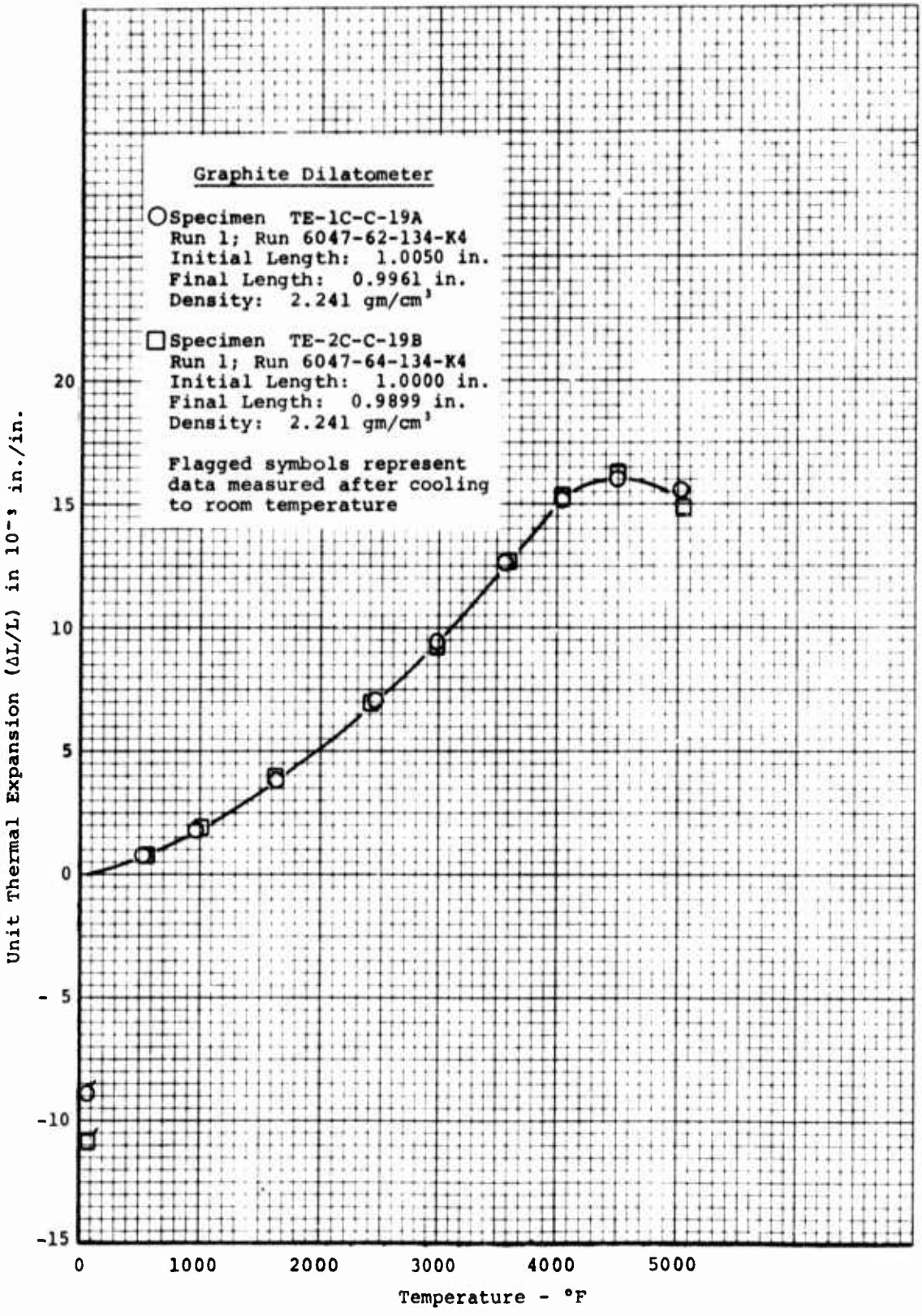

Figure 6. Thermal Expansion of Codeposited Pyrolytic Graphite Plate with 13 Percent SiC in the 'C' Direction

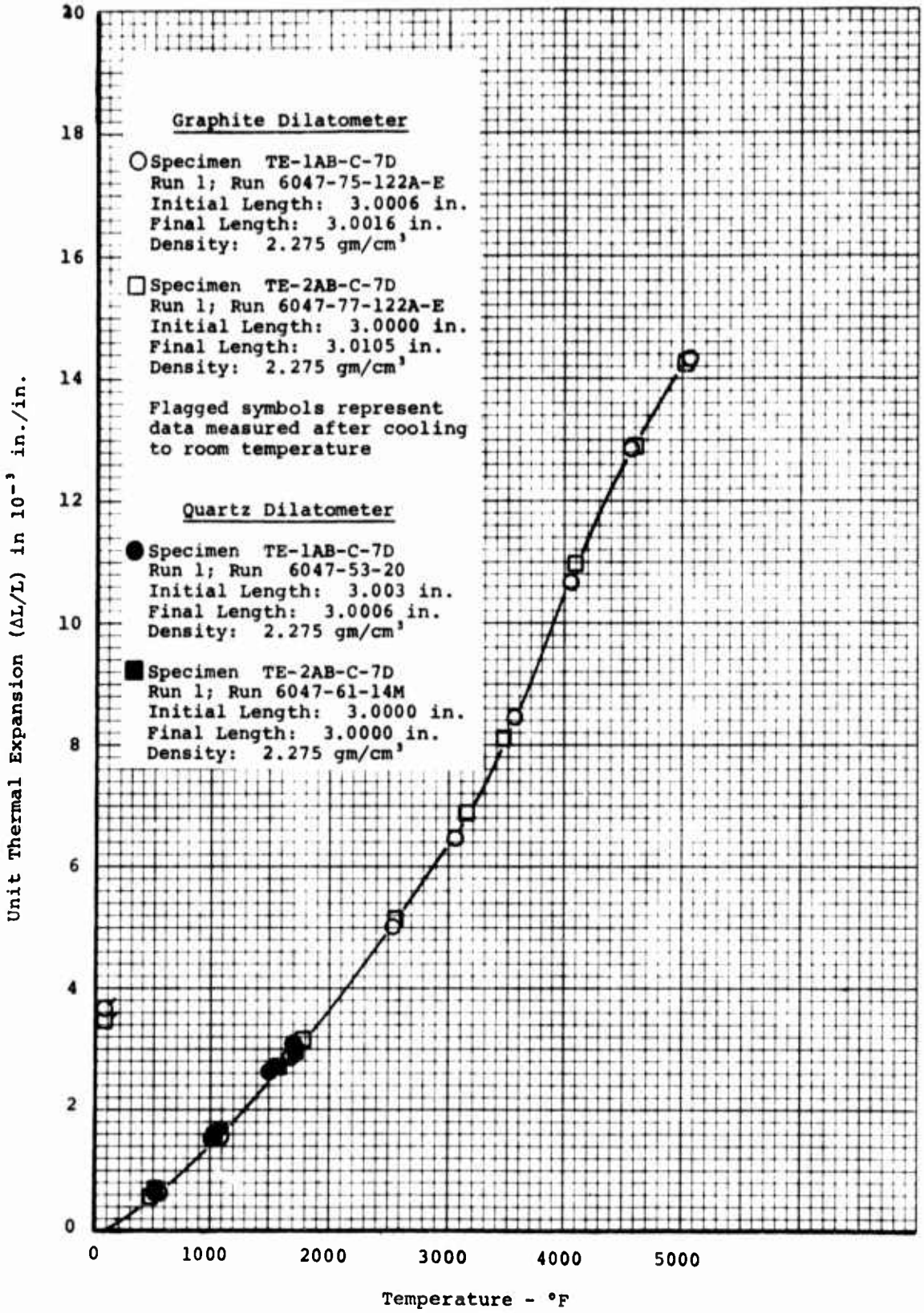

Figure 7. Thermal Expansion of Codeposited Pyrolytic Graphite Plate with 18 Percent SiC in the 'A-B' Direction

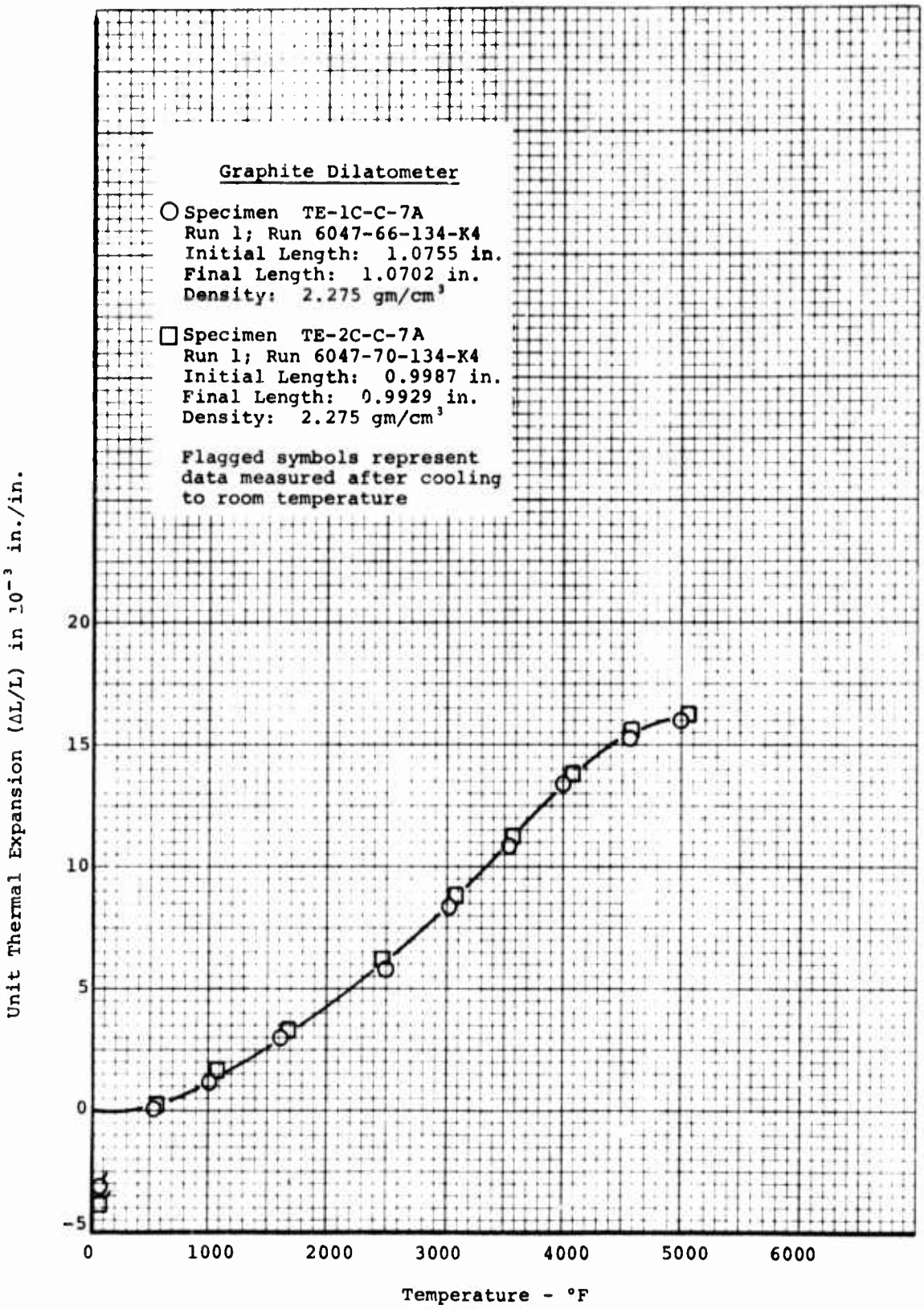

Figure 8. Thermal Expansion of Codeposited Pyrolytic Graphite Plate with 18 Percent SiC in the 'C' Direction

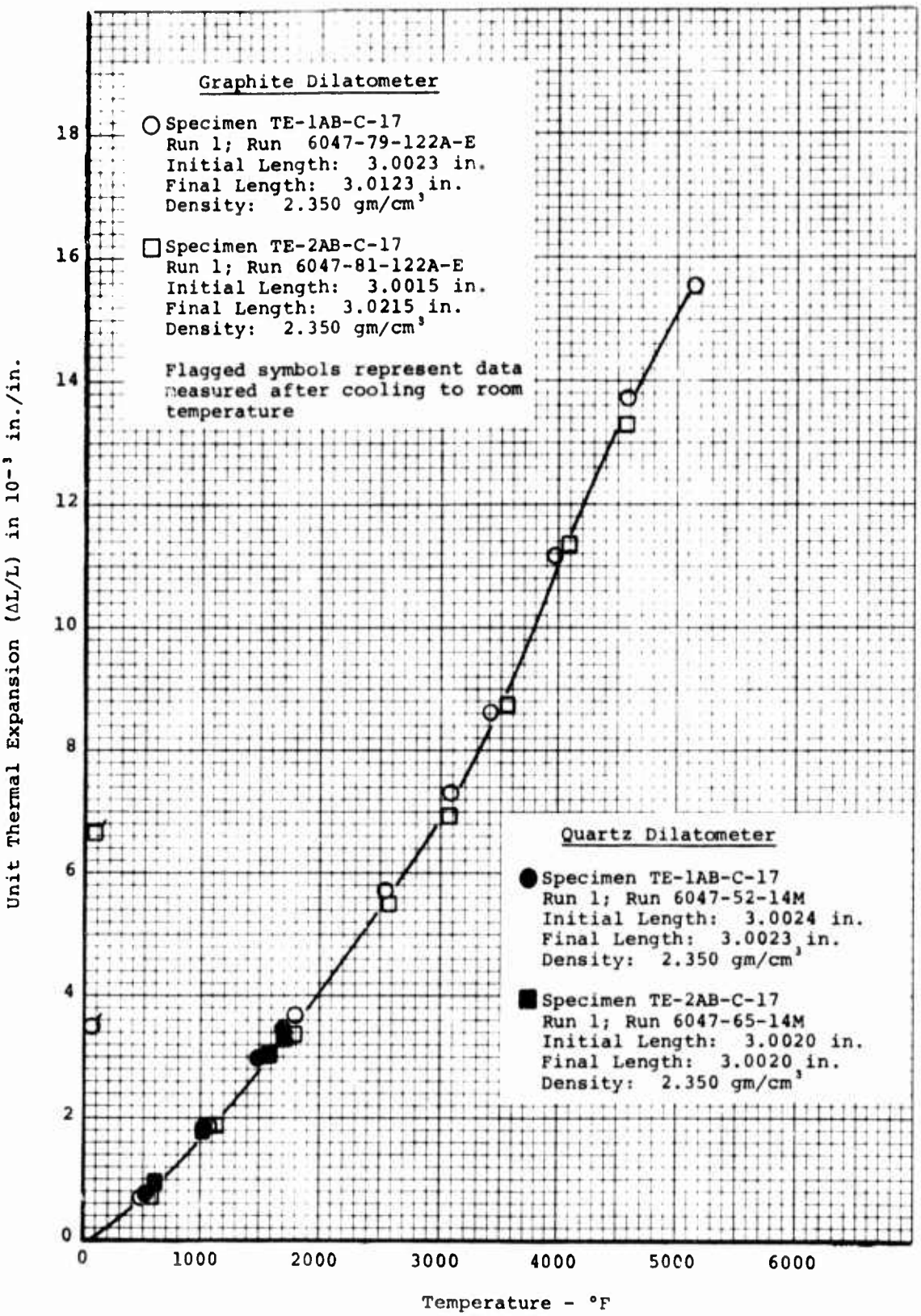

Figure 9. Thermal Expansion of Codeposited Pyrolytic Graphite Sleeve (Coupon Specimen) with 27 Percent SiC in the 'A-B' Direction

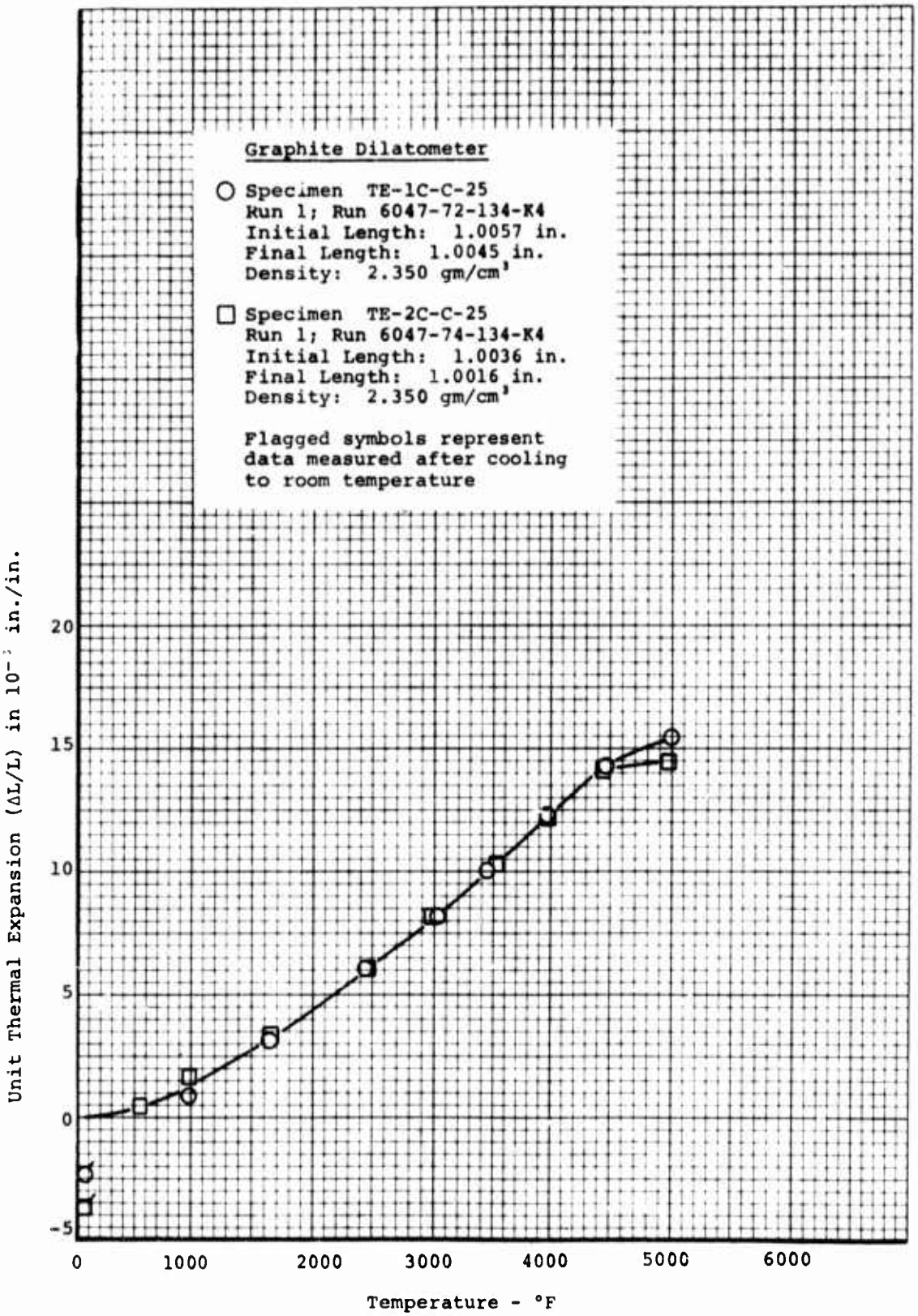

Figure 10. Thermal Expansion of Codeposited Pyrolytic Graphite Plate with 27 Percent SiC in the 'C' Direction

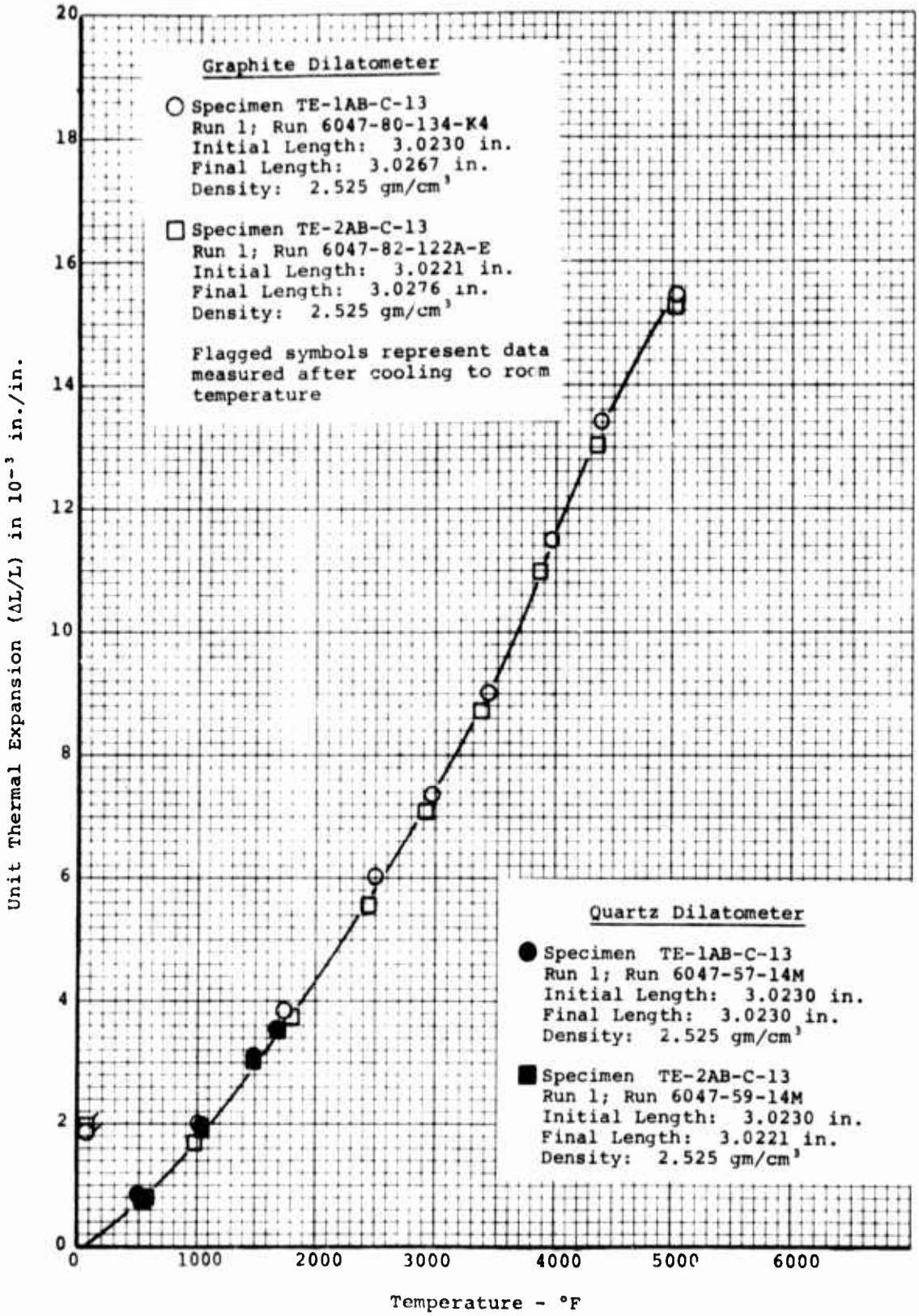

Figure 11. Thermal Expansion of Codeposited Pyrolytic Sleeve (Coupon Specimen) with 41 Percent SiC in the 'A-B' Direction

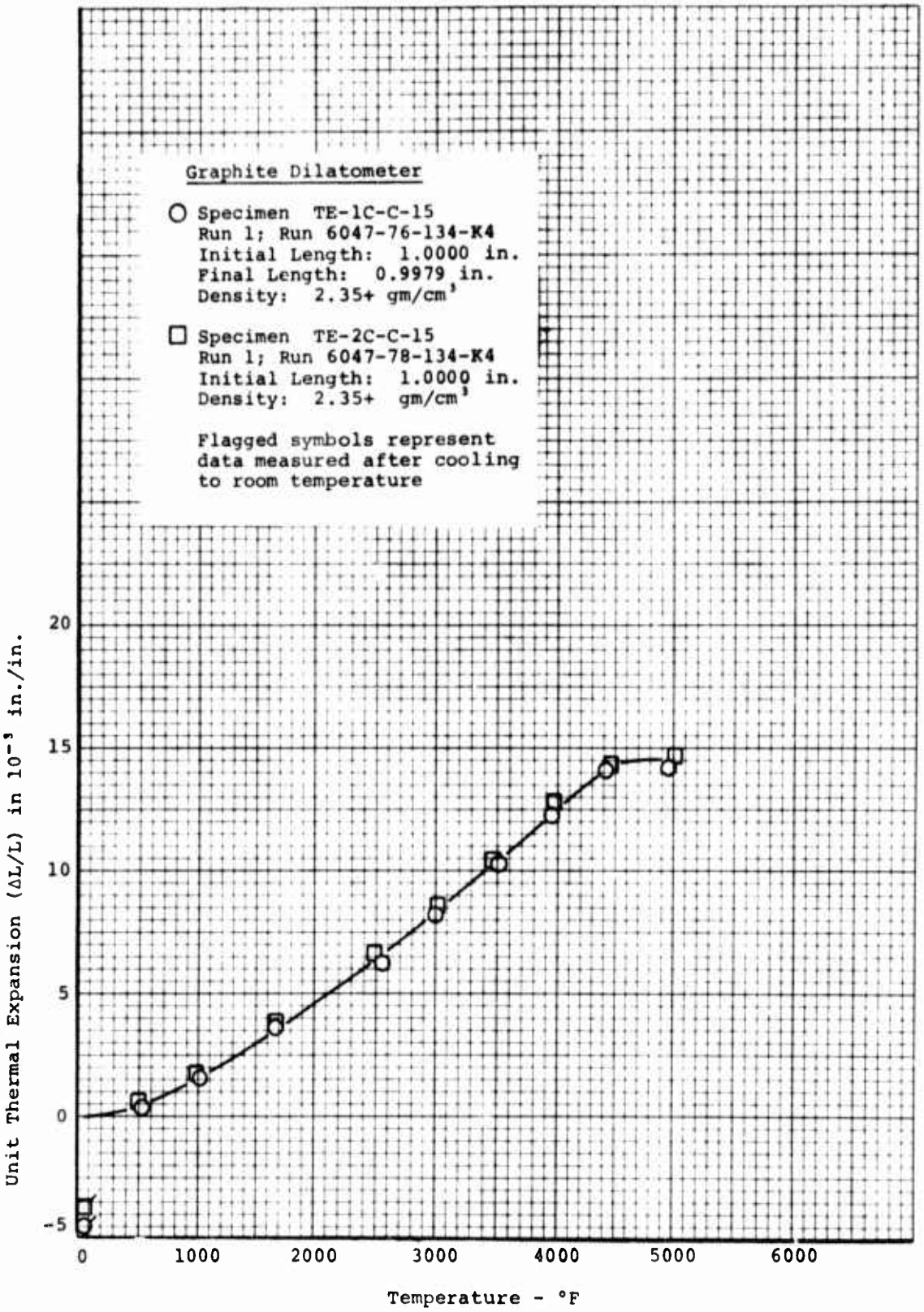

Figure 12. Thermal Expansion of Codeposited Pyrolytic Graphite Sleeve (Coupon Specimen) with 30 Percent SiC in the 'C' Direction

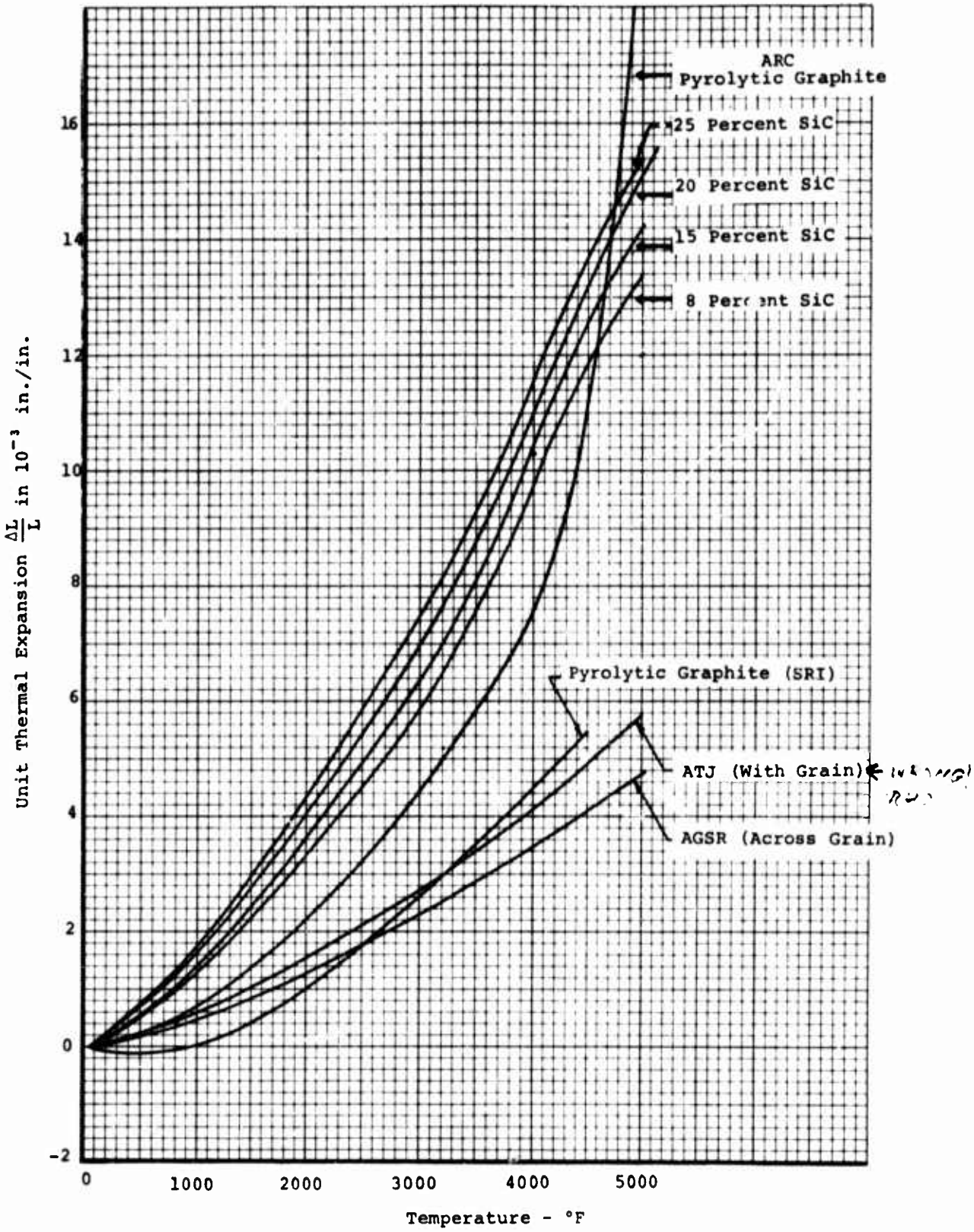

Figure 13. A Composite Plot of Thermal Expansion in the 'A-B' Direction

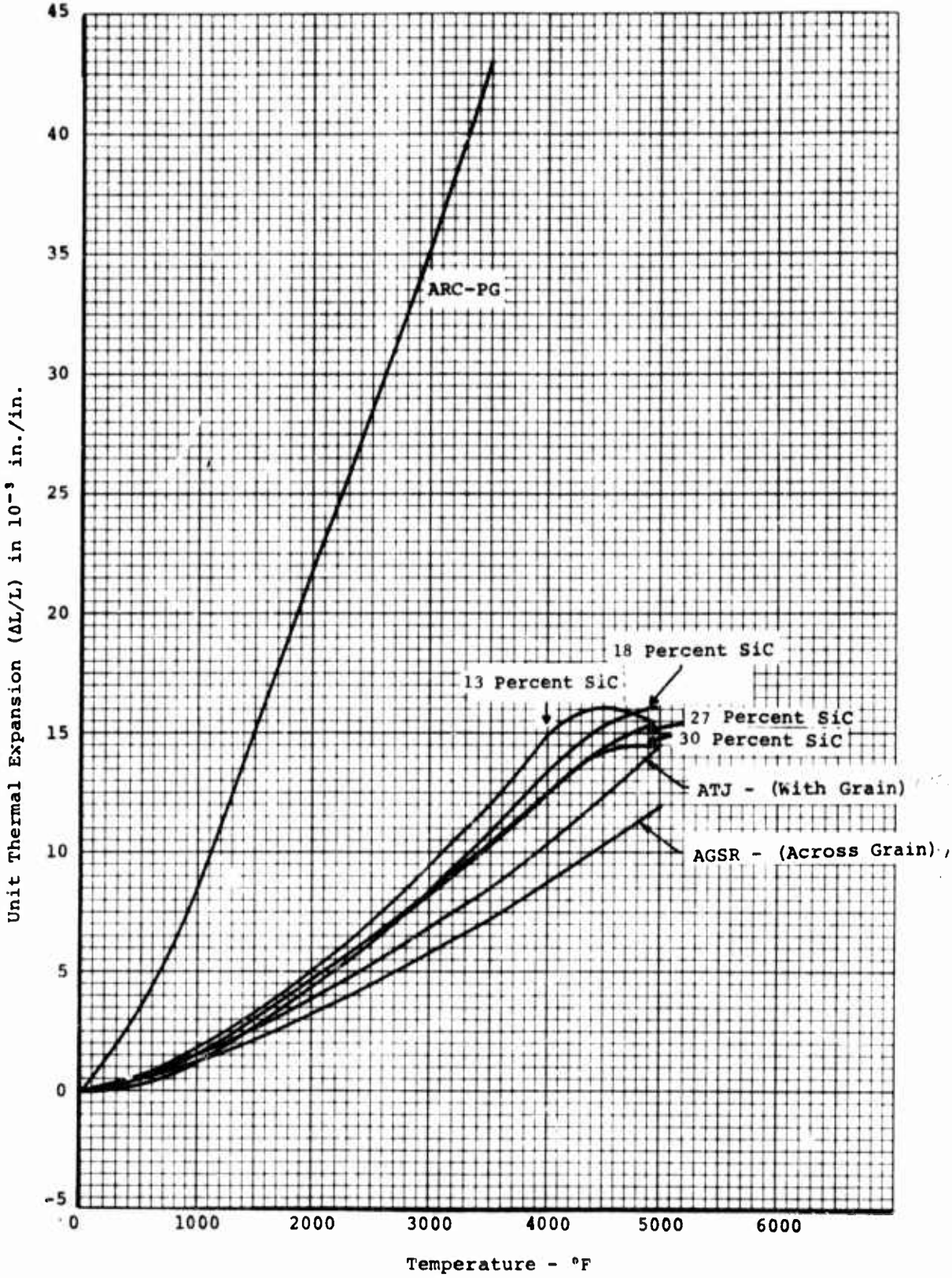

Figure 14. A Composite Plot of the Thermal Expansion in the 'C' Direction

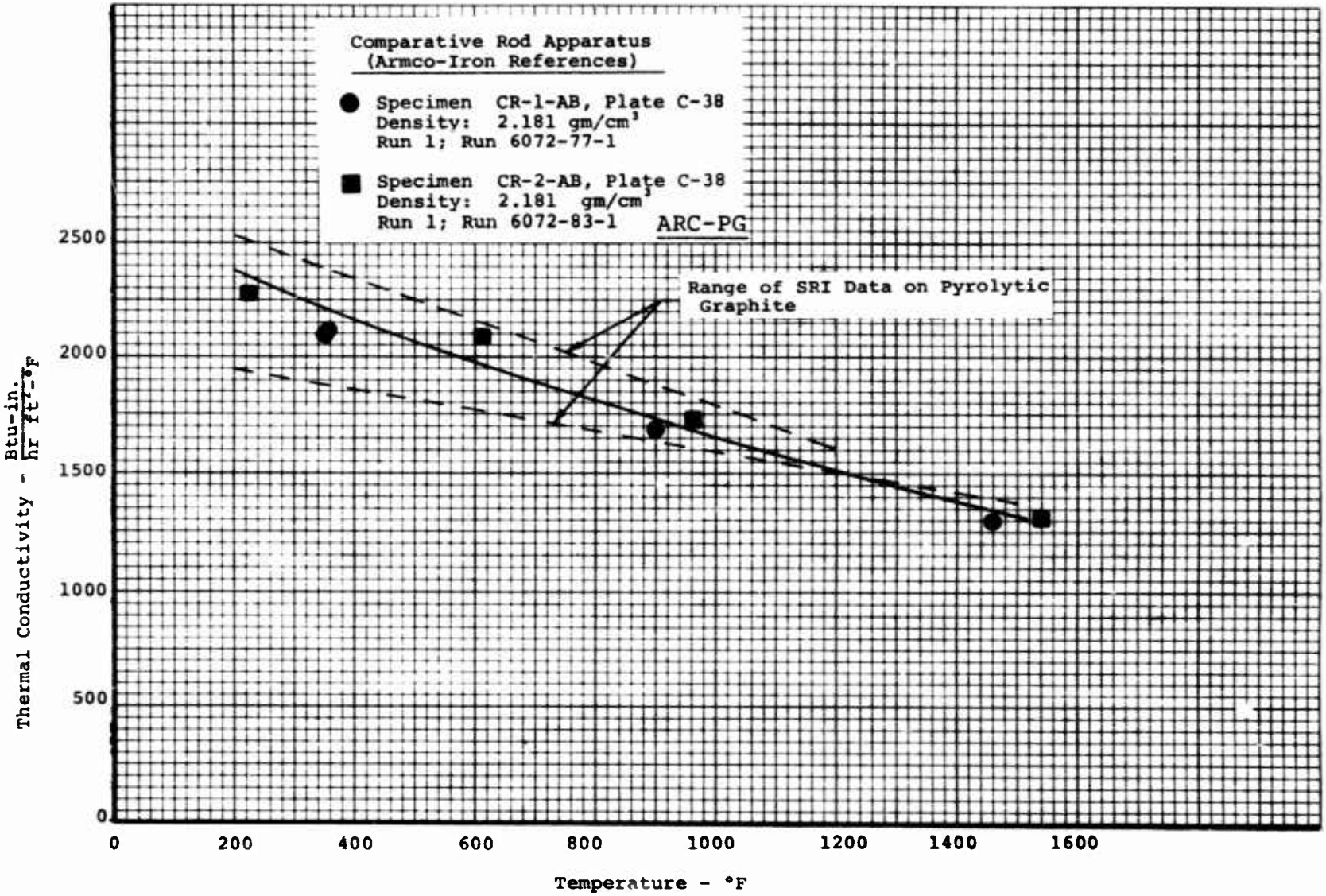

Figure 15. Thermal Conductivity of Pyrolytic Graphite in the 'A-B' Direction

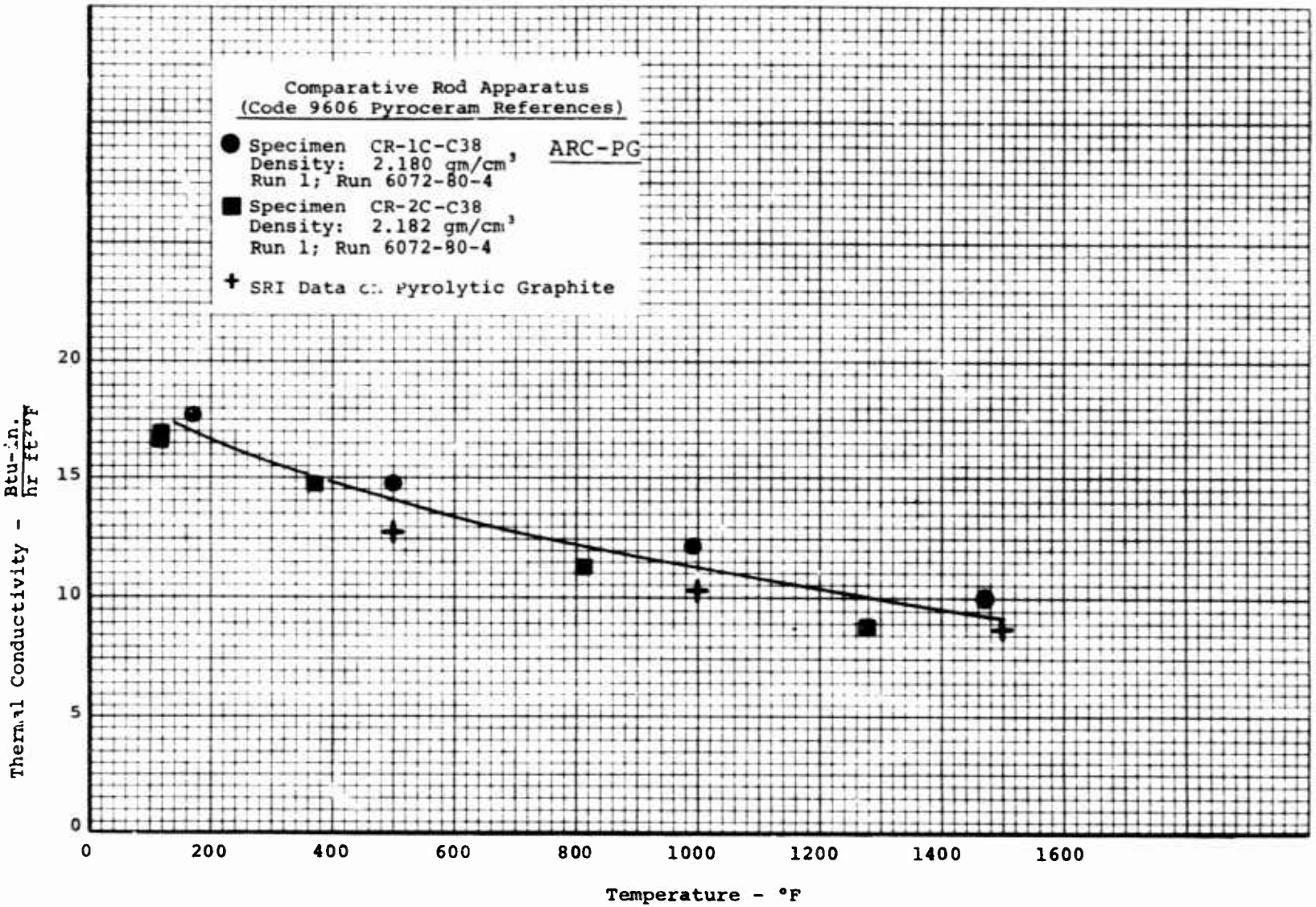

Figure 16. Thermal Conductivity of Pyrolytic Graphite in the 'C' Direction

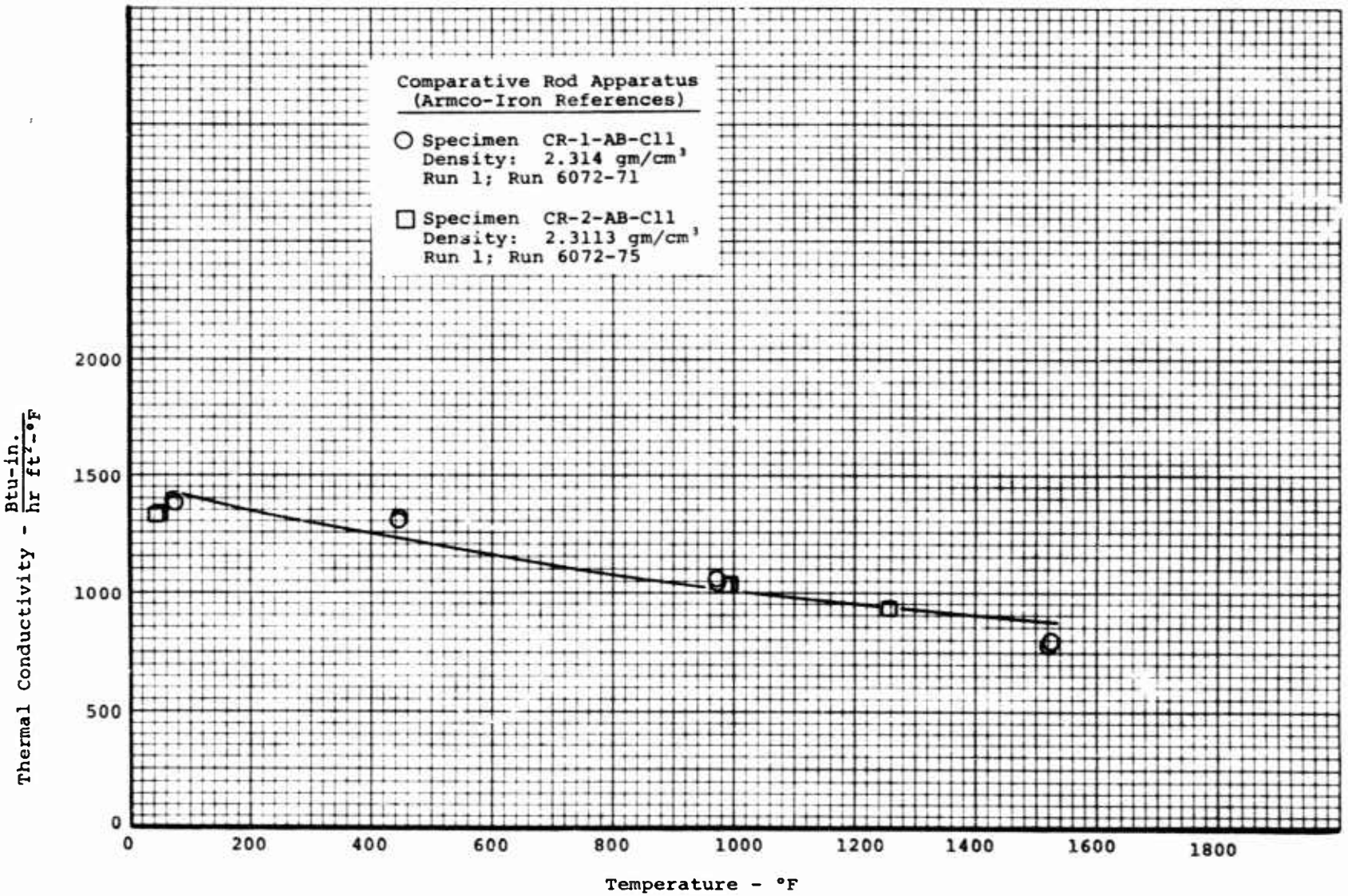

Figure 17. Thermal Conductivity of Codeposited Pyrolytic Graphite with 20 Percent SiC in the 'A-B' Direction

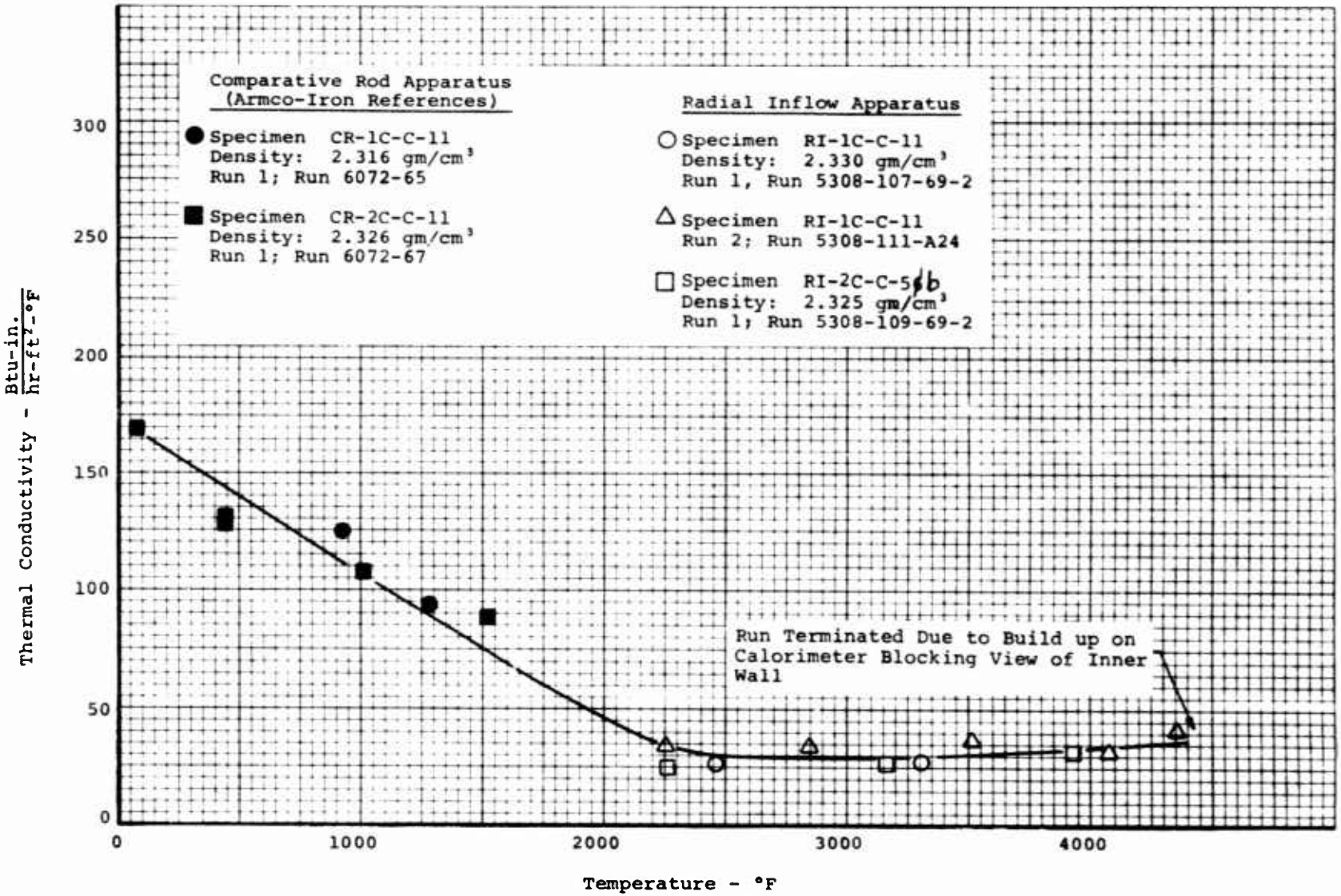

Figure 18. Thermal Conductivity of Codeposited Pyrolytic Graphite with 20 Percent SiC in the 'C' Direction

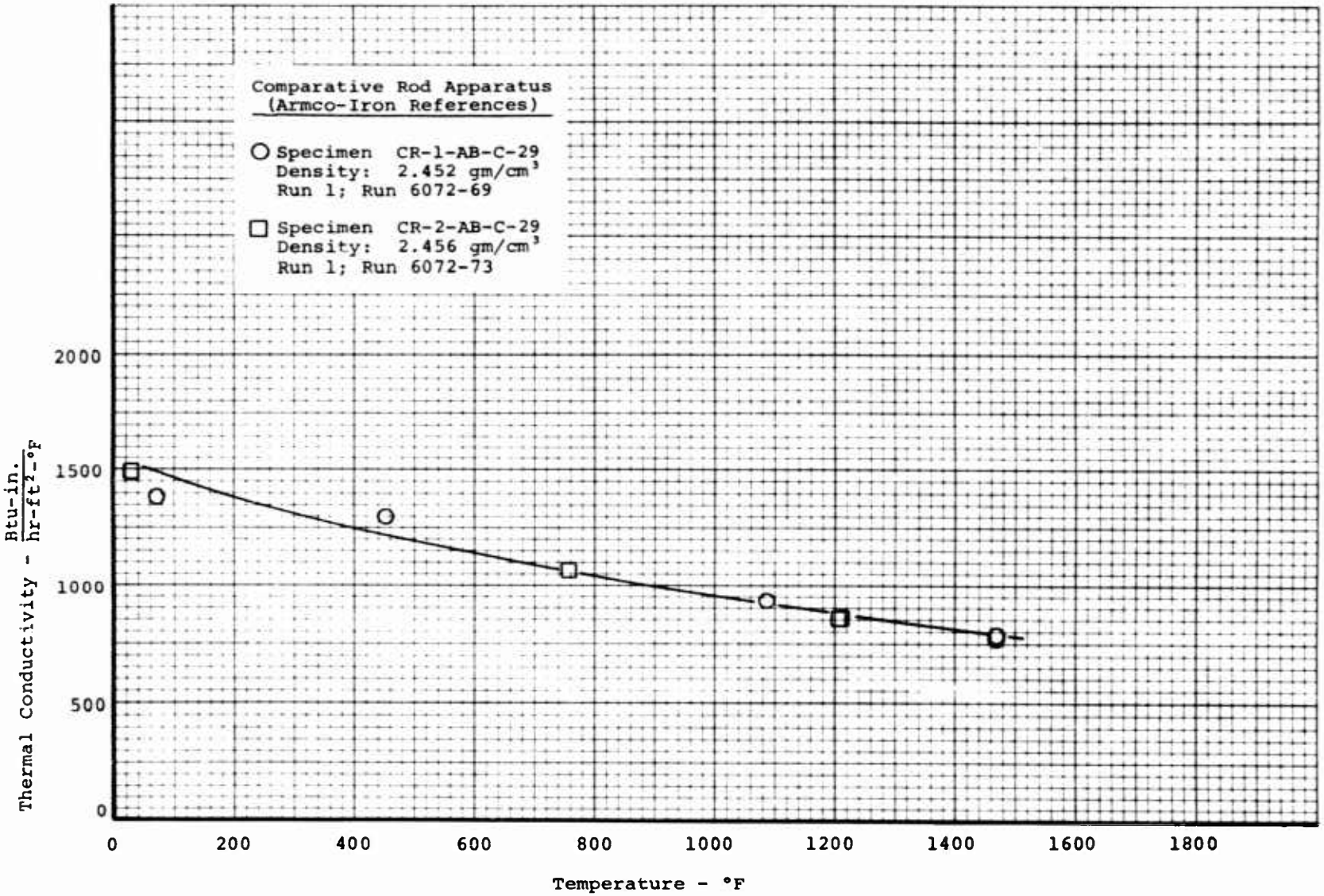

Figure 19. Thermal Conductivity of Codeposited Pyrolytic Graphite with 37 Percent SiC in the 'A-B' Direction

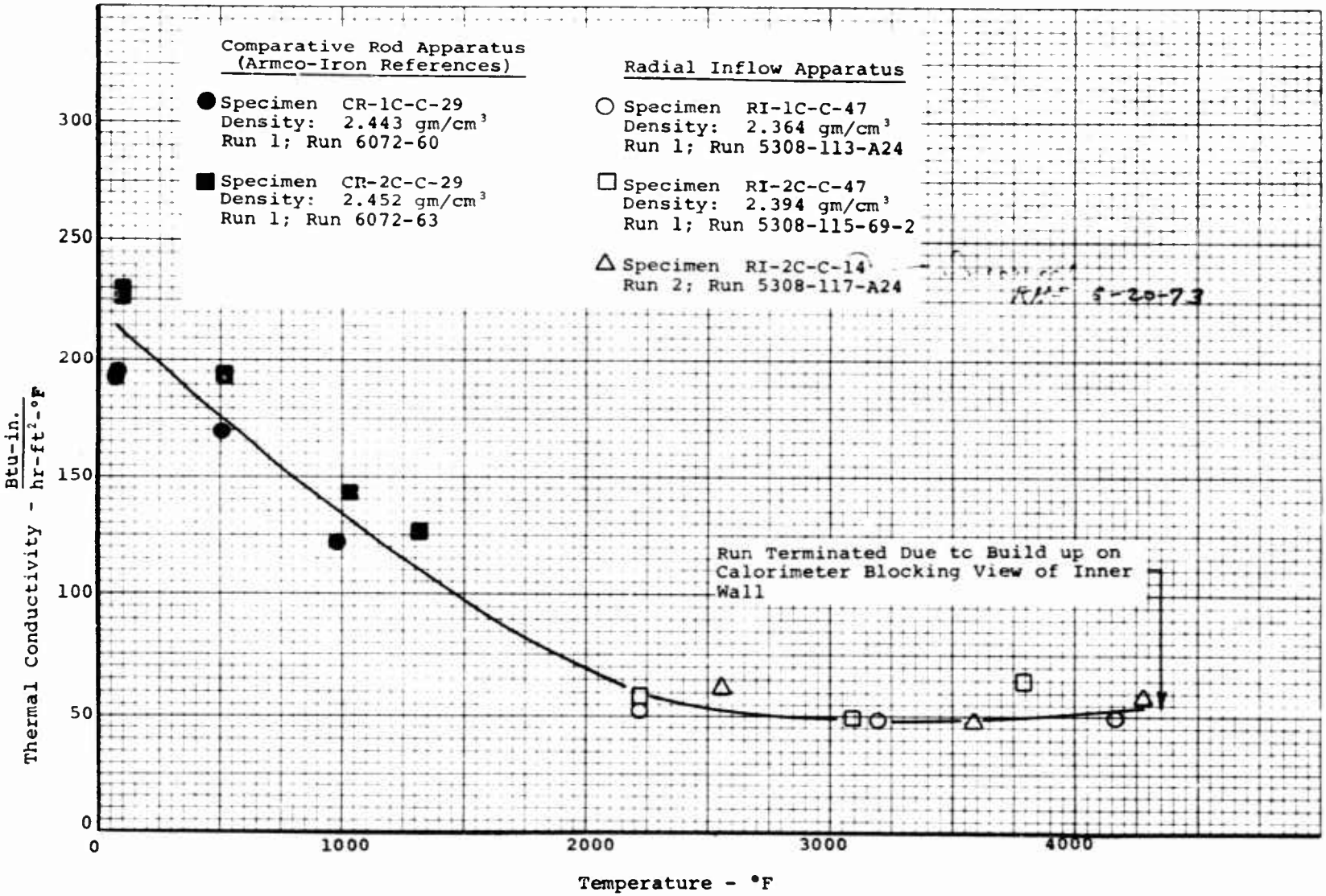

Figure 20. Thermal Conductivity of Codeposited Pyrolytic Graphite Sleeve with 37 Percent SiC in the 'C' Direction

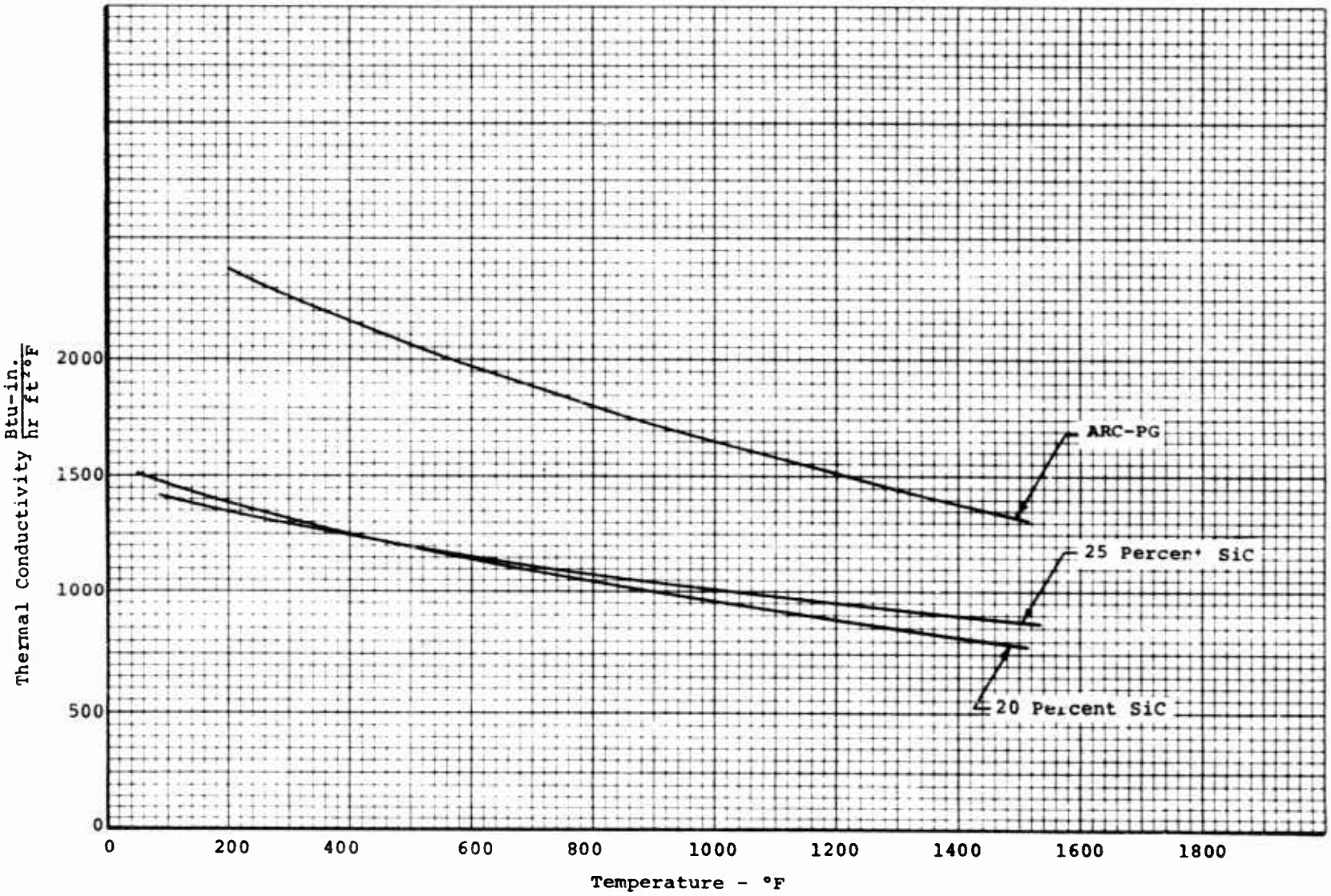

Figure 21. A Composite Plot of Thermal Conductivity in the 'A-B' Direction

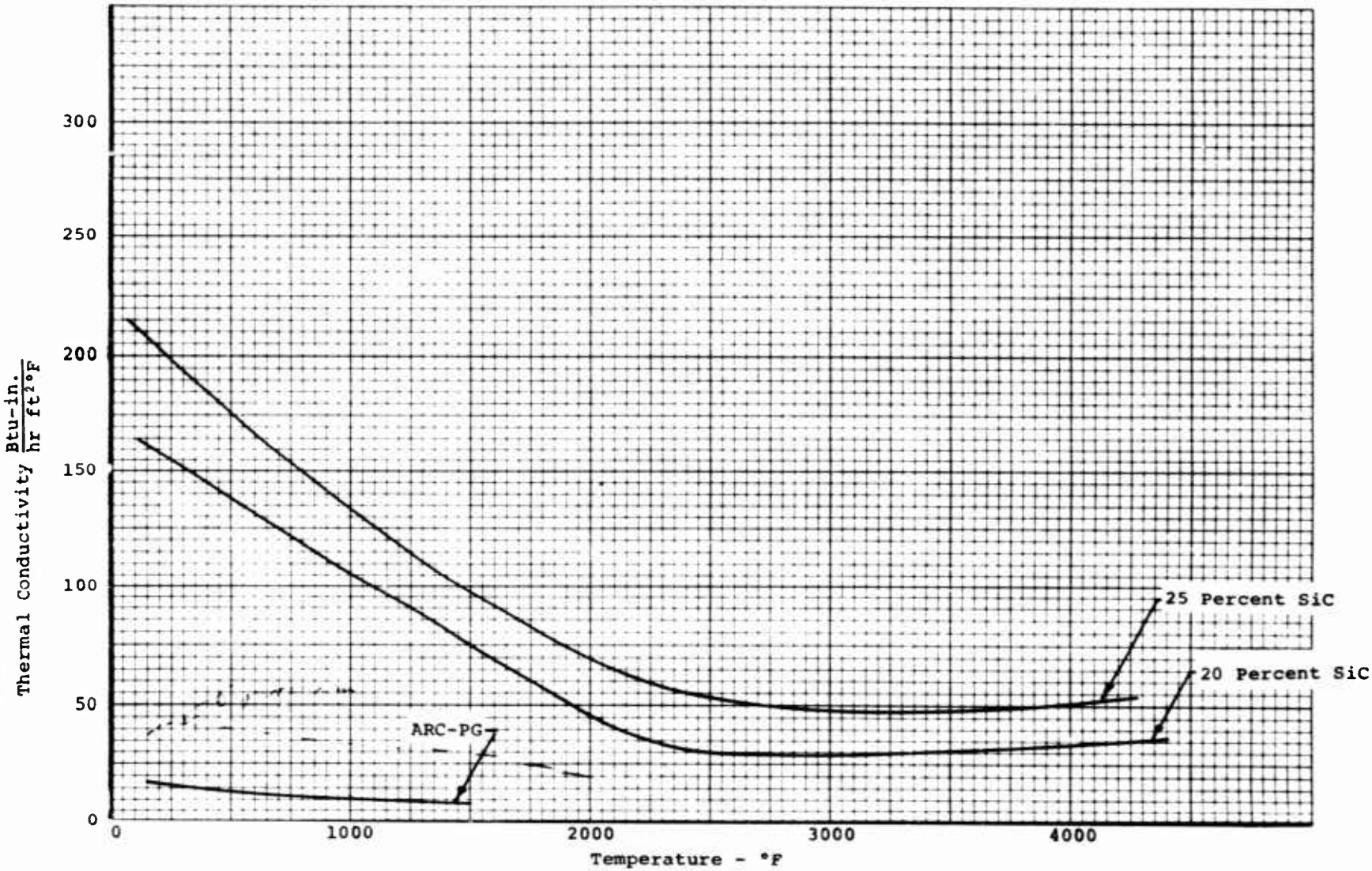

Figure 22. A Composite Plot of Thermal Conductivity in the 'C' Direction

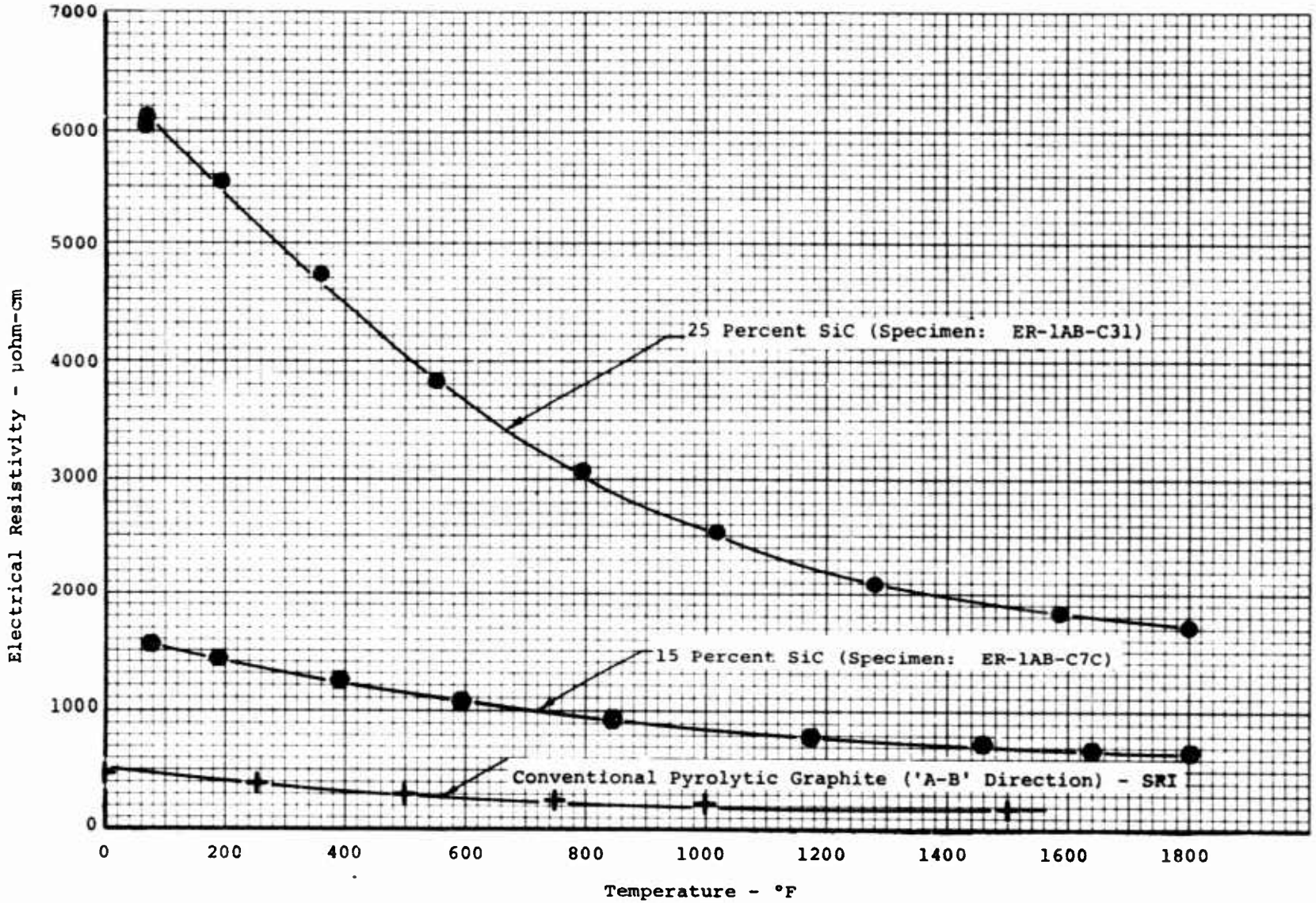

Figure 23. Electrical Resistivity of Codeposited Pyrolytic Graphite with 25 Percent and 15 Percent SiC in the 'A-B' Direction

Table 1

Test Matrix for ARC Pyrolytic Graphite and Codeposited SiC/PG with Various Weight Percentages of SiC

Test	Material	Direction	Temperature °F
Thermal Expansion	ARC PG	'a-b' and 'c'	70 to 5000
	SiC/PG with 8% SiC	'a-b' and 'c'	70 to 5000
	SiC/PG with 15% SiC	'a-b' and 'c'	70 to 5000
	SiC/PG with 20% SiC	'a-b' and 'c'	70 to 5000
	SiC/PG with 25% SiC	'a-b' and 'c'	70 to 5000
Thermal Conductivity	ARC PG	'a-b' and 'c'	70 to 1700
	SiC/PG with 20% SiC	'ab'	70 to 1700
		'c'	70 to 5000
	SiC/PG with 25% SiC	'ab'	70 to 1700
		'c'	70 to 5000
Electrical Resistivity	ARC PG	'ab'	70 to 1800
	SiC/PG with 15% SiC	'ab'	70 to 1800
	SiC/PG with 25% SiC	'ab'	70 to 1800

Table 2

Thermal Expansion of Pyrolytic Graphite in the 'A-B' Direction
Measured in Quartz Dilatometer

Specimen	Time	Specimen Temperature - °F: Top	Middle	Bottom	Average	Observed Total Elongation 10^{-3} in.	Observed Unit Elongation 10^{-3} in./in.	Unit Elongation Correction for Dilatometer Motion 10^{-3} in./in.	Corrected Specimen Unit Elongation 10^{-3} in./in.
Specimen: TE-1AB-C2		Initial Length: 3.0010 in.				Initial Weight: 2.7344 gm			
		Final Length: 3.0022 in.				Final Weight: 2.7328 gm			
Run: 1									
Run: 6047-51-20	11:00	73	73	73	73	0.00	0.00	0.00	0.00
Density: 2.195 gm/cm³	12:35	500	500	500	500	0.40	0.13	0.10	0.23
	1:15	1000	1000	1000	1000	1.63	0.54	0.27	0.81
	2:00	1485	1500	1504	1496	3.12	1.04	0.44	1.48
	2:30	1701	1700	1702	1701	3.79	1.26	0.50	1.76
	7:20	74	74	74	74	0.30	0.10	0.00	0.10
Specimen: TE-2AB-C2		Initial Length: 3.0123 in.				Initial Weight: 2.7836 gm			
		Final Length: 3.0125 in.				Final Weight: 2.7865 gm			
Run: 1									
Run: 6047-55-14M-Q	11:20	72	72	72	72	0.00	0.00	0.00	0.00
Density: 2.195 gm/cm³	12:50	500	500	500	500	0.32	0.11	0.12	0.23
	1:25	1000	1000	1000	1000	1.57	0.52	0.22	0.74
	1:55	1517	1521	1525	1521	3.45	1.15	0.28	1.43
	2:20	1706	1710	1717	1711	4.22	1.40	0.31	1.71
	7:40	72	72	72	72	-0.01	0.00	0.00	0.00

Table 3

Thermal Expansion of Pyrolytic Graphite in the 'A-B' Direction
Measured in Graphite Dilatometer

Specimen and Run No.	Temp. °F	Time	Observed Total Elongation (10^{-3} in.)	Observed Unit Elongation (10^{-3} in./in.)	Unit Correction for Dilatometer Motion (10^{-3} in./in.)	Corrected Specimen Unit Elongation (10^{-3} in./in.)
Specimen: TE-1AB-C2	77	8:55	0.00	0.00	0.00	0.00
Run: 1	438	9:30	- 0.19	- 0.06	0.25	0.19
Run: 6047-67-122A-E	1000	10:00	- 0.45	- 0.15	0.86	0.71
Initial length:	1614	10:35	- 0.55	- 0.18	1.80	1.62
3.0022 in.	2261	11:05	- 0.45	- 0.15	3.00	2.85
Final length:	2821	11:30	- 0.21	- 0.07	4.13	4.06
3.0452 in.	3523	12:20	0.67	0.22	5.69	5.91
Initial Weight:	4009	12:50	2.50	0.83	6.80	7.63
2.7328 gm	4416	1:25	8.50	2.83	7.78	10.61
Final Weight:	4993	2:00	39.28	13.08	9.20	22.28
2.7321 gm	77	7:15	44.08	14.68	0.00	14.68
Density: 2.195 gm/cm³						
Specimen: TE-2AB-C2	78	8:10	0.00	0.00	0.00	0.00
Run: 1	475	8:40	- 0.15	- 0.05	0.28	0.23
Run: 6047-69-122A-E	1033	9:15	- 0.37	- 0.12	0.98	0.86
Initial length:	1620	10:00	- 0.41	- 0.14	1.81	1.67
3.0125 in.	2415	10:35	- 0.25	- 0.08	3.30	3.22
Final length:	3063	11:05	- 0.04	- 0.01	4.68	4.67
3.0586 in.	3473	11:30	- 0.26	0.09	5.57	5.56
Initial weight:	3969	12:25	3.10	1.03	6.70	7.73
2.7865 gm	4374	1:00	7.87	2.61	7.66	10.27
Final weight:	5034	1:30	40.44	13.42	9.32	22.74
2.7852 gm	78	7:30	45.45	15.08	0.00	15.08
Density: 2.195 gm/cm³						

Table 4

Thermal Expansion of Pyrolytic Graphite in the 'A-B' Direction (Second Exposure)
Measured in Graphite Dilatometer

Specimen and Run No.	Temp. °F	Time	Observed Total Elongation (10^{-3} in.)	Observed Unit Elongation (10^{-3}in./in.)	Unit Correction for Dilatometer Motion (10^{-3} in./in.)	Corrected Specimen Unit Elongation (10^{-3} in./in.)
Specimen: TE-2AB-C2	79	8:00	0.00	0.00	0.00	0.00
Run: 2	483	8:45	- 1.22	-0.40	0.65	0.25
Run: 6047-83-134-K4	1019	9:20	- 2.70	-0.88	1.68	0.80
Initial length:	1696	9:50	- 4.29	-1.40	3.08	1.68
3.0586 in.	2392	10:20	- 5.60	-1.83	4.67	2.84
Final length:	2997	10:55	- 6.86	-2.24	6.16	3.92
3.0624 in.	3422	11:25	- 7.64	-2.50	7.30	4.80
Initial weight:	3999	12:20	- 9.05	-2.96	9.00	6.04
2.7852 gm	4445	1:00	-10.53	-3.44	10.30	6.86
Final weight:	4973	1:30	- 9.63	-3.15	12.05	8.90
2.7852 gm	79	7:25	3.37	1.10	0.00	1.10
Density: 2.195 gm/cm^3						

Table 5

Thermal Expansion of Pyrolytic Graphite in the 'C' Direction
Measured in Graphite Dilatometer

Specimen and Run No.	Temp. °F	Time	Observed Total Elongation (10^{-3} in.)	Observed Unit Elongation (10^{-3} in./in.)	Unit Correction for Dilatometer Motion (10^{-3} in./in.)	Corrected Specimen Unit Elongation (10^{-3} in./in.)
Specimen: TE-1C-C-14	80	8:15	0.00	0.00	0.00	0.00
Run: 1	563	9:30	2.44	2.44	1.30	3.74
Run: 6047-58-134-K4	1025	10:00	6.92	6.91	2.63	9.54
Initial length:	1620	10:30	12.70	12.67	4.50	17.17
1.0020 in.	2324	11:00	20.29	20.25	6.86	27.11
Final length:	2916	11:30	26.62	26.57	9.05	35.62
0.9772 in.	3523	12:00	32.85	32.78	11.51	44.29
Initial weight:	4090	12:40	38.60	38.52	13.90	52.42
2.2181 gm	4435	1:15	40.86	40.78	15.33	56.11
Final weight:	4983	1:55	19.51	19.47	17.85	37.32
2.2178 gm	79	7:30	-26.66	-26.61	0.00	-26.61
Density: 2.200 gm/cm³						
Specimen: TE-2C-C-14	79	8:25	0.00	0.00	0.00	0.00
Run: 1	569	9:00	2.11	2.11	1.32	3.43
Run: 6047-60-134-K4	995	9:30	6.05	6.04	2.55	8.59
Initial length:	1665	10:15	12.55	12.53	4.67	17.20
1.0014 in.	2432	10:50	20.60	20.57	7.25	27.82
Final length:	2982	11:25	26.58	26.54	9.32	35.86
0.9728 in.	3564	12:15	32.15	32.10	11.70	43.80
Initial weight:	4055	12:45	36.99	36.94	13.78	50.72
2.2262 gm	4465	1:15	39.29	39.23	15.67	54.90
Final weight:	5014	1:45	15.55	15.53	18.00	33.53
2.2260 gm	79	7:25	-30.91	-30.87	0.00	-30.87
Density: 2.200 gm/cm³						

Table 6

Thermal Expansion of Codeposited Pyrolytic Graphite Plate
with 8 Percent SiC in the 'A-B' Direction (Measured in Quartz Dilatometer)

Specimen	Time	Specimen Temperature - °F				Observed Total Elongation 10^{-3} in.	Observed Unit Elongation 10^{-3} in./in.	Unit Elongation Correction for Dilatometer Motion 10^{-3} in./in.	Corrected Specimen Unit Elongation 10^{-3} in./in.
		Top	Middle	Bottom	Average				
Specimen: TE-1AB C-19-A		Initial length: 3.003 in. Final length: 3.003 in.				Initial weight: 3.2992 gm Final weight: 3.2982 gm			
Run: 1									
Run: 6047-50-14M	11:00	73	73	73	73	0.00	0.00	0.00	0.00
Density: 2.241 gm/cm³	12:35	500	500	500	500	1.34	0.45	0.12	0.57
	1:15	1000	1000	1000	1000	3.49	1.16	0.22	1.38
	2:00	1495	1500	1503	1499	5.98	1.99	0.27	2.26
	2:30	1694	1700	1704	1699	6.97	2.32	0.30	2.62
	7:20	74	74	74	74	-0.13	-0.04	0.00	-0.04
Specimen: TE-2AB C-19-B		Initial length: 3.0000 in. Final length: 3.0000 in.				Initial weight: 3.0665 gm Final weight: 3.0660 gm			
Run: 1									
Run: 6047-63-14M-Q	11:00	70	70	70	70	0.00	0.00	0.00	0.00
Density: 2.241 gm/cm³	12:45	500	500	500	500	1.47	0.49	0.12	0.61
	1:25	1000	1000	1000	1000	3.82	1.27	0.22	1.49
	2:05	1496	1500	1506	1501	6.46	2.15	0.27	2.42
	2:25	1694	1700	1709	1701	7.53	2.51	0.30	2.81
	8:15	70	70	70	70	-0.13	-0.04	0.00	-0.04

Table 7

Thermal Expansion of Codeposited Pyrolytic Graphite Plate
with 8 Percent SiC in the 'A-B' Direction
Measured in Graphite Dilatometer

Specimen and Run No.	Temp. °F	Time	Observed Total Elongation (10^{-3} in.)	Observed Unit Elongation (10^{-3} in./in.)	Unit Correction for Dilatometer Motion (10^{-3} in./in.)	Corrected Specimen Unit Elongation (10^{-3} in./in.)
Specimen: TE-1AB-C-19-A	78	8:15	0.00	0.00	0.00	0.00
	475	8:45	0.78	0.26	0.28	0.54
Run: 1	1043	9:15	1.59	0.53	0.90	1.43
Run: 6047-71-122A-E	1533	9:45	2.25	0.75	1.67	2.42
Initial length:	2470	10:15	3.30	1.10	3.40	4.50
3.0003 in.	3048	10:45	4.08	1.36	4.61	5.97
Final length:	3574	11:20	6.38	2.13	5.80	7.93
3.0094 in.	3928	12:00	8.64	2.88	6.62	9.50
Initial weight:	4435	12:30	11.48	3.83	7.80	11.63
3.2982 gm	5044	1:00	12.56	4.19	9.32	13.51
Final weight:	78	7:55	9.70	3.23	0.00	3.23
2.9211 gm						
Density: 2.241 gm/cm³						
Specimen: TE-2AB-C-19-B	77	8:30	0.00	0.00	0.00	0.00
	475	9:00	0.78	0.26	0.28	0.54
Run: 1	998	9:35	1.54	0.51	0.85	1.36
Run: 6047-122A-E	1685	10:05	2.35	0.78	1.93	2.71
Initial length:	2498	10:35	3.29	1.10	3.45	4.55
3.0000 in.	3083	11:05	4.18	1.39	4.71	6.10
Final length:	3549	11:35	6.27	2.09	5.72	7.81
3.0095 in.	3994	12:05	9.10	3.03	6.74	9.77
Initial weight:	4526	12:35	11.66	3.87	8.05	11.92
3.0660 gm	4993	1:05	12.05	4.02	9.21	13.23
Final weight:	77	7:30	9.30	3.10	0.00	3.10
2.7183 gm						
Density: 2.241 gm/cm³						

Table 8

Thermal Expansion of Codeposited Pyrolytic Graphite Plate
with 8 Percent SiC in the 'C' Direction
Measured in Graphite Dilatometer

Specimen and Run No.	Temp. °F	Time	Observed Total Elongation (10^{-3} in.)	Observed Unit Elongation (10^{-3} in./in.)	Unit Correction for Dilatometer Motion (10^{-3} in./in.)	Corrected Specimen Unit Elongation (10^{-3} in./in.)
Specimen: TE-1C-C-19-A	30	8:00	0.00	0.00	0.00	0.00
	523	8:40	-0.26	-0.26	1.18	0.92
Run: 1	983	9:20	-0.66	-0.66	2.50	1.84
Run: 6047-62-134-K4	1638	10:05	-0.64	-0.64	4.57	3.93
Initial length:	2442	10:40	-0.23	-0.23	7.30	7.07
1.0050 in.	2992	11:15	0.12	0.12	9.34	9.46
Final length:	3559	12:15	1.04	1.03	11.65	12.68
0.9961 in.	4014	12:50	1.52	1.51	13.60	15.11
Initial weight:	4496	1:30	0.21	0.21	15.80	16.01
2.2771 gm	5014	2:05	-2.47	-2.46	18.00	15.54
Final weight:	80	7:30	-8.95	-8.91	0.00	- 8.91
2.1381 gm						
Density: 2.241 gm/cm³						
Specimen: TE-2C-C-19-B	80	8:00	0.00	0.00	0.00	0.00
	539	8:35	- 0.49	- 0.49	1.24	0.75
Run: 1	1002	9:05	- 0.58	- 0.58	2.56	1.98
Run: 6047-64-134-K4	1617	10:10	- 0.50	- 0.50	4.50	4.00
Initial length:	2407	10:40	- 0.19	- 0.19	7.19	7.00
1.0000 in.	2982	11:15	0.03	0.03	9.30	9.33
Final length:	3564	12:15	1.03	1.03	11.68	12.71
0.9899 in.	4019	12:45	1.81	1.81	13.60	15.41
Initial weight:	4496	1:15	0.53	0.53	15.80	16.33
2.2247 gm	5024	1:50	- 3.05	- 3.05	18.01	14.96
Final weight:	80	7:30	-10.80	-10.80	0.00	-10.80
2.0788 gm						
Density: 2.241 gm/cm³						

Table 9

Thermal Expansion of Codeposited Pyrolytic Graphite Plate
with 15 Percent SiC in the 'A-B' Direction Measured in Quartz Dilatometer

Specimen	Time	Specimen Temperature - °F				Observed Total Elongation 10^{-3} in.	Observed Unit Elongation 10^{-3} in./in.	Unit Elongation Correction for Dilatometer Motion 10^{-3} in./in.	Corrected Specimen Unit Elongation 10^{-3} in./in.
		Top	Middle	Bottom	Average				
Specimen: TE-1AB C-7-D		Initial length: 3.0003 in.				Initial weight: 3.7492 gm			
		Final length: 3.0006 in.				Final weight: 3.7485 gm			
Run: 1									
Run: 6047-53-20	11:00	72	72	72	72	0.00	0.00	0.00	0.00
Density: 2.275 gm/cm³	12:40	500	500	500	500	1.55	0.52	0.10	0.62
	1:20	1000	1000	1000	1000	3.85	1.28	0.27	1.55
	2:05	1498	1500	1503	1500	6.55	2.18	0.44	2.62
	2:30	1696	1700	1704	1700	7.75	2.58	0.50	3.08
	7:30	76	76	76	76	-0.16	-0.05	0.00	-0.05
Specimen: TE-2AB C-7-D		Initial length: 3.0000 in.				Initial weight: 3.1616 gm			
		Final length: 3.0000 in.				Final weight: 3.1611 gm			
Run: 1									
Run: 6047-61-14M-Q	10:30	71	71	71	71	0.00	0.00	0.00	0.00
Density: 2.275 gm/cm³	12:25	500	500	500	500	1.62	0.54	0.12	0.66
	1:05	1000	1000	1000	1000	4.00	1.33	0.22	1.55
	1:45	1566	1571	1575	1571	7.27	2.42	0.28	2.70
	2:10	1694	1700	1705	1700	7.98	2.66	0.30	2.96
	8:15	71	71	71	71	-0.05	-0.02	0.00	-0.02

Table 10

Thermal Expansion of Codeposited Pyrolytic Graphite Plate
with 15 Percent SiC in the 'A-B' Direction (Measured in Graphite Dilatometer)

Specimen and Run No.	Temp. °F	Time	Observed Total Elongation (10^{-3} in.)	Observed Unit Elongation (10^{-3} in./in.)	Unit Correction for Dilatometer Motion (10^{-3} in./in.)	Corrected Specimen Unit Elongation (10^{-3} in./in.)
Specimen: TE-1AB-C-7	78	8:20	0.00	0.00	0.00	0.00
D	528	9:05	0.85	0.28	0.32	0.60
Run: 1	1072	9:35	1.83	0.61	0.95	1.56
Run: 6047-75-122A-E	1658	10:05	2.84	0.95	1.90	2.85
Initial length:	2523	10:35	4.53	1.51	3.51	5.02
3.0006 in.	3018	11:15	5.70	1.91	4.55	6.45
Final length:	3543	12:10	8.21	2.74	5.70	8.44
3.0016 in.	4029	12:45	11.50	3.83	6.82	10.65
Initial weight:	4547	1:15	14.31	4.77	8.10	12.87
3.7485 gm	5054	1:50	14.90	4.96	9.40	14.36
Final weight:	78	7:30	11.00	3.67	0.00	3.67
3.0337 gm						
Density: 2.275 gm/cm³						
Specimen: TE-2AB-C-	78	8:20	0.00	0.00	0.00	0.00
7-D	481	9:00	0.86	0.29	0.29	0.58
Run: 1	1029	9:40	1.91	0.64	0.90	1.54
Run: 6047-77-122-A-E	1759	10:15	3.37	1.12	2.06	3.18
Initial length:	2530	10:55	4.85	1.62	3.53	5.15
3.0000 in.	3119	11:30	6.25	2.08	4.79	6.87
Final length:	3447	12:10	7.90	2.63	5.49	8.12
3.0105 in.	4080	12:45	12.02	4.01	6.98	10.99
Initial weight:	4367	1:15	14.22	4.74	8.14	12.88
3.1611 gm	5003	1:45	14.94	4.98	9.26	14.24
Final weight:	78	7:35	10.46	3.49	0.00	3.49
2.7160 gm						
Density: 2.275 gm/cm³						

Table 11

Thermal Expansion of Codeposited Pyrolytic Graphite Plate
with 15 Percent SiC in the 'C' Direction (Measured in Graphite Dilatometer)

Specimen and Run No.	Temp. °F	Time	Observed Total Elongation (10^{-3} in.)	Observed Unit Elongation (10^{-3} in./in.)	Unit Correction for Dilatometer Motion (10^{-3} in./in.)	Corrected Specimen Unit Elongation (10^{-3} in./in.)
Specimen: TE-1C-C-7A	78	8:45	0.00	0.00	0.00	0.00
Run: 1	535	9:15	-1.25	-1.16	1.21	0.05
Run: 6047-66-134-K4	1006	9:50	-1.49	-1.39	2.60	1.21
Initial length:	1596	10:20	-1.46	-1.36	4.41	3.05
1.0755 in.	2392	10:50	-1.30	-1.21	7.10	5.89
Final length:	3007	11:20	-1.07	-0.99	9.42	8.43
1.0702 in.	3543	12:20	-0.70	-0.65	11.57	10.92
Initial weight:	3999	12:50	-0.10	-0.09	13.50	13.41
2.4275 gm	4526	1:25	-0.65	-0.60	15.95	15.35
Final weight:	4993	2:00	-1.96	-1.82	17.90	16.08
2.2688 gm	78	7:35	-3.30	-3.07	0.00	- 3.07
Density: 2.275 gm/cm³						
Specimen: TE-2C-C-7A	78	8:10	0.00	0.00	0.00	0.00
Run: 1	554	8:40	-0.96	-0.96	1.28	0.32
Run: 6047-70-134-K-4	1057	9:10	-1.04	-1.04	2.78	1.74
Initial length:	1623	9:40	-1.07	-1.07	4.50	3.43
0.9987 in.	2455	10:10	-0.96	-0.96	7.35	6.39
Final length:	3083	10:40	-0.77	-0.77	9.71	8.94
0.9929 in.	3548	11:15	-0.32	-0.32	11.61	11.29
Initial weight:	4065	12:05	+0.08	+0.08	13.78	13.86
2.2623 gm	4537	12:30	-0.20	-0.20	15.90	15.70
Final weight:	5044	1:00	-1.84	-1.84	18.10	16.26
2.1081 gm	78	7:55	-3.46	-3.86	0.00	- 3.86
Density: 2.275 gm/cm³						

Table 12

Thermal Expansion of Codeposited Pyrolytic Graphite (Coupon Specimen) with 20 Percent SiC in the 'A-B' Direction Measured in Quartz Dilatometer

Specimen	Time	Specimen Temperature - °F				Observed Total Elongation 10^{-3} in.	Observed Unit Elongation 10^{-3} in./in.	Unit Elongation Correction for Dilatometer Motion 10^{-3} in./in.	Corrected Specimen Unit Elongation 10^{-3} in./in.
		Top	Middle	Bottom	Average				
Specimen: TE-2AB -C-17		Initial length: 3.0020 in.				Initial weight: 4.9111 gm			
Run: 1		Final length: 3.0020 in.				Final weight: 4.7215 gm			
Run: 6047-65-14M-Q	10:00	74	74	74	74	0.00	0.00	0.00	0.00
Density: 2.350 gm/cm³	10:45	598	598	598	598	2.40	0.80	0.15	0.95
	1:10	1000	1000	1000	1000	4.66	1.55	0.22	1.77
	1:50	1565	1569	1577	1570	8.19	2.73	0.28	3.01
	2:15	1694	1700	1709	1701	9.04	3.01	0.31	3.32
	7:30	74	74	74	74	-0.02	-0.01	0.00	-0.01
Specimen: TE-1AB -C-17		Initial length: 3.0024 in.				Initial weight: 4.9048 gm			
		Final length: 3.0023 in.				Final weight: 4.9037 gm			
Run: 1	11:00	72	72	72	72	0.00	0.00	0.00	0.00
Run: 6047-65-14M-Q	12:40	500	500	500	500	1.96	0.65	0.12	0.77
Density: 2.350 gm/cm³	1:20	1000	1000	1000	1000	4.90	1.63	0.22	1.85
	2:00	1496	1500	1505	1500	8.11	2.70	0.27	2.97
	2:20	1693	1700	1708	1700	9.43	3.14	0.30	3.44
	7:30	76	76	76	76	-0.36	-0.12	0.00	-0.12

Table 13

Thermal Expansion of Codeposited Pyrolytic Graphite (Coupon Specimen) with 20 Percent SiC in the 'A-B' Direction Measured in Graphite Dilatometer

Specimen and Run No.	Temp. °F	Time	Observed Total Elongation (10^{-3} in.)	Observed Unit Elongation (10^{-3} in./in.)	Unit Correction for Dilatometer Motion (10^{-3} in./in.)	Corrected Specimen Unit Elongation (10^{-3} in./in.)
Specimen: TE-1AB-C-17	78	8:35	0.00	0.00	0.00	0.00
Run: 1	482	9:10	1.17	0.39	0.29	0.68
Run: 6047-79-122A-E	1035	9:40	2.79	0.93	0.90	1.83
Initial length:	1781	10:10	4.74	1.58	2.10	3.68
3.0023 in.	2536	10:40	6.53	2.17	3.55	5.72
Final length:	3078	11:15	8.06	2.68	4.65	7.33
3.0123 in.	3402	11:45	9.80	3.26	5.36	8.62
Initial weight:	3964	12:15	13.72	4.57	6.61	11.18
4.9037 gm	4567	12:45	16.85	5.61	8.15	13.76
Final weight:	5146	1:15	17.97	5.98	9.60	15.58
3.6071 gm	78	8:00	10.50	3.50	0.00	3.50
Density: 2.350 gm/cm³						
Specimen: TE-2AB-C-17	77	8:45	0.00	0.00	0.00	0.00
Run: 1	527	9:30	1.12	0.37	0.32	0.69
Run: 6047-81-122A-E	1106	10:00	2.54	0.85	1.00	1.85
Initial length:	1760	10:30	3.95	1.32	2.06	3.38
3.0015 in.	2575	11:00	5.56	1.85	3.62	5.47
Final length:	3068	11:30	6.72	2.24	4.68	6.92
3.0215 in.	3543	12:00	9.17	3.05	5.70	8.75
Initial weight:	4095	12:30	13.17	4.39	6.98	11.37
4.7215 gm	4557	1:00	15.52	5.17	8.13	13.30
Final weight:	77	8:00	19.97	6.65		6.65
3.3812 gm						
Density: 2.350 gm/cm³						
	Heater tube burned out while going for 5000°F data-specimen maximum exposure temperature not known.					

Table 14

Thermal Expansion of Codeposited Pyrolytic Graphite Plate
with 20 Percent SiC in the 'C' Direction (Measured in Graphite Dilatometer)

Specimen and Run No.	Temp. °F	Time	Observed Total Elongation (10^{-3} in.)	Observed Unit Elongation (10^{-3} in./in.)	Unit Correction for Dilatometer Motion (10^{-3} in./in.)	Corrected Specimen Unit Elongation (10^{-3} in./in.)
Specimen: TE-1C-C-25	68	8:40	0.00	0.00	0.00	0.00
Run: 1	975	9:40	-1.52	-1.51	2.48	0.97
Run: 6047-72-134-K4	1628	10:10	-1.41	-1.40	4.55	3.15
Initial length:	2444	10:40	-1.24	-1.23	7.30	6.07
1.0057 in.	3005	11:10	-1.20	-1.19	9.40	8.21
Final length:	3442	11:40	-1.13	-1.12	11.16	10.04
1.0045 in.	3969	12:10	-0.99	-0.98	13.37	12.39
Initial weight:	4445	12:40	-1.16	-1.15	15.52	14.37
2.4371 gm	4993	1:10	-2.42	-2.41	17.90	15.49
Final weight:	68	7:30	-2.37	-2.36	0.00	- 2.36
2.1854 gm						
Density: 2.350 gm/cm³						
Specimen: TE-2C-C-25	66	8:25	0.00	0.00	0.00	0.00
Run: 1	517	9:10	-0.69	-0.69	1.18	0.49
Run: 6047-74-134-K4	991	9:40	-0.90	-0.90	2.52	1.62
Initial length:	1633	10:10	-1.24	-1.24	4.57	3.33
1.0036 in.	2445	10:40	-1.19	-1.19	7.28	6.09
Final length:	2992	11:15	-1.23	-1.23	9.34	8.11
1.0016 in.	3508	12:10	-1.21	-1.21	11.48	10.27
Initial weight:	3958	12:45	-1.20	-1.20	13.38	12.18
2.4250 gm	4415	1:15	-1.37	-1.37	15.41	14.04
Final weight:	4983	1:50	-3.39	-3.38	17.86	14.48
2.1775 gm	56	7:30	-3.69	-3.68	0.00	- 3.68
Density: 2.350 gm/cm³						

Table 15

Thermal Expansion of Codeposited Pyrolytic Graphite (Coupon Specimen) with 25 Percent SiC in the 'A-B' Direction (Measured in Quartz Dilatometer)

Specimen	Time	Specimen Temperature - °F				Observed Total Elongation 10^{-3} in.	Observed Unit Elongation 10^{-3} in./in.	Unit Elongation Correction for Dilatometer Motion 10^{-3} in./in.	Corrected Specimen Unit Elongation 10^{-3} in./in.
		Top	Middle	Bottom	Average				
Specimen: TE-2AB-C-13		Initial length: 3.0230 in.				Initial weight: 5.0520 gm			
Run: 1		Final length: 3.0221 in.				Final weight: 5.0510 gm			
Run: 6047-59-14M-Q	9:45	72	72	72	72	0.00	0.00	0.00	0.00
	11:15	500	500	500	500	1.90	0.63	0.12	0.75
Density: 2.525 gm/cm³	12:30	1022	1022	1025	1023	5.08	1.69	0.23	1.92
	1:25	1496	1500	1505	1500	8.39	2.79	0.27	3.06
	1:50	1687	1694	1701	1694	9.83	3.27	0.30	3.57
	8:30	72	72	72	72	-0.22	-0.07	0.00	-0.07
Specimen: TE-1AB-C-13		Initial length: 3.0230 in.				Initial weight: 5.0235 gm			
		Final length: 3.0230 in.				Final weight: 5.0229 gm			
Run: 1	8:45	75	75	75	75	0.00	0.00	0.00	0.00
Run: 6047-57-14M-Q	9:20	500	500	500	500	2.08	0.69	0.12	0.81
	10:00	1037	1039	1039	1038	5.36	1.77	0.23	2.00
Density: 2.525 gm/cm³	10:30	1496	1500	1504	1500	8.62	2.85	0.27	3.12
	11:00	1630	1700	1705	1699	9.92	3.28	0.30	3.58
	8:20	75	75	75	75	-0.25	-0.08	0.00	-0.08

Table 16

Thermal Expansion of Codeposited Pyrolytic Graphite (Coupon Specimen) with 25 Percent SiC in the 'A-B' Direction (Measured in Graphite Dilatometer)

Specimen and Run No.	Temp. °F	Time	Observed Total Elongation (10^{-3} in.)	Observed Unit Elongation (10^{-3} in./in.)	Unit Correction for Dilatometer Motion (10^{-3} in./in.)	Corrected Specimen Unit Elongation (10^{-3} in./in.)
Specimen: TE-1AB-C-13	73	8:50	0.00	0.00	0.00	0.00
Run: 1	499	9:30	0.62	0.21	0.67	0.88
Run: 6047-80-134-K4	1000	10:00	1.28	0.42	1.63	2.05
Initial length:	1707	10:30	2.23	0.74	3.13	3.87
3.0230 in.	2500	11:00	3.31	1.09	4.94	6.03
Final length:	2962	11:30	3.91	1.29	6.10	7.39
3.0267 in.	3412	12:00	5.23	1.73	7.30	9.03
Initial weight:	3959	12:30	7.95	2.63	8.88	11.51
5.0229 gm	4395	1:00	9.79	3.24	10.18	13.42
Final weight:	5034	1:30	9.85	3.26	12.24	15.50
3.9385 gm	73	7:30	5.73	1.89	0.00	1.89
Density: 2.525 gm/cm³						
Specimen: TE-2AB-C-13	78	8:30	0.00	0.00	0.00	0.00
Run: 1	527	9:00	1.32	0.44	0.35	0.79
Run: 6047-82-122A-E	984	9:30	2.59	0.86	0.83	1.69
Initial length:	1792	10:00	5.01	1.66	2.10	3.76
3.0221 in.	2420	10:30	6.91	2.29	3.30	5.59
Final length:	2910	11:00	8.32	2.75	4.32	7.07
3.0276 in.	3371	11:30	10.33	3.42	5.32	8.74
Initial weight:	3888	12:20	13.59	4.50	6.49	10.99
5.0510 gm	4369	12:55	16.21	5.36	7.67	13.03
Final weight:	5004	1:30	18.12	5.99	9.27	15.26
3.4192 gm	78	7:30	5.92	1.96	0.00	1.96
Density: 2.525 gm/cm³						

Table 17

Thermal Expansion of Codeposited Pyrolytic Graphite (Coupon Specimen) with 25 Percent SiC in the 'C' Direction (Measured in Graphite Dilatometer)

Specimen and Run No.	Temp. °F	Time	Observed Total Elongation (10^{-3} in.)	Observed Unit Elongation (10^{-3} in./in.)	Unit Correction for Dilatometer Motion (10^{-3} in./in.)	Corrected Specimen Unit Elongation (10^{-3} in./in.)
Specimen: TE-1C-C-15	74	8:20	0.00	0.00	0.00	0.00
Run: 1	517	9:00	-0.70	-0.70	1.19	0.49
Run: 6047-76-134-K4	1015	9:40	-1.05	-1.05	2.60	1.55
Initial length:	1678	10:15	-1.13	-1.13	4.70	3.57
1.0000 in.	2528	10:55	-1.20	-1.20	7.55	6.35
Final length:	3002	11:30	-1.12	-1.12	9.38	8.26
0.9979 in.	3508	12:10	-1.20	-1.20	11.48	10.28
Initial weight:	3963	12:45	-1.08	-1.08	13.35	12.27
2.4221 gm	4415	1:15	-1.41	-1.41	15.42	14.01
Final weight:	4983	1:45	-3.70	-3.70	17.90	14.20
2.1739 gm	74	7:35	-4.40	-4.40	0.00	- 4.40
Density: 2.35 gm/cm³						
Specimen: TE-2C-C-15	78	8:35	0.00	0.00	0.00	0.00
Run: 1	491	9:10	-0.46	-0.46	1.10	0.64
Run: 6047-78-134-K4	975	9:40	-0.64	-0.64	2.49	1.85
Initial length:	1685	10:10	-0.76	-0.76	4.71	3.95
1.0000 in.	2480	10:40	-0.79	-0.79	7.43	6.64
Final length:	3008	11:15	-0.82	-0.82	9.43	8.61
	3463	11:45	-0.76	-0.76	11.24	10.48
Initial weight:	3979	12:15	-0.61	-0.61	13.45	12.84
2.4320 gm	4476	1:15	-1.41	-1.41	15.75	14.34
Final weight:	5014	8:00	-3.26	-3.26	18.00	14.74
2.2511 gm	78		-3.66	-3.66	0.00	- 3.66
Density: 2.35+ gm/cm³						
	Final length of specimen not obtained due to SiC deposites causing specimen to stick to bottom of dilatometer					

Table 18

Thermal Conductivity of Pyrolytic Graphite in the 'A-B' Direction
Measured in Comparative Rod Apparatus with Armco-Iron References

Specimen and Time	Mean Temperature of Specimen °F	Thermal Conductivit of Specimen K_s Btu-in./hr ft²°F	ΔT through Specimen °F	Mean Tempera-ture of Lower Reference °F	Thermal Conductivity of Lower Reference K_1 Btu-in./hr ft²°F	ΔT through Lower Reference ΔT_1 °F	Mean Tempera-ture of Upper Reference °F	Thermal Conductivity of Upper Reference K_2 Btu-in./hr ft²°F	ΔT through Upper Reference ΔT_2 °F
Specimen: CR-1-AB-C-38	$l_1 = l_2 = 0.750$ in.		Initial Thickness:	1.4998 in.		Initial Weight:	8.5005 gm		
Run: 1	$l_s^1 = 1.2500$ in.		Final Thickness:	1.5000 in.		Final Weight:	8.4633 gm		
Density: 2.181 gm/cm³									
Run: 6072-77-1									
11:45	364	2103	18.80	302	440	53.13	435	406	59.25
1:20	351	2078	18.50	297	442	50.95	421	409	57.75
2:55	899	1675	40.78	766	331	125.9	1055	275	146.6
3:30	899	1667	41.00	766	331	125.6	1055	275	146.8
7:00	1457	1303	46.60	1299	234	157.7	1631	193	186.4
7:30	1458	1305	46.5	1300	234	157.3	1633	193	186.6
Specimen: CR-2-AB	$l_1 = l_2 = 0.750$ in.		Initial Thickness:	1.5731 in.		Initial Weight:	11.0282 gm		
Run: 1	$l_s^1 = 1.3231$ in.		Final Thickness:	1.5736 in.		Final Weight:	10.9848 gm		
Run: 6072-83-1									
Density: 2.181 gm/cm³									
9:20	225	2274	9.34	191	470	25.24	258	451	27.10
9:45	226	2283	9.28	192	470	25.30	259	451	26.90
1:40	612	2085	39.15	483	393	112.5	755	345	140.2
2:00	615	2095	39.00	486	392	113.1	758	343	140.2
10:15	961	1724	39.72	823	319	123.8	1106	268	142.4
3:00	1541	1309	44.94	1373	222	171.0	1706	196	178.8

Notes: 1. All measurements made with helium purge.
2. Thermal conductivity (k_s) of specimen calculated from following equation

$$k_s = \left[\frac{k_1 \Delta T_1}{l_1} + \frac{k_2 \Delta T_2}{l_2}\right] \frac{l_s}{2\Delta T_s}$$

where

k = thermal conductivity
ΔT = temperature drop over gage length
l = gage length

and subscripts 1, 2, and s refer to lower reference, upper reference, and specimen, respectively.

Table 19

Thermal Conductivity of Pyrolytic Graphite in the 'C' Direction
Measured in Comparative Rod Apparatus with Code 9606 Pyroceram References

Specimen and Time	Mean Temperature of Specimen °F	Thermal Conductivity of Specimen K_s Btu-in./hr ft²°F	ΔT through Specimen °F	Mean Temperature of Lower Reference °F	Thermal Conductivity of Lower Reference K_1 Btu-in./hr ft²°F	ΔT through Lower Reference ΔT_1 °F	Mean Temperature of Upper Reference °F	Thermal Conductivity of Upper Reference K_2 Btu-in./hr ft²°F	ΔT through Upper Reference ΔT_2 °F
Specimen: CR-1C-C-38 Run: 1 Run: 6072-80-4 Density: 2.180 gm/cm³	$l_1 = l_2 = 0.750$ in. $l_s = 0.1585$ in.		Initial Thickness: Final Thickness:		0.1585 in. 0.1583 in.	Initial Weight: Final Weight:	4.4575 gm 4.4493 gm		
8:15	168	17.6	9.16	142	28.0	26.62	192	26.0	30.1
10:00	168	17.9	9.05	142	26.6	28.0	192	26.0	30.4
3:20	504	14.7	26.61	435	24.05	75.7	573	23.38	80.4
1:00									
2:00	990	12.32	38.6	902	22.05	100.4	1087	21.4	106.7
5:20	1472	9.99	47.95	1276	8.72	44.0	1578	19.82	119.2
Specimen: CR-2C Plate C-38 Run: 1 Run: 6072-80-4 Density: 2.182 gm/cm³	$l_1 = l_2 = 0.750$ in. $l_s = 0.1398$ in.		Initial Thickness: Final Thickness:		0.1398 in. 0.1396 in.	Initial Weight: Final Weight:	3.9318 gm 3.9279 gm		
8:15	118	16.6	8.60	92	27.30	28.6	142	26.62	28.0
10:00	118	16.8	8.50	92	27.3	28.8	142	26.62	28.0
3:20	373	14.78	22.8	308	24.8	72.3	435	24.1	75.7
1:00	809	11.35	35.0	729	22.7	89.3	899	22.0	101.7
2:00	810	11.25	36.9	722	22.7	98.3	902	22.0	100.4
5:20	1276	8.72	44.0	1188	21.1	92.3	1374	20.4	106.3

Notes: 1. All measurements made with helium purge.
2. Thermal conductivity (k_s) of specimen calculated from following equation

$$k_s = \left[\frac{k_1 \Delta T_1}{l_1} + \frac{k_2 \Delta T_2}{l_2}\right] \frac{l_s}{2\Delta T_s}$$

where

k = thermal conductivity
ΔT = temperature drop over gage length
l = gage length

and subscripts 1, 2, and s refer to lower reference, upper reference, and specimen, respectively.

Table 20

Thermal Conductivity of Codeposited Pyrolytic Graphite with 20 Percent SiC in the 'A-B' Direction (Measured in Comparative Rod Apparatus with Armco Iron References)

Specimen and Time	Mean Temperature of Specimen °F	Thermal Conductivity of Specimen K_s Btu-in./hr ft²°F	ΔT through Specimen °F	Mean Temperature of Lower Reference °F	Thermal Conductivity of Lower Reference K_1 Btu-in./hr ft²°F	ΔT through Lower Reference ΔT_1 °F	Mean Temperature of Upper Reference °F	Thermal Conductivity of Upper Reference K_2 Btu-in./hr ft²°F	ΔT through Upper Reference ΔT_2 °F
Specimen: CR-1 AB-C-11 Run: 6072-71 Density: 2.314 gm/cm³	$l_1 = l_2 = 0.750$ in. $l_s^1 = 0.600$ in.		Initial Thickness: 0.9010 in. Final Thickness: 0.9010 in.			Initial Weight: 6.7184 gm Final Weight: 6.7110 gm			
10:30	77	1384	19.39	11	525	63.85	144	484	69.34
11:00	77	1392	19.32	10	527	63.75	145	485	69.33
3:40	444	1323	18.67	371	423	72.85	519	389	79.58
4:05	44[illegible]	1302	18.95	373	423	72.73	521	388	79.63
10:45	97[illegible]	1040	27.25	869	313	112.92	1098	268	132.60
11:15	97[illegible]	1058	27.17	870	312	11[illegible].00	1113	268	136.70
2:00	1522	799	18.60	1443	211	85.33	1611	195	98.15
2:30	1521	788	18.95	1442	212	85.46	1610	196	98.03
Specimen: CR-2A B-C-11 Run: 6072-75 Density: 2.3113 gm/cm³	$l_1 = l_2 = 0.750$ in. $l_s^1 = 0.600$ in.		Initial Thickness: 0.9008 in. Final Thickness: 0.9008 in.			Initial Weight: 6.7080 gm Final Weight: 6.6983 gm			
10:00	45	1328	26.06	-62	552	80.50	144	485	86.75
10:30	49	1332	26.25	-59	548	82.00	154	483	88.00
12:20	989	1044	43.36	805	325	176.17	1200	254	220.19
12:50	990	1043	43.43	808	325	176.40	1202	254	220.10
2:00	1258	938	45.70	1021	284	182.85	1506	200	276.00

Notes: 1. All measurements made with helium purge.
2. Thermal conductivity (k_s) of specimen calculated from following equation

$$k_s = \left[\frac{k_1 \Delta T_1}{l_1} + \frac{k_2 \Delta T_2}{l_2}\right] \frac{l_s}{2\Delta T_s}$$

where

k = thermal conductivity
ΔT = temperature drop over gage length
l = gage length

and subscripts 1, 2, and s refer to lower reference, upper reference, and specimen, respectively.

Table 21

Thermal Conductivity of Codeposited Pyrolytic Graphite with 20 Percent SiC in the 'C' Direction (Measured in Comparative Rod Apparatus with Type 316 Stainless Steel References)

Specimen and Time	Mean Temperature of Specimen °F	Thermal Conductivity of Specimen K_s Btu-in./hr ft²°F	Corrected* ΔT through Specimen °F	Mean Temperature of Lower Reference °F	Thermal Conductivity of Lower Reference K_1 Btu-in./hr ft²°F	ΔT through Lower Reference ΔT_1 °F	Mean Temperature of Upper Reference °F	Thermal Conductivity of Upper Reference K_2 Btu-in./hr ft²°F	ΔT through Upper Reference ΔT_2 °F
Specimen: CR-2C--C-11	$l_1 = l_2 = 0.750$ in.		Initial Thickness:		0.1254 in.	Initial Weight:		0.9379 gm	
Run: 1	$l_s^1 = 0.1254$ in.		Final Thickness:		0.1254 in.	Final Weight:		0.9373 gm	
Run: 6072-67									
Density: 2.326 gm/cm³									
8:50	62	169	14.49	-95	80.0	177.25	206	100.7	149.35
9:15	64	170	14.54	-95	80.0	178.90	209	101.0	150.57
2:40	443	128	17.10	325	108.0	120.60	556	120.8	109.20
3:30	444	132	16.81	324	108.0	120.68	562	123.0	109.05
12:15	1010	109	34.12	841	140.0	155.66	1179	160.8	140.22
12:45	1011	108	34.40	838	140.0	155.55	1178	160.8	140.40
2:40	1519	89	40.75	1358	170.1	126.92	1676	186.0	118.16
3:15	1521	90	40.62	1358	170.1	127.08	1678	186.0	118.25
Specimen: CR-1-C-C-II	$l_1 = l_2 = 0.750$ in.		Initial Thickness:		0.1255 in.	Initial Weight:		0.9325 gm	
	$l_s^1 = 0.1255$ in.		Final Thickness:		0.1255 in.	Final Weight:		0.9320 gm	
Run: 1									
Run: 6072-65									
Density: 2.316									
3:10	472	181	13.13	375	110	83.9	557	123	78.67
3:25	472	182	13.10	376	111	83.9	557	123	78.7
1:00	1034	125	24.54	924	145	81.8	1141	159	79.5
3:05	1519	94	48.62	1348	170	107.1	1669	186	98.1

Notes: 1. All measurements made with helium purge.
2. Thermal conductivity (k_s) of specimen calculated from following equation

$$k_s = \left[\frac{k_1 \Delta T_1}{l_1} + \frac{k_2 \Delta T_2}{l_2}\right] \frac{l_s}{2\Delta T_s}$$

where

k = thermal conductivity
ΔT = temperature drop over gage length
l = gage length

and subscripts 1, 2, and s refer to lower reference, upper reference, and specimen, respectively.

*Temperature gradient corrected for grafoil at interfaces from known in-house thermal conductivity of grafoil.

Table 22

The Thermal Conductivity of Codeposited Pyrolytic Graphite Sleeve with 20 Percent SiC in the 'C' Direction (Measured in Radial Inflow Apparatus Using an Optical Technique)

Time	Outer Surface Temperature PG-SiC °F	Inner Wall Temperature PG-SiC °F	Specimen ΔT PG-SiC °F	Heat to Calorimeter $\frac{Btu}{hr}$	Specimen Mean Temperature °F	Thermal Conductivity $\frac{Btu\text{-}in.}{hr\ ft^2\,°F}$
Specimen Sleeve: RI-1C-C-11 Run: 1 Run: 5308-107-69-2 Density: 2.330 gm/cm³			R_2 = Outside Radius 2.000 in. R_1 = Inside Radius 1.7190 in.			
11:00	2478	2430	48	181	2454	26.2
1:00	3366	3238	128	509	3302	27.6
2:00	Run terminated due to build-up on calorimeter blocking optical view of inner wall					
Specimen: RI-1C-C-11 Run: 2 Run: 5308-111-A24						
10:30	2277	2236	41	206	2256	34.8
12:15	2887	2800	87	426	2844	34.0
1:15	3591	3443	148	791	3517	37.1
2:15	4206	3963	243	1141	4085	32.6
3:00	4484	4222	262	1562	4353	41.3
3:45	Run terminated due to build-up on calorimeter blocking optical view of inner wall					
Specimen Sleeve: RI-2C-C-5b Run: 1 Run: 5308-109-69-2 Density: 2.325 gm/cm³			R_2 = Outside Radius 2.000 in. R_1 = Inside Radius 1.7150 in.			
9:30	2277	2233	44	152	2255	24.3
11:15	3221	3101	120	450	3161	26.4
12:45	4047	3816	231	1040	3932	31.7
1:20	Run terminated due to build-up on calorimeter blocking optical view of inner wall					

The thermal conductivity was calculated from the Equation:

$$K = \frac{\ln (R_2/R_1)}{2\pi L} \cdot \frac{Q}{\Delta T}$$

where

K = thermal conductivity
Q = heat to calorimeter
ΔT = temperature difference between outside and inside radii
L = gage length of calorimeter 0.500 in.

Notes:

[1]All measurements made in 1 atm helium purge after evacuating and back filling furnace twice with helium.

Table 23

Thermal Conductivity of Codeposited Pyrolytic Graphite with 25 Percent SiC in the 'AB' Direction (Measured in Comparative Rod Apparatus with Armco-Iron References)

Specimen and Time	Mean Temperature of Specimen °F	Thermal Conductivity of Specimen K_s Btu-in./hr ft²°F	ΔT through Specimen °F	Mean Temperature of Lower Reference °F	Thermal Conductivity of Lower Reference K_1 Btu-in./hr ft²°F	ΔT through Lower Reference ΔT_1 °F	Mean Temperature of Upper Reference °F	Thermal Conductivity of Upper Reference K_2 Btu-in./hr ft²°F	ΔT through Upper Reference ΔT_2 °F
Specimen: CR-1AB -C-29	$l_1 = l_2 = l_s = 0.750$ in.		Initial Thickness:		1.1406 in.	Initial Weight:		14.0974 gm	
Run: 1			Final Thickness:		1.1406 in.	Final Weight:		14.0752 gm	
Run: 6072-69									
Density: 2.452 gm/cm³									
2:15	73	1392	12.65	35	517	33.25	110	494	36.47
2:45	73	1395	12.65	36	518	33.30	111	494	36.53
8:30	454	1303	14.50	406	414	43.74	502	391	50.36
9:00	454	1304	14.55	407	415	43.83	503	392	50.37
12:30	1087	941	29.57	994	290	93.50	1199	251	113.57
1:00	1088	941	29.55	994	290	93.58	1200	251	113.35
2:20	1467	791	36.33	1344	230	123.60	1613	195	149.02
3:00	1468	784	36.50	1348	228	123.73	1512	195	148.82
Specimen: CR-2AB -C-29	$l_1 = l_2 = l_s = 0.750$ in.		Initial Thickness:		1.1400 in.	Initial Weight:		14.1067 gm	
Run: 1			Final Thickness:		1.1400 in.	Final Weight:		14.0922 gm	
Run: 6072-73									
Density: 2.456 gm/cm³									
9:50	31	1500	21.15	-37	541	58.25	97	498	64.10
10:20	31	1493	21.25	-36	541	58.30	97	498	64.10
2:30	754	1059	34.97	649	361	100.48	874	310	121.95
3:10	754	1061	34.97	650	361	100.65	877	310	122.20
10:30	1206	854	33.35	1100	270	103.50	1328	230	126.25
11:00	1207	865	32.95	1102	270	103.17	1329	230	126.70

Notes: 1. All measurements made with helium purge.
2. Thermal conductivity (k_s) of specimen calculated from following equation

$$k_s = \left[\frac{k_1 \Delta T_1}{l_1} + \frac{k_2 \Delta T_2}{l_2}\right] \frac{l_s}{2\Delta T_s}$$

where

k = thermal conductivity
ΔT = temperature drop over gage length
l = gage length

and subscripts 1, 2, and s refer to lower reference, upper reference, and specimen, respectively.

Table 24

Thermal Conductivity of Codeposited Pyrolytic Graphite with 25 Percent SiC in the 'C' Direction Measured in Comparative Rod Apparatus with Armco-Iron References

Specimen and Time	Mean Temperature of Specimen °F	Thermal Conductivity of Specimen K_s Btu-in./hr ft²°F	Corrected* ΔT through Specimen °F	Mean Temperature of Lower Reference °F	Thermal Conductivity of Lower Reference K_1 Btu-in./hr ft²°F	ΔT through Lower Reference ΔT °F[1]	Mean Temperature of Upper Reference °F	Thermal Conductivity of Upper Reference K_2 Btu-in./hr ft²°F	ΔT through Upper Reference ΔT_2 °F
Specimen: CR-1C-C-29 Run: 1 Run: 6072-60 Density: 2.443 gm/cm³	$l_1 = l_2 = 0.750$ in. $l_s = 0.1563$ in.		Initial Thickness: 0.1563 in. Final Thickness: 0.1563 in.			Initial Weight: 4.9355 gm Final Weight: 4.9346 gm			
2:30	67	193	16.62	4	527	28.85	138	484	32.05
3:00	67	195	16.56	4	527	29.35	138	484	32.11
1:30	501	168	14.19	451	403	27.30	557	380	31.33
2:00	502	170	14.14	452	403	27.30	558	380	31.81
7:00	973	122	34.25	869	313	62.83	1099	269	76.25
7:30	972	123	34.13	868	313	62.82	1098	269	76.50
Specimen: CR-2C-C-29 Run: 1 Run: 6072-63 Density: 2.452 gm/cm³	$l_1 = l_2 = 0.750$ in. $l_s = 0.1563$ in.		Initial Thickness: 0.1563 in. Final Thickness: 0.1563 in.			Initial Weight: 4.9389 gm Final Weight: 4.9382 gm			
2:20	94	226	8.20	2	87.0	102.40	179	99.0	89.90
2:50	94	230	8.10	5	87.2	102.50	183	99.1	90.60
7:45	507	195	7.29	451	116.0	59.60	564	123.2	54.35
8:20	508	194	7.29	452	116.0	59.56	565	123.2	54.35
12:30	1039	144	21.87	925	145.2	104.25	1153	159.2	94.52
1:00	1039	144	21.89	925	145.2	104.28	1153	159.2	94.45
4:30	1315	127	25.84	1203	162.0	95.75	1432	173.5	91.48
5:00	1315	127	25.83	1203	162.0	95.75	1433	173.5	91.49

Notes: 1. All measurements made with helium purge.
2. Thermal conductivity (k_s) of specimen calculated from following equation

$$k_s = \left[\frac{k_1 \Delta T_1}{l_1} + \frac{k_2 \Delta T_2}{l_2}\right] \frac{l_s}{2\Delta T_s}$$

where

k = thermal conductivity
ΔT = temperature drop over gage length
l = gage length

and subscripts 1, 2, and s refer to lower reference, upper reference, and specimen, respectively.

*Temperature gradient corrected for grafoil at interfaces from known in house thermal conductivity of grafoil

Table 25

The Thermal Conductivity of Codeposited Pyrolytic Graphite Sleeve with 25 Percent SiC in the 'C' Direction (Measured in Radial Inflow Apparatus Using an Optical Technique)

Time	Outer Surface Temperature PG-SiC °F	Inner Wall Temperature PG-SiC °F	Specimen ΔT PG-SiC °F	Heat to Calorimeter $\frac{Btu}{hr}$	Specimen Mean Temperature °F	Thermal Conductivity $\frac{Btu\text{-}in.}{hr\ ft^2\ °F}$
Specimen Sleeve: RI-1C-C-47 Run: 1 Run: 5308-113-A24 Density: 2.364 gm/cm³				R_2 = Outside Radius 2.0000 in. R_1 = Inside Radius 1.8400 in.		
12:10	2216	2201	15	208	2208	52.7
1:15	3221	3173	48	618	3197	49.0
2:45	4214	4107	107	1388	4160	49.3
3:30	Run terminated due to build-up on calorimeter blocking optical view of inner wall					
Specimen Sleeve: RI-2C-C-47 Run: 1 Run: 5308-115-69-2 Density: 2.394 gm/cm³						
11:00	2214	2198	16	180	2206	58.3
12:10	3108	3055	53	498	3082	48.7
2:05	3824	3745	79	991	3785	65.0
3:00	Run terminated due to build-up on calorimeter blocking optical view of inner wall					
Run: 2 RI-2C-C-47 Run: 5308-117-A24						
9:45	2564	2542	22	284	2553	66.9
10:45	3615	3541	74	691	3578	48.4
11:45	4341	4209	131	1481	4275	58.6
12:15	Run terminated due to build-up on calorimeter blocking optical view of inner wall					

The thermal conductivity was calculated from the Equation:

$$K = \frac{\ln (R_2/R_1)}{2\pi L} \frac{Q}{\Delta T}$$

where

K = thermal conductivity
Q = heat to calorimeter
ΔT = temperature difference between outside and inside radii
L = gage length of calorimeter 0.500 in.

Notes:

[1]All measurements made in 1 atm helium purge after evacuating and back filling furnace twice with helium

Table 26

Electrical Resistivity of Codeposited Pyrolytic Graphite with 25 Percent and 15 Percent Silicon Carbide in the 'a-b' Direction

Time	Specimen Temperature °F	Current Through Circuit Amps	Closed Circuit minus Open Circuit Potential mv	Electrical Resistivity μohm-cm
	Specimen: ER-1AB-C7C (15% SiC) Run: 1 Run: 6621-37			
8:30	76	0.3 -0.3	5.55 -5.47 Avg. 5.51	1557
9:15	195	0.3 -0.3	5.12 -5.15 Avg. 5.14	1453
9:35	393	0.3 -0.3	4.38 -4.37 Avg. 4.37	1237
10:00	593	0.3 -0.3	3.89 -3.75 Avg. 3.82	1080
10:30	846	0.3 -0.3	3.24 3.31 Avg. 3.28	927
11:25	1173	0.3 -0.3	2.76 2.81 Avg. 2.79	789
12:10	1458	0.3 -0.3	2.55 2.56 Avg. 2.56	724
12:35	1638	0.3 -0.3	2.37 2.40 Avg. 2.38	674
1:00	1810	0.3 -0.3	2.32 2.33 Avg. 2.32	657
	Cool Down Point			
2:20	74	0.3 -0.3	5.55 5.44 35.50	1555

Table 26 (Continued)

Time	Specimen Temperature °F	Current Through Circuit Amps	Closed Circuit minus Open Circuit Potential mv	Electrical Resistivity μohm-cm
	Specimen: ER-1AB-C31 (25% SiC)			
9:30	73	0.3 -0.3	21.63 -21.63 Avg. 21.63	6114
10:00	190	0.3 -0.3	20.12 -19.16 Avg. 19.64	5552
10:20	359	0.3 -0.3	16.89 -16.49 Avg. 16.69	4718
10:40	552	0.3 -0.3	13.65 -13.47 Avg. 13.56	3833
11:00	794	0.3 -0.3	10.84 -10.86 Avg. 10.85	3067
11:20	1021	0.3 -0.3	8.98 - 8.88 Avg. 8.93	2524
11:40	1283	0.3 -0.3	7.45 - 7.43 Avg. 7.44	2103
12:00	1590	0.3 -0.3	6.34 - 6.52 Avg. 6.43	1818
12:25	1799	0.3 -0.3	5.98 - 5.05 Avg. 6.02	1702
	Cool Down Point (RT)			
1:10	78	0.3 -0.3	21.60 21.16 Avg. 21.38	6043

Note:
Negative sign indicates that the direction of the current through the circuit was reversed.

APPENDICES

APPENDIX A

THERMAL EXPANSION TO 1800°F

Thermal expansion measurements are made utilizing quartz tube dilatometers of the Bureau of Standards design. The dial gages (B. C. Ames Co., Model 212, Shockless) are graduated in 0.0001-inch divisions with a total range of 0.500 inch. The manufacturer's stated mechanical accuracy for any given reading is ±0.0001 inch at any point in the range. This accuracy has been checked with a precision micrometer.

The extensions from the dial, which are made of stainless steel, are finned to facilitate cooling. The temperatures of the fins are continually monitored and air cooled when necessary to eliminate differential expansion between the dial gage mount and the extension; see Figure 1.

For temperatures above room temperature, each dilatometer is heated by an individual heater. The temperature of the heater is maintained by a manual setting of a variable voltage transformer.

Cold specimen temperatures are obtained by use of a Dewar flask filled with dry ice and trichloroethylene. The flask surrounds the dilatometer tubes and the cold liquid level rises to a height above the specimens.

Liquid nitrogen is used in the Dewar flask for temperatures down to -300°F. A cooling coil has also been designed to provide better control of temperatures in the cryogenic range.

Thermocouples are placed at each end and the center of the specimens to monitor the temperature throughout. The specimens are nominally 1/2-inch diameter by 3 inches in length with the ends rounded on a 3-inch radius. Other diameters and cross-sectional configurations are employed where necessary due to configuration of supplied material.

To calibrate the dilatometers we employ a fused silica specimen, the expansion of which is known and is shown in Figure 2.

The accuracy of the apparatus to 1800°F has been checked by running the NBS copper standard and other in-house standards of graphite and nickel. Figures 3, 4, and 5 include the expansion values measured in the quartz dilatometers on these standards. Note the excellent agreement between the measured values and the data reported by NBS on the copper. For the graphite and nickel standards, good agreement was observed between the values measured in the quartz dilatometer and that reported in the literature and the values measured at SRI by optically tracking.

The above data and our experience have demonstrated the excellent precision and accuracy of this equipment. We have observed no systematic uncertainty with the equipment and, based on 5 runs with the graphite standard, the random uncertainty is $\pm 0.05 \times 10^{-3}$ in./in. at 1500°F with a 95 percent confidence interval.

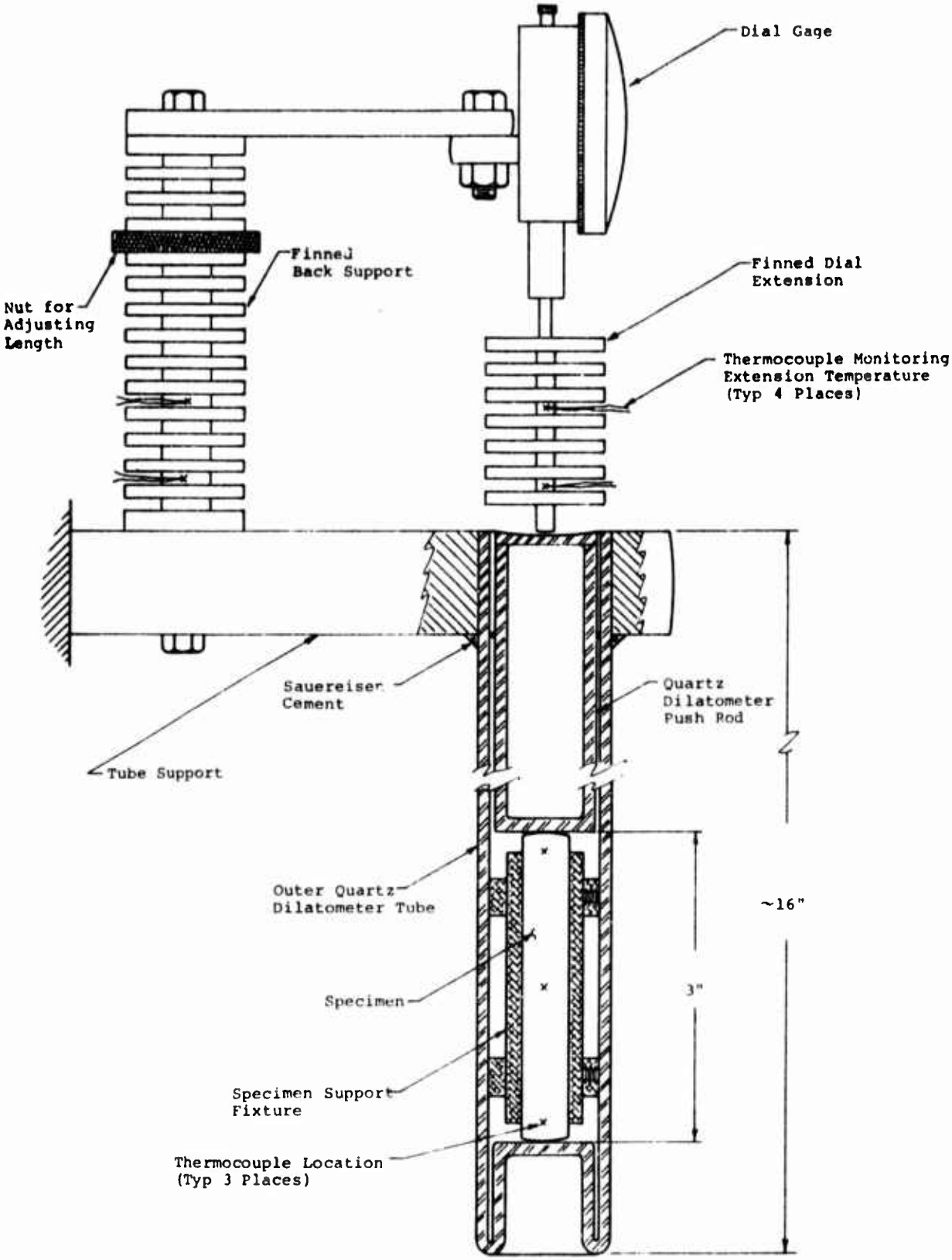

Figure 1. Assembly of Quartz Tube Dilatometer for Thermal Expansion Measurements

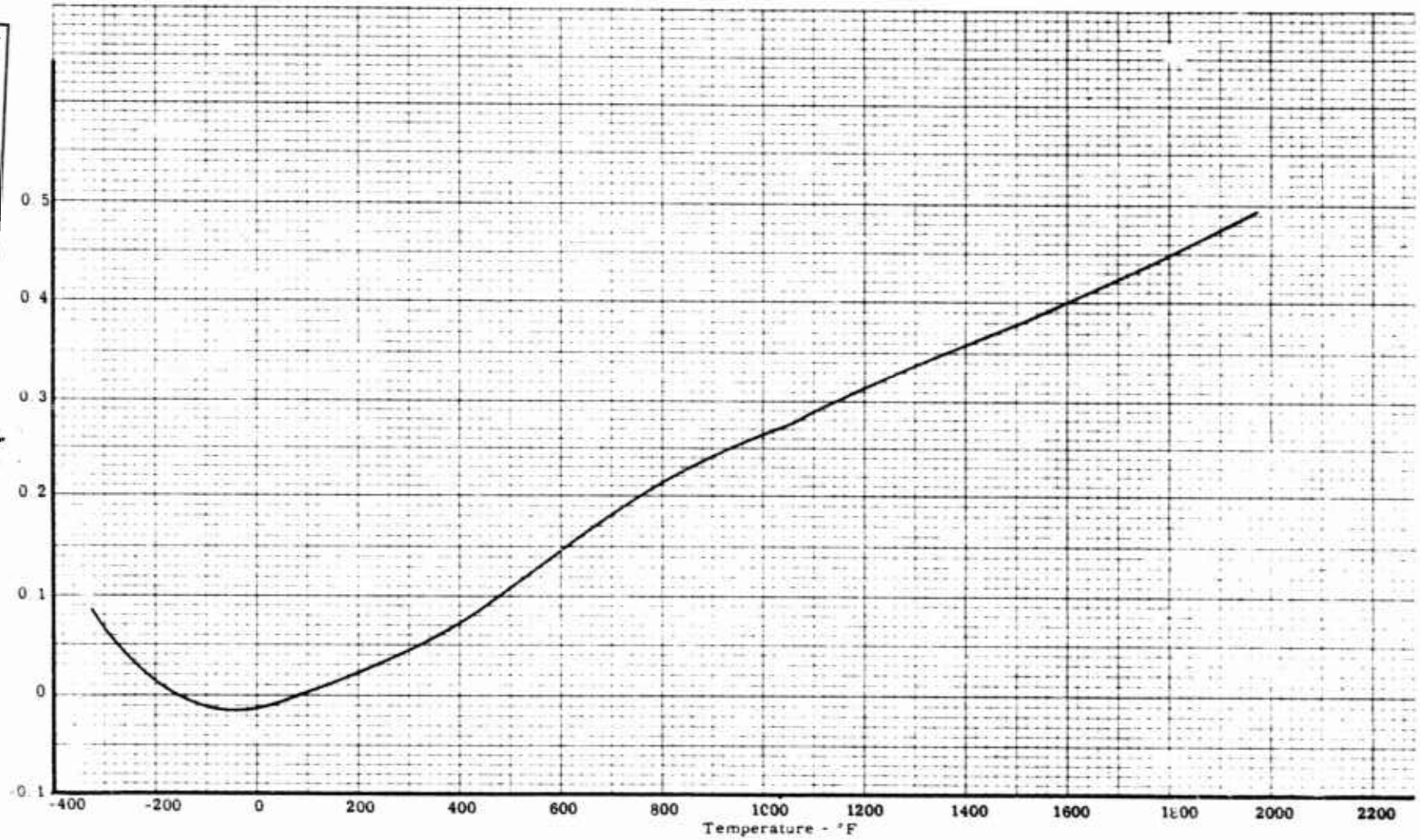

Figure 2. Thermal Expansion of Fused Silica (Taken from Souder and Hidnert, "Measurements on Thermal Expansion of Fused Silica" Scientific Papers of the Bureau of Standards, No. 524)

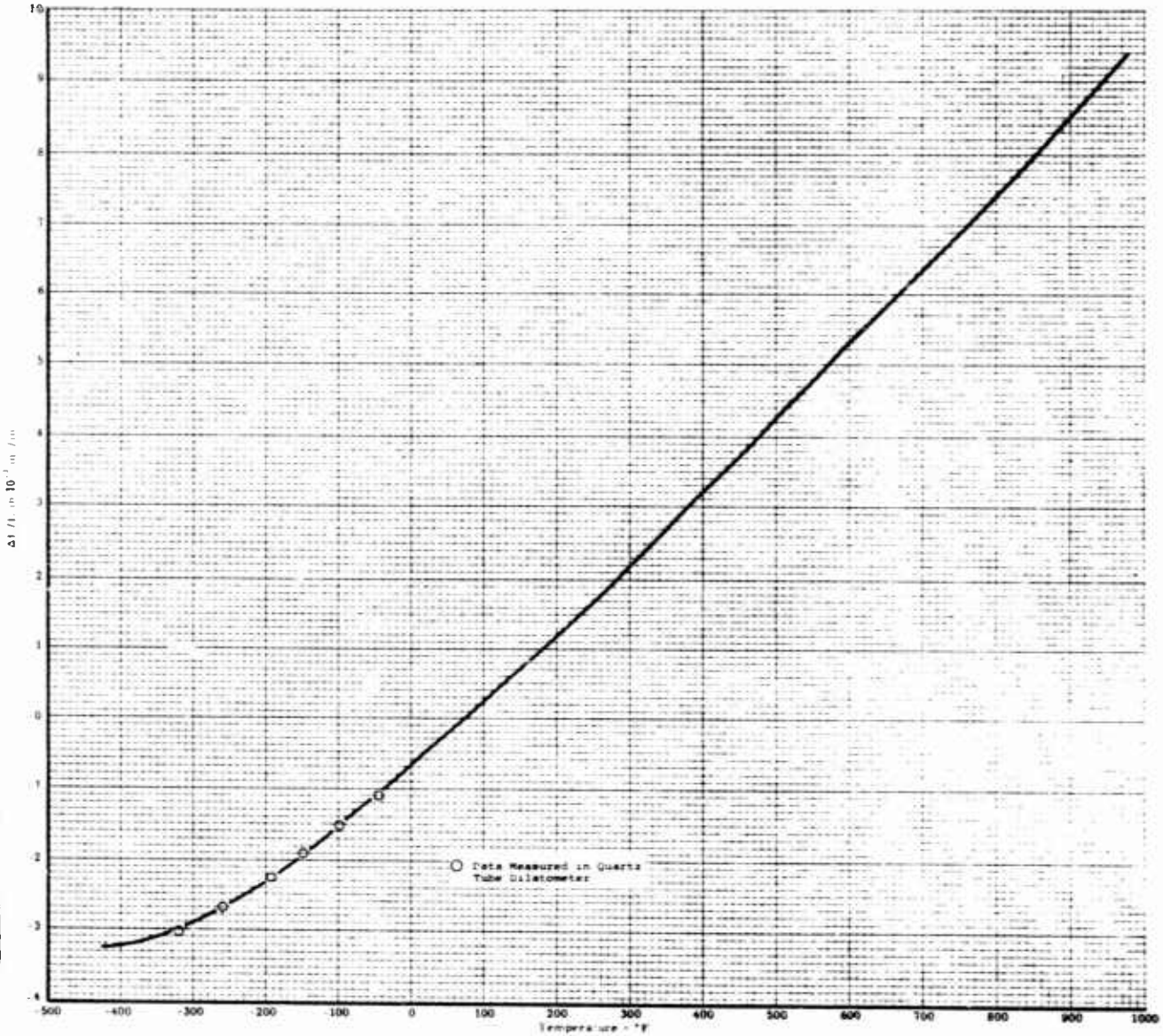

Figure 3. Thermal Expansion of NBS Copper Standard SRM 736

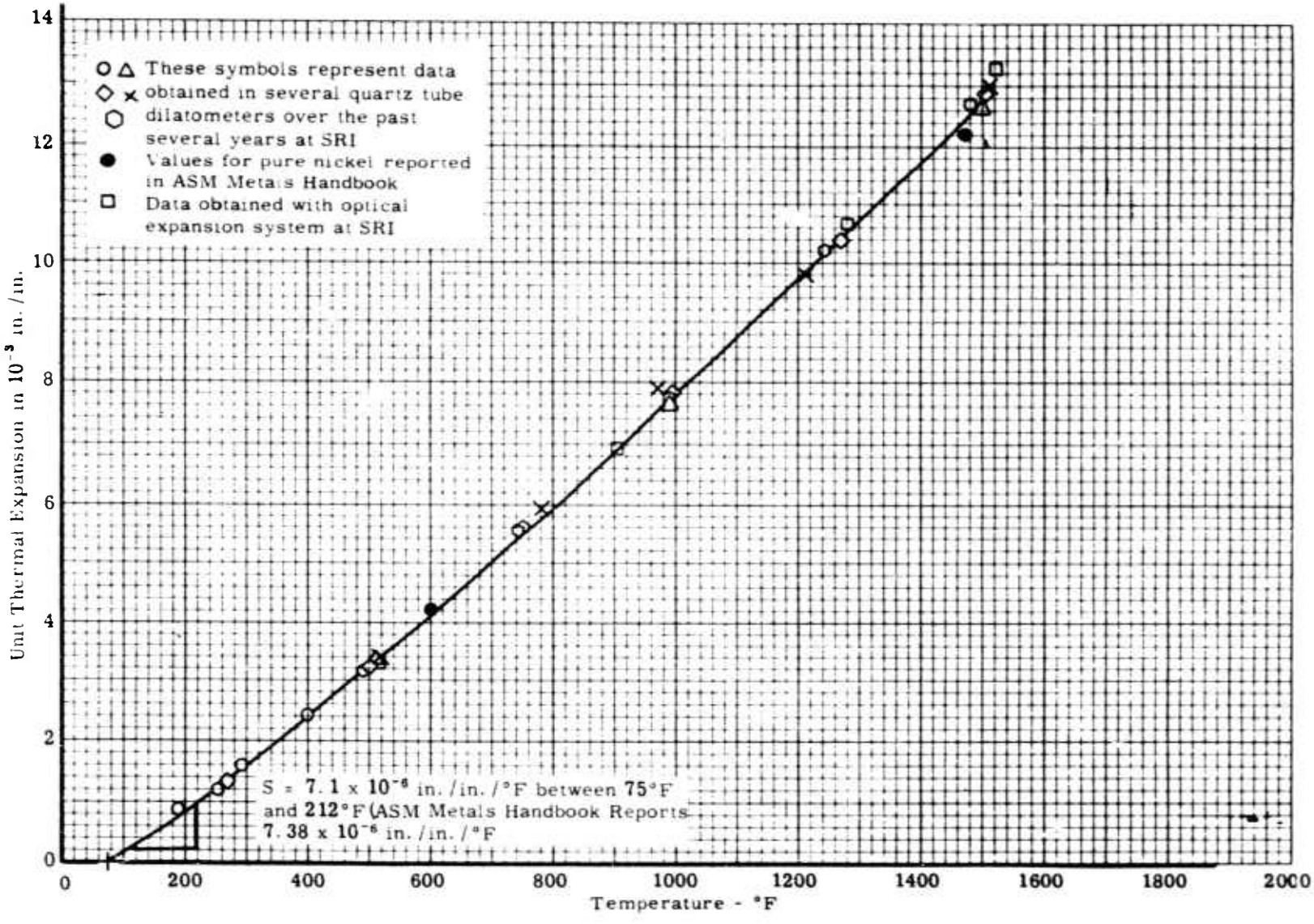

Figure 4. Expansion of "A" Nickel (Calibration Standard Specimen)

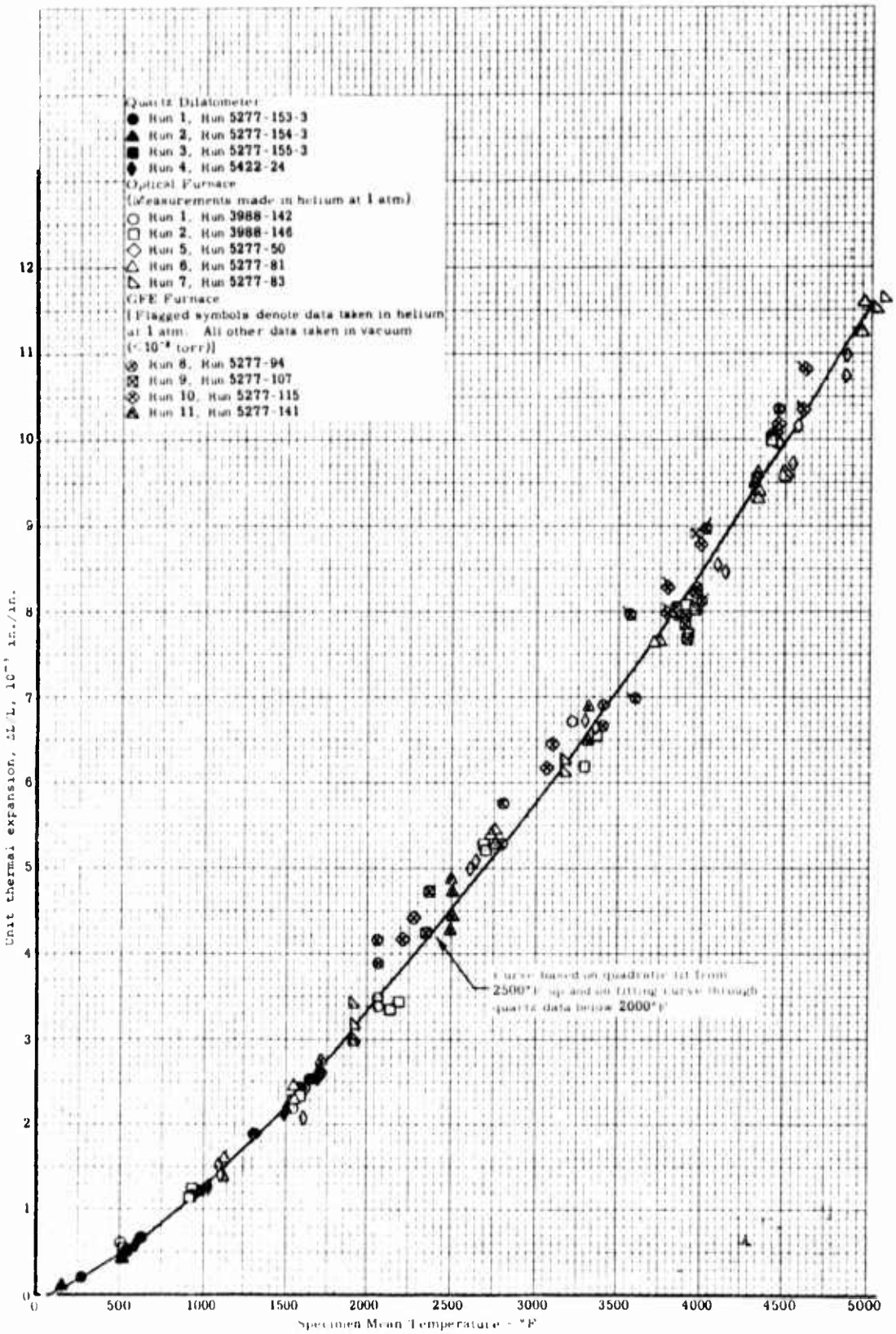

Figure 5. Thermal Expansion of ATJ Graphite (wg) Standard No. 5 by In-House Optical Calibration

APPENDIX B

THERMAL EXPANSION TO 5500°F

Thermal expansion is measured in a graphite tube dilatometer developed by Southern Research Institute for performance to 5500°F, see Figure 1. The specimen required is about 1/2" diameter and 3" long, although the exact size can vary somewhat if it appears desirable from the standpoint of specimen availability. Specimens 3/4" in diameter and only 1/4" thick can be evaluated, but with a reduced precision. Discs can be stacked to provide more length in many cases. Of course, specimens can always be pinned together from smaller pieces to provide both length and columnar strength.

In the dilatometer, the specimen rests on the bottom of the cylinder with a graphite extension rod resting on the specimen to extend to the top of the cylinder. When required, tungsten pads are inserted at the ends of the specimens to eliminate graphite diffusion from the dilatometer parts into the specimen. This entire assembly is inserted into one of the 5000°F furnaces described in another brochure.

The motion of the specimen is measured by a dial gage attached to the upper end of the cylinder with the stylus bearing on the extension rod. The system accurately indicates total motions of 0.0001" - or less than 0.00004" per inch of specimen.

Either a helium or an argon environment can be employed. Nitrogen has been used on occasion. The equipment will permit operation at hard vacuums, but this procedure is rarely used.

A CS graphite, which has a fairly low expansion relative to other grades of graphite, is used as the material for the dilatometer. Prior to calibrations, the dilatometers are heat soaked to a temperature several hundred degrees above the maximum temperature to which they would be exposed during normal service. Dimensional stability is confirmed by measuring the lengths of the dilatometer tube and rod after each run. Past experience has shown that following the initial heat soak the expansion is reproducible in subsequent repeated cycles to lower temperatures. Reproducibility is also confirmed by repeated runs on standards.

To calibrate the dilatometers we have developed in-house primary and secondary standards of ATJ graphite. ATJ graphite was selected as a standard because of our vast experience with it, its stability after repeated exposure to high temperatures, and its relatively low expansion.

The true expansion of the primary standard was determined by a direct optical technique using a traveling Gaertner telescope. The total error in the telescope readings, based on calibration data, was estimated to be 0.2×10^{-3} in./in. For the direct optical measurements, the 3.5 inch long specimen was heated in a graphite furnace, and the expansion was determined by sighting on "knife" edges machined on the ends of the specimen. Typically a total of 11 runs have been made in two different furnaces both in vacuum and helium environments. The two environments are used to check effects of refraction as reported in the literature. The same standard was then machined to the configuration of a regular dilatometer specimen and several runs were made in our precision quartz dilatometers. The optical expansion data were fitted to a quadratic equation over the temperature range from 2500°F to 5000°F using the method of least squares and statistically analyzed to determine the uncertainty (primarily the scatter). Below 2500°F, the quartz dilatometer data were fitted by hand since the uncertainty of this apparatus has been well established, and the imprecision is small ($<0.1 \times 10^{-3}$ in./in.). A typical plot of all data points with the curve fit is shown in Figure 2.

A check of the expansion of the standard was obtained by making runs on round robin specimens of various graphites and synthetic sapphire which had been previously evaluated by others, including the National Bureau of Standards. Our data on these specimens agreed within a 2.5 percent random difference with the data reported by the other laboratories.

After establishing the expansion of the ATJ standard, several graphite dilatometers were then calibrated by making runs on this standard. These dilatometers were used to establish the expansion of secondary standards (also ATJ graphite) which are used to calibrate new dilatometers and to make periodic checks on dilatometers currently in service. This use of secondary standards thus minimizes the wear and tear on the primary standard and prolongs its life.

Table 1 lists the uncertainties in the dilatometer measurements in 10^{-3} in./in. Observe that most of the uncertainty is in the expansion of the standard and includes both random and systematic uncertainties. Other sources of uncertainty, resulting from such factors as dial gage and temperature measurement, are small amounting to less than 0.2×10^{-3} in./in. at any temperature. The precision in the dilatometer measurements is quite good and amounts to about 0.1×10^{-3} in./in. From Table 1, it can be seen that the maximum total uncertainty, which occurs at a temperature of 4500°F, is $\pm 0.45 \times 10^{-3}$ in./in. For a low expansion graphite, such as ATJ, this amounts to an uncertainty of ±4.5 percent at 4500°F (see Figure 2). For graphites having higher expansions, the percentage uncertainty would be lower.

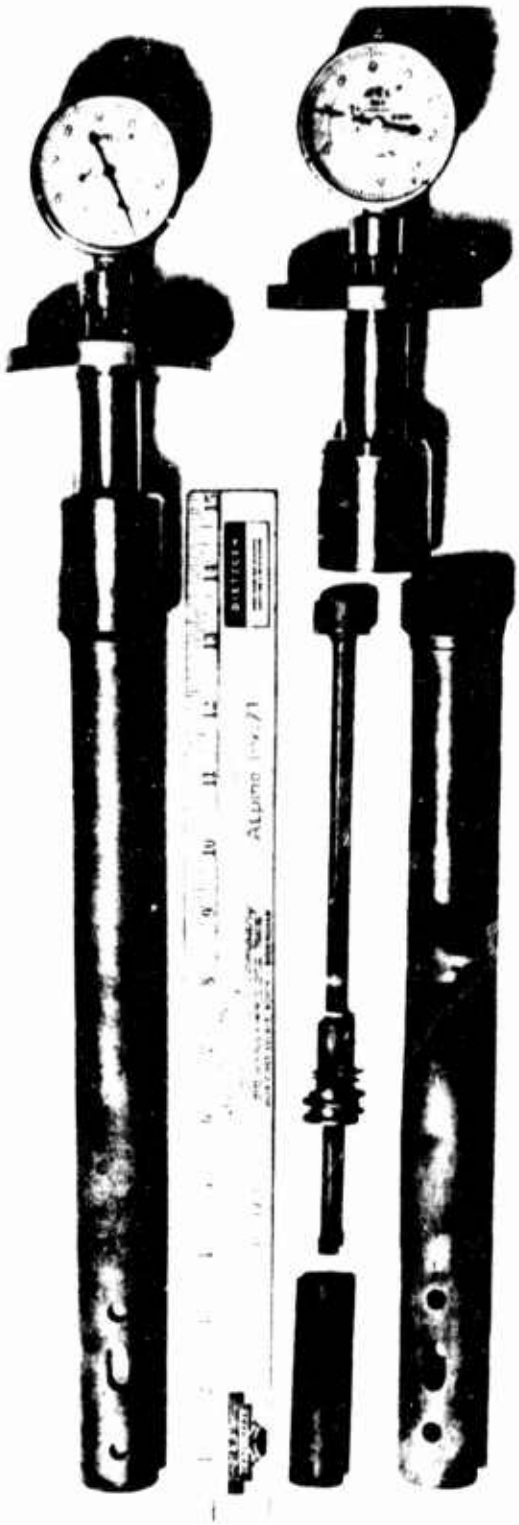

Figure 1. Picture of the Graphite Dilatometer Tubes for Measuring Thermal Expansion to 5500°F

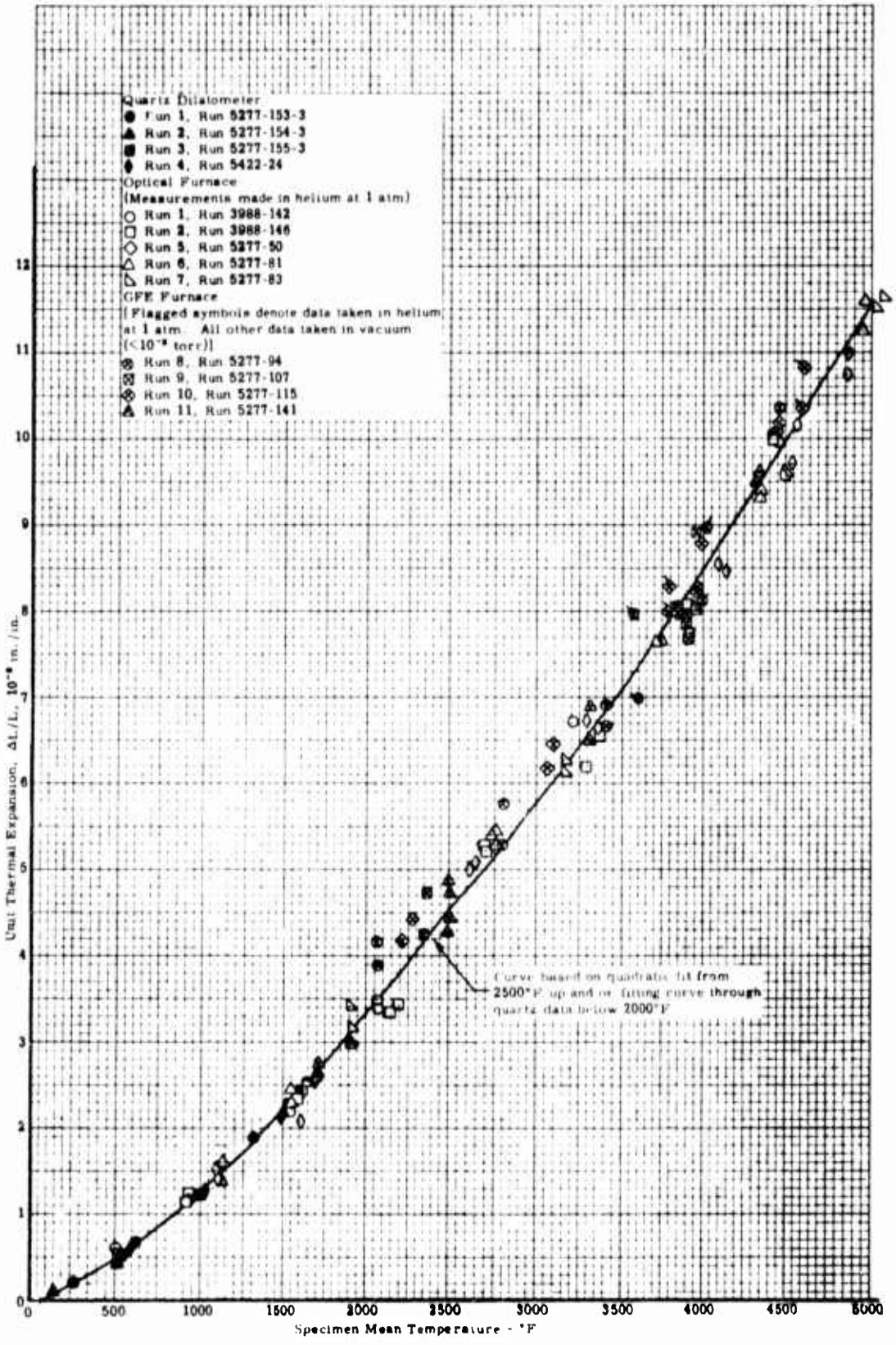

Figure 2. The Thermal Expansion of ATJ Graphite (wg) Standard No. 5 by In-House Optical Calibration

Table 1

Uncertainty in Thermal Expansion Measurements
Made in Graphite Dilatometers

Temperature °F	Uncertainty in Expansion of Standard in 10^{-3} in./in. Random Uncertainty (See Note 1)	Systematic Uncertainty (See Note 2)	Random Uncertainty in Dilatometer Measurements in 10^{-3} in./in.	Total Uncertainty in Dilatometer Measurements from all Sources in 10^{-3} in./in. +	-
500	±0.04	0	±0.03	0.05	0.05
1000	±0.04	0	±0.03	0.05	0.05
1500	±0.05	0	±0.04	0.07	0.07
2000	±0.17	+0.03	±0.05	0.21	0.18
2500	±0.11	+0.20	±0.07	0.33	0.13
3000	±0.12	+0.21	±0.08	0.35	0.14
3500	±0.19	-0.02	±0.10	0.21	0.23
4000	±0.14	-0.09	±0.12	0.18	0.27
4500	±0.14	±0.25	±0.14	0.45	0.45
5000	±0.19	-0.12	±0.16	0.25	0.37

Notes: 1. 95% confidence limits.

2. Represents deviation between average measured value and least squares curve through all data.

APPENDIX C

A COMPARATIVE ROD APPARATUS FOR MEASURING THERMAL CONDUCTIVITY TO 2000°F

Southern Research Institute's comparative rod apparatus is used to measure thermal conductivities of a wide variety of materials from -300°F to 2000°F. This apparatus, shown schematically in Figure 1, consists basically of two cylindrical reference pieces of known thermal conductivity stacked in series with the cylindrical specimen. Heat is introduced to one end of the rod, composed of the references and specimen, by a small electrical heater. A cold sink or heater is employed at the opposite end of the rod as required to maintain the temperature drop through the specimen at the preferred level. Cylinders of zirconia may be inserted in the rod assembly to assist in controlling the temperature drop. Radial losses are minimized by means of radial guard heaters surrounding the rod and consisting of three separate coils of 16, 18 or 20-gage Kanthal wire wound on a 2 or 4-inch diameter alumina core. The annulus between the rod and the guard heaters is filled with diatomaceous earth, thermatomic carbon, bubbled alumina or zirconia powder. Surrounding the guard is an annulus of diatomaceous earth enclosed in an aluminum or transite shell.

The specimens and references (see Figure 2) are normally 1-inch diameter by 1-inch long. Thermocouples located 3/4 inch apart in radially drilled holes measure the axial temperature gradients. Thermocouples located at matching points in each guard heater are used to monitor guard temperatures, which are adjusted to match those at corresponding locations in the test section.

In operation, the apparatus is turned on and allowed to reach steady state. The guard and rod heaters are adjusted to minimize radial temperature gradients between the rod and guard sections consistent with maintaining equal heat flows in the references. Temperatures are measured on a Leeds and Northrup Type K-3 potentiometer, and the temperature gradients calculated. A typical temperature profile in the test section is shown in Figure 3.

The thermal conductivity of the specimen is calculated from the relation

$$K_s = \frac{K_1 \Delta T + K_2 \Delta T}{2 \Delta T_s} \quad \frac{\Delta X_s}{\Delta X_r}$$

where K_1 and K_2 are the thermal conductivities of the upper and lower references; ΔT_1, ΔT_2 and ΔT_s are the temperature differences in the upper and lower references and specimen, respectively; ΔX_s and ΔX_r are the distances between thermocouples in the specimen and references.

Note that for purely axial heat flow, the products $K_1 \Delta T_1$ and $K_2 \Delta T_2$ should be equal. Due to imperfectly matched guarding and other factors, this condition is seldom attained in practice; therefore, the average of the two values is used in the calculations. Their difference is maintained as small as possible, usually within 5 percent of the smaller.

For identical specimens, the radio $\Delta X_s/\Delta X_r$ should be unity but may vary due to the uncertainty in hold locations. To prevent introducing an additional error in calculations, ΔX is determined as follows: the depth of the hole is measured by inserting a snugly fitting drill rod in the hole, measuring the projecting length and subtracting it from the total length of the rod. The slope, or angle the hole makes with the perpendicular to the specimen axis, is determined by making measurements to the face of the hole and the outer end of the drill rod with respect to a datum plane, using a dial gage. From these measurements, the location of the bottom of the hole can be calculated.

Generally, measurements with the comparative rod apparatus are performed in an inert helium environment. The apparatus can also be operated in vacuum and at gas pressures of up to 100 psig. We have had experience operating under all conditions.

The primary reference materials which we use are Code 9606 Pyroceram and Armco iron for measurements on materials with low and high thermal conductivities, respectively. Primary standard reference sets are kept and are used to calibrate other references made from the same materials. The standards of Code 9606 Pyroceram were made from a batch of material which NBS purchased shortly after their measurements on a sample of Code 9606 Pyroceram. The curve which Flynn presented for the thermal conductivity of the Pyroceram is given in Figure 4.[1] Note that the curve is in good

---

[1] Robinson, H. E. and Flynn, D. R., Proceedings of Third Conference on Thermal Conductivity, pages 308-321, 1963 (with author's permission)

agreement with the recommended values from NSRDS-NBS 8[2]. The standards of Armco iron were made from the stock which was used in the round-robin investigations from which Powell[3] developed the most probable values for Armco iron. The curve used for the Armco iron standards is shown in Figure 5. Powell estimated the uncertainty to be within ±2 percent over the temperature range from 0° to 1000°C. Note in Figure 5 that numerous evaluations of Armco iron from other batches of material have agreed within ±3 percent (coefficient of variation about curve) with Powell's original data.

In addition to Code 9606 Pyroceram and Armco iron, several other materials have been used as references. These include copper for high conductivity specimens, 316 stainless steel for specimens of intermediate thermal conductivity and Teflon or Pyrex for low conductivity materials.

Copper references have been calibrated against Armco iron and excellent agreement with literature data has been obtained. Thermal conductivity values obtained from calibrations of 316 stainless steel against Pyroceram, Armco iron and a set of 316 stainless steel standards are presented in Figure 6. Note the consistency of the data obtained with the three different sets of references. The coefficient of variation of the data shown in Figure 6, about the curve value, was ±3.3 percent. These data indicate the internal consistency of the stainless steel and the reference materials. Note that the thermal conductivity values for 316 stainless steel presented in Figure 6 lie between values reported by several steel manufacturers and Lucks and Deem.[4]

The calibrations indicate that for materials with moderate to high thermal conductivities the apparatus operates with a precision of about ±3 percent and a total uncertainty of about ±5 percent at temperatures above 0°F if temperatures between the guard and test section are closely matched. Below 0°F, the precision achieved to date has been about ±7 percent with a total uncertainty of about ±10 percent. We anticipate that the precision and uncertainty at cryogenic temperatures can be improved by additional calibrations.

---

[2] Powell, R. W., C. Y. Ho and P. E. Liley, Thermal Conductivity of Selected Materials, NSRDS-NBS 8, Department of Commerce, November 25, 1966.

[3] Powell, R. W., Proceedings of Third Conference on Thermal Conductivity, pages 322-341, 1963.

[4] WADC TR58-476, "The Thermophysical Properties of Solid Materials", Armour Research Foundation, November, 1960.

Some additional data obtained on the comparative rod apparatus are shown in Figures 7 and 8. Figure 7 shows thermal conductivity data for ATJ graphite, with grain, using Armco iron as the referene material. These data show excellent agreement with earlier data obtained here and by other sources [5-7]. The maximum scatter of the comparative rod points was about 5 percent.

Figure 8 shows data for thermocouple grade constantan obtained on the comparative rod apparatus using Armco iron references and on Southern Research Institute's high temperature radial inflow apparatus. Note the excellent agreement. These data also show close agreement with data obtained by Silverman[4] on an alloy of very similar composition.

---

[5] ASD-TDR-62-765, "The Thermal Properties of Twenty-Six Solid Materials to 5000°F or Their Destruction Temperatures," Southern Research Institute, August, 1962.

[6] Pears, C. D., Proceedings of Third Conference on Thermal Conductivity, 453-479, 1963.

[7] NSRDS-NBS 16, "Thermal Conductivity of Selected Materials", Part 2, by C. Y. Ho, R. W. Powell and P. E. Liley, National Bureau of Standards, 1968.

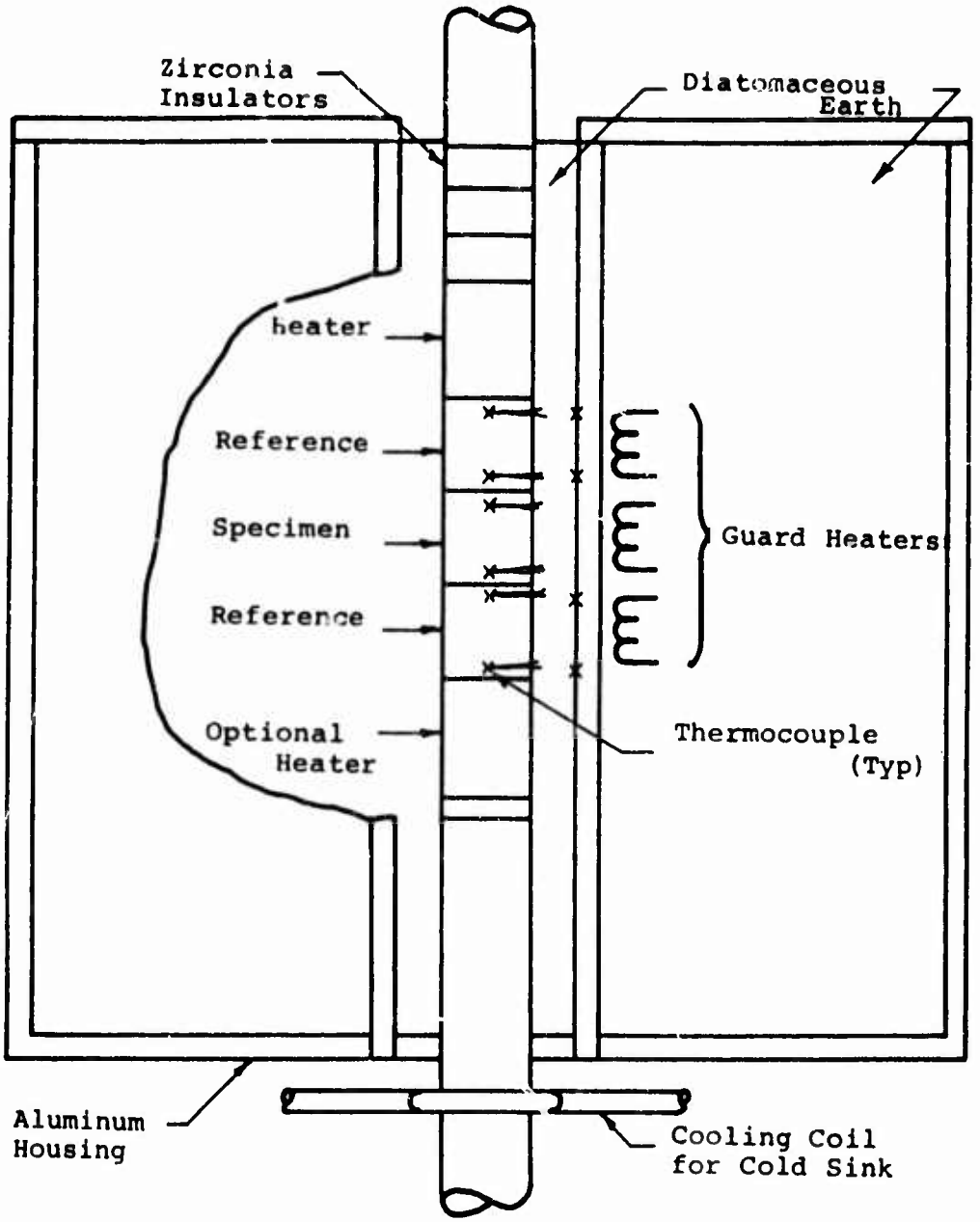

Figure 1. Schematic of Comparative Rod Thermal Conductivity Apparatus

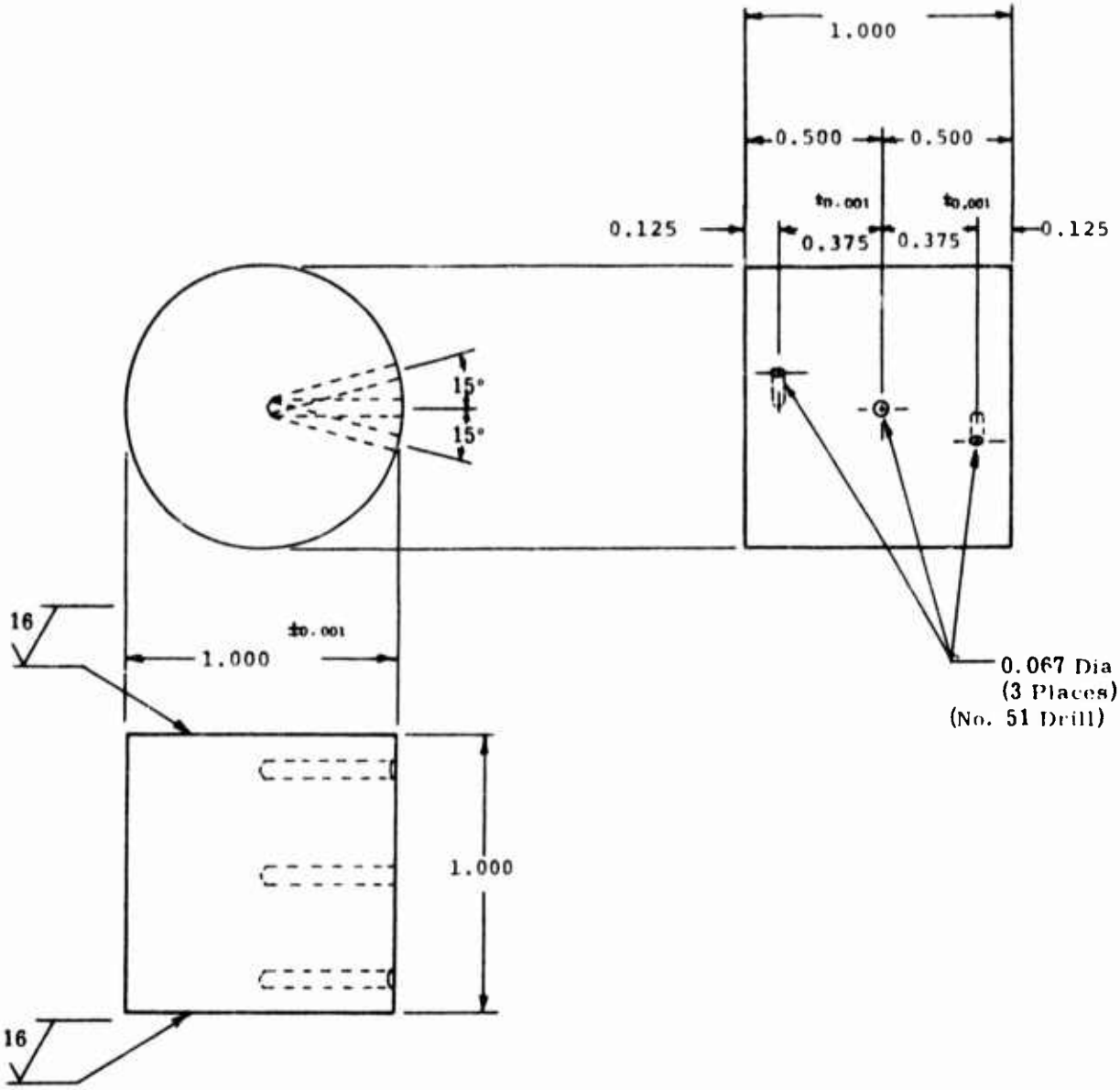

Note: All dimensions ±0.005 except where noted

Figure 2. Drawing of Specimen for Thermal Conductivity Measurements in Comparative Rod Apparatus to 1800°F

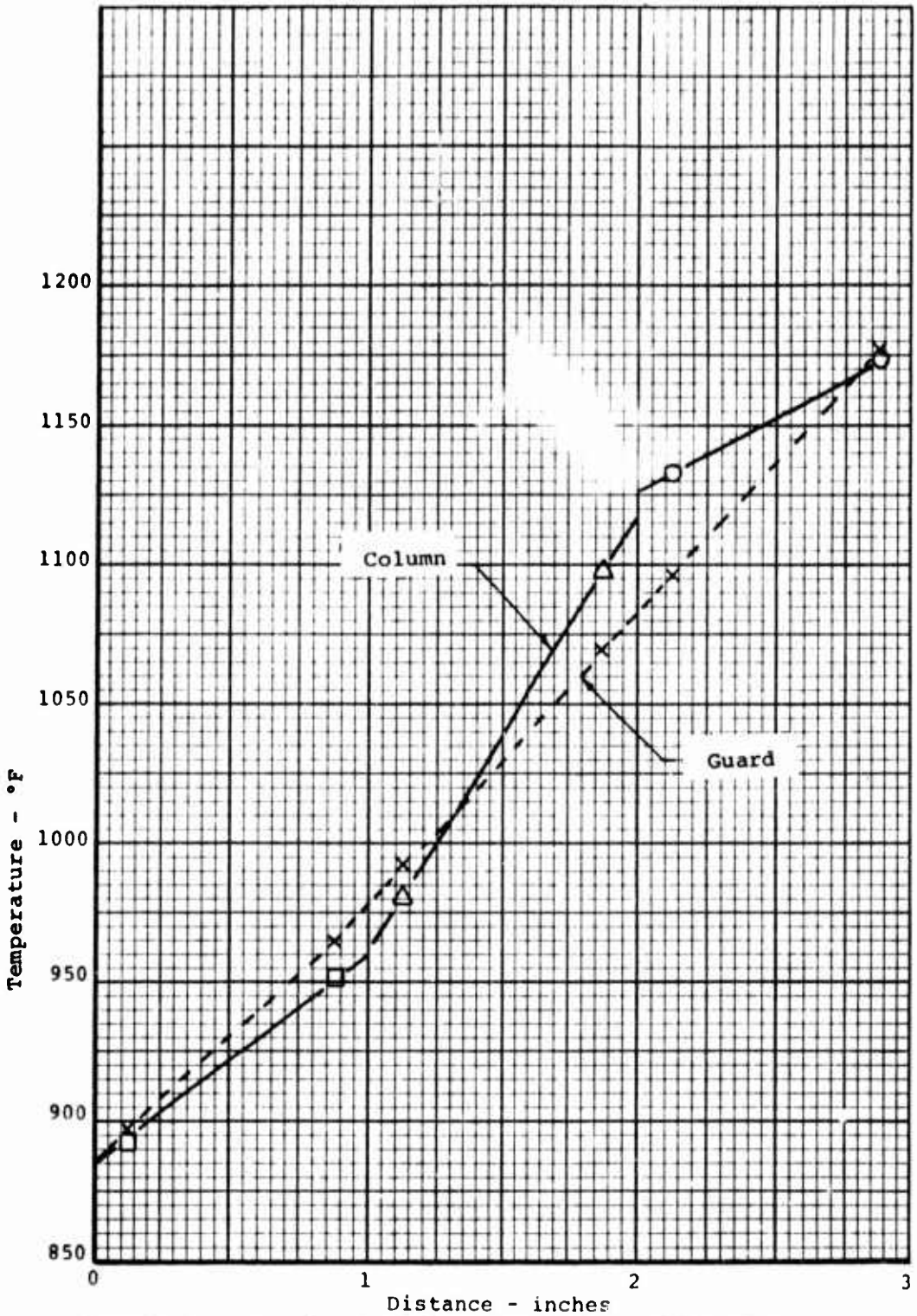

Figure 3. Typical Temperature Profile in Test Section

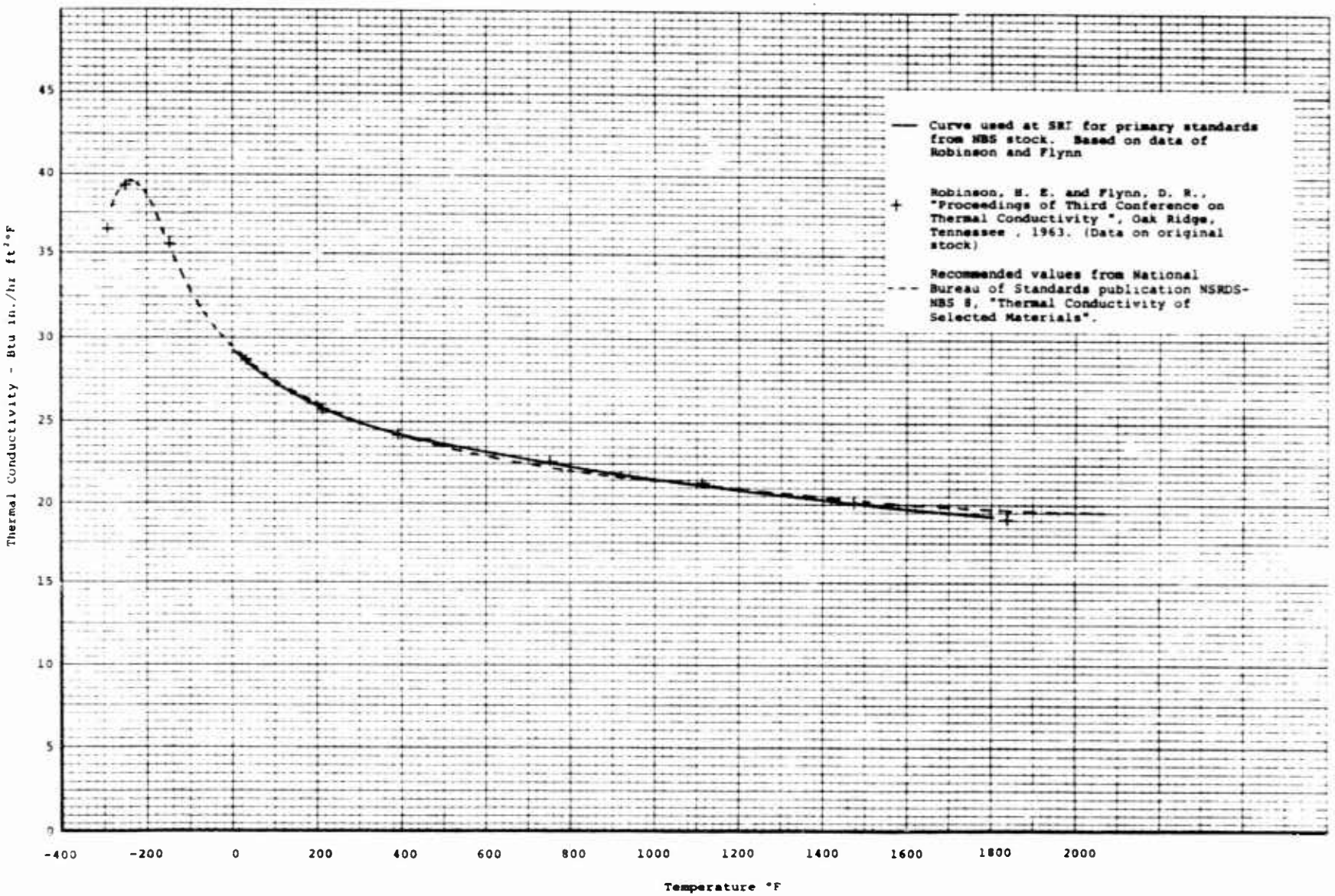

Figure 4. The Thermal Conductivity of Primary SRI Standards from NBS Stock of Code 9606 Pyroceram

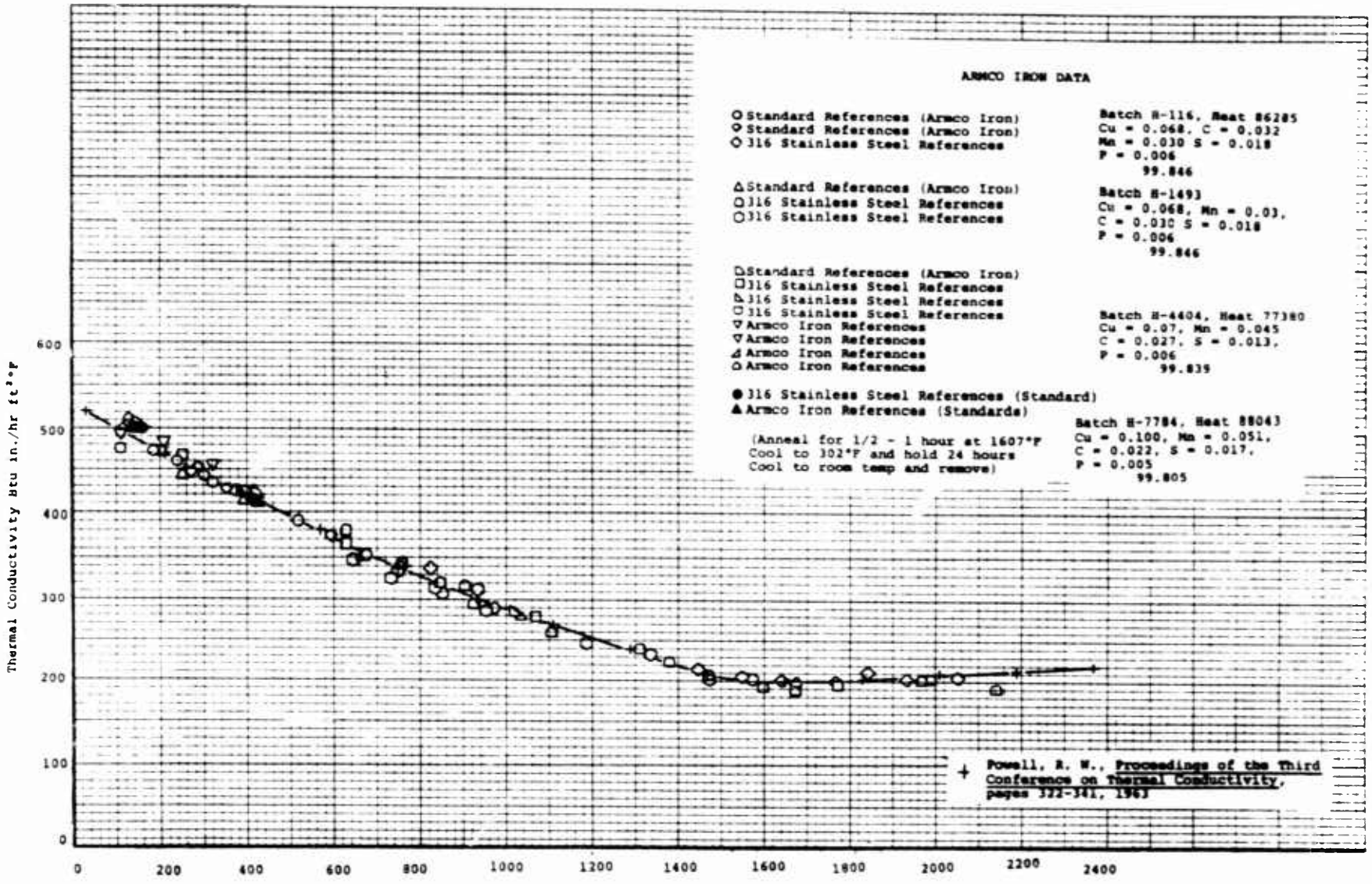

Figure 5. The Thermal Conductivity of Armco Iron

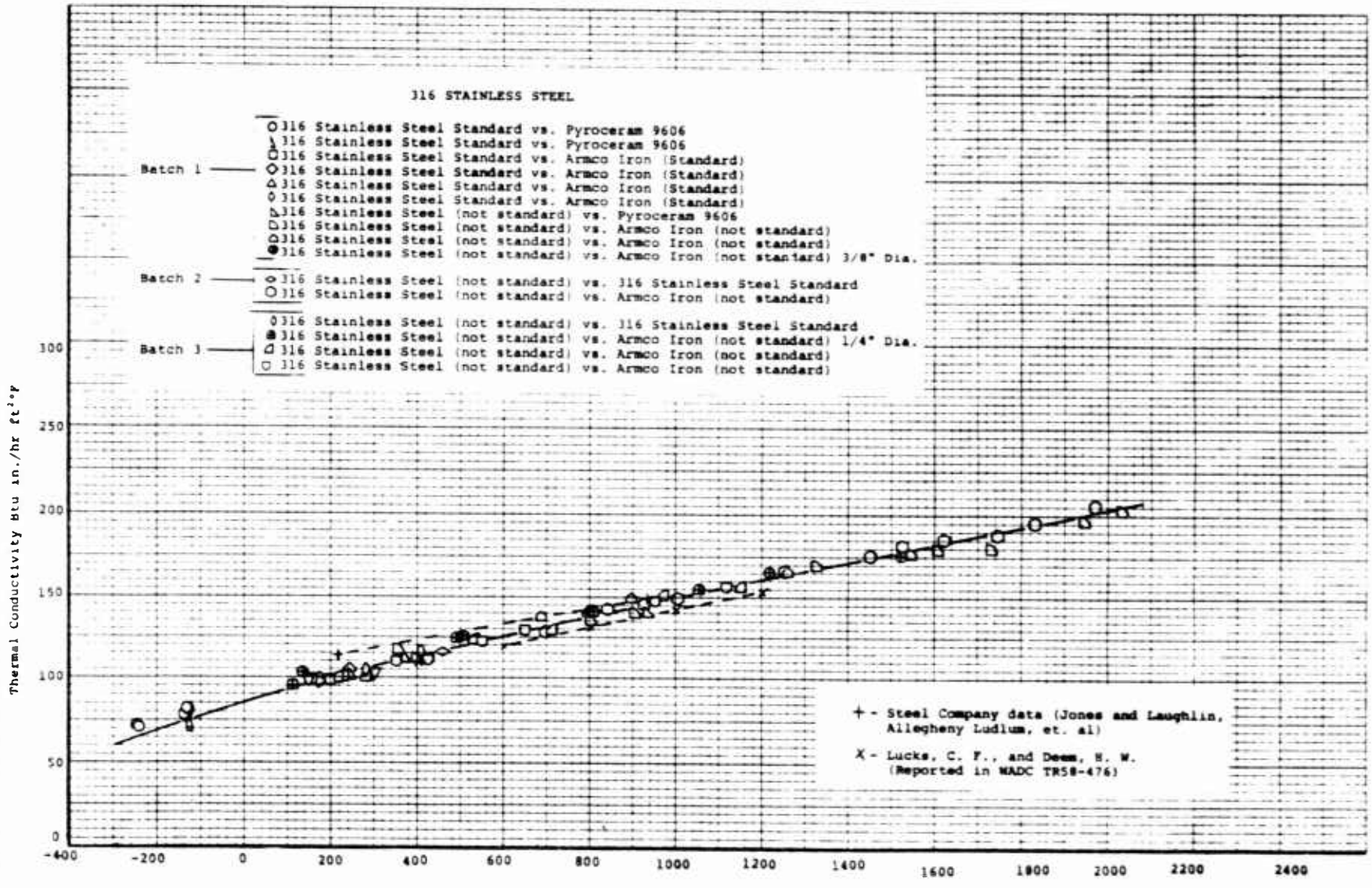

Figure 6. The Thermal Conductivity of 316 Stainless Steel

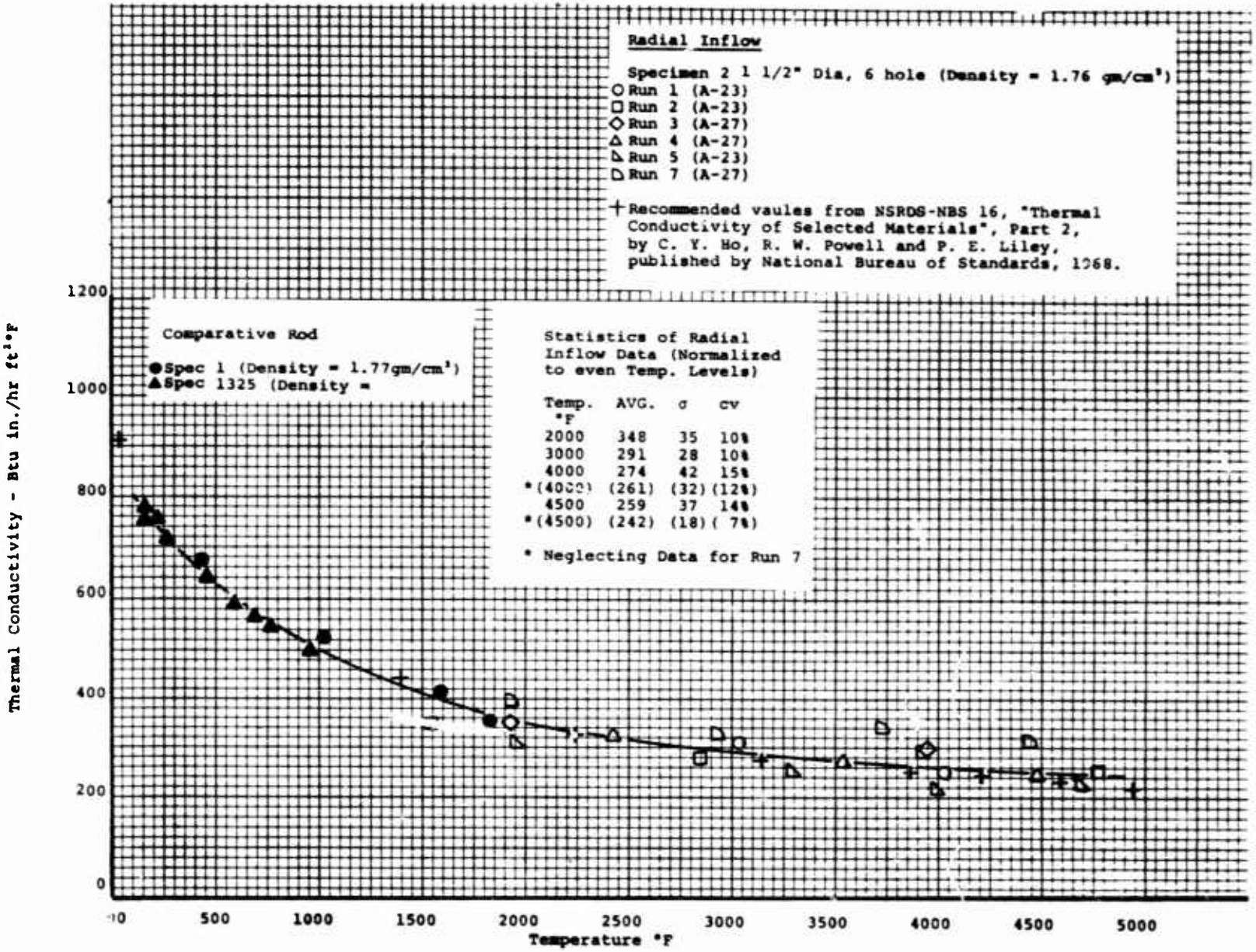

Figure 7. The Thermal Conductivity of ATJ Graphite, With Grain

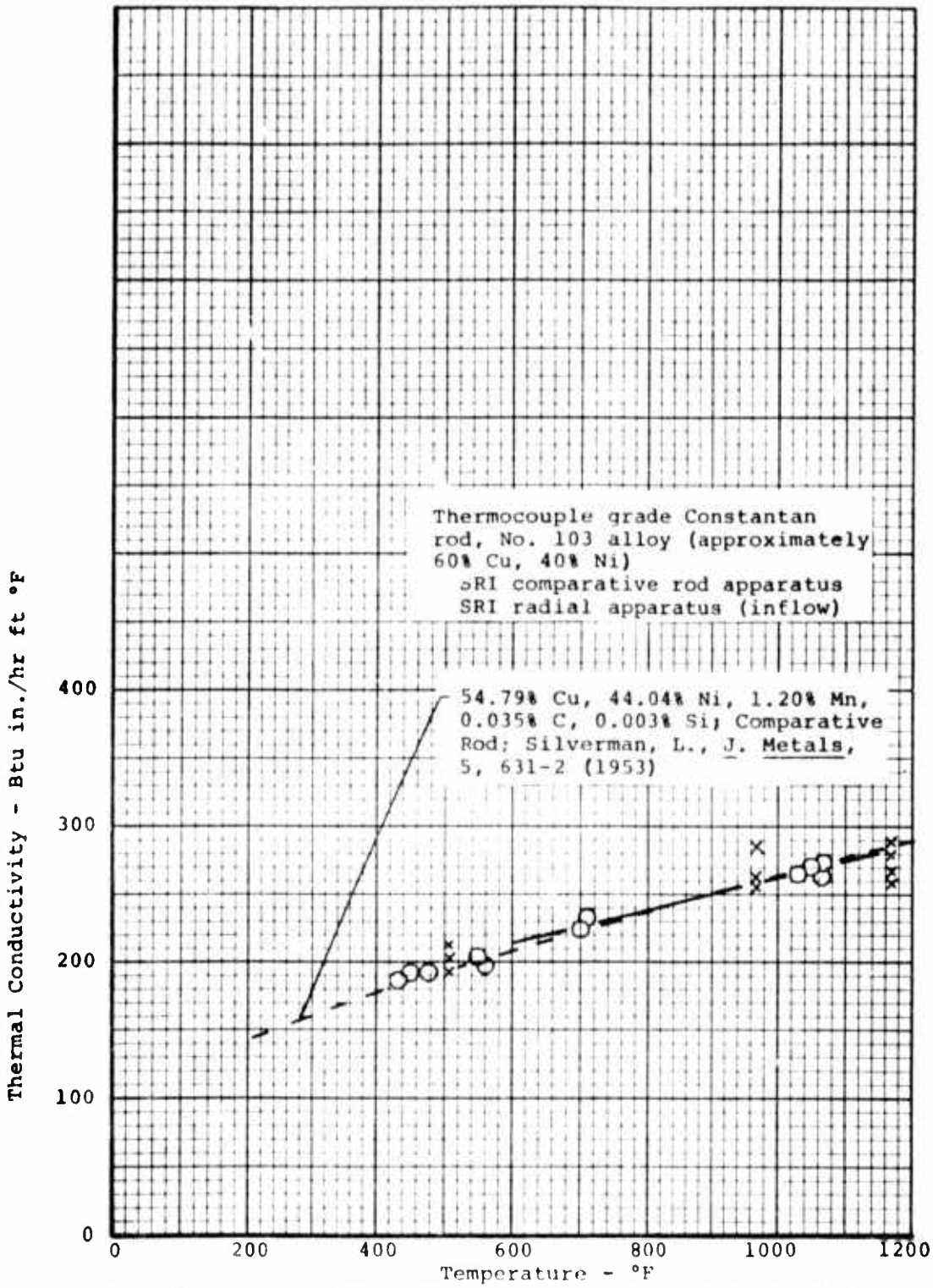

Figure 8. The Thermal Conductivity of Thermocouple Grade Constantan Rod

APPENDIX D

THERMAL CONDUCTIVITY TO 5500°F BY RADIAL INFLOW METHOD

The thermal conductivity is determined with a radial heat inflow apparatus that utilizes a central specimen 1" long. This apparatus is normally employed for measurements over the temperature range from 1500°F to 5500°F. Comparative rod apparatus is used at temperatures below 1500°F where radiant heating is less effective. The radial inflow apparatus gives a direct measurement of the thermal conductivity rather than a measurement relative to some standard reference material. A picture of the apparatus ready to be installed in the furnace is shown in Figure 1. The furnace and associated equipment for the thermal conductivity work is shown in Figure 2. In addition to the specimen, the apparatus consists primarily of (1) a water calorimeter that passes axially through the center of the specimen, (2) guards made from the same specimen material at both ends of the specimens to reduce axial heat losses, (3) sight tubes that allow the temperature at selected points in the specimen to be determined either by thermocouples or optical pyrometer and (4) an external radiant heat source (see Figure 3). The water calorimeter provides a heat sink at the center of the specimen to create a substantial heat flow through the specimen and allows the absolute value of the heat flow to be determined. Thermocouples mounted 1/2" apart in the calorimeter water stream measure the temperature rise of the water as it passes through the gage portion of the specimen. By metering the water flow through the calorimeter, it is possible to calculate the total radial heat flow through the 1/2" gage section of the specimen from the standard relationship $Q = MC\Delta T$. M is the weight of water flowing per hour, C is the specific heat of water and ΔT is the temperature rise of the water as it passes through the gage section.

The standard specimen configuration is shown in Figure 4. The specimen is 1.062" O.D. x 0.250" I.D. x 1" long. Holes 0.073" in diameter are drilled on radii of 0.233 and 0.437" to permit measurement of the radial temperature gradient. In specimens which are anisotropic in the diametral plane (for example, certain graphites) a second pair of holes is drilled 90° to the first pair. The diameters joining each pair of holes is located to coincide with the principal planes of anisotropy in the material.

A 1/2" long upper guard and a 1/2" long lower guard of specimen material are placed above and below the 1" long specimen to maintain a constant radial temperature gradient throughout the entire specimen length and thereby prevent axial heat flow in the

specimen. The outer ends of the specimen guards are insulated with graphite tubes filled with thermatomic carbon. These tubes also hold the specimen in alignment. The combined effect of specimen guards and thermatomic carbon insulation permits a minimum axial temperature gradient within the specimen. This gradient is not detectable by optical pyrometer readings. Visual inspection of the specimens after runs have verified that no large axial temperature gradient exists in the specimen. The guards, made of specimen material, display axial distortion of the isothermal lines for approximately 1/4" from the outer ends before reaching an apparent constant axial temperature.

When sufficient material is available the alternate specimen configuration shown in Figure 5 is employed. This specimen, being 1.5" in diameter, provides a larger gage length (0.357") between temperature wells and allows the installation of three holes on each radius without excessively distorting the radial temperature profiles. Thus this specimen configuration permits a more precise measurement of the average temperature at each radial location. As with the smaller specimen, the location of the temperature wells must be altered for transversely anisotropic specimens.

The annulus between the specimen inside diameter and the 7/32" outside diameter of the calorimeter tube is packed with either copper granules, graphite or zirconia powder. This packing provides a positive method for centering the calorimeter within the specimen and promotes good heat transfer between specimen and calorimeter.

Temperatures up to 2000°F are measured with Chromel/Alumel thermocouples inserted into the specimen through the sight tubes. At high temperatures, the temperatures are measured through the cer-tical sight tubes using a right-angle mirror device and optical pyrometer.

In Figures 1 and 3 showing a typical conductivity calorimeter apparatus ready for insertion into a furnace for a run, a water-cooled copper section can be seen at the top of the unit. This section provides permanent sight tubes to within about 2-1/2" of the guard specimen, in addition to a permanent mount for the right-angle mirror device used with the optical pyrometer. Within the short zone between the water-cooled section and the top guard, thin-walled graphite sight tubes are fitted. The remainder of the annulus is filled with thermatomic carbon insulation.

During thermal conductivity runs, the following data are recorded: (1) power input, (2) specimen face temperature, (3) specimen temperatures in the gage section at the two radii, (4) temperature of the calorimeter water at two points 1/2" apart axially within the specimen center and (5) water flow rate through the calorimeter. At least 5 readings are made at each general temperature range to determine the normal data scatter and to minimize the error that might be encountered in a single reading.

All thermocouple readings are measured on a Leeds and Northrup K-3 null balance potentiometer used in conjunction with a galvanometer of 0.43 microvolts per mm deflection sensitivity. All optically measured temperatures are read with a Leeds and Northrup Type 8622 optical pyrometer. The flow rate of the calorimeter water is measured with a Fischer and Porter Stabl-Vis Flowrater.

The thermal conductivity values are computed from the relation

$$K = \frac{Q \ln \frac{r_2}{r_1}}{2\pi L \, (T_{r_2} - T_{r_1})}$$

where

Q = the heat flow to and measured by the calorimeter
r_2 = the radius to the outer temperature well
r_1 = the radius to the inner temperature well
T_{r_2} = temperature at r_2
T_{r_1} = temperature at r_1
L = the gage length over which the calorimeter ΔT is measured, for our present calorimeter is 1/2 inch

Based on an extensive error analysis and calibrations on homogeneous isotropic materials of known thermal conductivities, such as Armco iron and tungsten, the precision (coefficient of variation) in the measurements has been established at ±7 percent over the temperature range. For multiple runs on samples having similar properties, the uncertainty in a smooth curve through the data can be established to within ±7 percent. A detailed error analysis has been presented in a paper by Mann and Pears.[1]

Data obtained here on several high temperature materials are presented in Figures 6, 7 & 8. Figure 6 is a plot of data obtained here on tungsten. The specimen for these determinations were fabricated from stacks of 0.060 inch washers cut from hot rolled sheet stock. Also plotted are values reported by other investigators including "recommended values" given by Powell, Ho and Liley[2] based on a compilation of 103 sets of data. Agree-

---

[1] Mann, W. H. Jr., and C. D. Pears, "A Radial Heat Flow Method for the Measurement of Thermal Conductivity to 5200°F", presented at the Conference on Thermal Conductivity Methods, Battelle Memorial Institute, October 26-28, 1961.

[2] Powell, R. W., C. Y. Ho and P. E. Liley, "Thermal Conductivity of Selected Materials", NSRDS-NBS 8, National Standard Reference Data Series - National Bureau of Standards - 8, 1966, pp. 11, 54-59.

the recommended values is excellent throughout the temperature range.

Figure 7 shows data obtained here on ATJ graphite, with grain. This material is premium grade, medium grain graphite having a density range of 1.73 to 1.78 gm/cm^3. The crosses (+) shown in the figure are "recommended values" given by Ho, Powell and Liley.[3] Again agreement is excellent.

Figure 8 shows data obtained on AXM-5Q1. These data were obtained under a program sponsored by the Air Force Materials Laboratory to develop high temperature thermal conductivity standards. Measurements were made on this material by four laboratories in addition to Southern Research Institute. The bands shown in Figure 8 represent the range of data reported by the other participating organizations. A complete presentation and discussion of the data are given in AFML-TR-69-2.[4]

---

[3] Ho, C. Y., R. W. Powell and P. E. Liley, "Thermal Conductivity of Selected Materials, Part 2," NSRDS-NBS 16 National Standard Reference Data Series - National Bureau of Standards-16, pp. 89-128.

[4] AFML-TR-69-2, "Development of High Temperature Thermal Conductivity Standards" submitted by Arthur D. Little, Inc., under Contract AF33(615)-2874, 1969, pp. 115-127.

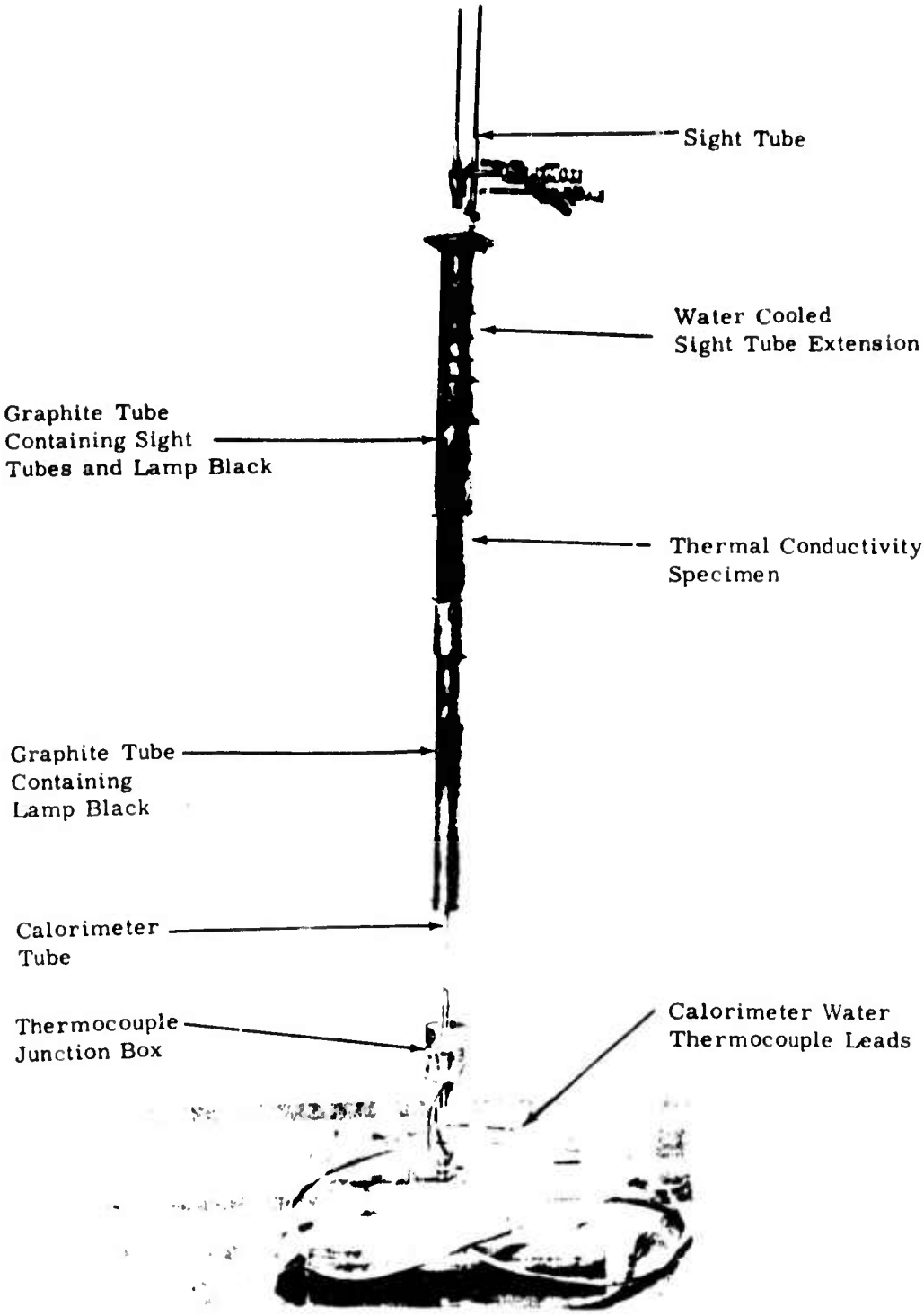

Figure 1. Picture of the Radial Thermal Conductivity Apparatus

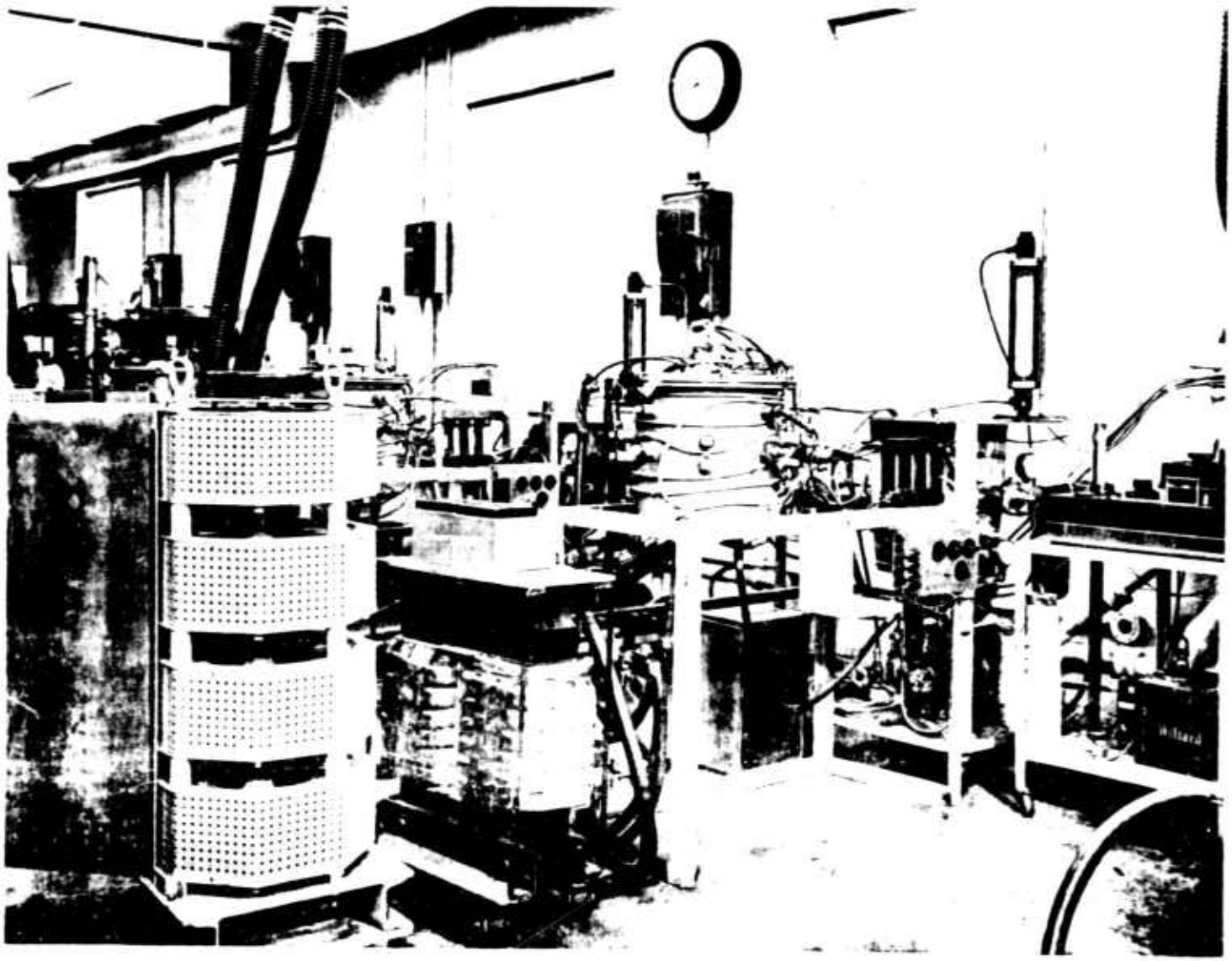

Figure 2. Furnace with Thermal Conductivity Apparatus Installed

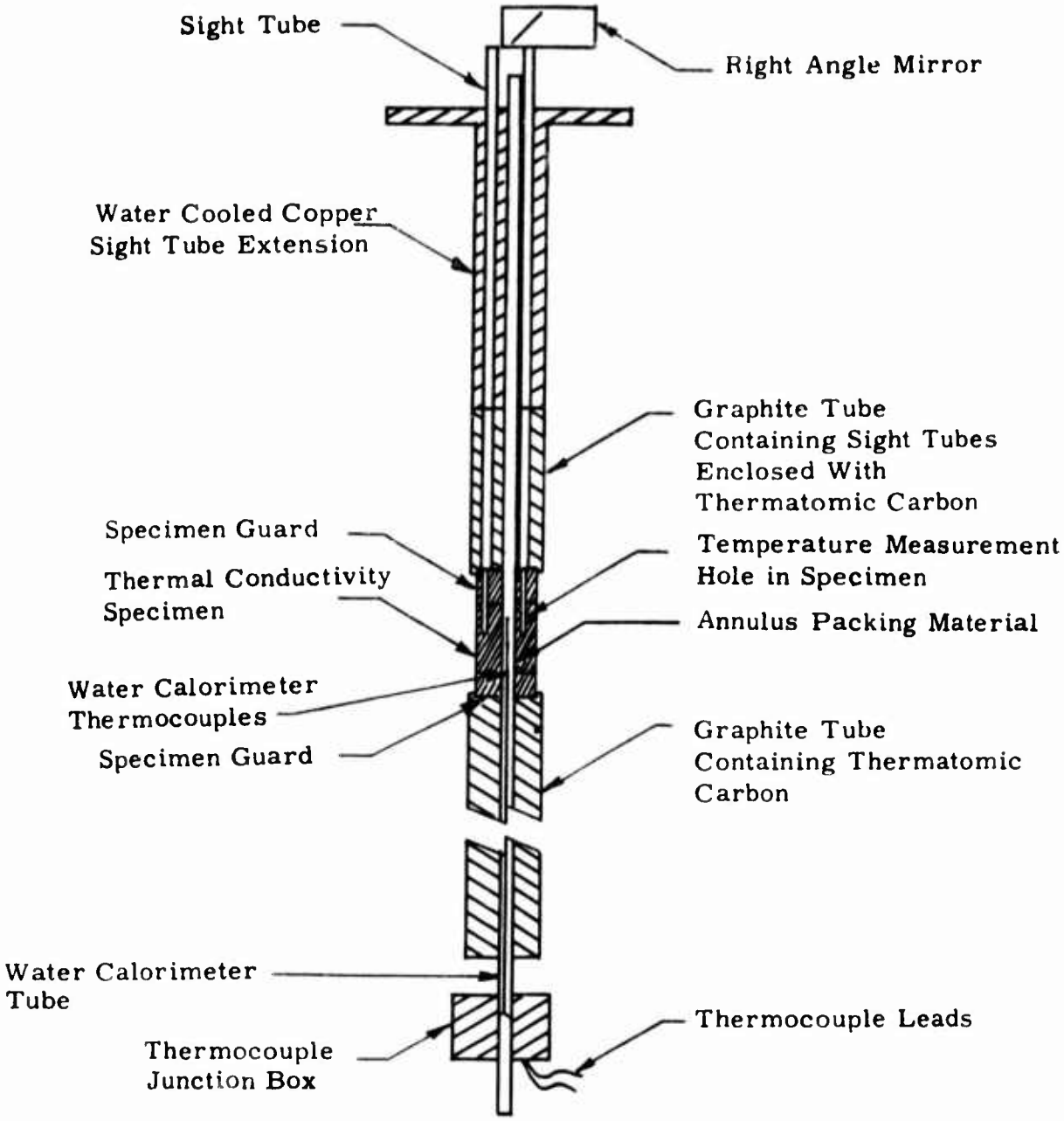

Figure 3. Cross-section Schematic of the Thermal Conductivity Apparatus

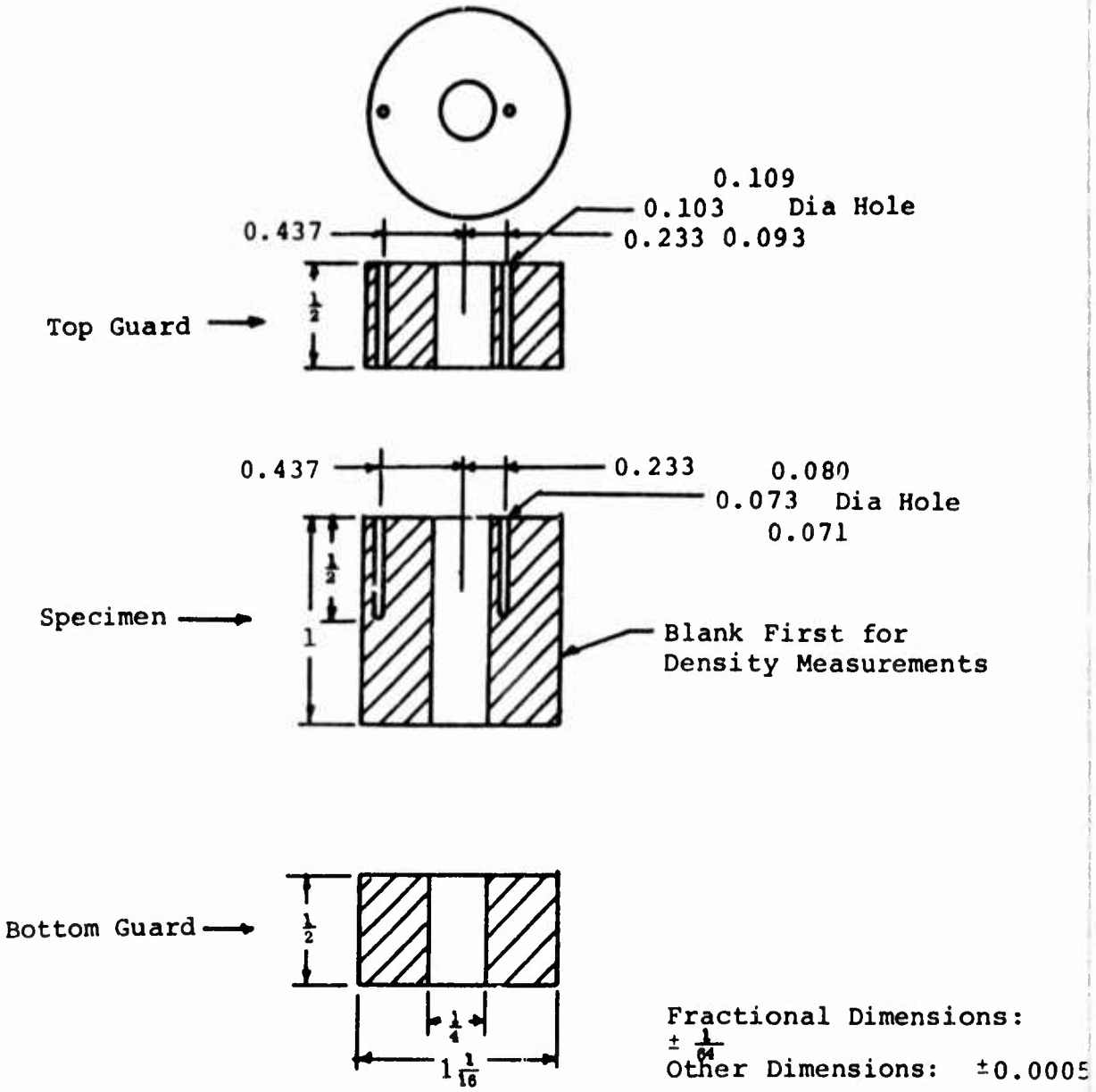

Figure 4. 1.06 Diameter Thermal Conductivity Specimen for Radial Inflow Apparatus

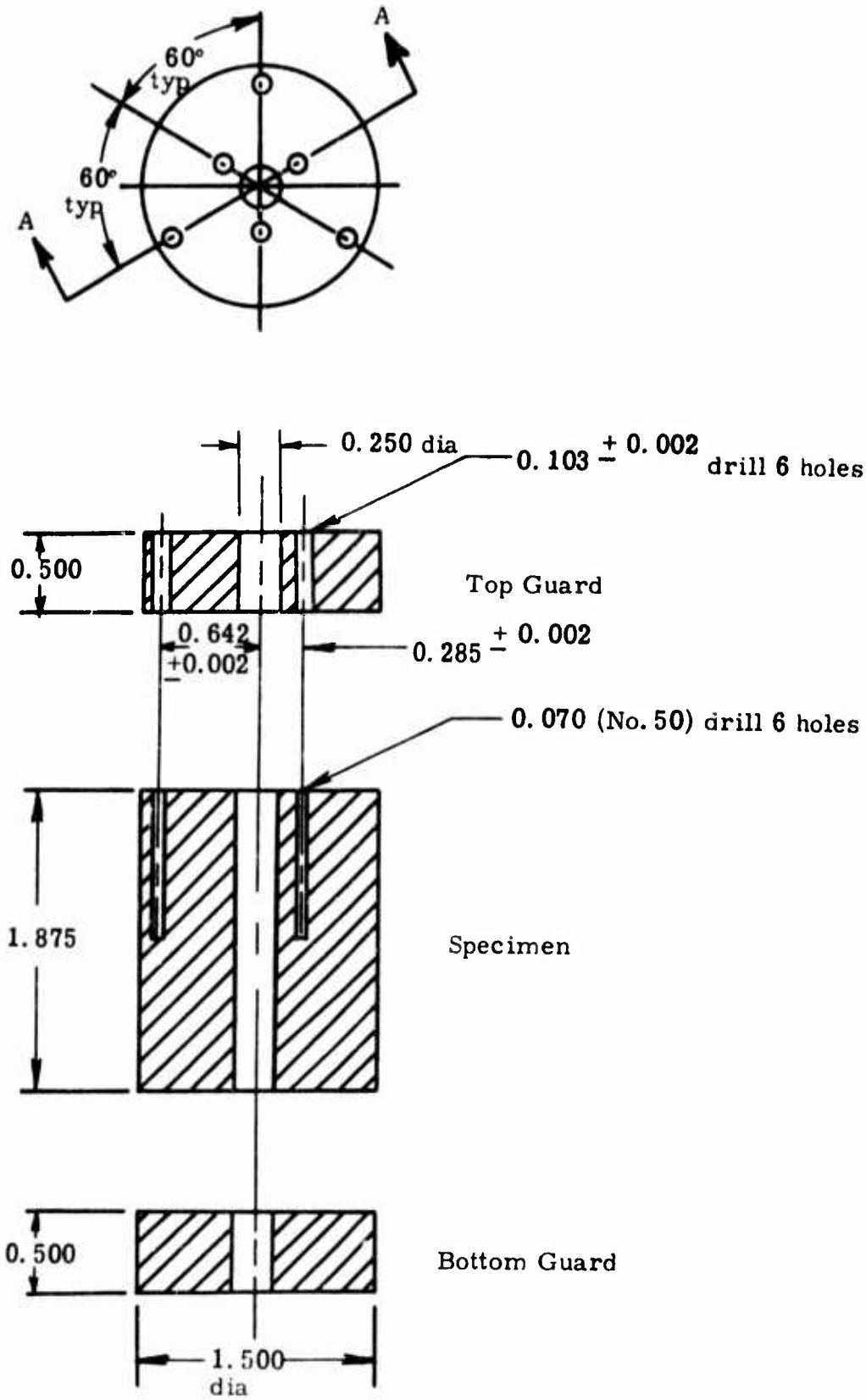

Figure 5. Dimensions of 1.50 Inch Diameter Specimen and Guards Used for Radial Inflow Thermal Conductivity Measurements

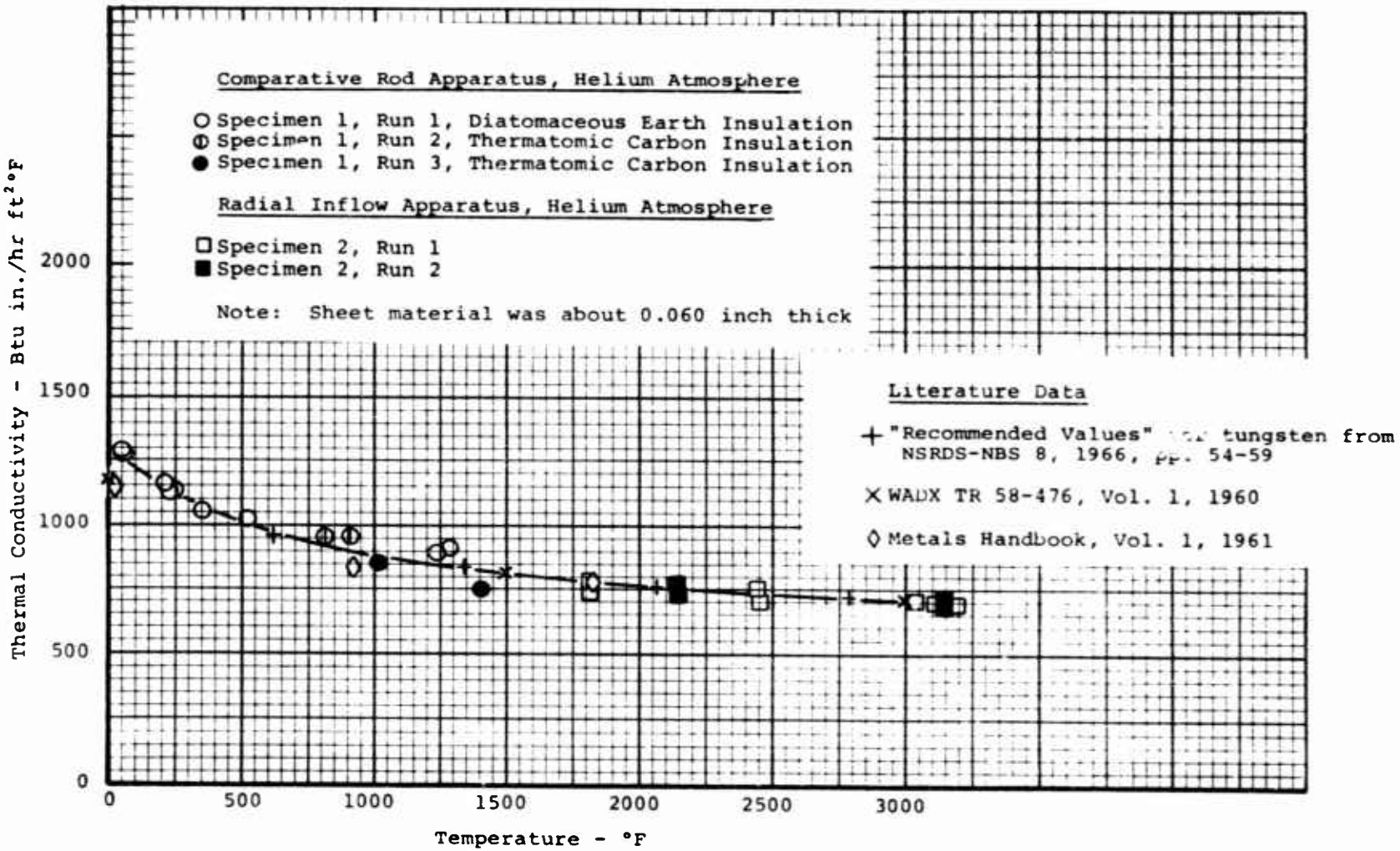

Figure 6. The Thermal Conductivity of Tungsten Sheet Parallel to the Plane of the Sheet

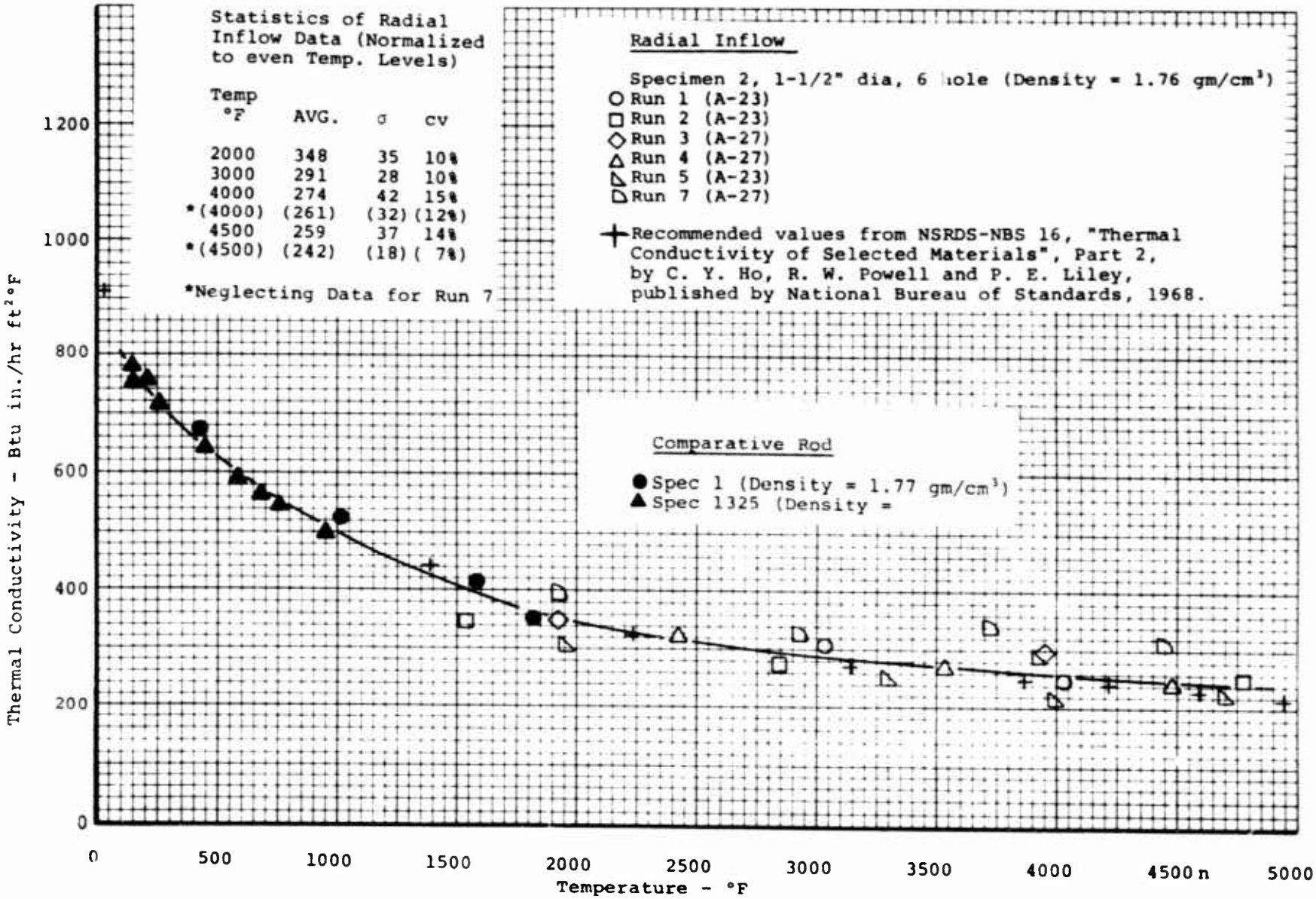

Figure 7. The Thermal Conductivity of ATJ Graphite, With Grain

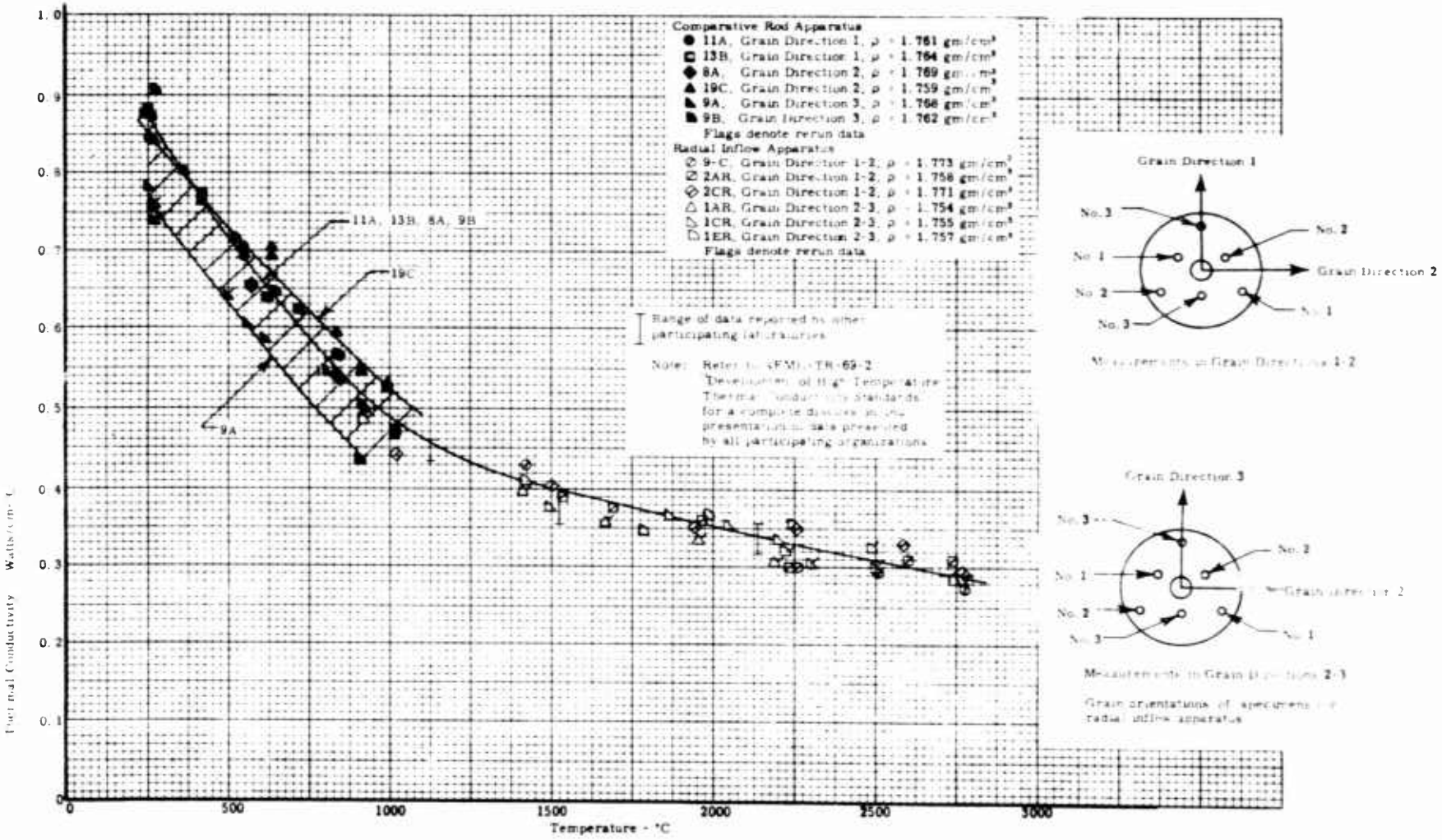

Figure 8. The Thermal Conductivity of AXM-5QI Graphite

APPENDIX II

MECHANICAL PROPERTIES SoRI

SoRI-EAS-73-183

MECHANICAL PROPERTIES OF PYROLYTIC GRAPHITE AND CODEPOSITED SiC/PG WITH VARIOUS WEIGHT PERCENTAGES OF SILICON-CARBIDE

FINAL REPORT

to

ATLANTIC RESEARCH CORPORATION
Alexandria, Virginia

Purchase Order 78119

Southern Research Institute
2000 Ninth Avenue South
Birmingham, Alabama 35205
June, 1973

Project 2931-II-F

TABLE OF CONTENTS

LIST OF ILLUSTRATIONS

LIST OF ILLUSTRATIONS - CONTINUED

135

Mechanical Properties of Pyrolytic Graphite and Codeposited SiC/PG with Various Weight Percentages of Silicon-Carbide

INTRODUCTION

This is the final report covering work performed under Atlantic Research Purchase Order 91138 (F04611-73-C-0012). The tensile and compressive properties were determined for Pyrolytic Graphite and Codeposited SiC/PG with various weight percentages of silicon carbide. The test matrix for the evaluations is presented in Table 1.

The thermal properties of these materials are reported in SoRI Report EAS-73-031 (January, 1973).

MATERIAL

The material was furnished by Atlantic Research Corporation primarily in the form of cylinders of various lengths up to 9 inches. The pyrolytic graphite was deposited on the 2 inch I.D. of AGSR graphite cylinders and the codeposited SiC/PG was deposited on the 2 inch I.D. of ATJ graphite cylinders. The thicknesses of the deposited layers varied from cylinder to cylinder and along each cylinder length. The pyrolytic graphite layers on the AGSR cylinders were not as thick as the codeposited SiC/PG on the ATJ and as a result, representative coupon specimens could not be obtained for the PG material.

In an attempt to supply thicker samples of PG, Atlantic Research prepared 6 strips of PG approximately 13 inches long x 1-3/4-inch wide x various thicknesses. Although thicker, the strips were warped and we were unable to obtain straight specimens with sufficient thickness.

In an effort to obtain some tensile information on the Atlantic Research PG material, two small pieces (033-25), with nominal dimensions of 3-1/4-inches x 2 inches x approximately 0.1 inch thickness were utilized to obtain four subsize tensile specimens. (See Figure 1.)

From the materials supplied, the following cylinders were selected for evaluation:

Material Designation	Nominal Composition	Number and Type of Specimen obtained
033-25[a]	PG	4 Coupon tensiles
C- 1	20% SiC/PG	1 Cylinder tensile
C- 3	20% SiC/PG	1 Cylinder tensile
C-39	20% SiC/PG	5 Coupon tensiles
C-43	20% SiC/PG	5 Coupon tensiles
C-35	20% SiC/PG	5 Coupon tensiles
C-55	8% SiC/PG	5 Coupon tensiles
C-53	8% SiC/PG	5 Coupon tensiles
C- 1[b]	20% SiC/PG	1 Cylinder compression[b]
C-16	PG	1 Cylinder compression
C-18	PG	1 Cylinder compression
C-45	20% SiC/PG	1 Cylinder compression
C-51	8% SiC/PG	1 Cylinder compression
C-49	20% SiC PG	1 Cylinder compression
C-23	20% SiC/PG	1 Cylinder compression
C-21	20% SiC/PG	5 Coupon compressions
C-33	20% SiC/PG	5 Coupon compressions
C-59	8% SiC/PG	5 Coupon compressions
C-30	PG	5 "C" Coupon tensiles

[a]Flate plate
[b]Specimen was initially evaluated in tension

APPARATUS AND PROCEDURES

Tension

The tensile evaluations were performed in a gas-bearing tensile facility. The tensile machine utilizes gas-bearing universals in the load linkage to prevent the introduction of unknown bending moments into the load train from crosshead motion and to allow monitoring of the straightness of the load train. The primary components of a facility are the load frame, the mechanical drive system, the gas-bearing universals, a 5500°F furnace, optical strain analyzers, and associated instrumentation for measurement of load and strain. The load capacity is 15,000 pounds.

The load frame and mechanical drive system are similar to those of many good facilities. The upper crosshead is positioned by a small electrical motor connected to a precision screw jack. This crosshead is stationary during loading and is moved only when assembling the load train. The lower crosshead is used to apply the load to the specimen through a precision screw jack, which is chain-driven by a variable speed motor and gear reducer.

The unique feature of the facility that distinguishes it from other good facilities is the use of gas-bearing universals in the specimen load train to eliminate bending moments and hence provide true uniaxial tensile loading of the specimen.

Strain measurements were made using optical strain analyzers. These analyzers track strain targets attached to the specimen and permit an automated continuous readout of strain. A complete tensile facility is described in Appendix A.

Initially, the evaluations were to be conducted on cylindrical specimens for both tension and compression in the ab direction. Two cylindrical tensile specimens (C-1 and C-3) were prepared to the design shown in Figure 2 to check out the feasibility of evaluating cylindrical tube specimens. The first tensile evaluation (C-1) at 70°F resulted in a specimen head failure at a relatively low stress level. Since the gage section wall thickness was already 0.030 inch, it seemed fruitless to attempt specimen redesign or modification. The decision was made to attempt to use coupon specimens designed as shown in Figure 3, and to modify the remaining cylinder specimen (C-3) so that it could be evaluated to gage failure at 70°F. Specimen C-3 was modified by machining away the ATJ substrate, replacing the ATJ with aluminum sleeves epoxy bonded to the codeposited SiC/PG, and then remachining the aluminum sleeves with the specimen shoulder profile shown in Figure 2.

The coupon tensile specimen design proved successful and modified C-3 cylinder specimen was only partially successful. Therefore, the coupon tensile specimen design was used for the "ab" tensile evaluations of the cylinders.

The "c" direction tensile evaluations at 70°F were also conducted in the gas-bearing tensile facility. Due to the thickness of the material, strain measurements were not possible and strength only was determined when the strength of the test material was less than that of the epoxy bonding used to transfer the load to the specimen. The specimen assembly is shown in Figure 4.

Compression

The compressive evaluations were performed in a gas-bearing compressive facility. The facility is similar in operation to the tensile facility, except the gas-bearing universals are used only to initially precision align the specimen load train and are not in operation during the actual evaluation. The compressive facility is described in Appendix B. The coupon compressive specimen used in the evaluations is shown in Figure 5. To evaluate this specimen in compression required laterally supporting the specimen with low friction inserts to increase the stability. This is a common technique in the evaluation of thin sheets and has been used successfully at SoRI on many past programs. To confirm that the coupons yielded representative data, six total cylinder specimens were machined to the design shown in Figure 6 and evaluated in compression. As discussed later, good agreement was obtained between the coupon specimens and these total cylinder specimens.

DATA AND RESULTS

Tension - "ab" Direction

The results of the tensile evaluations of the PG and SiC/PG in the "ab" direction are presented in Table 2 and Figures 7 through 12. Composite plots of the tensile stress-strain curves for 16% SiC/PG, 20% SiC/PG, and 27% SiC/PG are shown in Figures 13, 14, and 15, respectively. Individual stress-strain curves are presented in Appendix C.

The "ab" tensile strength versus temperature for various percentages of SiC are shown in Figure 7. The strengths of the codeposited SiC/PG, for 70°F to 3000°F, were significantly increased by the increasing weight percentage of SiC. The 20 to 27% SiC/PG material exhibited strengths 2 to 3 times greater than the Atlantic Research pure PG (ARC-PG). The 70°F strengths are shown as a function of percentage SiC in Figure 8. The increase in 70°F strengths appeared to be approximately linear with increasing SiC percentage between 10 and 30% SiC.

The strengths of material containing above 20% SiC peaked at about 3000°F, but the material containing 13 and 16% attained peak strengths at about 4000°F. This indicates that the strengthening effects of the SiC are probably maximum at about 3000°F and above 3000°F the effects decrease rapidly to 4500°F. Figures 8, 9, and 10 illustrate this observation. In Figures 8 and 9, the 70°F and 3000°F tensile strengths are shown to be a strong, almost linear, function of SiC content. At 4500°F (see Figure 10), the strengthing effect of the SiC has diminished significantly, suggesting very little correlation with SiC content.

The "ab" tensile elastic moduli versus temperature for various percentages of SiC/PG are presented in Figure 11. As with the strength, the elastic modulus was an increasing function of SiC content. At 70°F, the moduli of ARC-PG was about 3.5 x 10^6psi and for 27% SiC/PG was about 5.7 x 10^6psi. The stiffening effect of the SiC was observed in all the evaluations to above 4000°F. At 4500°F, the stiffening effect was diminished but could still be observed in the data. The moduli values for all the various percentages of SiC/PG peaked at 3000°F.

The "ab" tensile strains-to-failure versus temperature for the various percentages of SiC/PG are shown in Figure 12. The data indicate an increase in strains-to-failure with increasing SiC content from 70°F to above 4000°F. The data were not as ordered as the strength and modulus data but the 20 to 27% SiC content specimens exhibited higher total strains than the 13 to 16% SiC content specimens. At 4500°F, the results were mixed.

A composite of the tensile stress-strain curves for 16% SiC/PG (Cylinder C-55) are shown in Figure 13. The stress-strain response was linear to fracture at 70°F and 3000°F but became slightly bilinear between 3000°F and 4000°F. Bilinear response was recorded at 4500°F. The stress-strain response of the 20% SiC/PG (Cylinder C-35) was similar as shown in Figure 14. The stress-strain response of the 27% SiC/PG (Cylinder C-39) was slightly bilinear at 70°F and became increasingly bilinear with increasing temperature (See Figure 15).

Tension - "c" Direction

The results of the "c" direction tensile strength evaluations at 70°F are presented in Table 3. Tensile failures of specimen materials were obtained only in the ARC-PG specimens. In the SiC/PG specimens, tensile failures occurred in the epoxy bond (see Figure 4). The average "c" direction tensile strength of the ARC-PG at 70°F was 792 psi and the strengths of the SiC/PG specimens were greater than 3000 psi. Therefore, the additions of SiC to PG resulted in a significant increase in "c" direction tensile strength.

Compression

The results of the compressive evaluations of the PG and SiC/PG are presented in Table 4. The compressive moduli versus temperature are presented in Figure 16 and composite plots of the compressive stress-strain curves for 13% SiC/PG, 16% SiC/PG, and 25% SiC/PG materials are presented in Figures 17, 18, and 19. Individual stress-strain curves are presented in Appendix D.

The effect of SiC content on the compressive elastic modulus was approximately the same as in tension; increase in modulus with increasing SiC content (see Figure 16). Although the compressive runs at elevated temperatures were conducted at only 3000°F and 4500°F, the moduli apparently peaked at 3000°F; the same as the tensile moduli. The stiffening effects of the SiC content were diminished significantly at 4500°F.

As mentioned earlier, the majority of the compressive evaluations were performed on coupon specimens (see Figure 5) using lateral supports to increase stability. To confirm that the coupon specimens gave representative compressive data, several total cylinder specimens were evaluated at 70°F for comparison. Good agreement between the total cylinders and coupon specimens was obtained as shown in Figures 18 and 19. In these figures, the compressive stress-strain response of the total cylinder specimens are shown as dashed curves. The coupon specimens generally gave excellent stress-strain data at strains up to 0.010 to 0.020 in./in. In this strain range, most stress-strain records showed a sudden increase in slope (see Appendix D) indicating that the lateral supports were probably beginning to support some of the compressive load. Stress-strain data after the sudden increase in curve slope were disregarded.

For comparison, the compressive stress-strain curves for the total cylinders of ARC-PG (Cylinders C-16 and C-18) are included in the composite plots in Figures 17, 18, and 19. The addition of SiC changed the character of the stress-strain curves from linear to bilinear. Strength, stiffness, and strain-to-failure increased with increasing (13% to 25%) SiC content at 70°F and 3000°F. At 4500°F, the stress-strain responses appeared to be independent of SiC content.

CONCLUSIONS

The addition of SiC to PG increased the strength, stiffness, and strains-to-failure in both tension and compression over the temperature range 70°F to 3000°F. The increase in these properties appeared to be almost linear with increasing

SiC content between 10 and 30%. Above 3000°F, the strengthening effect of the SiC began to decrease and was significantly diminished at 4500°F.

Submitted by:

J. K. Legg

J. K. Legg, Head
Applied Mechanics Section

Approved:

C D Pears, by

C. D. Pears, Head
Mechanical Engineering and
Mechanics Division

SoRI-EAS-73-183
P-2931-II-F

(5:12) lh

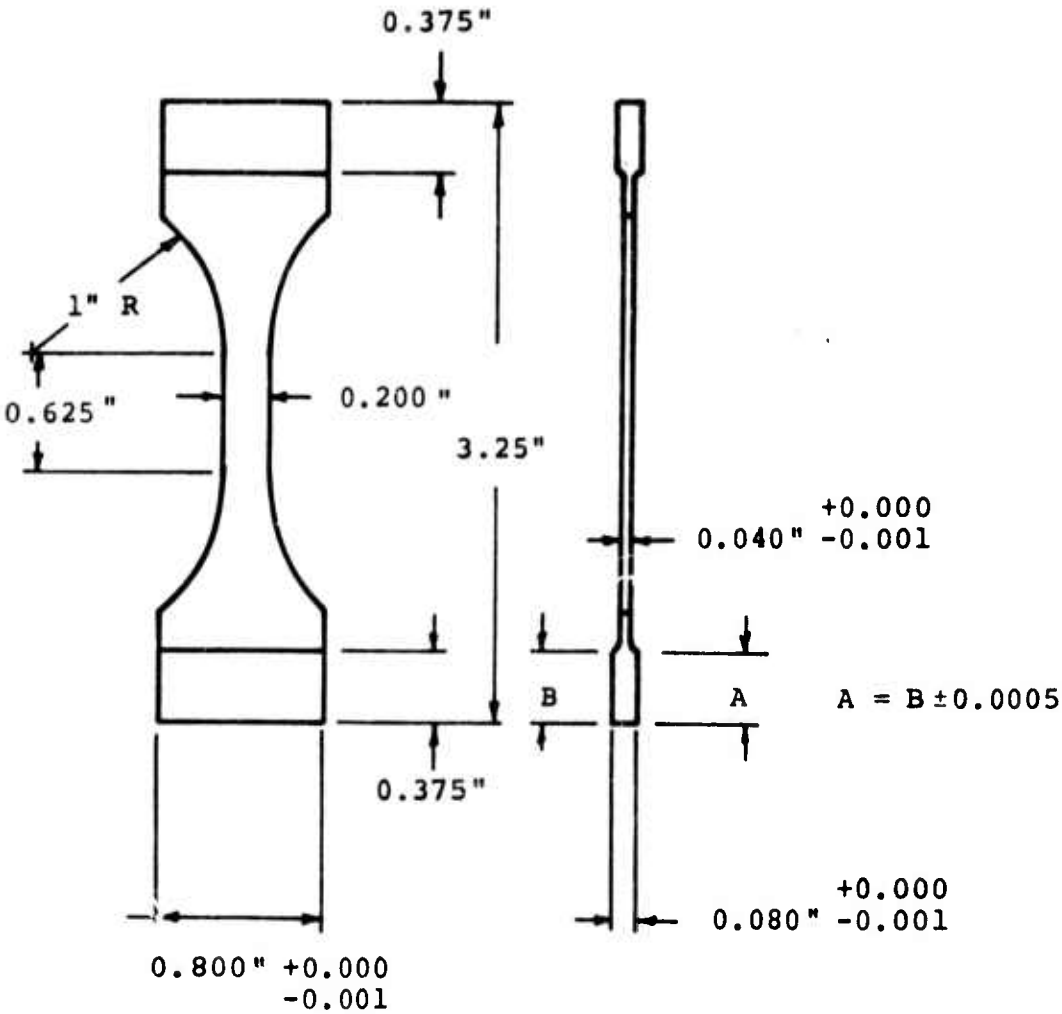

Figure 1. Subsize Tensile Specimen for PG Flat Plate

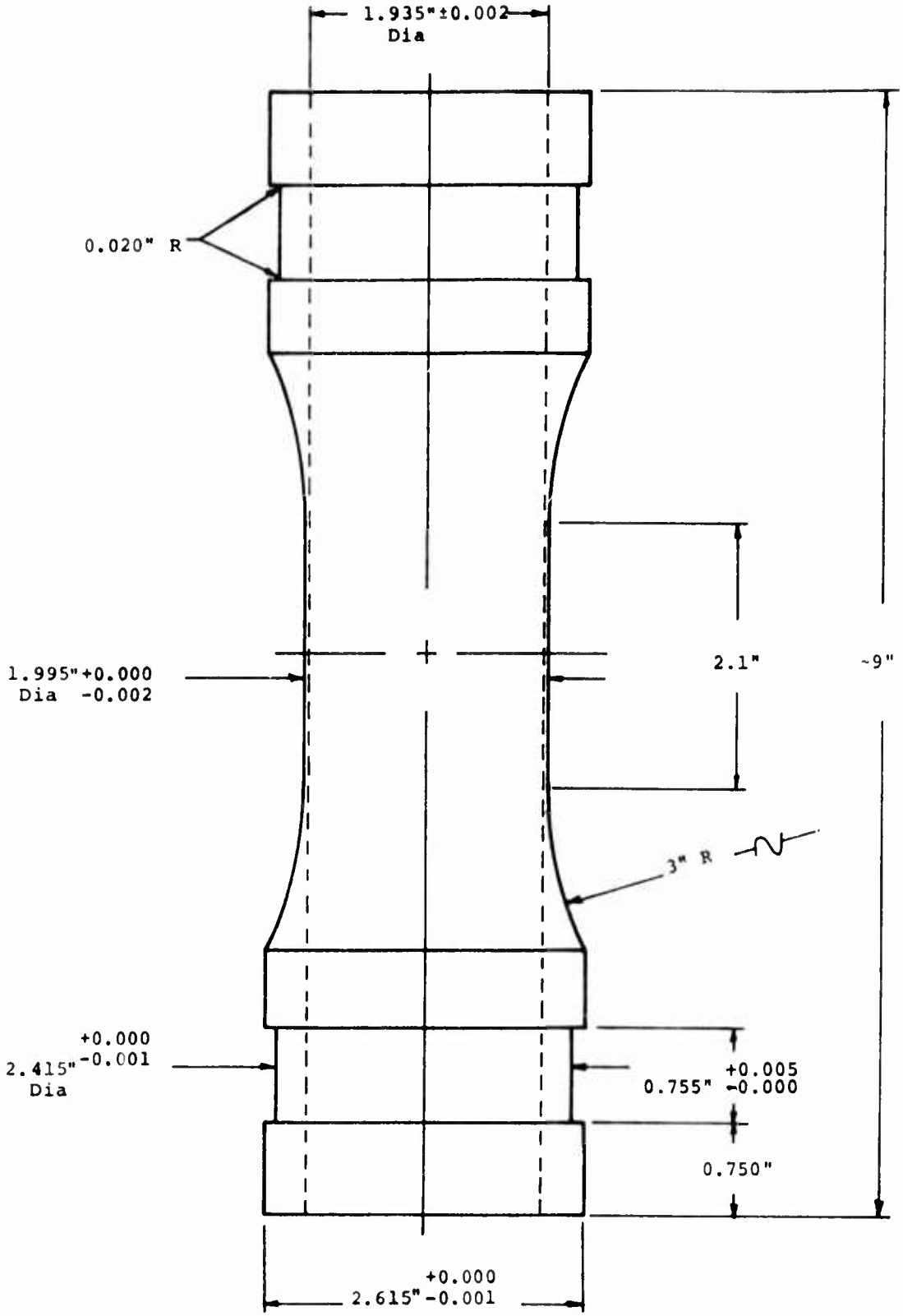

Figure 2. Axial Cylindrical Tensile Specimen for Codeposited PG/SiC on ATJ

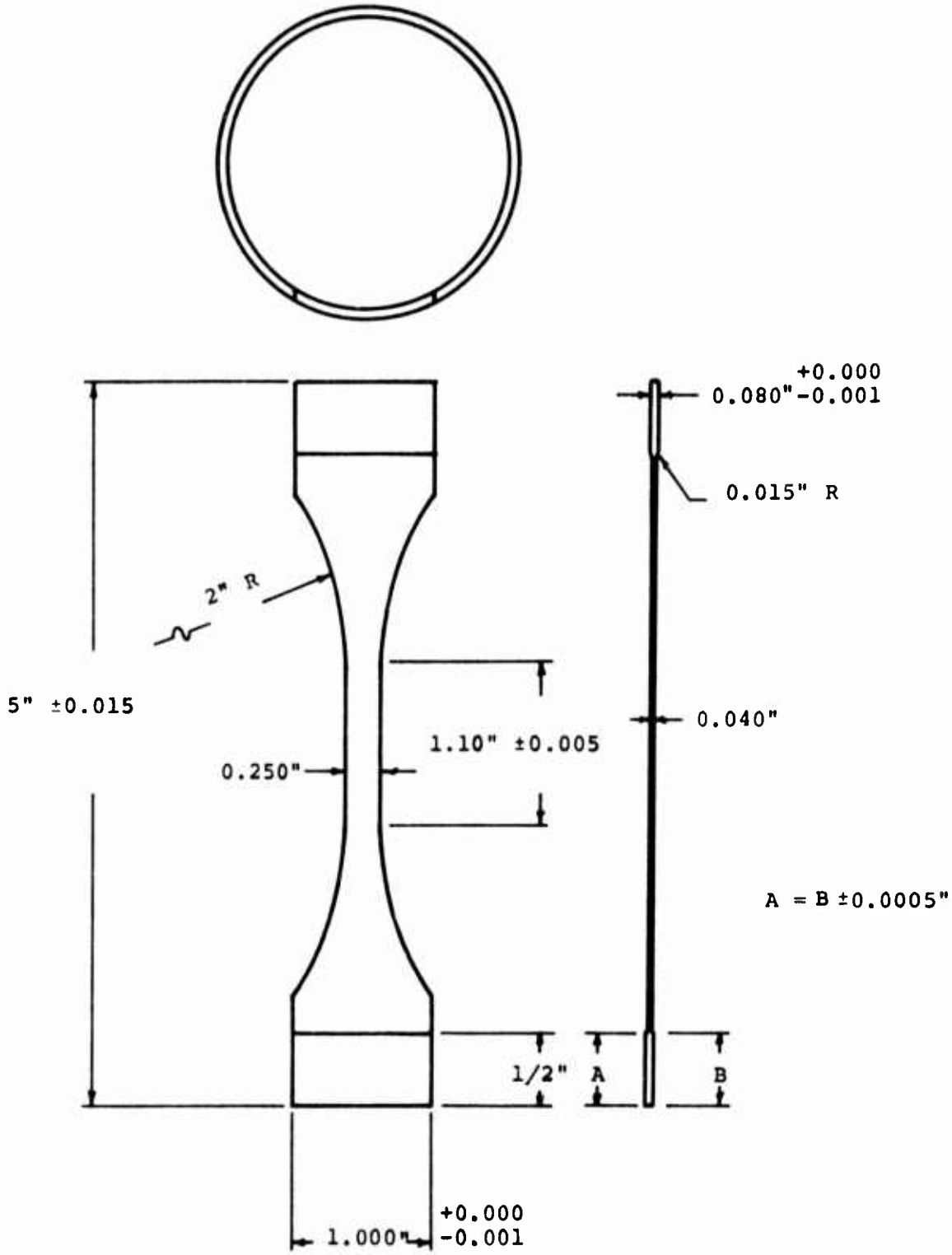

Figure 3. Coupon Tensile Specimen for Evaluation of Codeposited PG/Sic Cylinders in the ab Direction

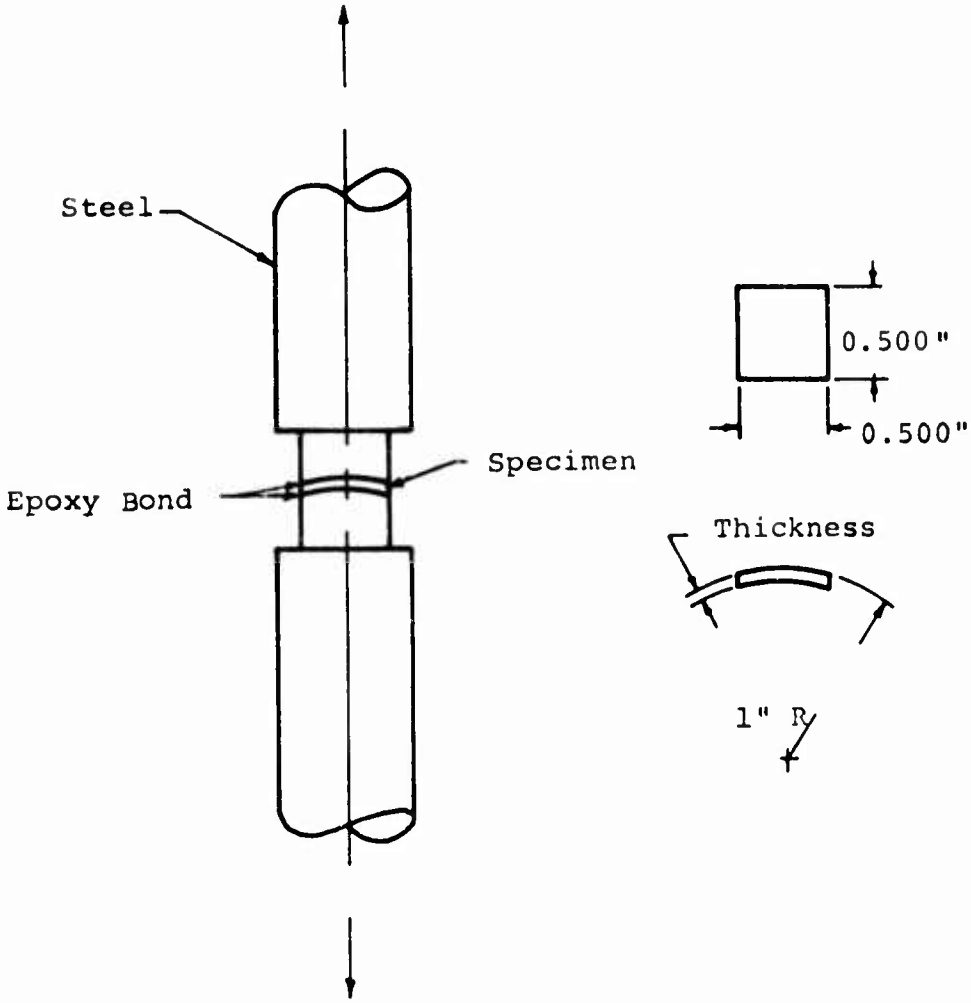

Figure 4. Specimen Assembly for Evaluation of PG and Codeposited SiC/PG Cylinders in the "c" Direction

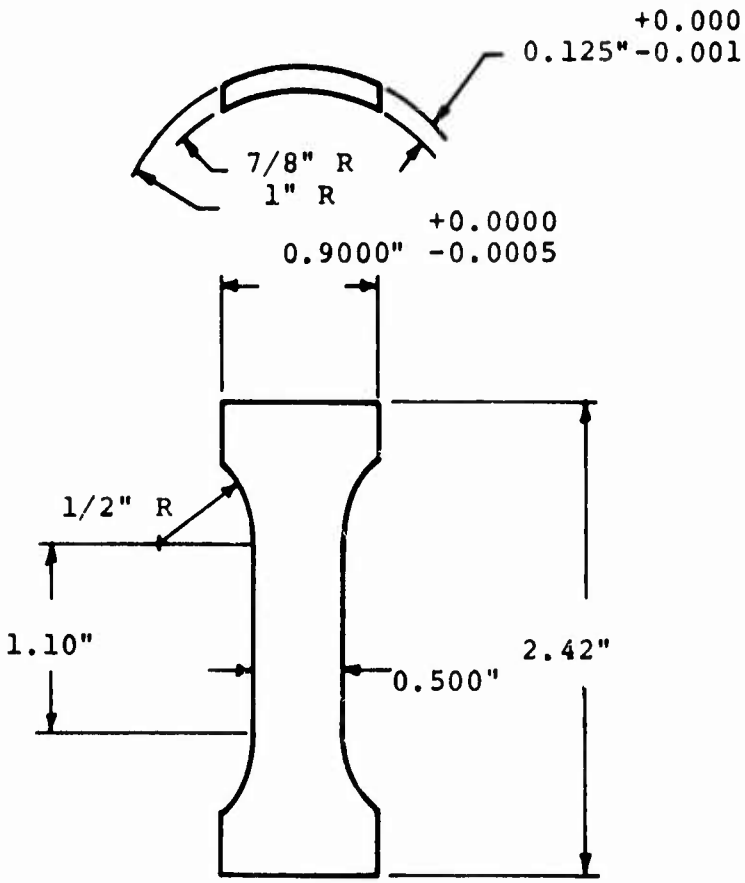

Figure 5. Compressive Specimen for Codeposited PG and SiC Cylinders

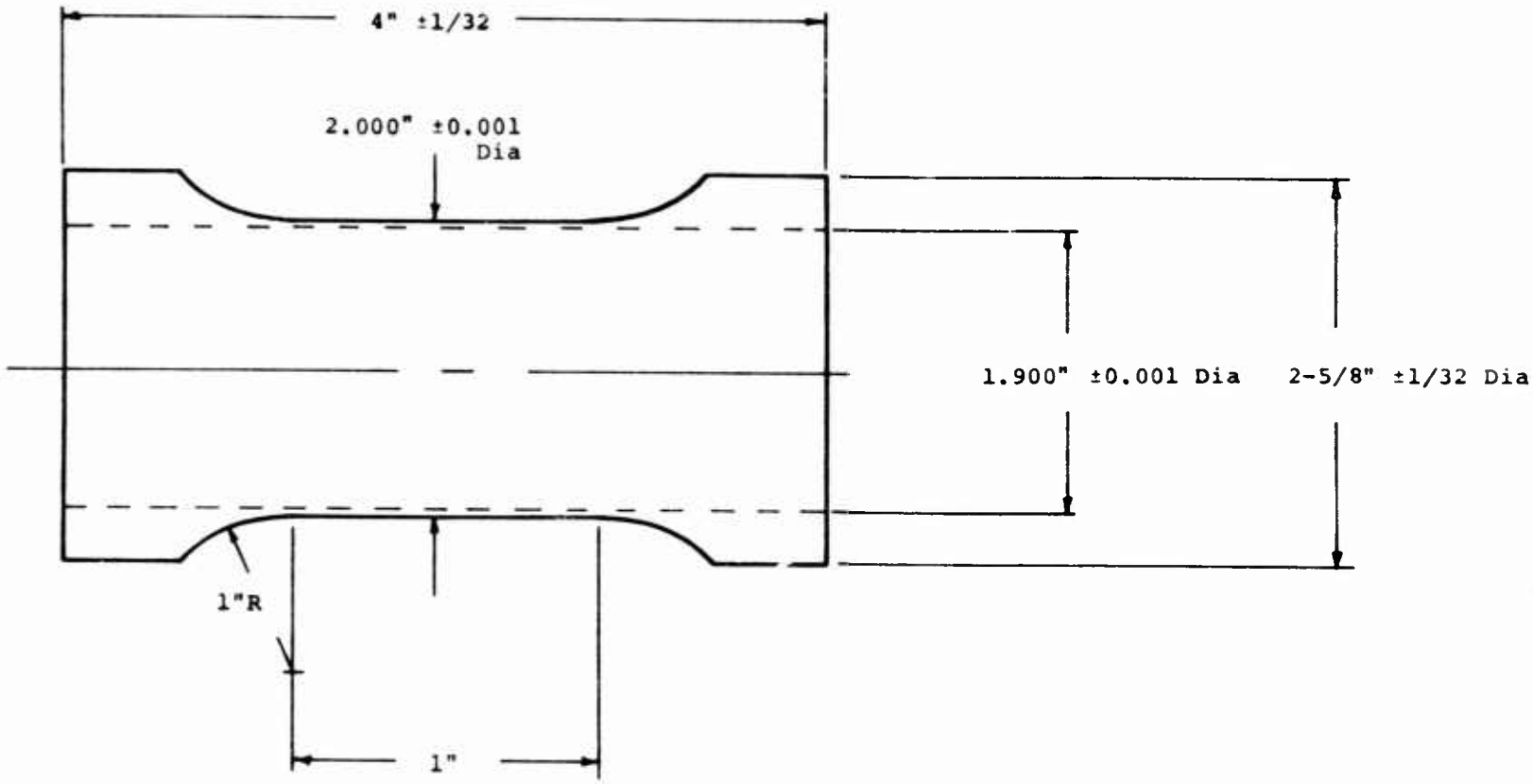

Figure 6. Cylindrical Compressive Specimen for the Evaluation of Codeposited PG/SIC in the ab direction

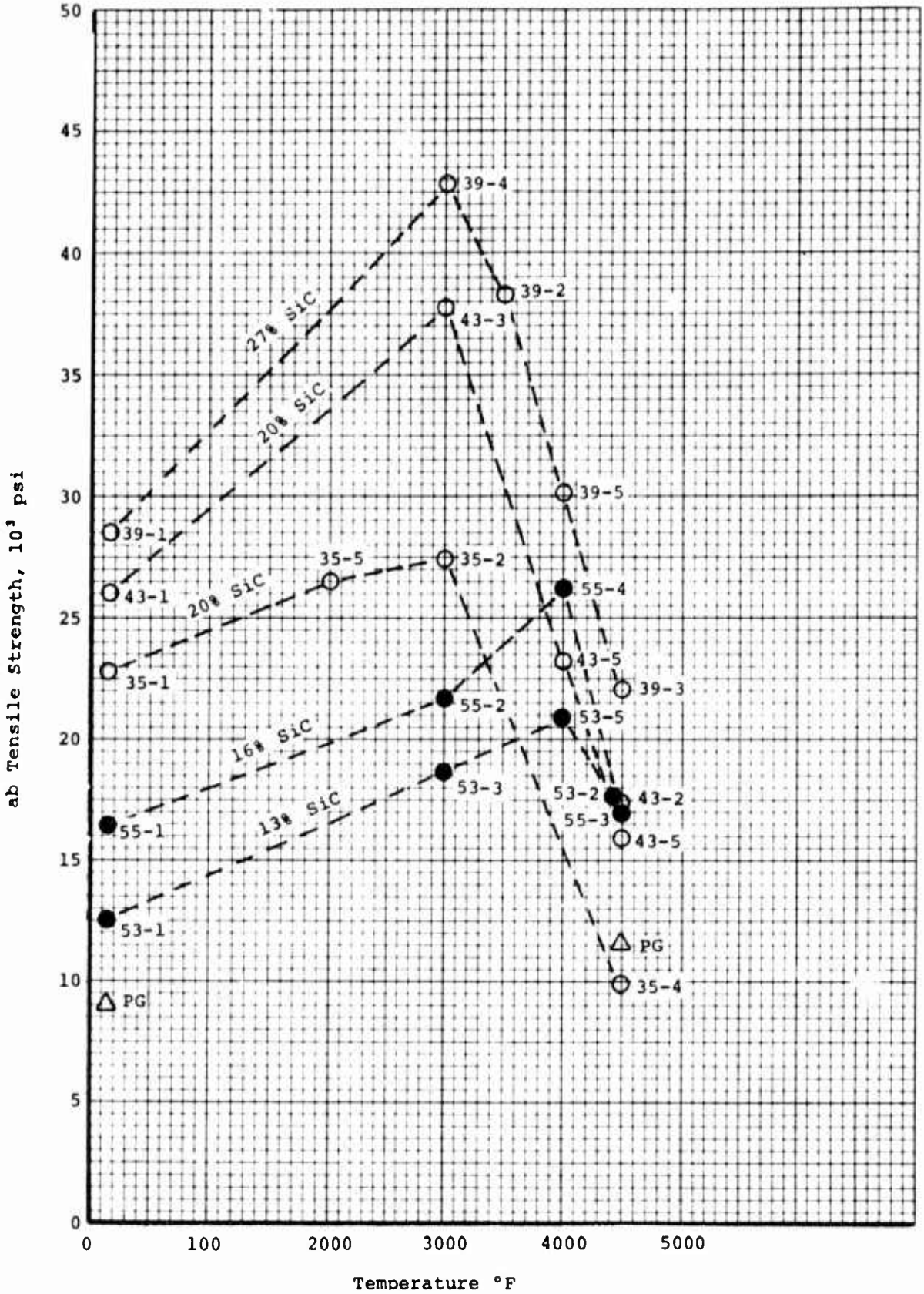

Figure 7. Tensile Strength Versus Temperature for Codeposited PG/SIC in the ab Direction

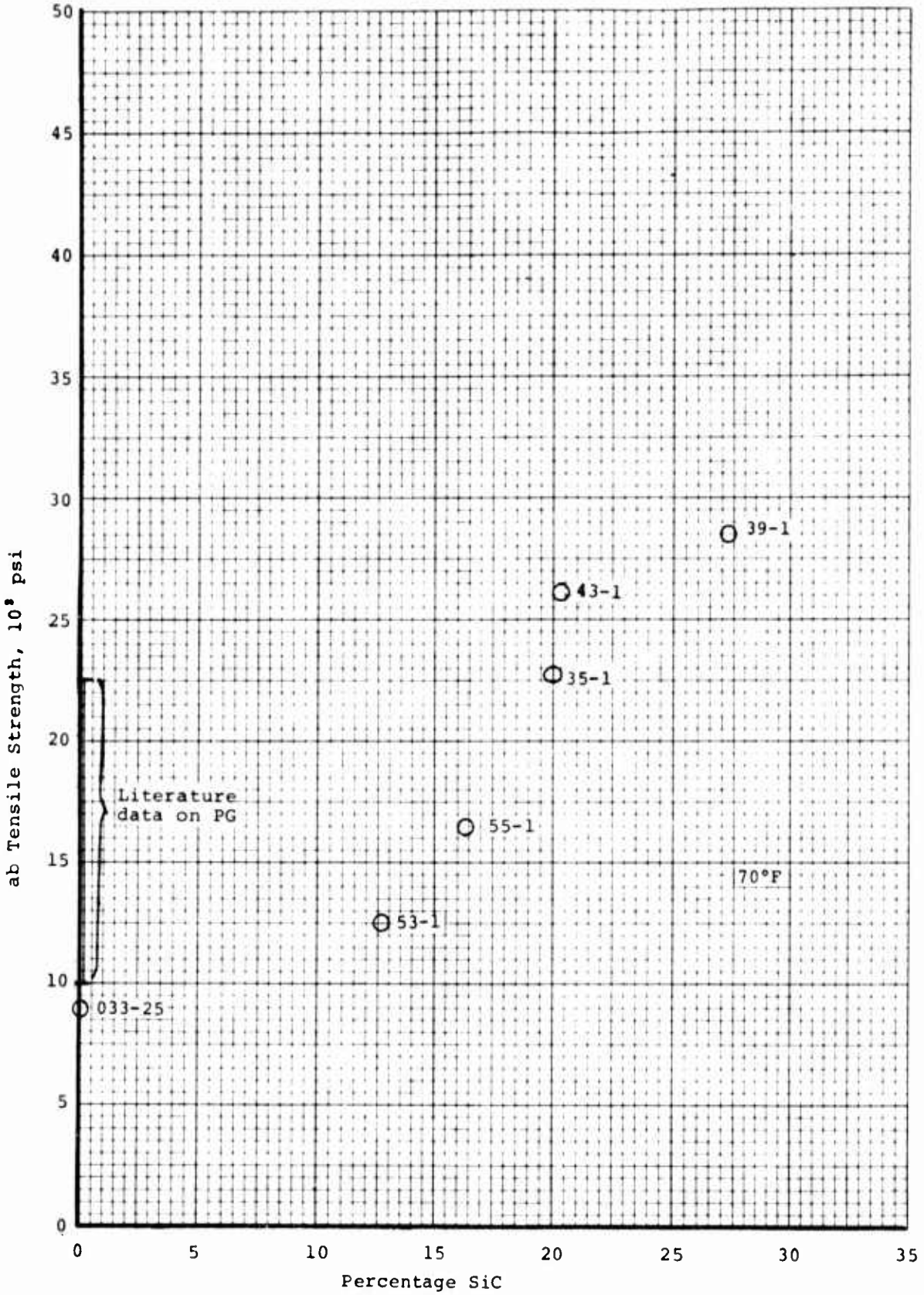

Figure 8. ab Tensile Strength at 70°F Versus Percentage SiC for Codeposited Sic/PG Cylinders

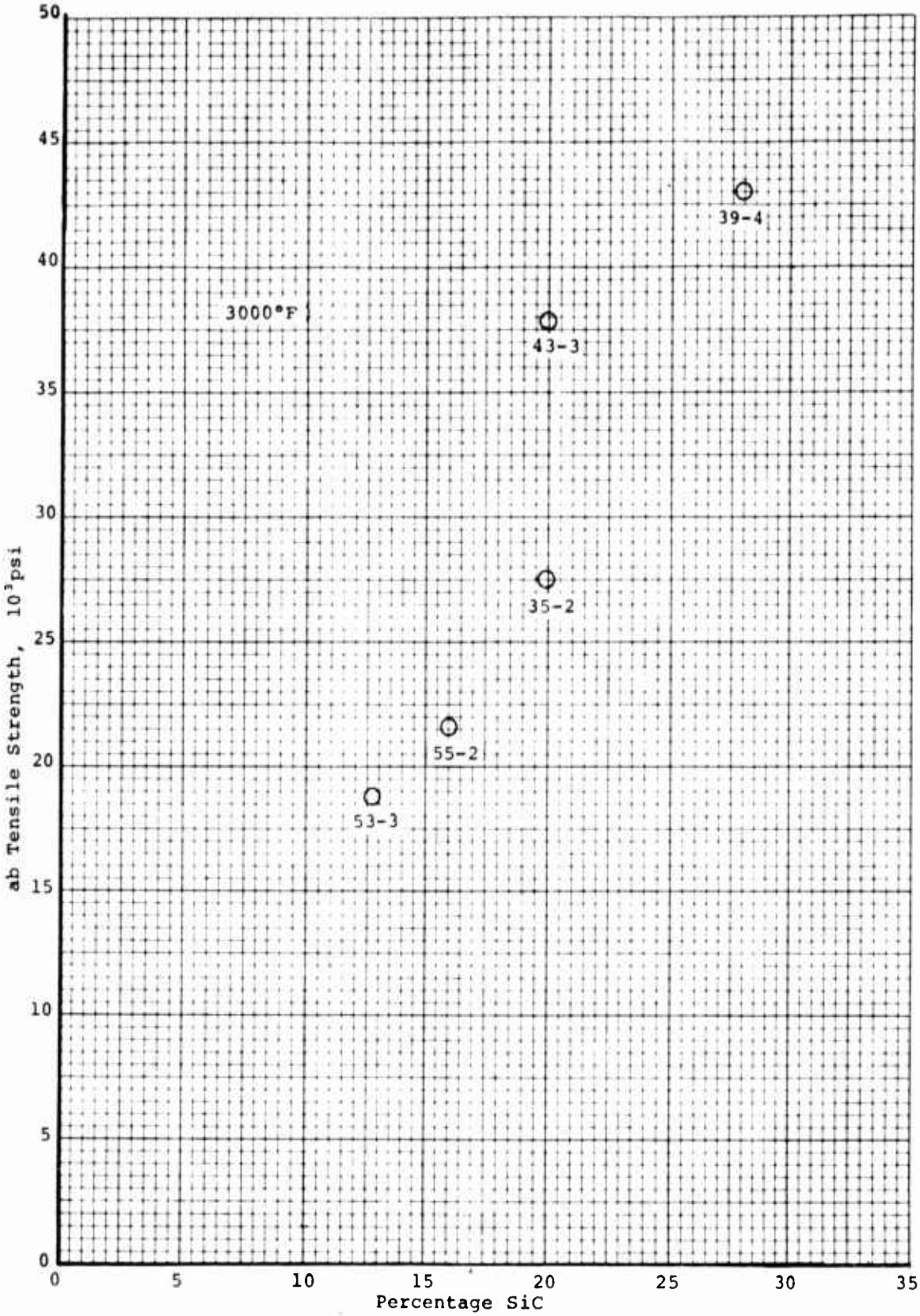

Figure 9. ab Tensile Strength at 3000°F versus Percentage SiC for Codeposited SiC/PG Cylinders

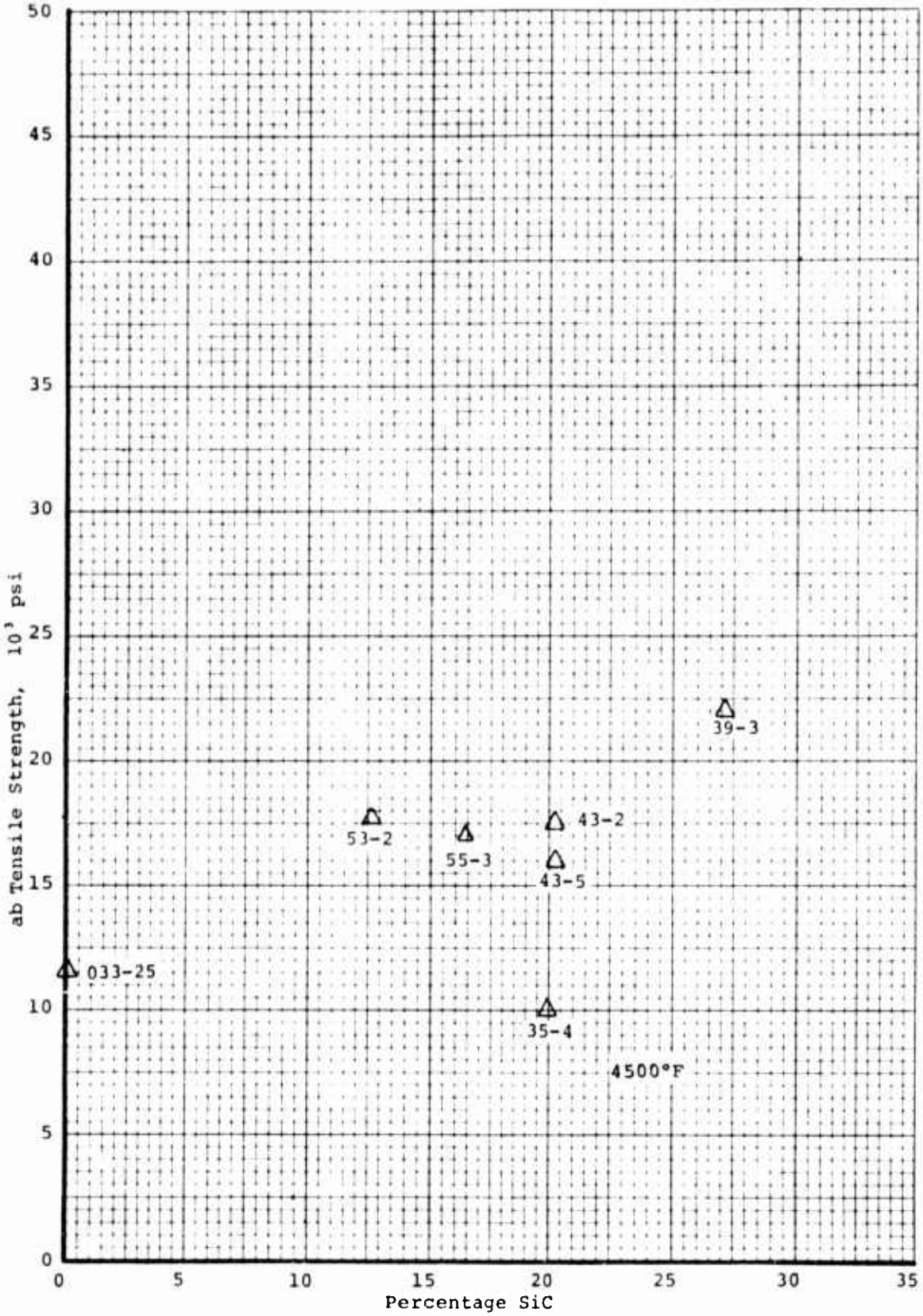

Figure 10. ab Tensile Strength at 4500°F Versus Percentage SiC for Codeposited SiC/PG Cylinders

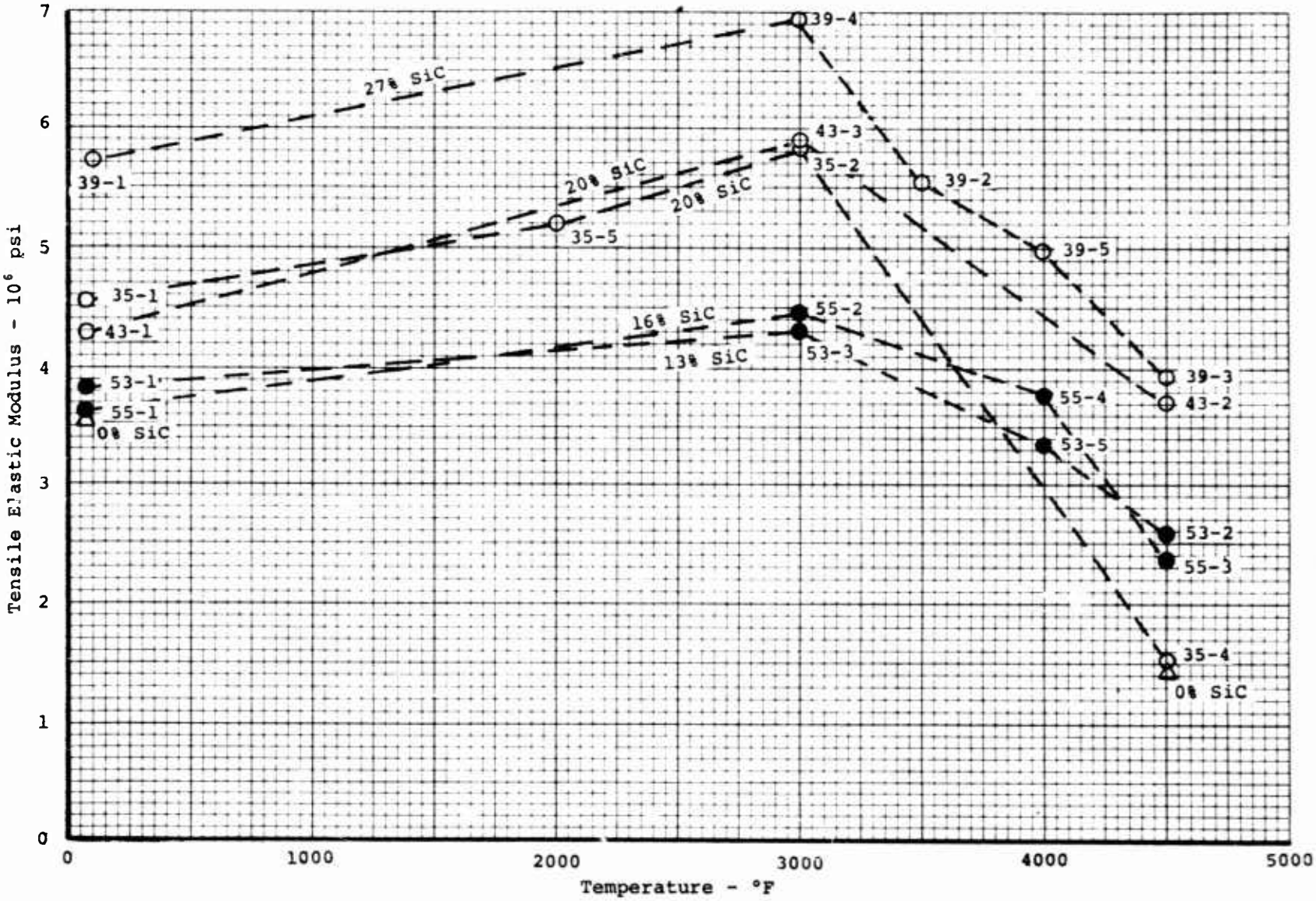

Figure 11. Tensile Elastic Modulus versus Temperature for Codeposited SiC/PG in the ab Direction

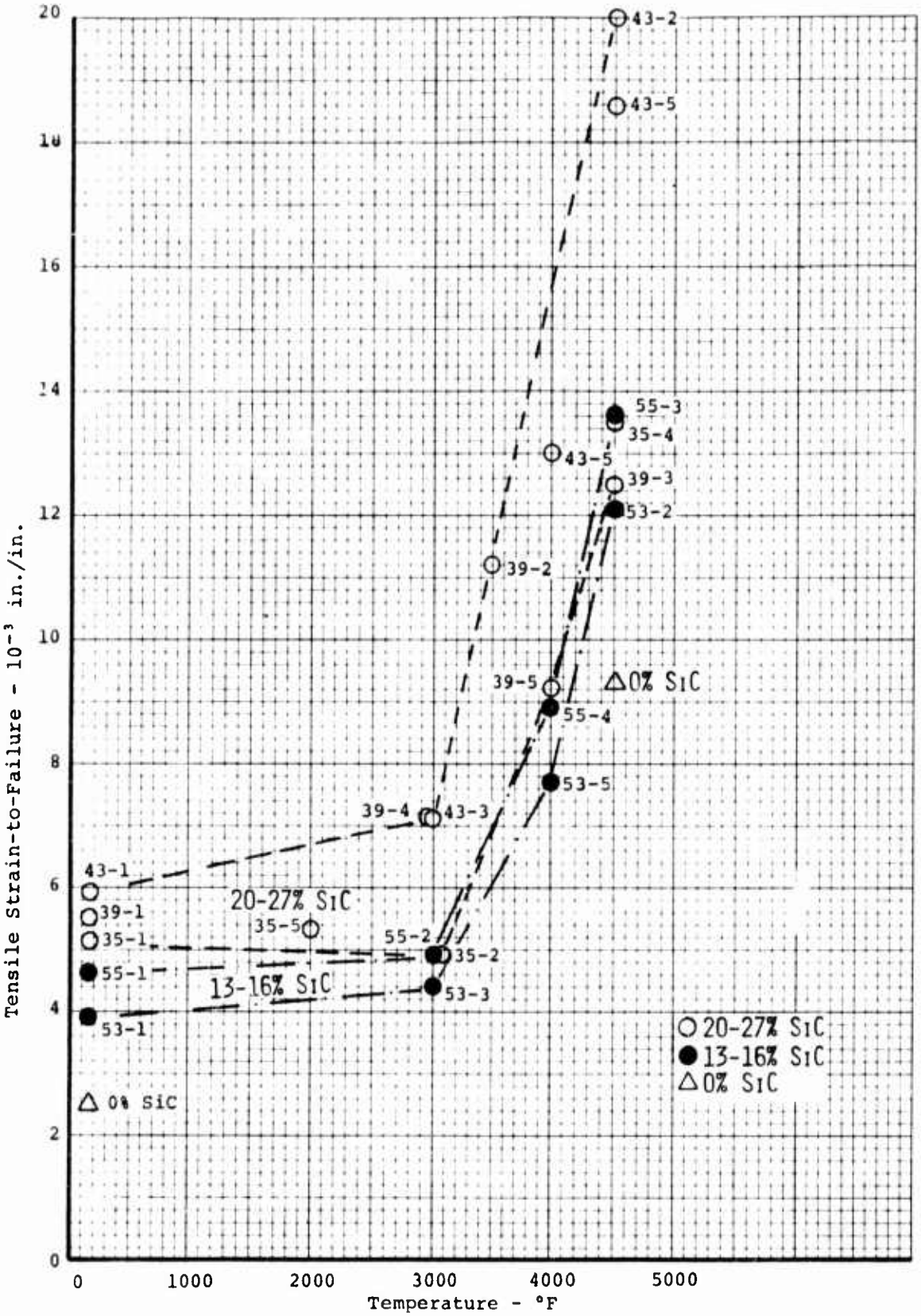

Figure 12. Tensile Strain-to-Failure versus Temperature for Codeposited SiC/PG in the ab Direction

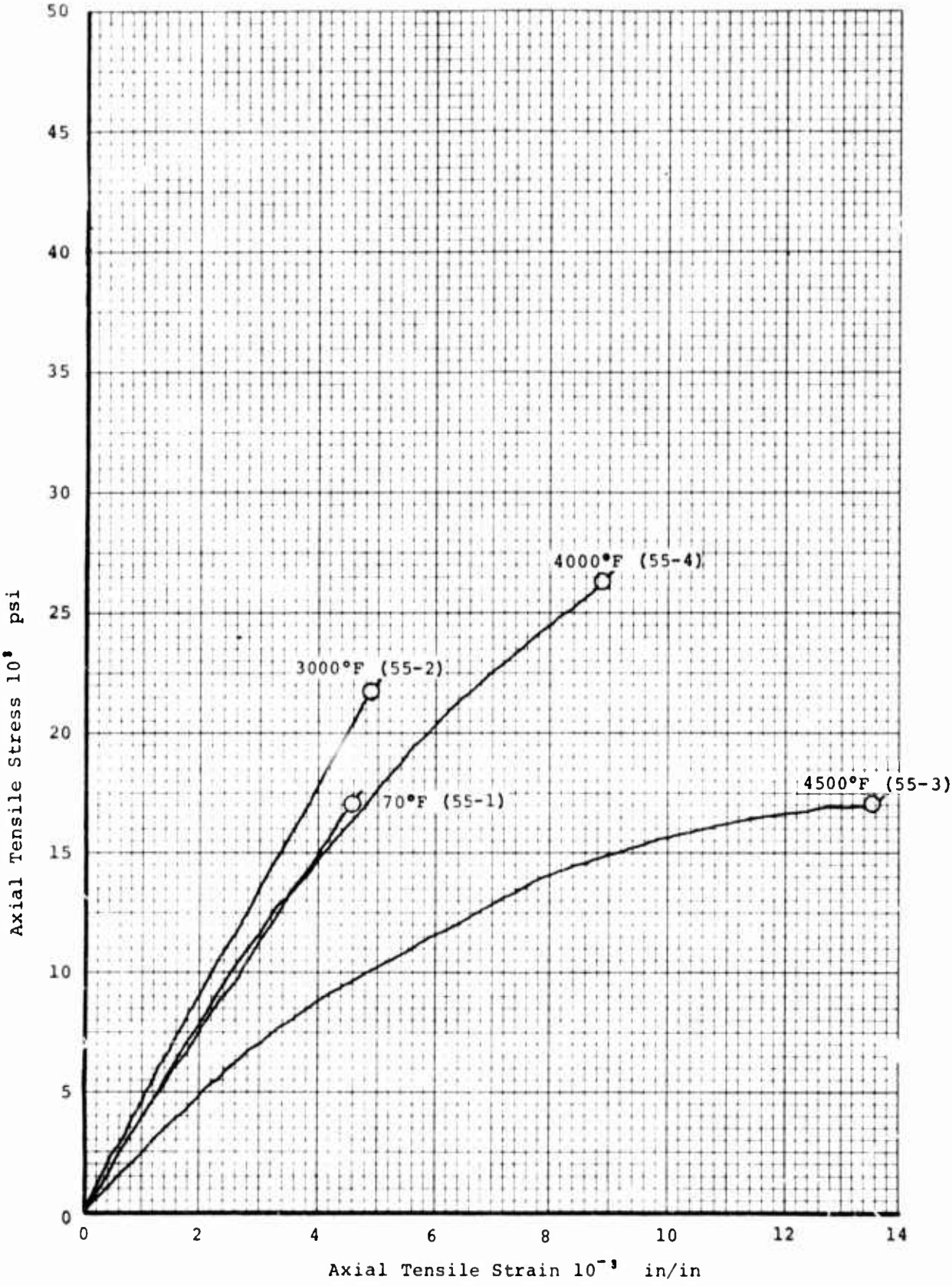

Figure 13. Tensile Stress-Strain Curves For Codeposited 16% SiC/PG (Cylinder C-55)

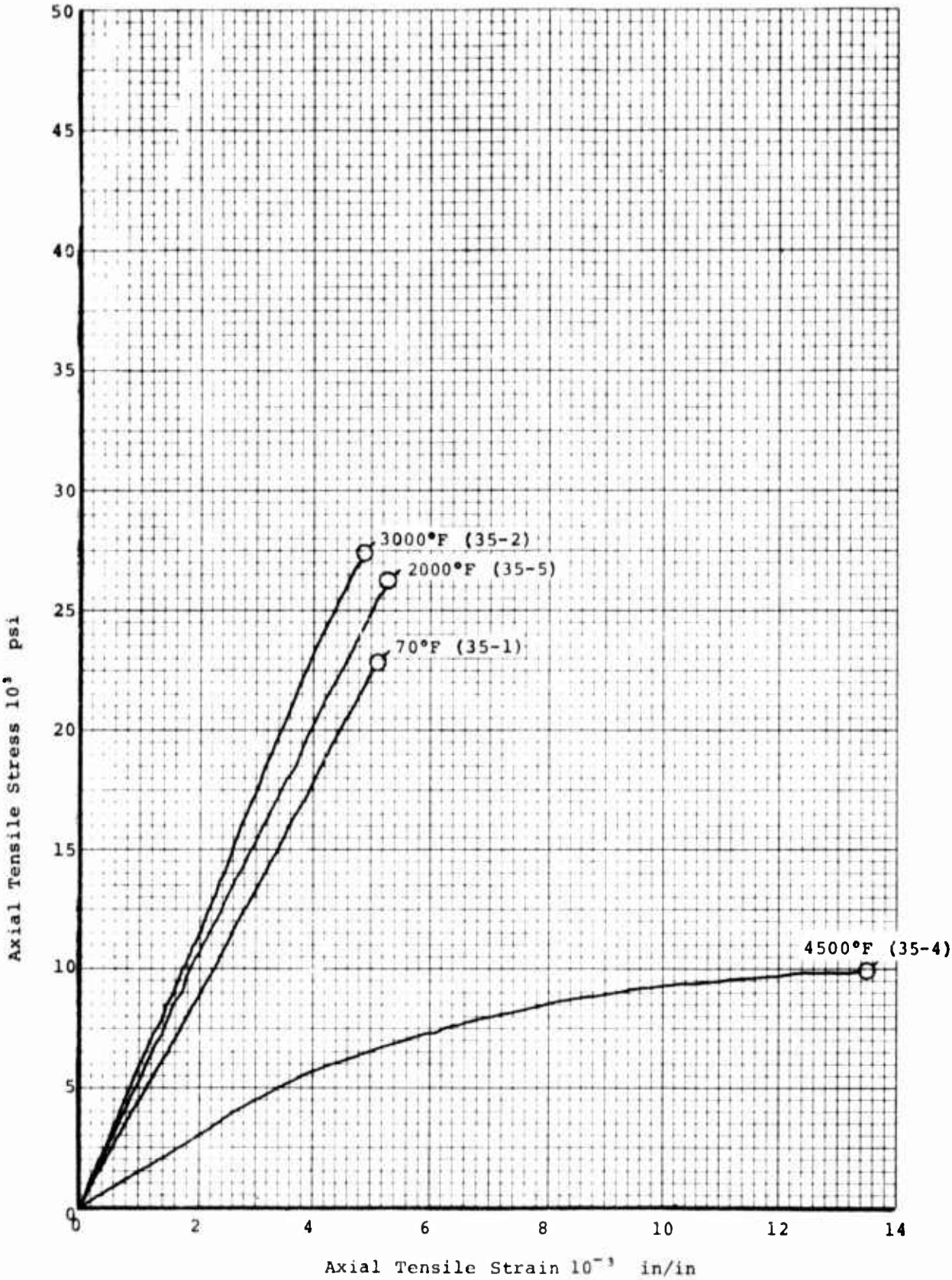

Figure 14. Tensile Stress-Strain Curves for Codeposited 20% SiC/PG (Cylinder C-35)

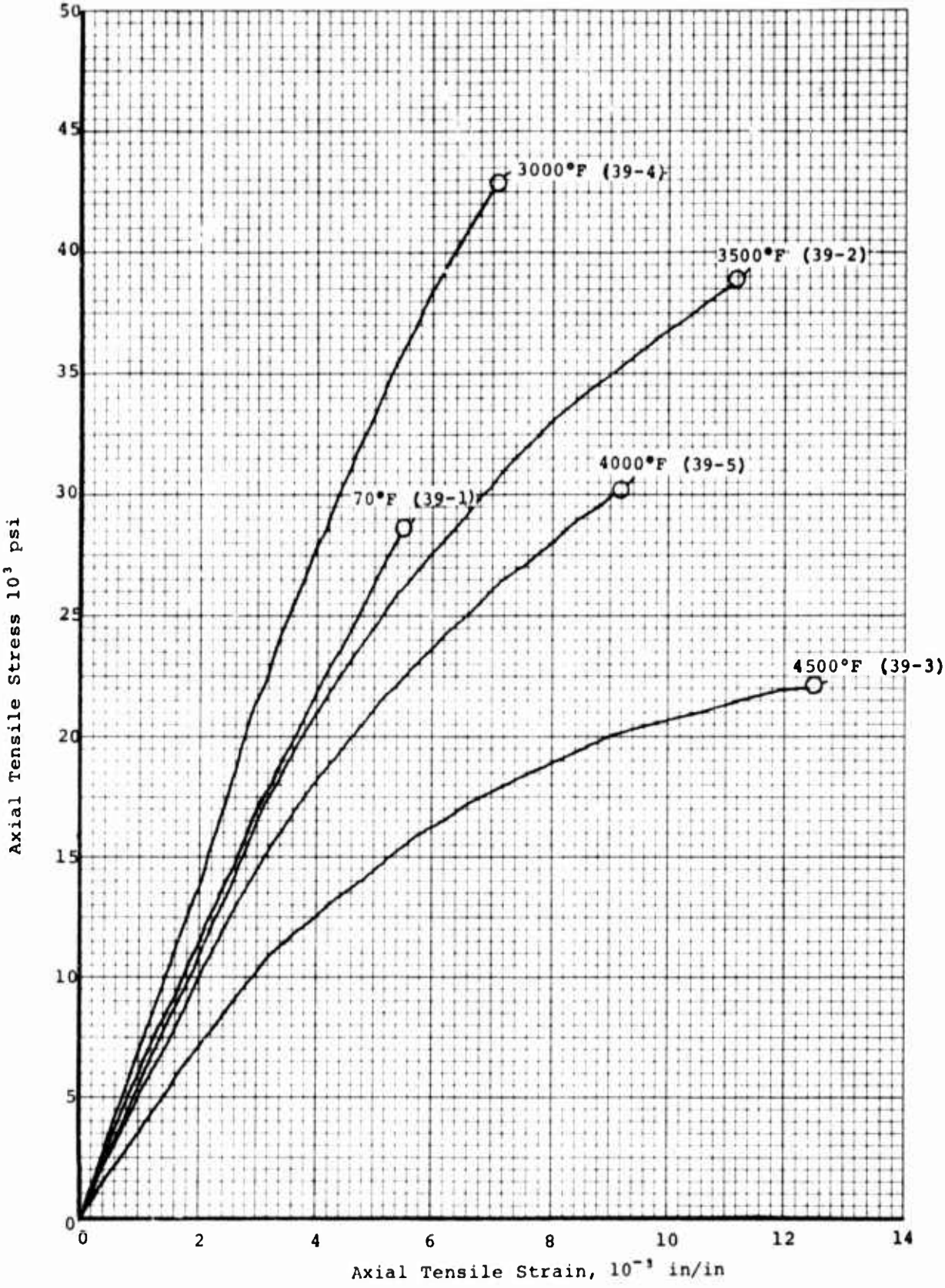

Figure 15. ab Tensile Stress-Strain Curves for Codeposited 27% SiC/PG (Cylinder C-39)

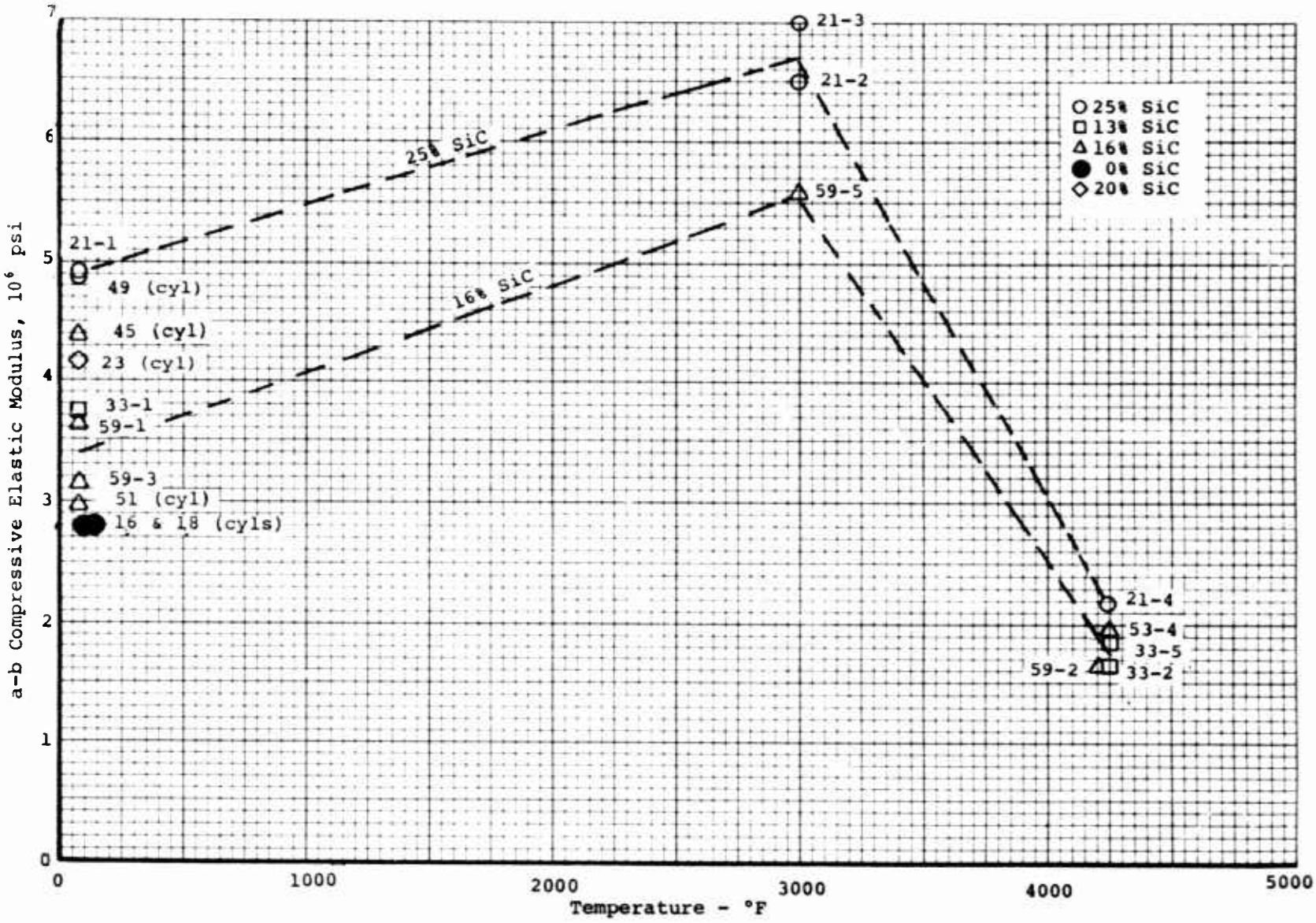

Figure 16. Compressive Elastic Modulus versus Temperature for Codeposited Pyrolytic Graphite and SiC in the a-b Direction

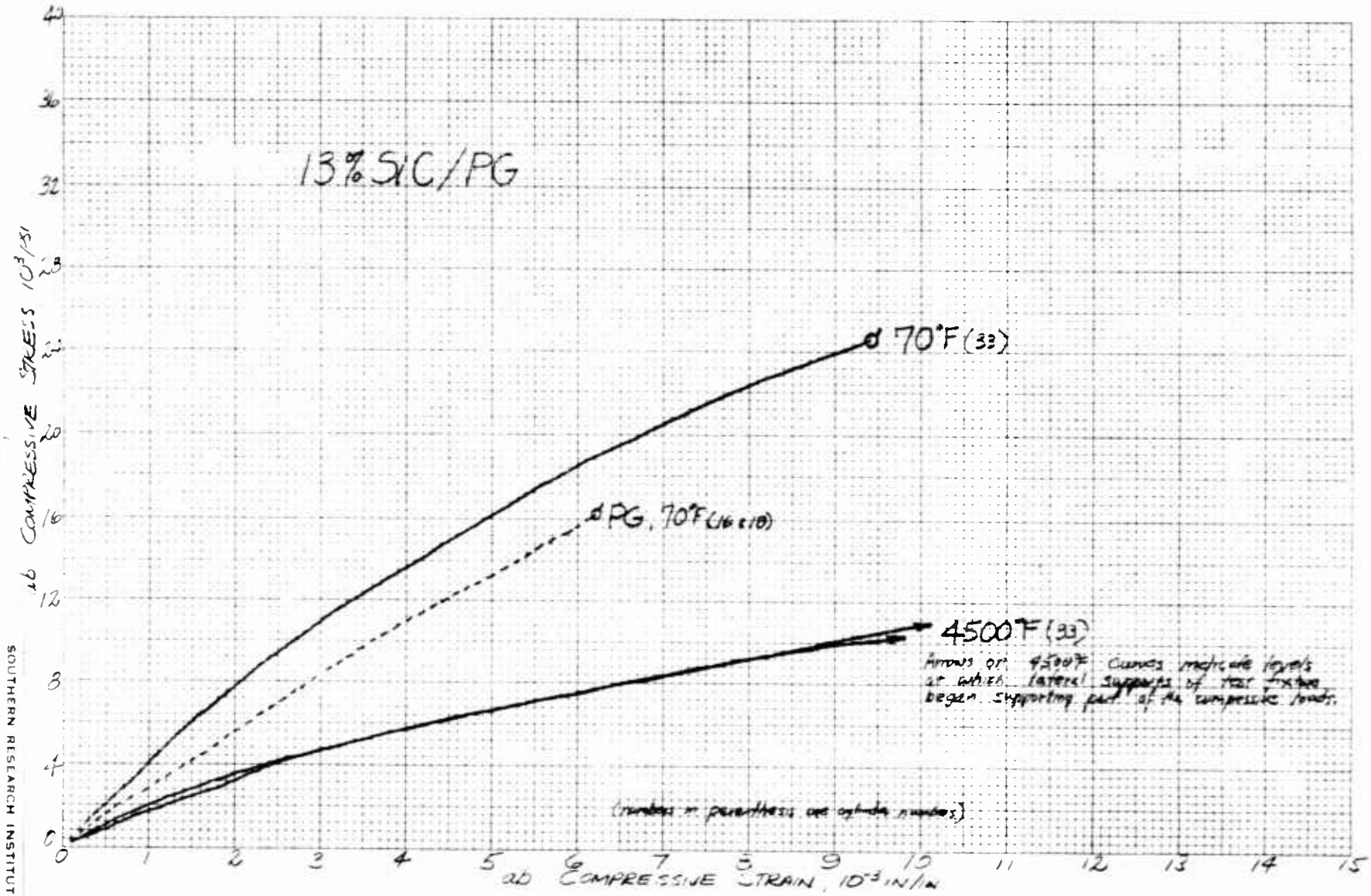

Figure 17. ab Compressive Stress-Strain Curves for Codeposited 13% SiC/PG (Cylinder 33)

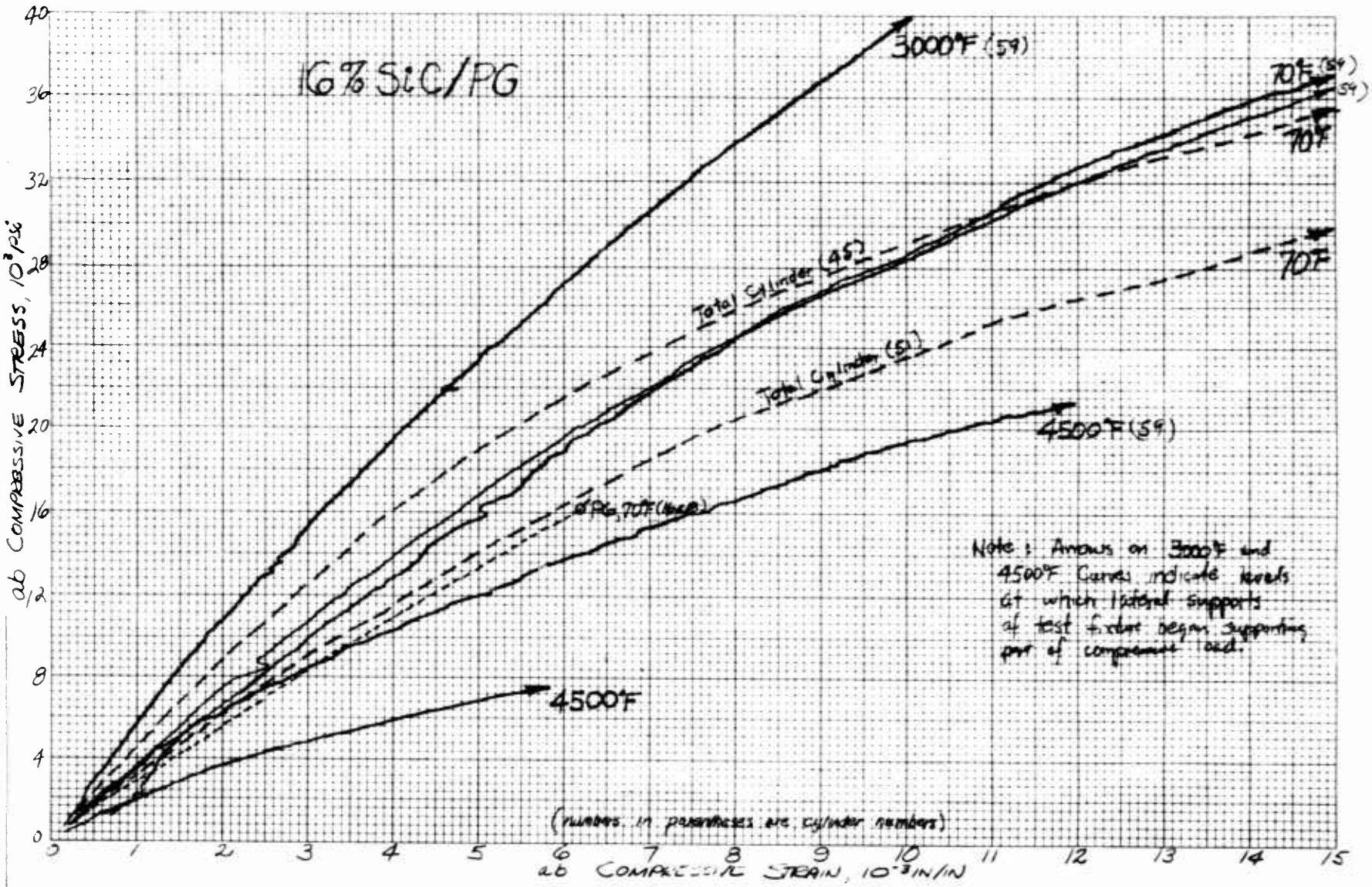

Figure 18. ab Compressive Stress-Strain Curves for Codeposited 16% SiC/PG (Cylinder 59)

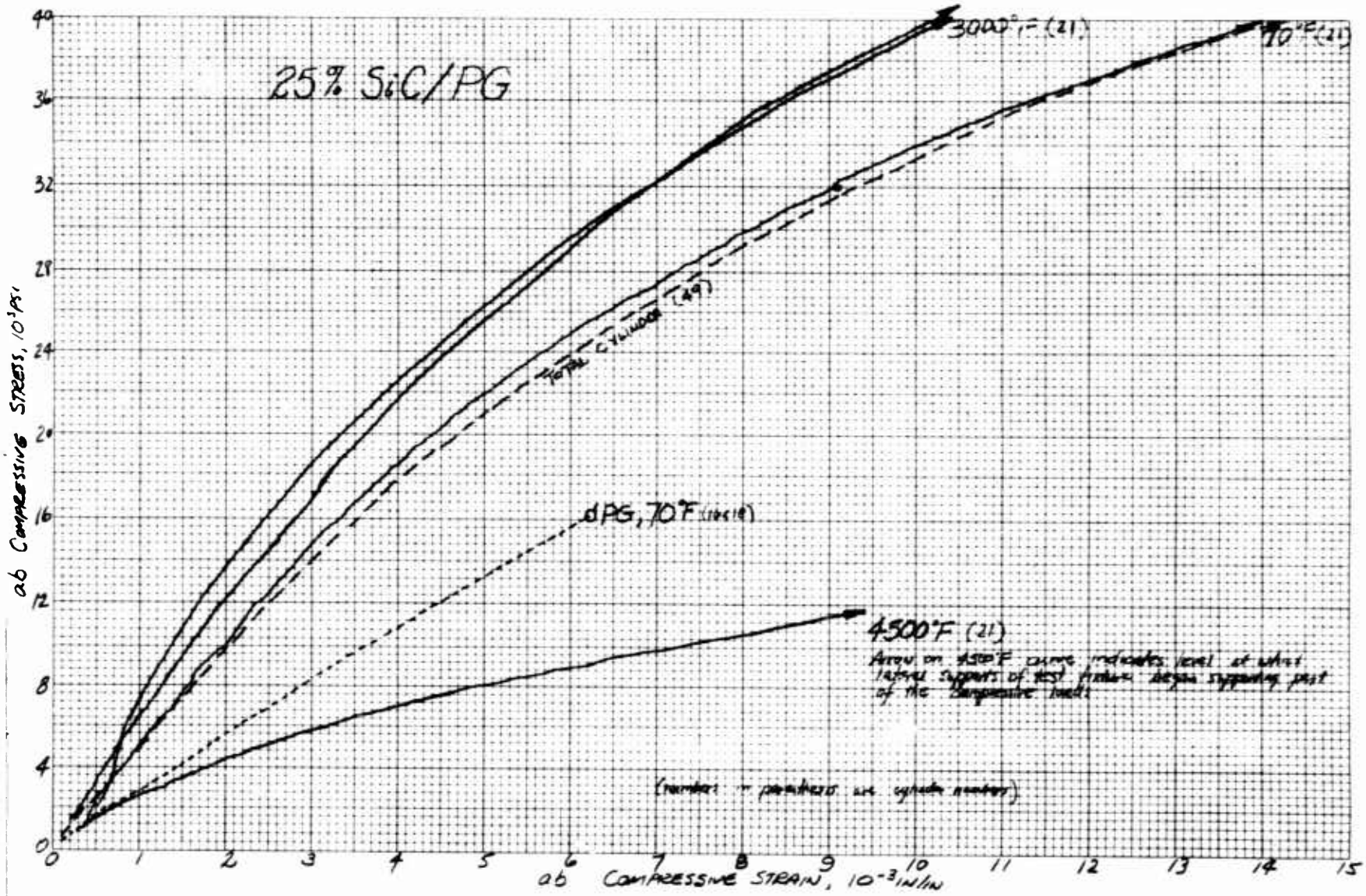

Figure 19. ab Compressive Stress-Strain Curves for Codeposited 25% SiC/PG (Cylinder 21)

TABLE 1

Mechanical Property Test Matrix for Evaluation of PG and Codeposited SiC/PG

Property	Orientation	Material	Temperature °F 70	2000	3000	3500	4000	4500
Tension	ab	PG	2(1)[a]	-	-	-	-	2(1)
		8% SiC/PG	2(2)	-	-(2)	-	-(2)	2(2)
		20% SiC/PG	2(5)	-(1)	2(3)	-(1)	-(2)	2(4)
	c	PG	3(3)	-	-	-	-	-
		8% SiC/PG	3(3)	-	-	-	-	-
		20% SiC/PG	4(4)	-	-	-	-	-
Compression	ab	PG	2(2)	-	-	-	-	2(0)
		8% SiC/PG	2(3)	-	-(1)	-	-	2(2)
		20% SiC/PG	2(5)	-	-(2)	-	-	2(3)

[a]Numbers in parentheses are the actual evaluations performed

Table 2

Tensile Data for PG and Codeposited SiC/PG Cylinders

Meas Wt % SiC	Loading Direction	Temp °F	Stress Rate psi/sec	Specimen Number	Bulk Density gm/cm	Ultimate Strength psi	Initial Elastic Modulus 10 psi	Total Unit Axial Strain in./in.	Nominal Weight % SiC	Remarks
0	ab	70	10,000	033-25-T1[a]	2.18	------	----	------	0	Broken in machining
				033-25-T2[a]	2.19	8,960	3.6	0.0025	0	
		4500	10,000	033-25-T3[a]	2.20	------	----	------	0	Broken in load
				033-25-T4[a]	2.20	11,600	1.45	0.0093	0	train assembly
13	ab	70	10,000	C-53-1T	----	12,600	3.82	0.0039	8	
		3000	10,000	C-53-3T	2.38	18,600	4.30	0.0044	8	
		4000	10,000	C-53-5T	----	20,800	3.32	0.0077	8	
		4500	10,000	C-53-2T	2.36	17,600	2.58	0.0121	8	
16	ab	70	10,000	C-55-1T	----	16,400	3.62	0.0046	8	
		3000	10,000	C-55-2T	2.35	21,600	4.46	0.0049	8	
		4000	10,000	C-55-4T	2.37	26,200	3.77	0.0089	8	
		4500	10,000	C-55-3T	2.37	16,900	2.36	0.0136	8	
20	ab	70	10,000	C-35-1T	----	22,800	4.55	0.0051	20	
		2000	10,000	C-35-5T	2.45	26,500	5.20	0.0053	20	
		3000	10,000	C-35-2T	2.44	27,400	5.82	0.0049	20	
		4500	10,000	C-35-4T	2.42	9,880	1.51	0.0135	20	
20	ab	70	10,000	C-43-1T	----	26,000	4.29	0.0059	20	
		3000	10,000	C-43-3T	2.41	37,800	5.90	0.0071	20	
		4000	10,000	C-43-4T	2.40	23,200	----[b]	~0.013	20	
		4500	10,000	C-43-2T	2.42	17,400	3.72	0.0204	20	
		4500	10,000	C-43-5T	2.42	15,800	~4.7	0.0186	20	
27	ab	70	10,000	C-39-1T	----	28,500	5.72	0.0055	20	
		3000	10,000	C-39-4T	2.47	42,900	6.95	0.0071	20	
		3500	10,000	C-39-2T	2.46	38,300	5.52	0.0112	20	
		4000	10,000	C-39-5T	2.48	30,100	4.98	0.0092	20	
		4500	10,000	C-39-3T	2.50	22,000	3.55	0.0125	20	
--	ab	70	10,000	C-1-TC[c]	----	> 9,640	5.25	>0.0019	20	Poisson's Ratio (ab/ab) = 0.14
--		70	10,000	C-3-TC[c]	----	>12,000	6.21	>0.0021	20	Poisson's Ratio (ab/ab) = 0.14

[a]Flat plate specimens

[b]Initial portion of stress-strain curve was erratic

[c]Total cylinder specimens

Table 3

Tensile Strength Data for PG and Codeposited Sic/PG at 70° F in the "C" Direction

Measured Weight Percentage SiC	Specimen No	Ultimate Tensile Strength, psi	Nominal Weight Percentage SiC
0	C-30-1	- [a]	0
	C-30-2	780	0
	C-30-3	725	0
	C-30-4	870	0
		792	
13	C-53-1	- [a]	8
	C-53-2	>3000[b]	8
	C-53-3	>3040[b]	8
	C-53-4	>2950[b]	
27	C-39-1	>4300[b]	20
	C-39-2	>3040[b]	20
	C-39-3	>3250[b]	20
	C-39-4	>3300[b]	20

[a]broken during assembly
[b]epoxy bond failure; specimen did not fail

Table 4

Compressive Data for PG and Codeposited SiC/PG

Meas Wt % SiC	Load Direction	Temp °F	Stress Rate psi/sec	Specimen Number	Bulk Density gm/cm³	Ultimate Strength psi	Initial Elastic Modulus 10^6 psi	Total Unit Axial Strain in./in.	Nominal Weight % SiC	Remarks
0	ab	70	10,000	C-16[a]	-	16,000	2.78	0.0062	0	Poisson's Ratio = -0.09 (ab/ab)
				C-18[a]	-	16,100	2.78	0.0062	0	Poisson's Ratio = -0.08 (ab/ab)
13	ab	70	10,000	C-33-1C	2.34	25,000	3.74	0.0094	20	
		4500	10,000	C-33-2C	2.33	10,400[b]	1.63	0.0097[b]	20	
				C-33-5C	2.34	11,000[b]	1.83	0.010 [b]	20	
16	ab	70	10,000	C-45[a]	-	46,500	4.41	0.026	20	Poisson's Ratio = 0.13 (ab/ab)
				C-51[a]	-	36,600	2.98	0.023	8	Poisson's Ratio = 0.14 (ab/ab)
		70	10,000	C-59-1C	2.34	43,200[b]	3.64	~0.020[b]	8	
				C-59-3C	2.34	44,500[b]	3.17	~0.021	8	
		3000	10,000	C-59-5C	2.35	40,000[b]	5.58	0.0101[b]	8	
		4500	10,000	C-59-2C	2.34	10,700[b]	1.63	0.012[b]	8	
				C-59-4C	2.34	7,360[b]	1.95	0.0059[b]	8	
20	ab	70	10,000	C-23[a]	-	32,700	4.19	0.019	20	Poisson's Ratio = 0.09 (ab/ab)
25	ab	70	10,000	C-49[a]	-	51,000	4.91	0.0220	20	Poisson's Ratio = 0.15 (ab/ab)
		70	10,000	C-21-1C	2.44	43,200[b]	4.92	0.0167[b]	20	
		3000	10,000	C-21-2C	2.43	40,500[b]	6.5	0.0105[b]	20	
				C-21-3C	2.42	44,000[b]	7.0	0.0118[b]	20	
		4500	10,000	C-21-4C	2.43	11,800[b]	2.18	0.0094[b]	20	

a. Total cylinder specimen
b. Stress and strain level at which lateral supports of the test fixture began supporting part of the load

APPENDICES

APPENDIX A

ULTIMATE STRENGTH, ELASTIC MODULUS AND POISSON'S RATIO TO 5500°F IN TENSION

A typical tensile facility is shown in the photograph in Figure 1 and in the schematic in Figure 2. The primary components are the gas-bearings, the load frame, the mechanical drive system, the 5500°F furnace, the optical strain analyzers and associated instrumentation for measurement of load and strain. The load capacity is 15,000 pounds.

The load frame and mechanical drive system are similar to those of many good facilities. The upper crosshead is positioned by a small electric motor connected to a precision screw jack. This crosshead is stationary during loading and is moved only when assembling the load train. The lower crosshead is used to apply the load to the specimen through a precision screw jack chain driven by a variable speed motor and gear reducer.

Nonuniaxial loading, and therefore bending stresses, may be introduced in tensile specimens not only from (1) misalignment of the load train at the attachment to the crossheads, but also from (2) eccentricity within the load train, (3) unbalance of the load train and (4) external forces applied to the load train by such items as electrical leads and clip-on extensometers. Although the bending moments from some of these sources may seem relatively slight, the resulting stress distortions are quite significant in the evaluation of the extremely sensitive brittle materials. Now consider each individually.

To confirm that the gas-bearings had eliminated nonuniaxial loading at the point of attachment of the load train to the crossheads, the frictional moment was determined at a load of 5000 pounds by measuring the torque required to produce initial motion within the system with the bearings in operation. This torque was found to be a maximum of 6.6×10^{-3} inch-pounds. The equation

$$M_O = \frac{2\mu P}{3} \left[\frac{R_2^{\,3} - R_1^{\,3}}{R_2^{\,2} - R_1^{\,2}}\right] \qquad (1)$$

was then applied to the system to calculate the kinetic friction where M_O was the resisting moment due to kinetic friction and μ represented the coefficient of kinetic friction. The calculated value of μ was then equal to a maximum of only 4.5×10^{-7}.

The classic equation

$$S = \frac{Mc}{I} \tag{2}$$

was then employed to obtain the stress that could be induced in the specimen due to this bending moment. This value was 0.16 psi, or less than 0.002 percent of the tensile stress produced within a typical graphite specimen. These low values clearly indicate the elimination of problems of bending stress in the pecimen imposed by misalignment at the crosshead attachments, either initially or during loading.

Emphases in the design of the load train were placed on (1) large length-to-diameter ratios at each connection, (2) close sliding fits (less than 0.005 inch) of all mating connections, (3) the elimination of threaded connections, (4) the use of pin connections wherever possible and (5) increasing the size of components to permit precise machining of all mating surfaces. All members were machined true and concentric to within 0.0005 inch, and the entire load train was checked regularly to ensure overall alignment following assembly of the individual members. This process ensures concentricity and no kinks in the system.

The problems of unbalance within the load train and of external forces applied to the load train have been explored and corrected. The entire load train is statically balanced to less than 0.01 inch-pound for normal operation.

One configuration of the tensile specimen is shown in Figure 3. This specimen provides a relatively large L/D ratio in the gripping area to ensure good alignment. All surfaces in the gripping area are cylindrical in order to make precision machining easier and repeatable from specimen to specimen. This specimen also has double breakdown radii from the gripping area to the gage section. This double breakdown allows a uniform transition of the stress pattern and reduces the frequency of radius (out of gage) fractures. This specimen provides a uniform gage section which gives a definable volume of material under stress and permits accurate measurements of strain. The flags for the measurement of axial strain are positioned one inch apart so that unit strain is recorded directly. The flag attachment for measurement of lateral strain is positioned between the flags for axial strain; see Figure 4.

A schematic of the precision tensile grip is shown in Figure 5. The design is much like the jaws of a lathe head or the chuck of a drill motor made with precision. Observe from the figure the long surface contact of the mating parts and the close fits to establish precise alignment with the specimen. As the load is applied, the wedges maintain alignment to fracture.

Figure 6 is a sketch of the 5500°F furnace used for tension showing the basic components. The furnace consists of a resistively heated graphite element insulated from a water-cooled shell by thermatomic carbon. The furnace and specimen are purged with helium to provide an inert atmosphere. Ports with visual openings are provided on opposite sides of the furnace as a means of allowing the strain analyzers to view the gage flags on the specimen. Specimen temperatures are determined by optical pyrometer readings taken through another small sight port containing a sapphire window. A calibration curve was established for the loss through the sapphire window, and since the furnace cavity acts essentially as a blackbody, true temperature readings are obtained. Power is supplied to the heating element by means of a 25 KVA variable transformer.

Strain measurement consists of measuring optically the elongation between two flags, or targets, which are mounted on the specimen and separated initially by a predetermined gage length. The travel of the targets is measured by sensing the displacemnt of the image of the edge of the targets and then electromechanically following the image displacement. The relative travel of the two targets provides the strain. Readout is continuous and automatic on a millivolt recorder. A schematic of the analyzer is shown in Figure 7.

A brief summary of the mechanical motions of the components involved in monitoring the strain is helpful in understanding the detailed performance. A tracking telescope follows the upper target and carries a second telescope mounted on its carriage. The second telescope is capable of independent motion to follow the lower target. The relative displacement between the upper and lower telescope, as strain occurs, defines the strain. The system usually is operated so that the tracking telescope follows the upper target and the strain is monitored by the relative displacement of the aperture rather than the telescope following the lower target. With this procedure the maximum range is the maximum displacement available for the lower aperture, of about 1/8 inch, and the sensitivity is limited by the optics and the noise level of the detector. Using both telescopes, the range is about 3/4 inch.

To provide optical references on the specimens, targets are affixed to the test specimen as mentioned. When the specimen is heated to temperature, the targets are self-luminous and are observed optically. The optics view past the luminous targets into a cooled cavity in the opposite furnace wall. The self-luminous targets are then visible against a dark background. To obtain data below 2000°F, a light beam is directed from behind the flags providing a shadow image for the detection system.

The image of the flowing target is focused through a rotating shutter (chopper) and onto a rectangular aperture. Small slits in the aperture pass a portion of the upper and lower edges of the light beam. A photocell receives the light thus transmitted, and an electronic circuit detects whether the energy passed by the two slits is equal. A servo drives the apertures to let a balanced quantity of light pass through the two slits and thus maintains an optical null.

To obtain lateral strain, a strain analyzer is supported horizontally on the tensile frame to view the diametrical or lateral strain of the specimen. A flag attachment, with the general configuration as shown in Figure 8, was developed to follow and transmit lateral motions of up to a few mils. The three-piece assembly consists of a ring and two rams bearing on the specimen.

Calibrations of the analyzers are performed in various ways including absolute correlations to precision micrometers, strain gage extensometers, and direct plots of stress-strain for reference materials such as steel, plexiglas, magnesium and aluminum. Precision is within ±0.000020 inch.

Instrumentation includes primarily a stress-strain measurement system composed of a 1000-pound SR-4 Baldwin load cell, constant d.c. voltage power supply, two optical strain analyzers, and two X-Y recorders. Specimen temperature is monitored with an optical pyrometer. Stress (load) is measured by a commercial load cell. The cell receives a constant d.c. voltage input from the power supply and transmits a millivolt signal (directly proportional to load) to an X-Y recorder. Simultaneously, the optical strain analyzers measure both the axial and lateral strain and transmit a millivolt signal (proportional to strain) to the X-Y recorders. Thus, continuous plots of stress-axial strain and axial strain-lateral strain are recorded simultaneously.

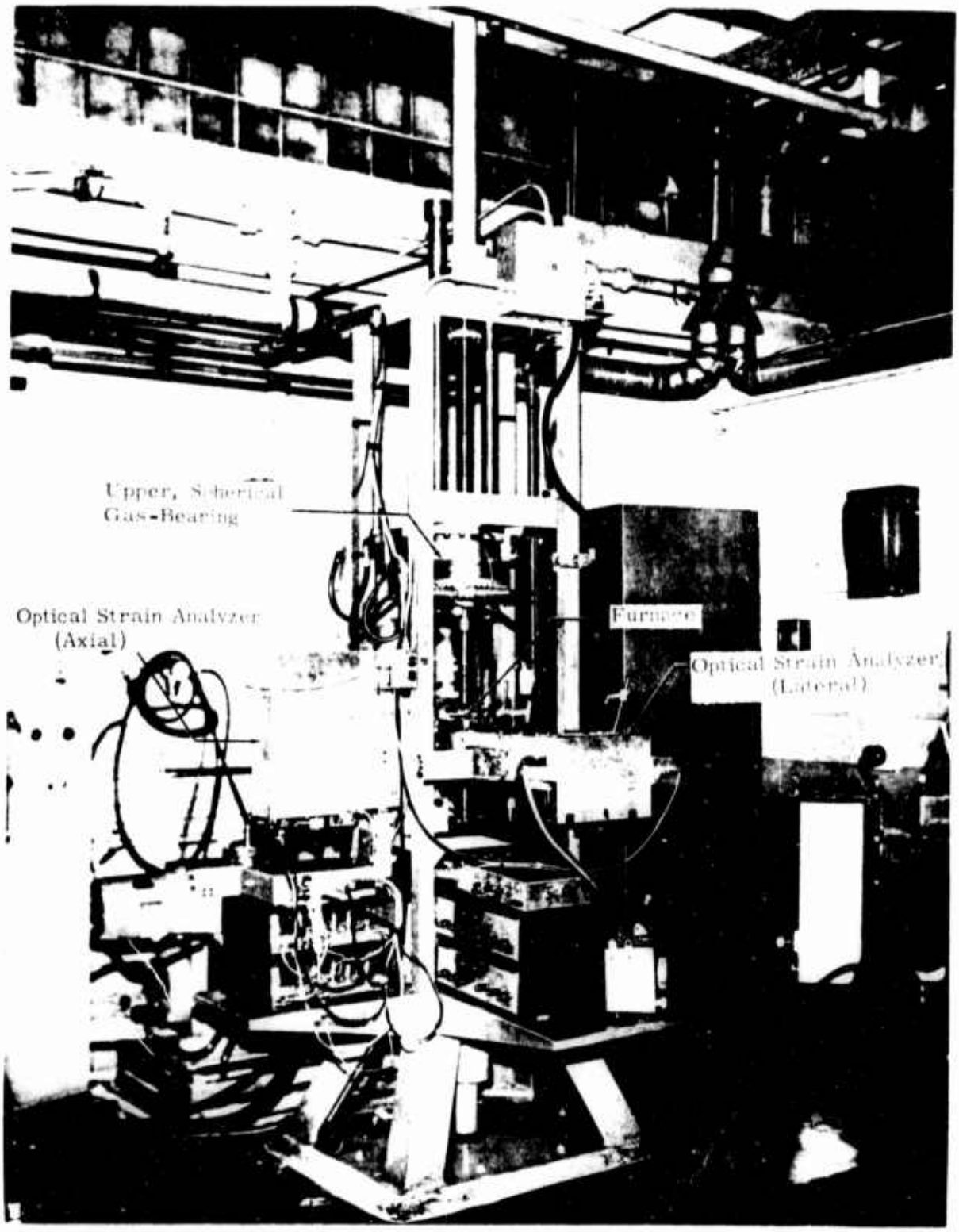

Figure 1. Picture of a Tensile Stress-Strain Facility

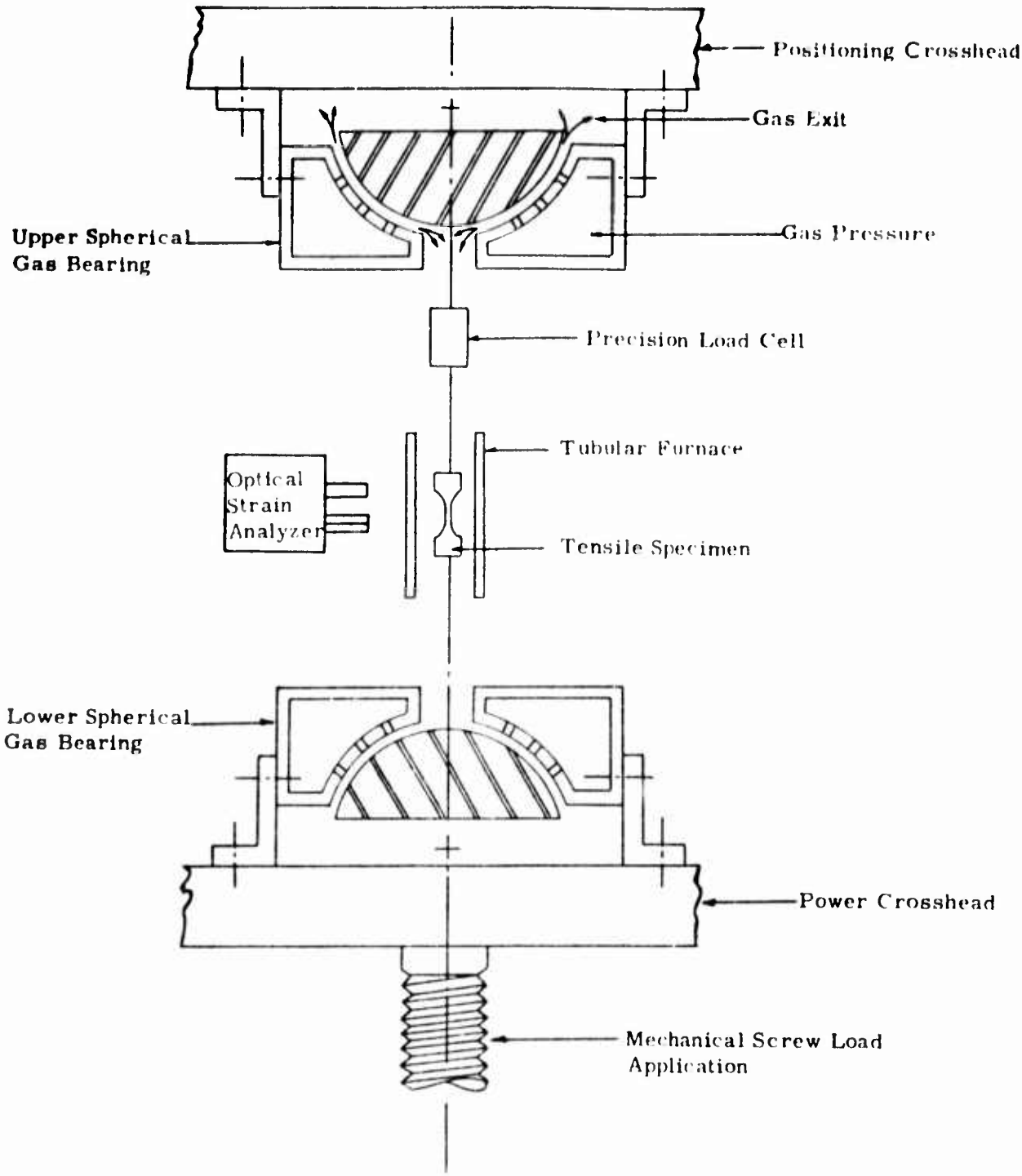

Figure 2. Schematic Arrangement of Gas-Bearing Universals, Specimen and Load Train

Notes:

1. All Diameters True and Concentric to Within 0.0005"
2. Do Not Undercut Radii At Tangent Points
3. Both Ends Flat and Perpendicular to and to Within 0.0005"
4. All Dimensions are in Inches
5. Tolerances are $\pm$ 0.001 on Diameters
   $\pm$ 0.005 on Lengths
   $\pm \frac{1}{64}$ on Fractions

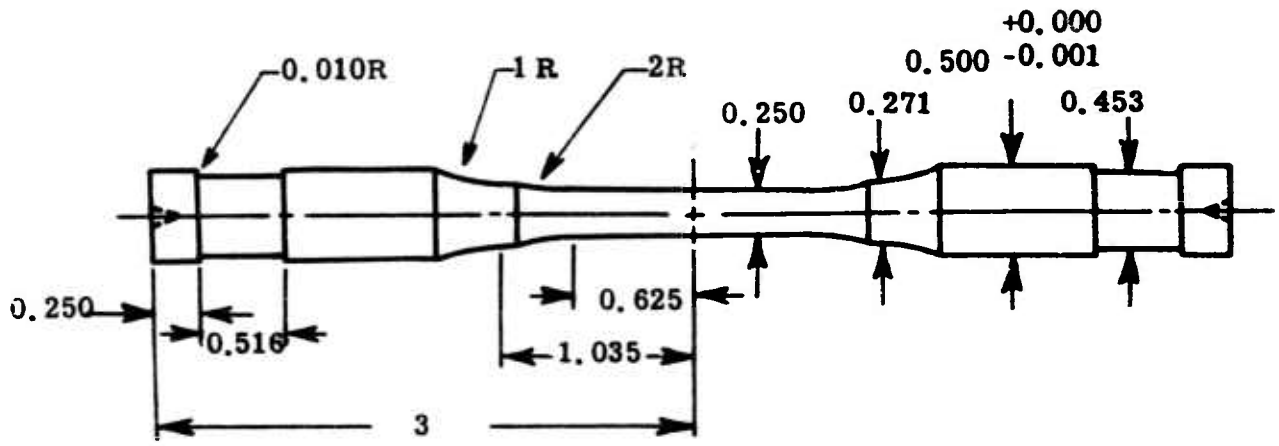

Figure 3. Tensile Specimen Configuration

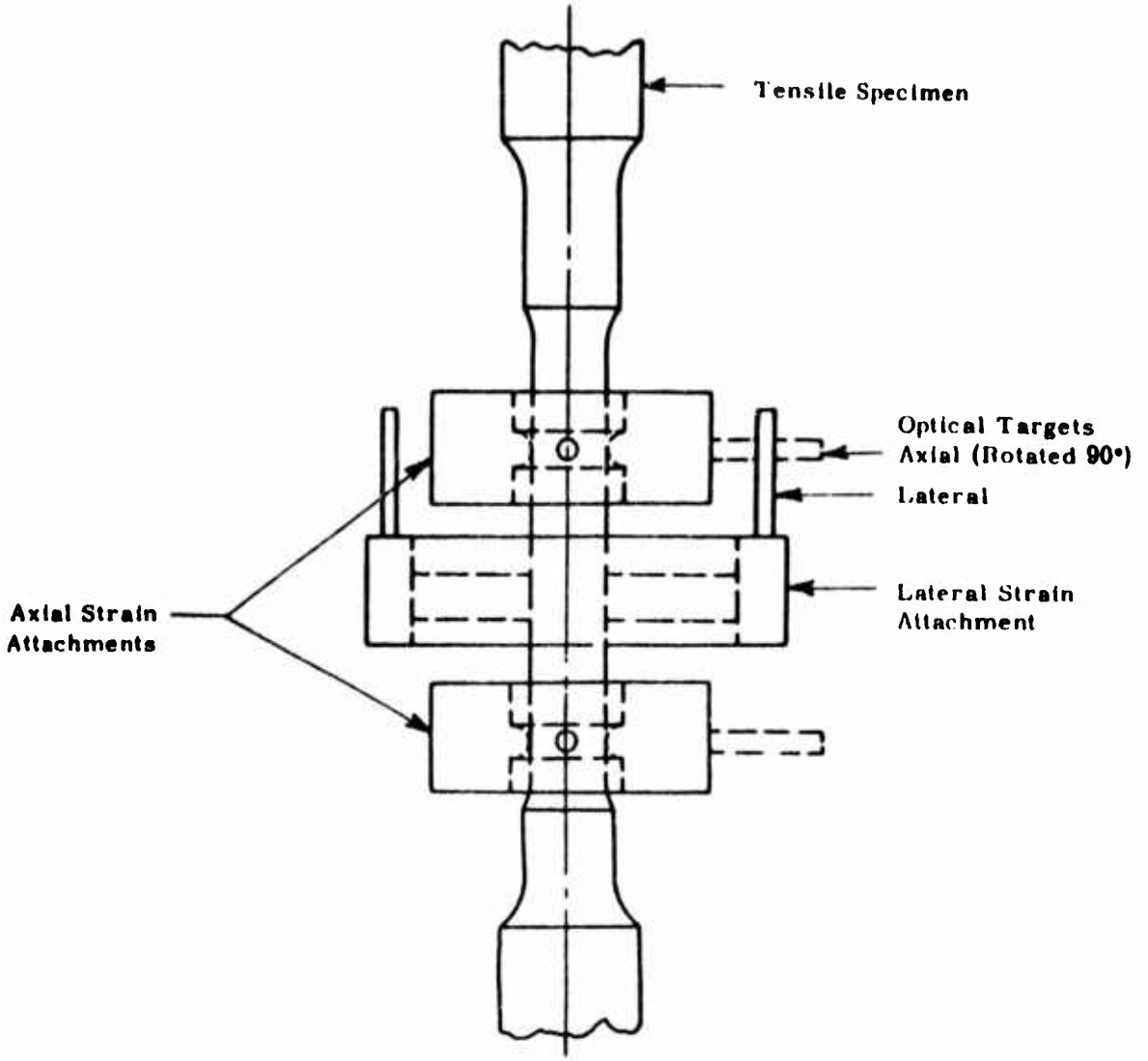

Figure 4. Location of the Flag Attachments on the Tensile Specimens

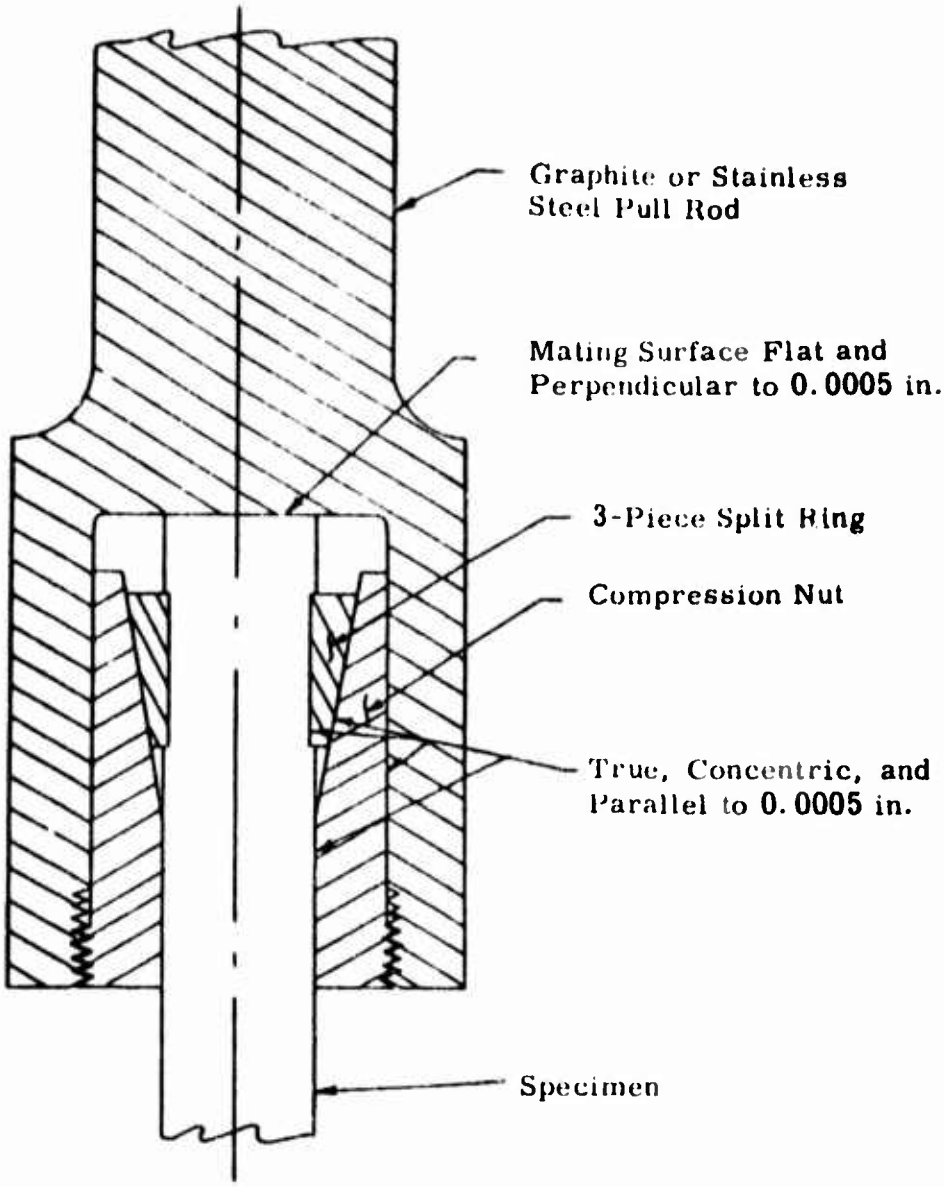

Figure 5. Precision Collet Grip for Tensile Specimen 2:1 Scale

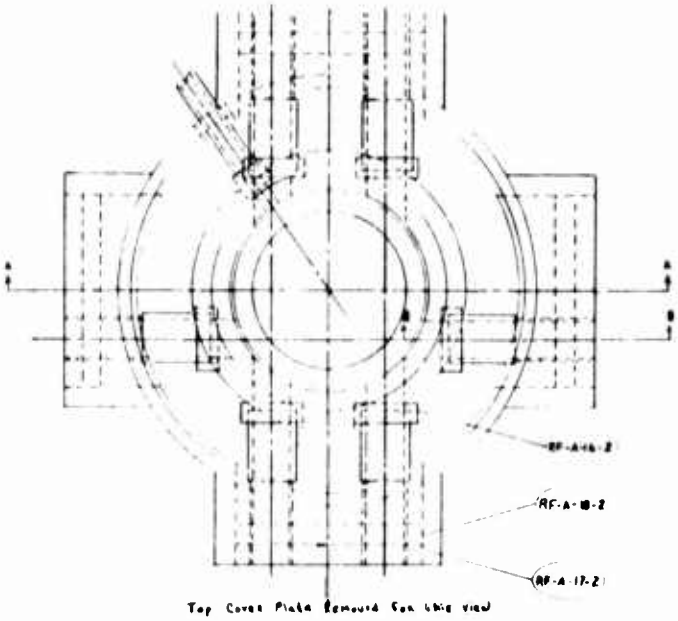

Item	Quan.	Description
A-2	1	Top pyrolytic graphite ring
A-3	1	Bottom pyrolytic graphite ring
A-4	1	Pyrolytic graphite temperature sight plate
A-5A	1	CS graphite protector tube
A-6	1	CS graphite temperature sight tube
A-7	1	Bottom Micarta insulating disc
A-8	1	Top steel base plate
C-9A	1	Steel shell
A-10	1	Top Micarta insulating disc
A-11	1	Top zirconia disc
A-12	1	Bottom steel base plate
A-13	1	Bottom zirconia disc
A-14A	1	CS graphite heater tube
A-15	2	Steel sight port tube
A-16-1	2	CS graphite sight port plate
A-16-2	2	CS graphite sight port plate
A-17-1	2	Firebrick sight port plate
A-17-2	2	Firebrick sight port plate
A-18-1	2	Zirconia sight port disc
A-18-2	2	Zirconia sight port disc
A-19	4	CS graphite sight tube
A-20	2	Fiberfrax insulator
A-21	1	Top electrode
A-22	1	Bottom electrode
A-23	1	Thermatomic carbon

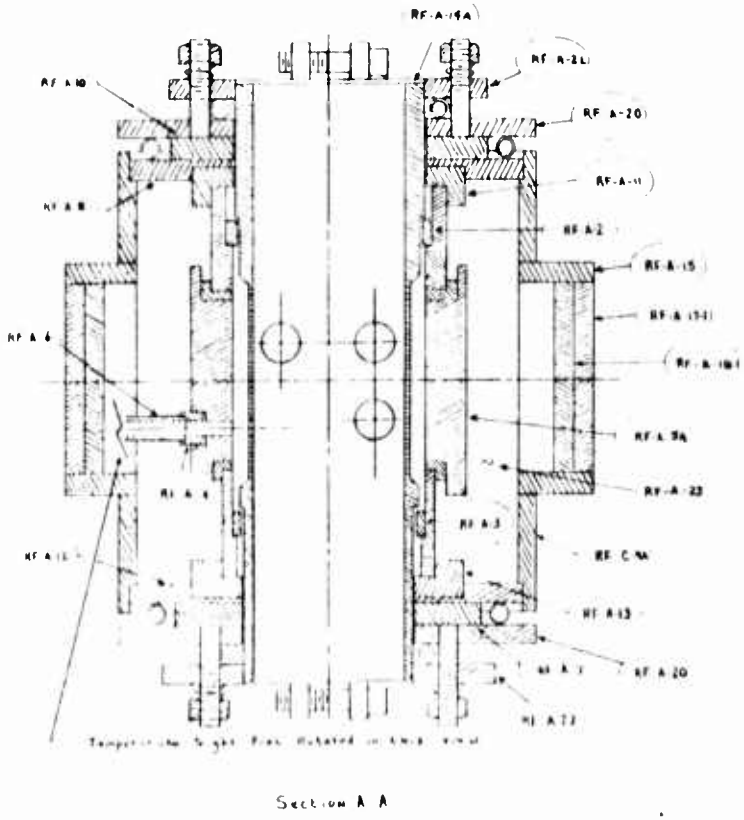

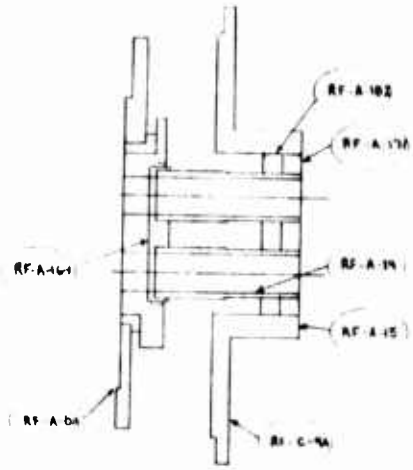

Figure 6. Small 5500°F Graphite Resistance Furnace

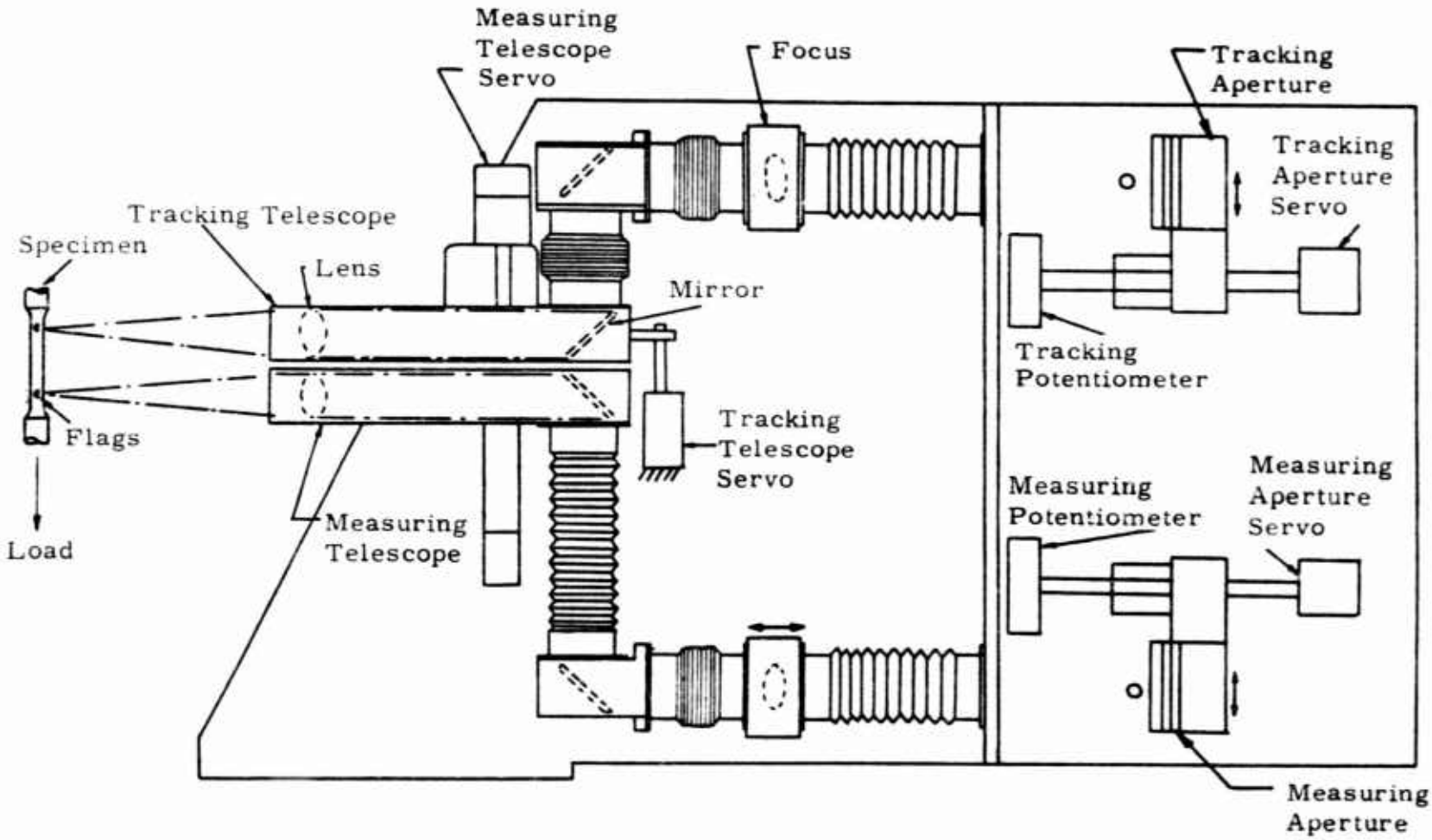

Figure 7. Arrangement of Optical Strain Analyzer

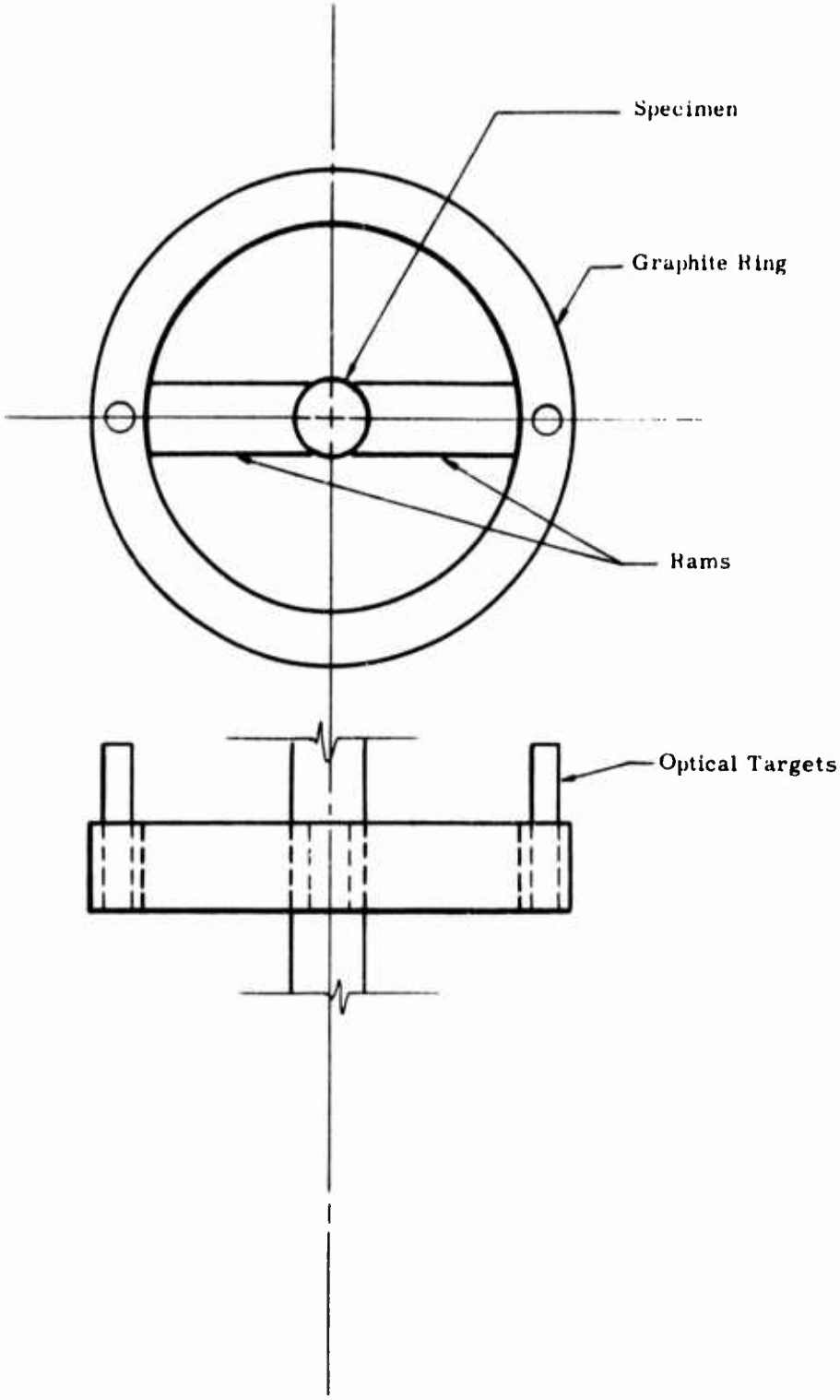

Figure 8. General Configuration of the Flag Attachment to Monitor Lateral Strain in Tension

APPENDIX B

ULTIMATE STRENGTH, ELASTIC MODULUS, AND POISSON'S RATIO TO 5500°F IN COMPRESSION

The compressive apparatus is shown in the photograph in Figure 1 and in the schematic in Figure 2 and consists primarily of a load frame, gas bearings, load train, 50-ton screw jack, variable speed mechanical drive system, strain analyzers, 5500°F furnace, and associated instrumentation for the measurement of load and strain.

The load frame is similar to most standard frames. It was designed to carry a maximum load of 100,000 pounds and to support the furnace optical strain analyzers, and other related equipment.

Gas bearings are installed at each end of the load train to permit precise alignment of the loading train to the specimen. The upper bearing is spherical on a radius of 6.5 inches. This radius is the distance from the top of the specimen to the spherical bearing surface. The load train, not the specimen, shifts to maintain radial alignment. The lower bearing is flat and is about 6 inches in diameter. The lower bearing permits transverse alignment of the load train. The gas bearings are floated for only a small initial amount of load so that precise alignment of the load train can be attained.

The load train near the furnace consists of the specimen loaded on each side by graphite and water-cooled steel push rods. The graphite push rods are counter-bored to permit insertion of a pyrolytic graphite disc which serves as a heat dam and to align the specimen to the center-line of the load train. Extreme care is exercised in the preparation of all parts of the load train to ensure concentricity of the mating parts to less than 0.0005 inch.

The 50-ton jack is a power screw type. The mechanical drive system consists of a gear reducer driven by a Louis Allis Synchro-Spede Unit (300-3000 rpm). The gear reducer is connected to the Synchro-Spede Unit through a chain coupling and to the 50-ton jack by a single roller chain and sprocket system. Different load rates are obtained by adjustment of the variable speed setting on the Synchro-Spede and by changeout of sprockets on the gear reducer and screw jack.

Figure 3 shows details of the "dumbbell" specimen which maintains a 0.500 inch diameter over the 1.2 inch long gage section. The specimen provides sufficient room for the flag attachments that follow the axial and lateral strains and also minimizes the influence of end restraint.

The flag attachments for the measurement of axial strain are positioned one inch apart so that unit strain is recorded directly. The flag attachment for the measurement of lateral strain is positioned between the flags for axial strain; see Figure 4. The lateral flag attachment used in compression is shown in Figure 5. The 4-piece assembly consists of a ring, two rams bearing on the specimen, and a screw to adjust the contact pressure. The ring was designed to track lateral motions as great as 0.030 inch without breaking.

Figure 6 is a sketch of the 5500°F furnace used for compression showing the basic components. The furnace consists of a resistivity heated graphite element insulated from a water-cooled shell by thermatomic carbon. The furnace and specimen are purged with helium to provide an inert atmosphere. Ports with visual openings are provided on opposite sides of the furnace as a means of allowing the strain analyzers to view the gage flags on the specimen. Specimen temperatures are determined by optical pyrometer readings taken through another small sight port containing a sapphire window. A calibration curve was established for the loss through the sapphire window, and since the furnace cavity acts essentially as a blackbody, true temperature readings are obtained. Power is supplied to the heating element by means of a 25 KVA variable transformer.

Strain measurement consists of measuring optically the elongation between two flags, or targets, which are mounted on the specimen and separated initially by a predetermined gage length. The travel of the targets is measured by sensing the displacement of the image of the edge of the targets and then electromechanically following the image displacement. The relative travel of the two targets provides the strain. Readout is continuous and automatic on a millivolt recorder. A schematic of the analyzer is shown in Figure 7.

A brief summary of the mechanical motions of the components involved in monitoring the strain is helpful in understanding the detailed performance. A tracking telescope follows the upper target and carries a second telescope mounted on its carriage. The second telescope is capable of independent motion to follow the lower target. The relative displacement between the upper and lower telescope, as strain occurs, defines the strain. The system usually is operated so that the tracking telescope follows the

upper target and the strain is monitored by the relative displacement of the aperture rather than the telescope following the lower target. With this procedure the maximum range is the maximum displacement available for the lower aperture, or about 1/8 inch, and the sensitivity is limited by the optics and the noise level of the detector. Using both telescopes, the range is about 3/4 inch.

To provide optical references on the specimens, targets are affixed to the test specimen as mentioned. When the specimen is heated to temperature, the targets are self-luminous and are observed optically. The optics view past the luminous targets into a cooled cavity in the opposite furnace wall. The self-luminous targets are then visible against a dark background. To obtain data at below 2000°F, a light beam is directed from behind the flags providing a shadow image for the detection system.

The image of the glowing target is focused through a rotating shutter (chopper) and onto a rectangular aperture. Small slits in the aperture pass a portion of the upper and lower edges of the light beam. A photocell receives the light thus transmitted, and an electronic circuit detects whether the energy passed by the two slits is equal. A servo drives the apertures to let a balanced quantity of light pass through the two slits and thus maintains an optical null.

To obtain lateral strain, a strain analyzer is supported horizontally on the load frame to view the diametrical or lateral strain of the specimen.

Calibrations of the analyzers are performed in various ways including absolute correlations to precision micrometers, strain gage extensometers, and direct plots of stress-strain for reference materials such as steel, plexiglas, magnesium, and aluminum. Precision is ±0.000020 inch.

Instrumentation includes primarily a stress-strain measurement system composed of a 20,000-pound SR-4 Baldwin load cell, constant d.c. voltage power supply, two optical strain analyzers, and two X-Y recorders. Specimen temperature is monitored with an optical pyrometer. Stress(load) is measured by a commercial load cell. The cell receives a constant d.c. voltage input from the power supply and transmits a millivolt signal (directly proportional to load) to an X-Y recorder. Simultaneously, the optical strain analyzers measure both the axial and lateral strain and transmit a millivolt signal (proportional to strain) to the X-Y recorders. Thus, continuous plots of stress-axial strain and axial strain-lateral strain are recorded simultaneously.

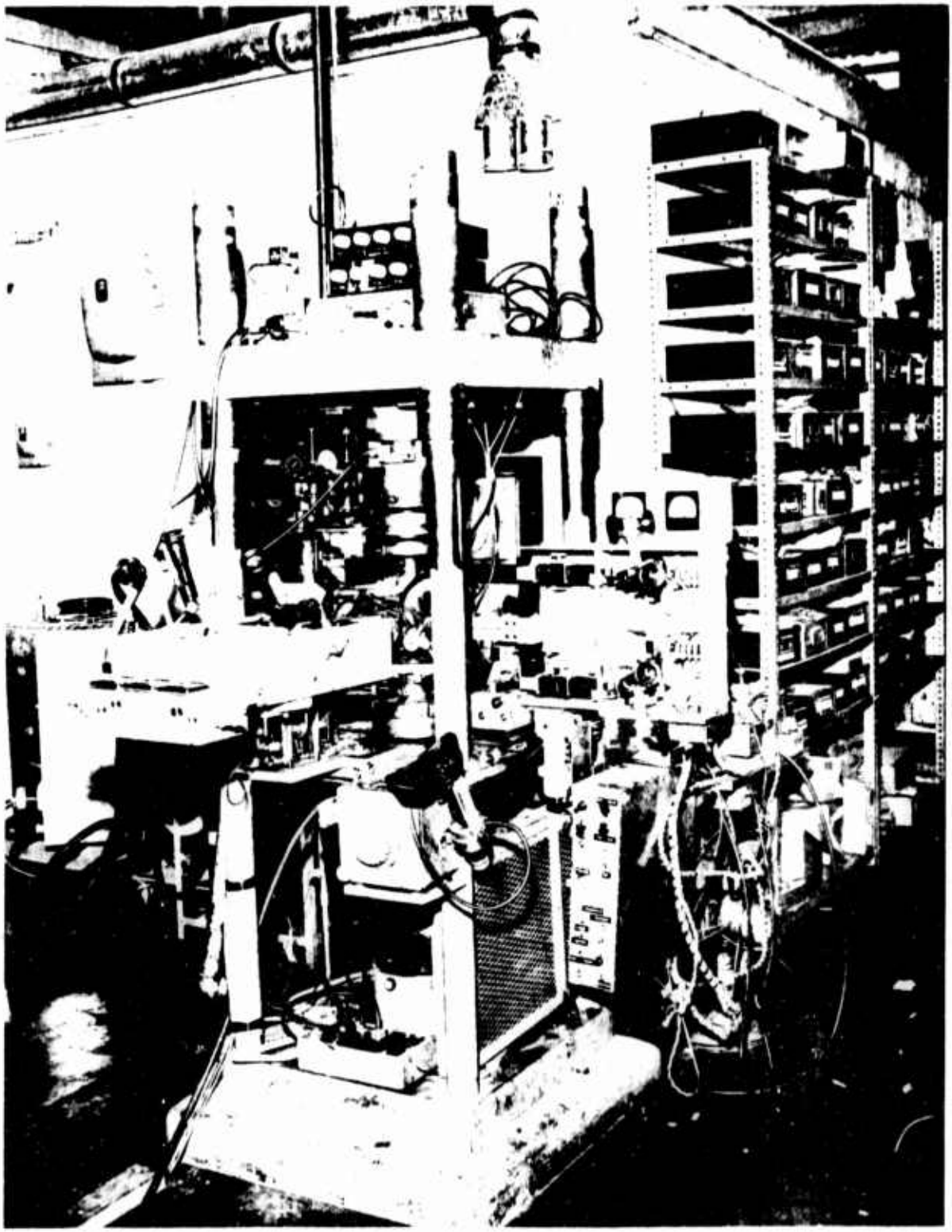

Figure 1. Picture of the Compressive Facility with Gas Bearings and Optical Strain Analyzer

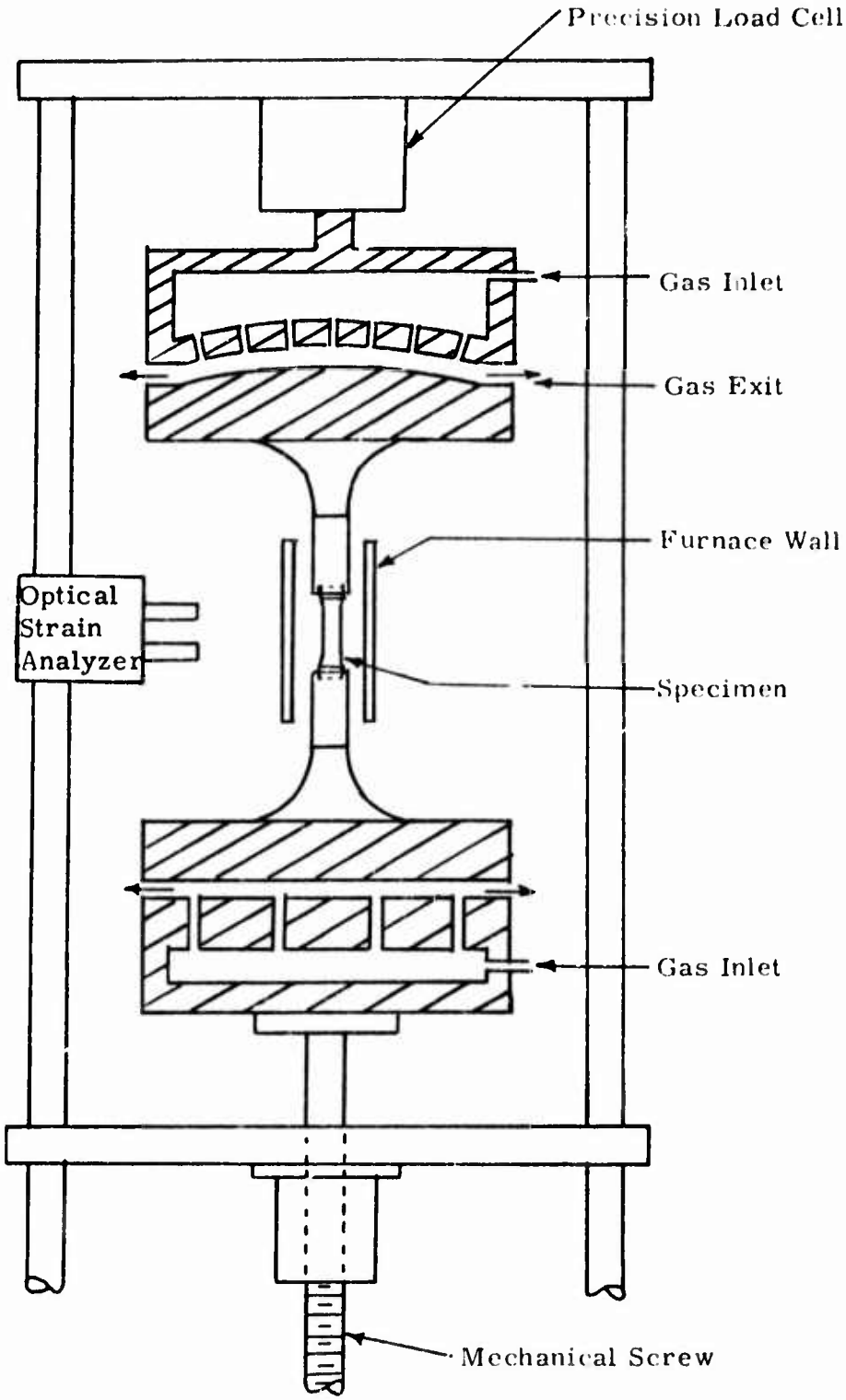

Figure 2. Schematic Arrangement of Gas-Bearing Universals, Specimen, and Load Train

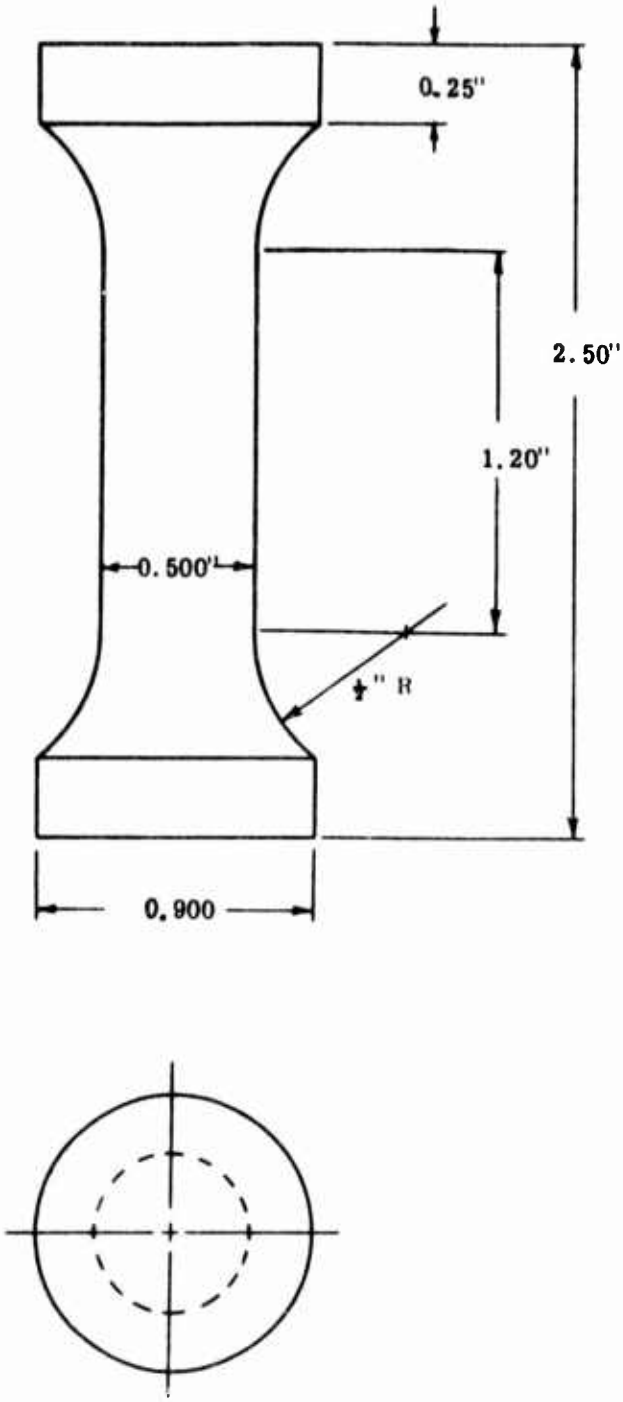

Figure 3. Compressive Specimen Configuration

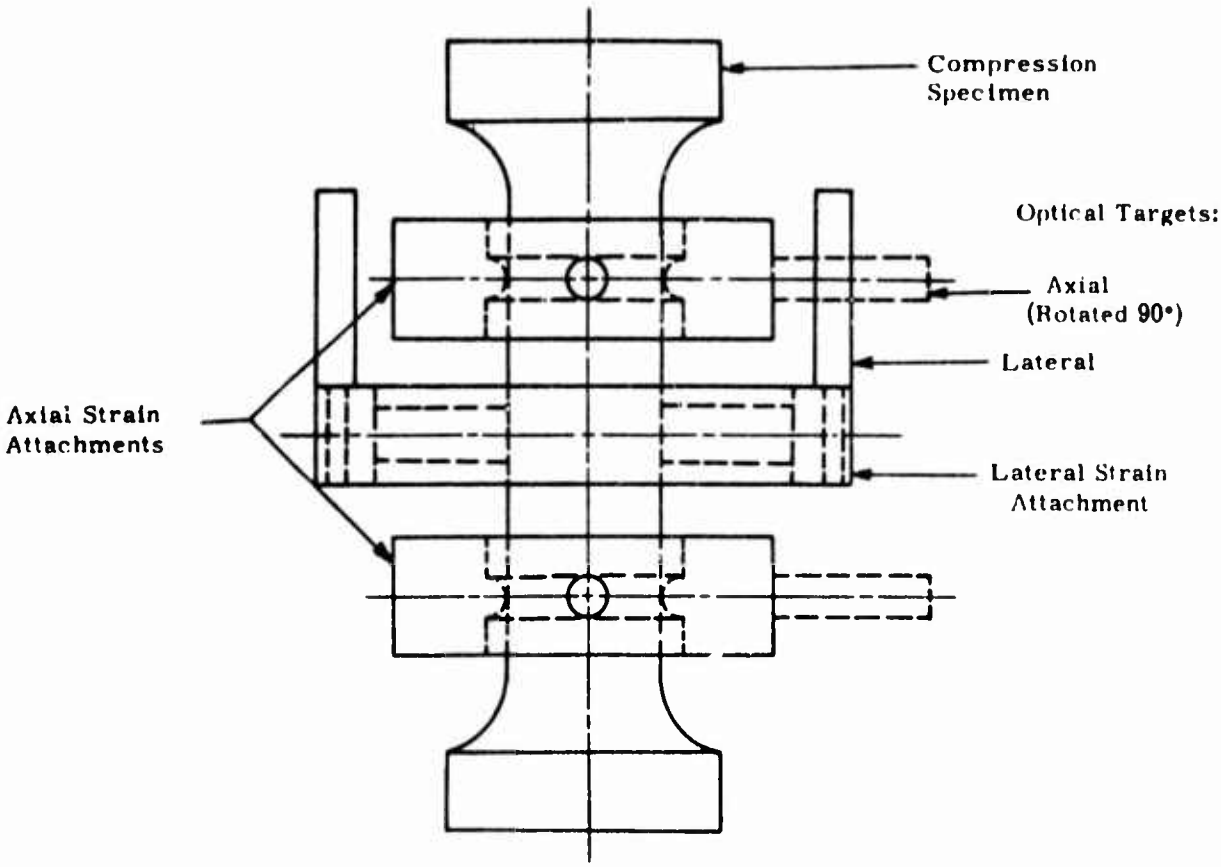

Figure 4. Location of the Flag Attachments on the Compressive Specimen

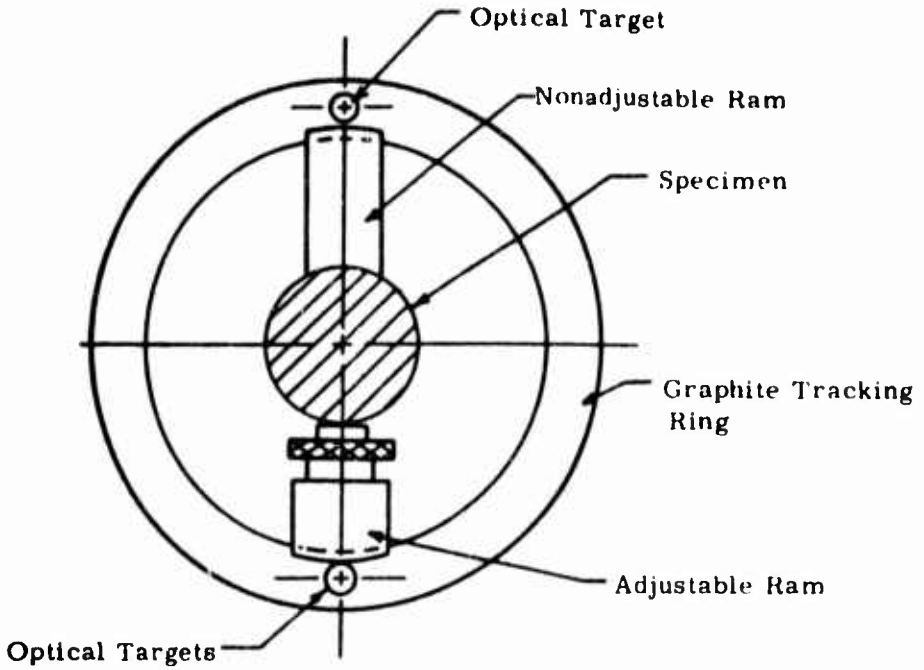

Figure 5. Lateral Strain Flag Attachment for Compressive Specimen

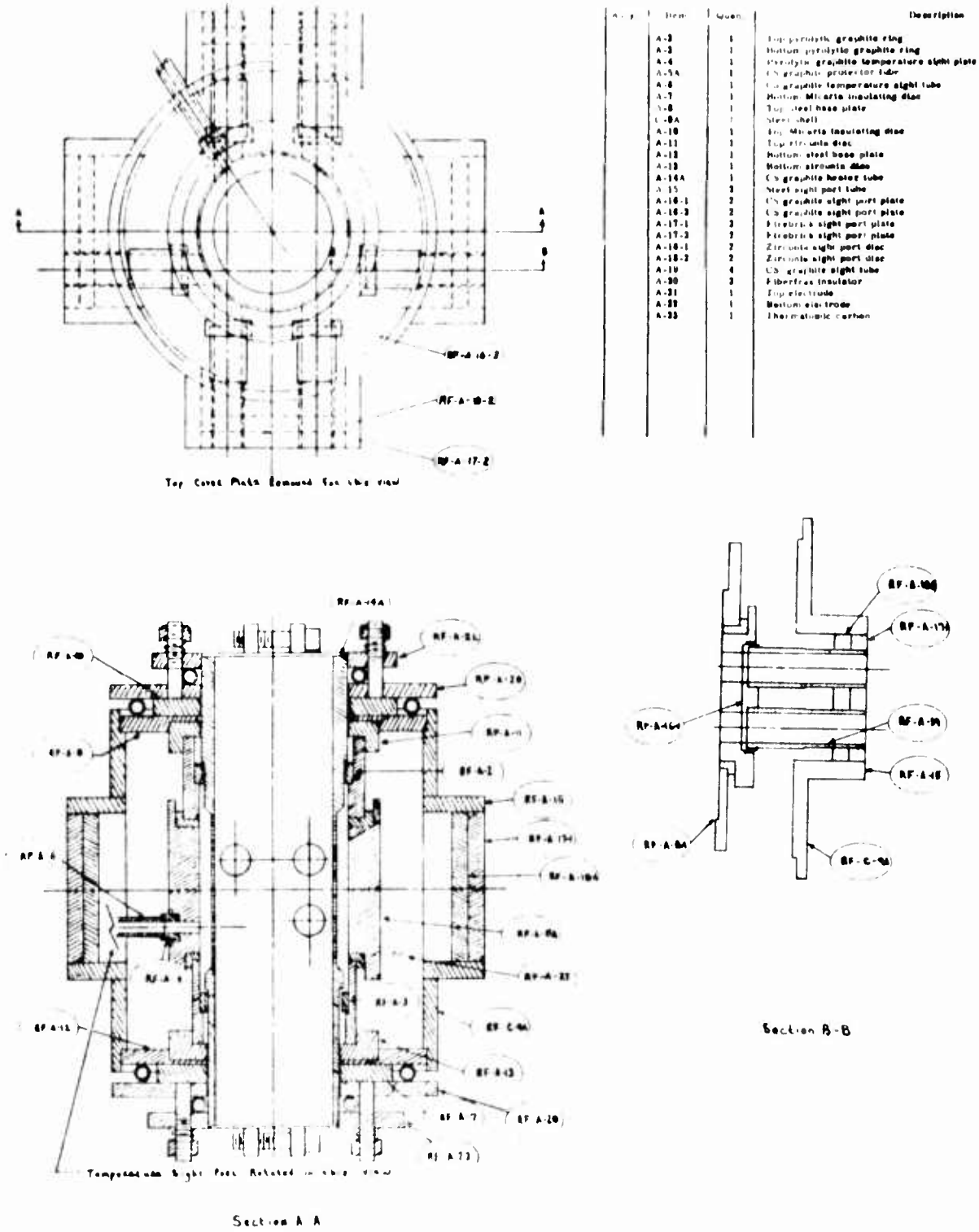

Figure 6. Small 5500°F Graphite Resistance Furnace

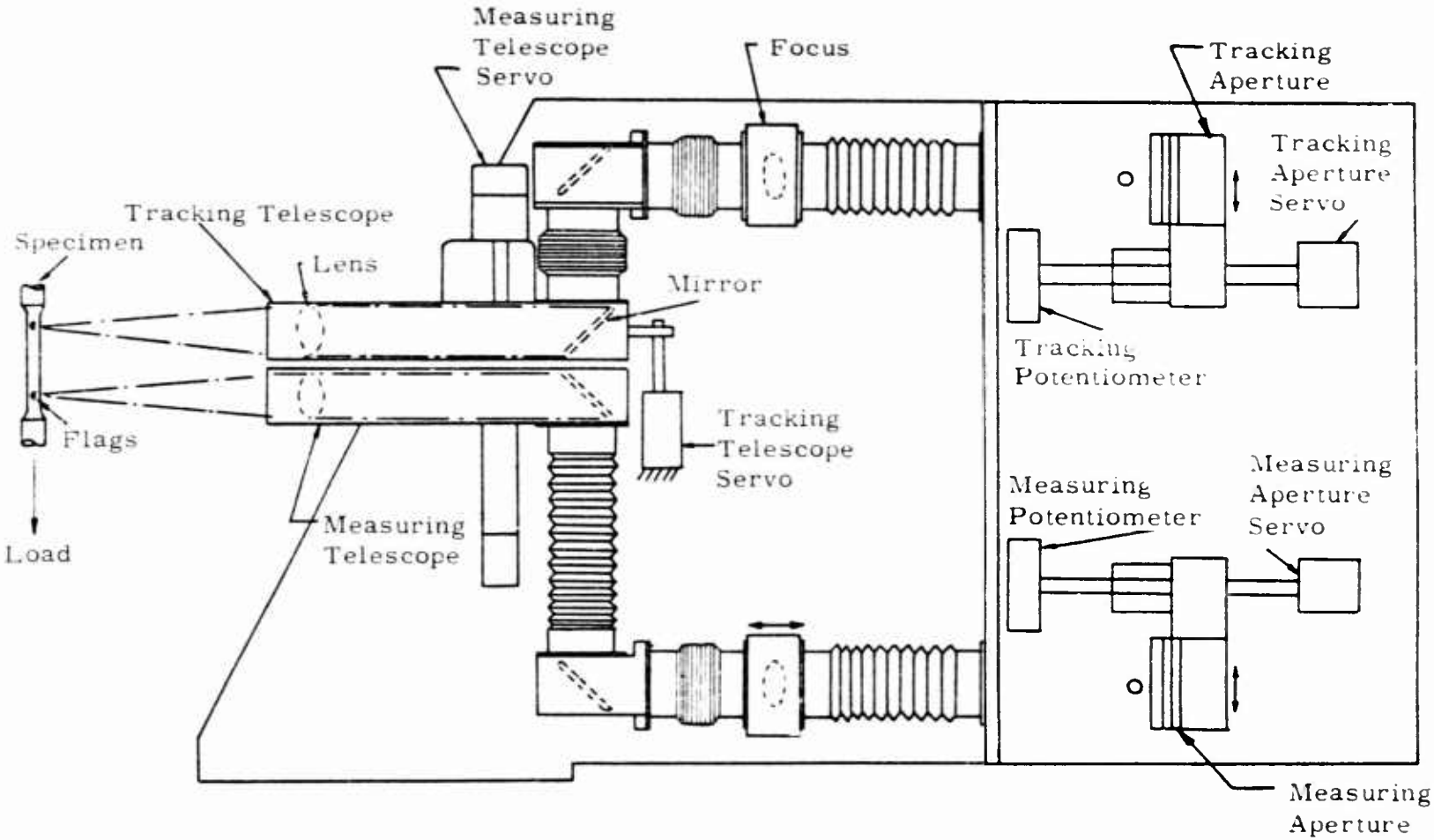

Figure 7. Arrangement of Optical Strain Analyzer

APPENDIX C

TENSILE STRESS-STRAIN CURVES FOR PG AND CODEPOSITED SiC/PG IN THE AB DIRECTION

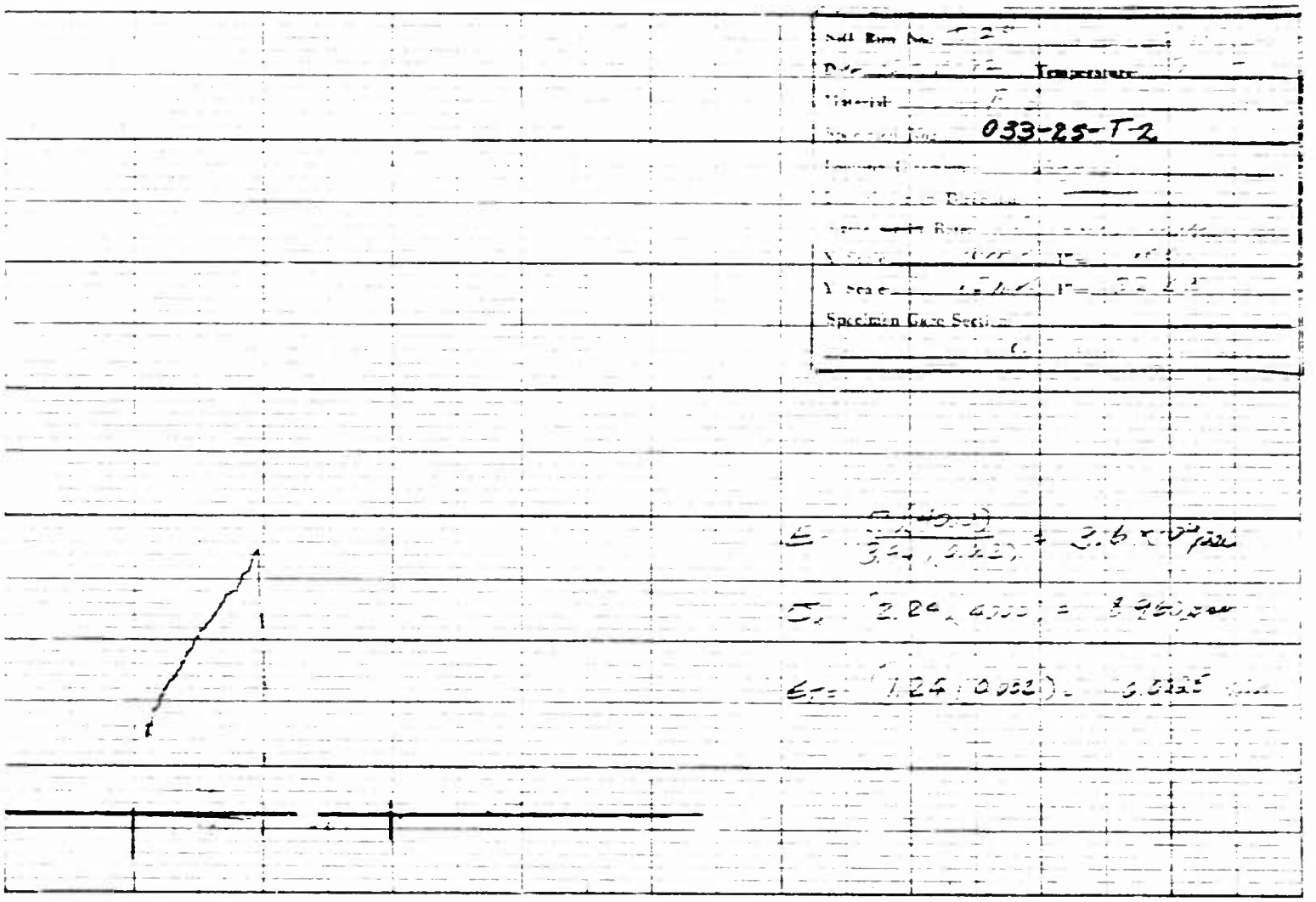

Figure C-1.

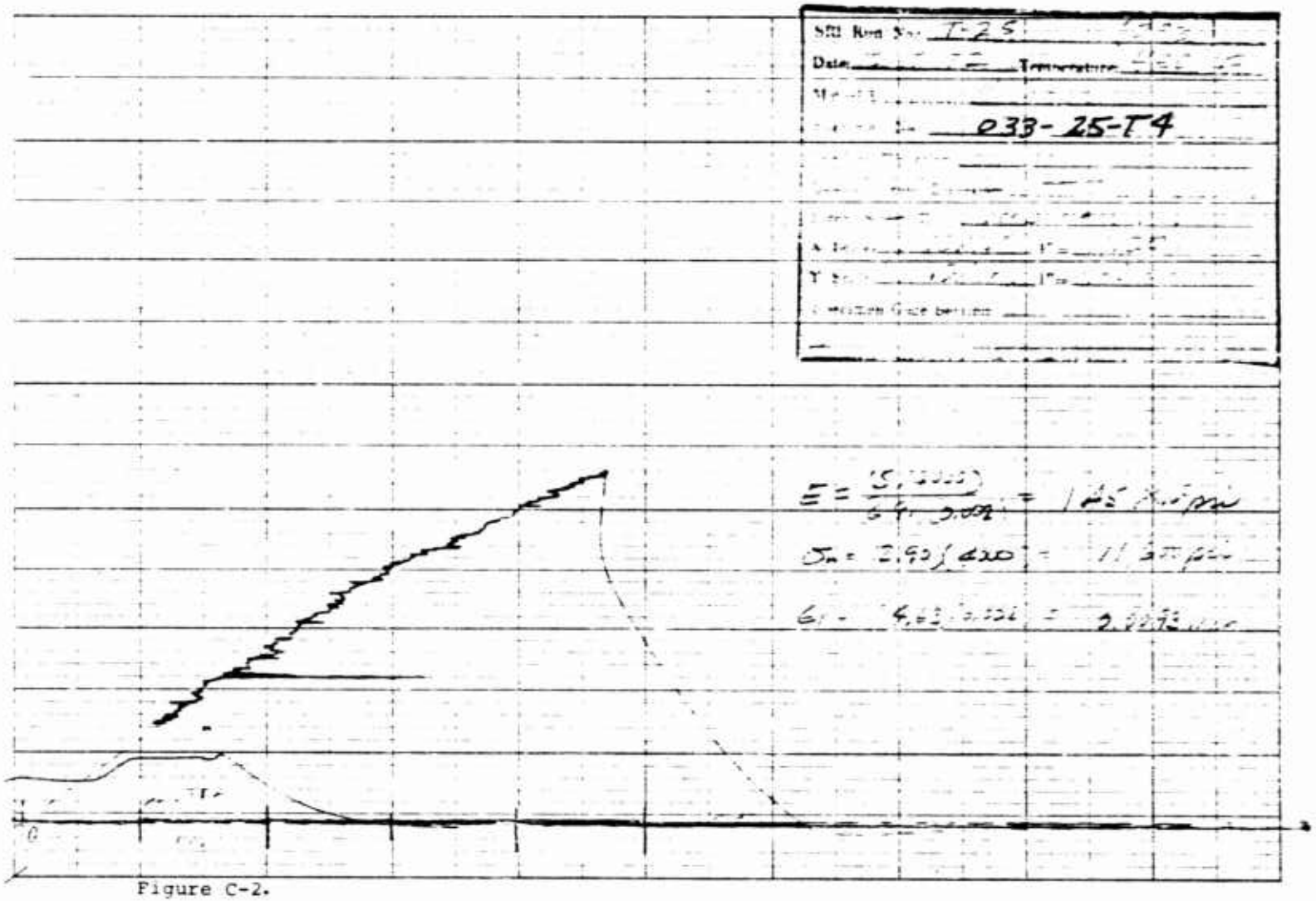

Figure C-2.

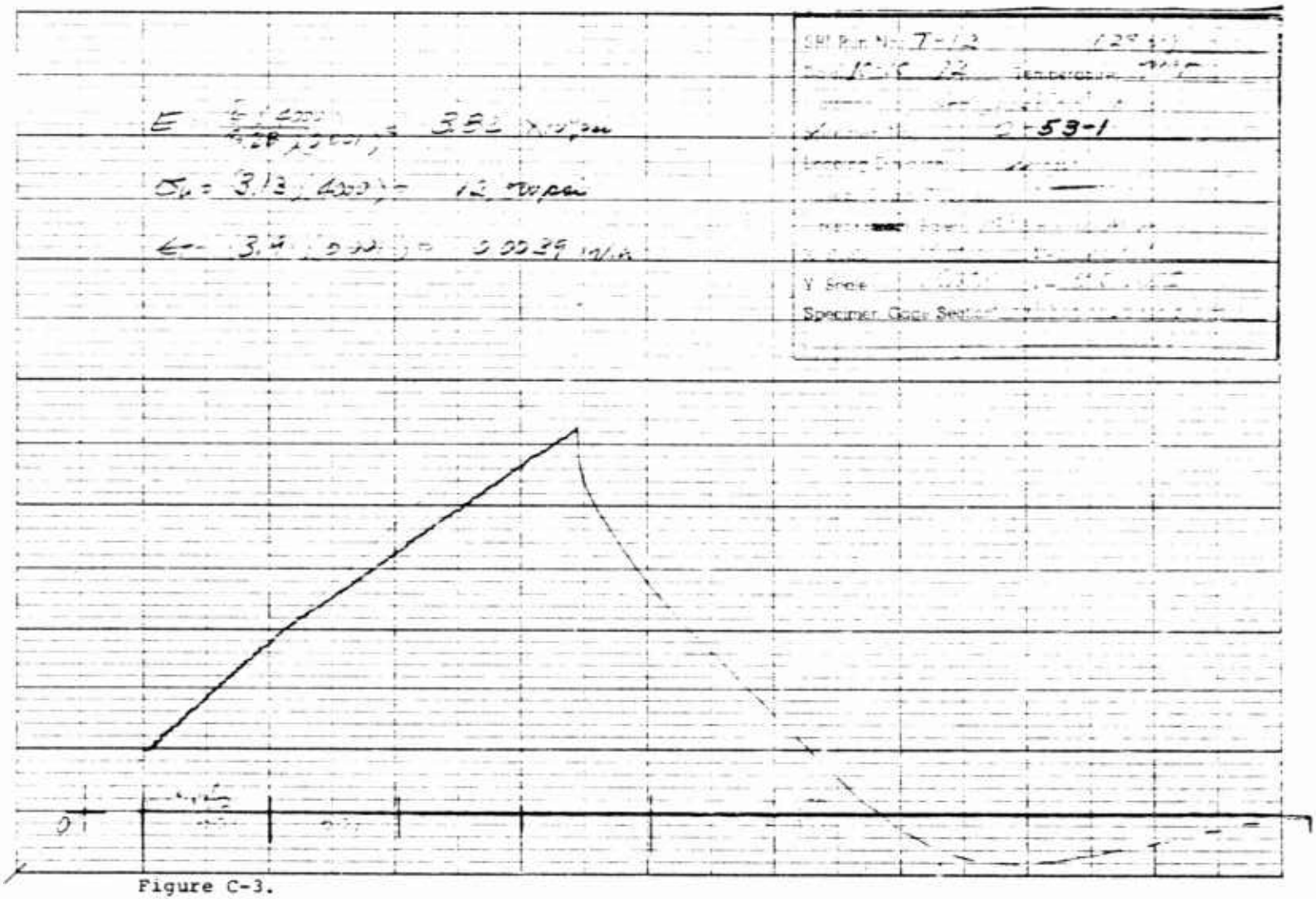

Figure C-3.

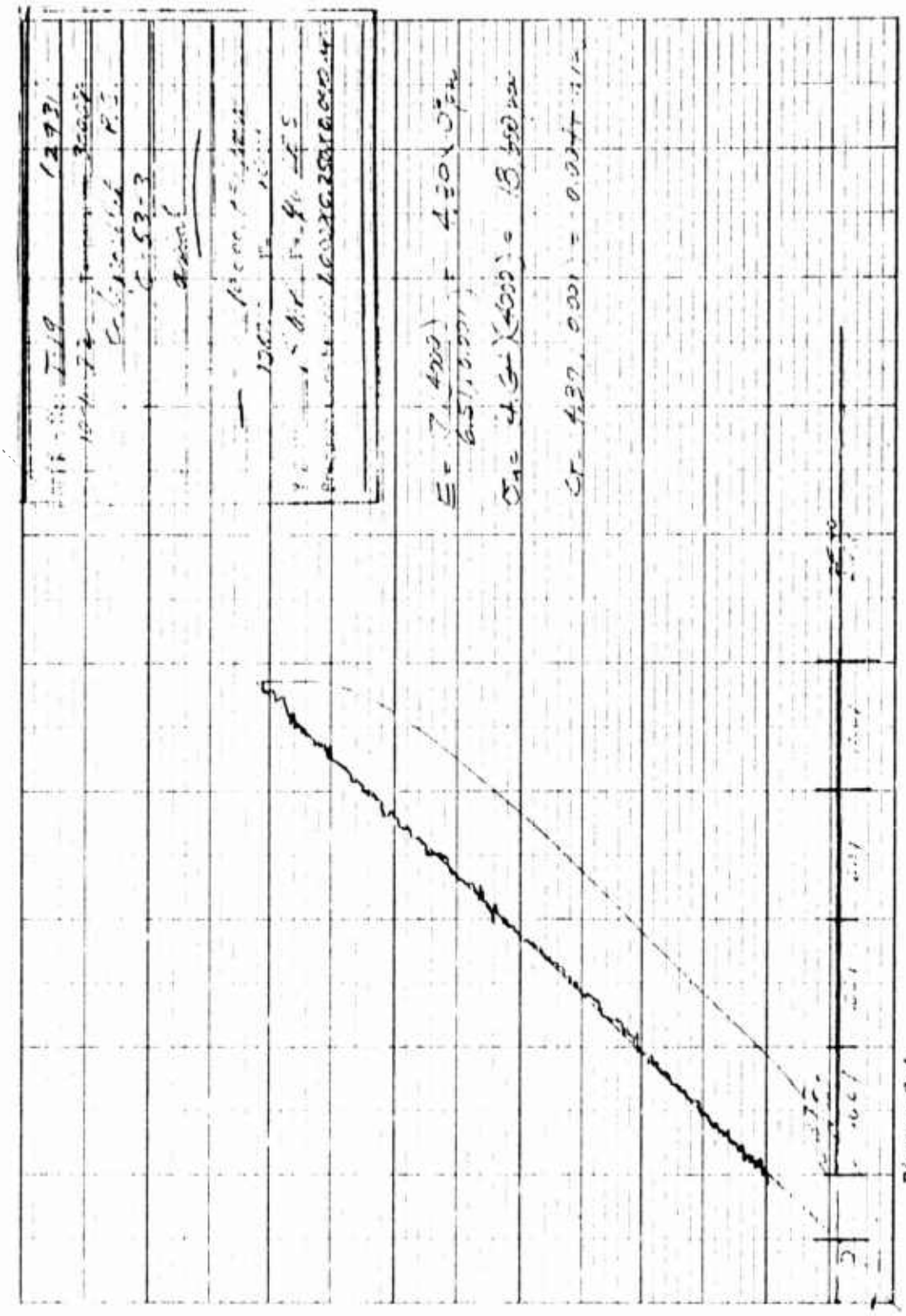

Figure C-4.

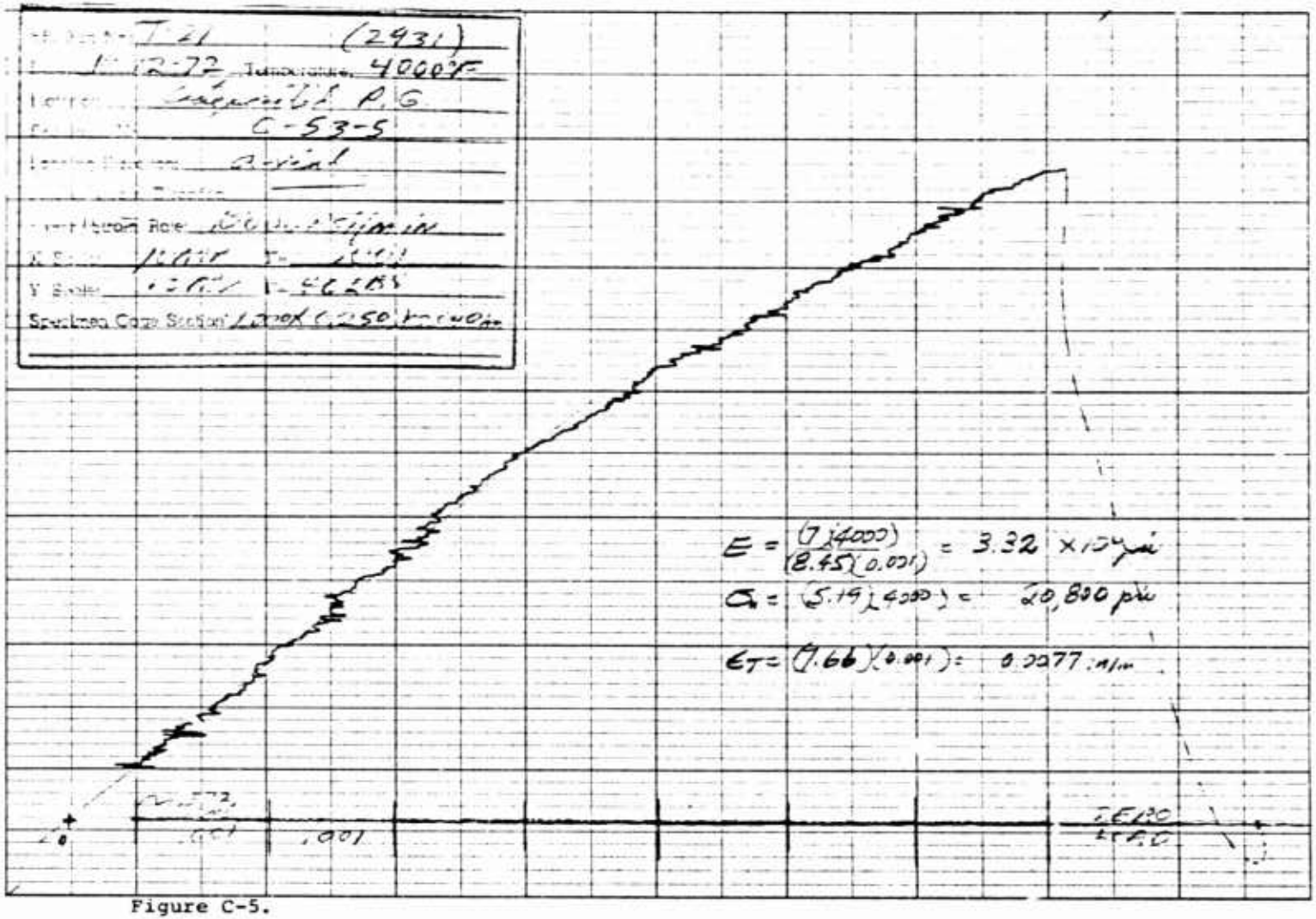

Figure C-5.

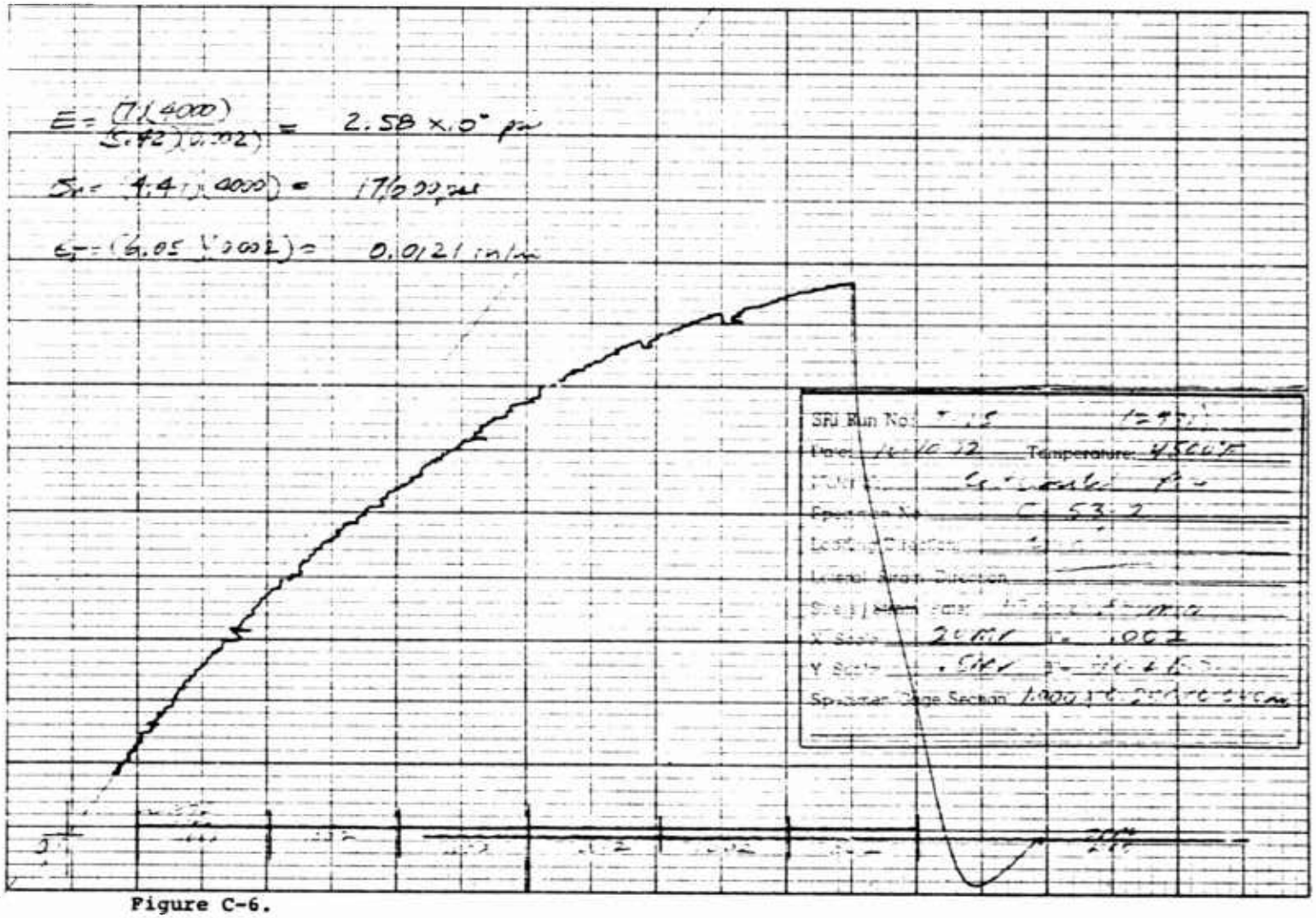

Figure C-6.

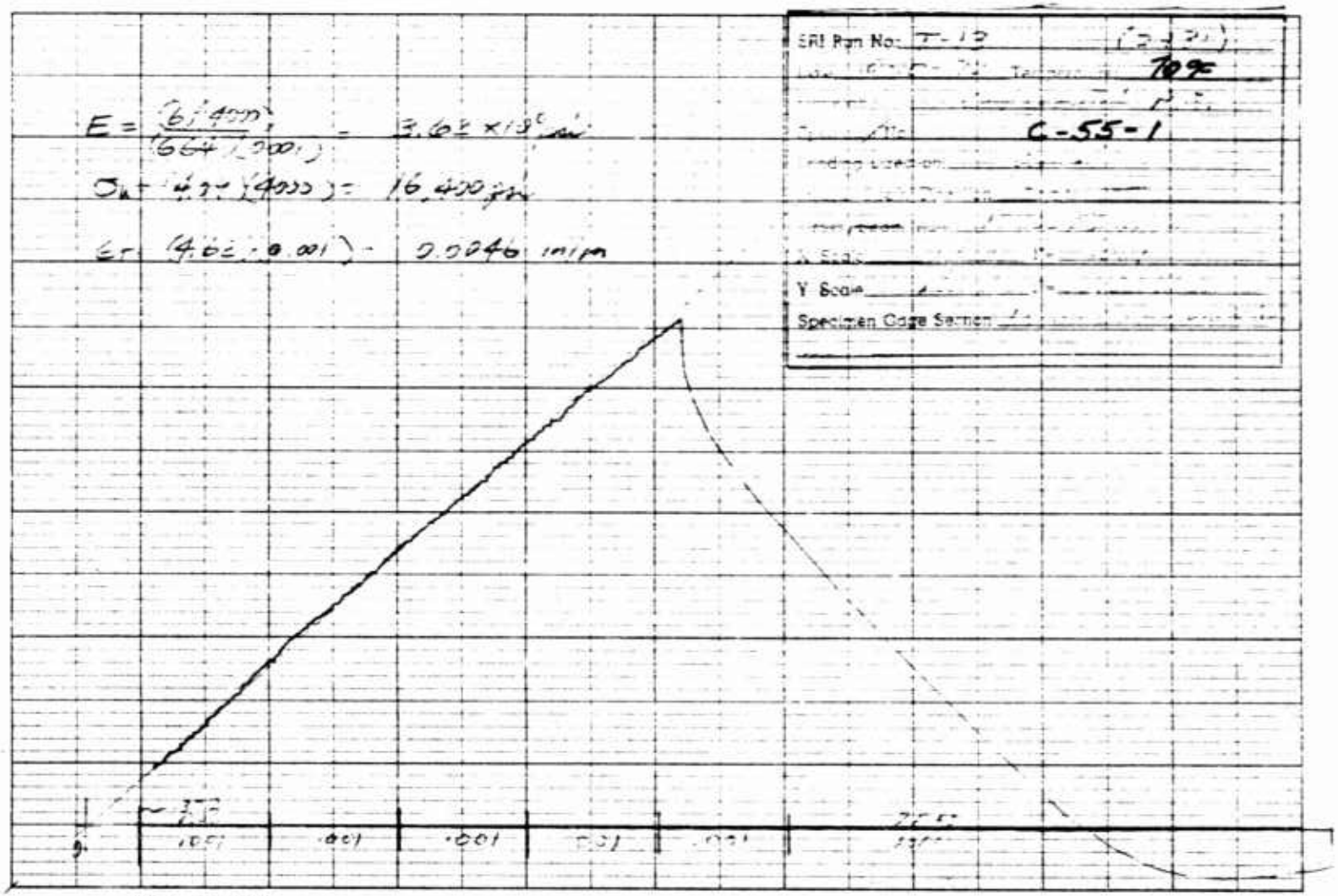

Figure C-7.

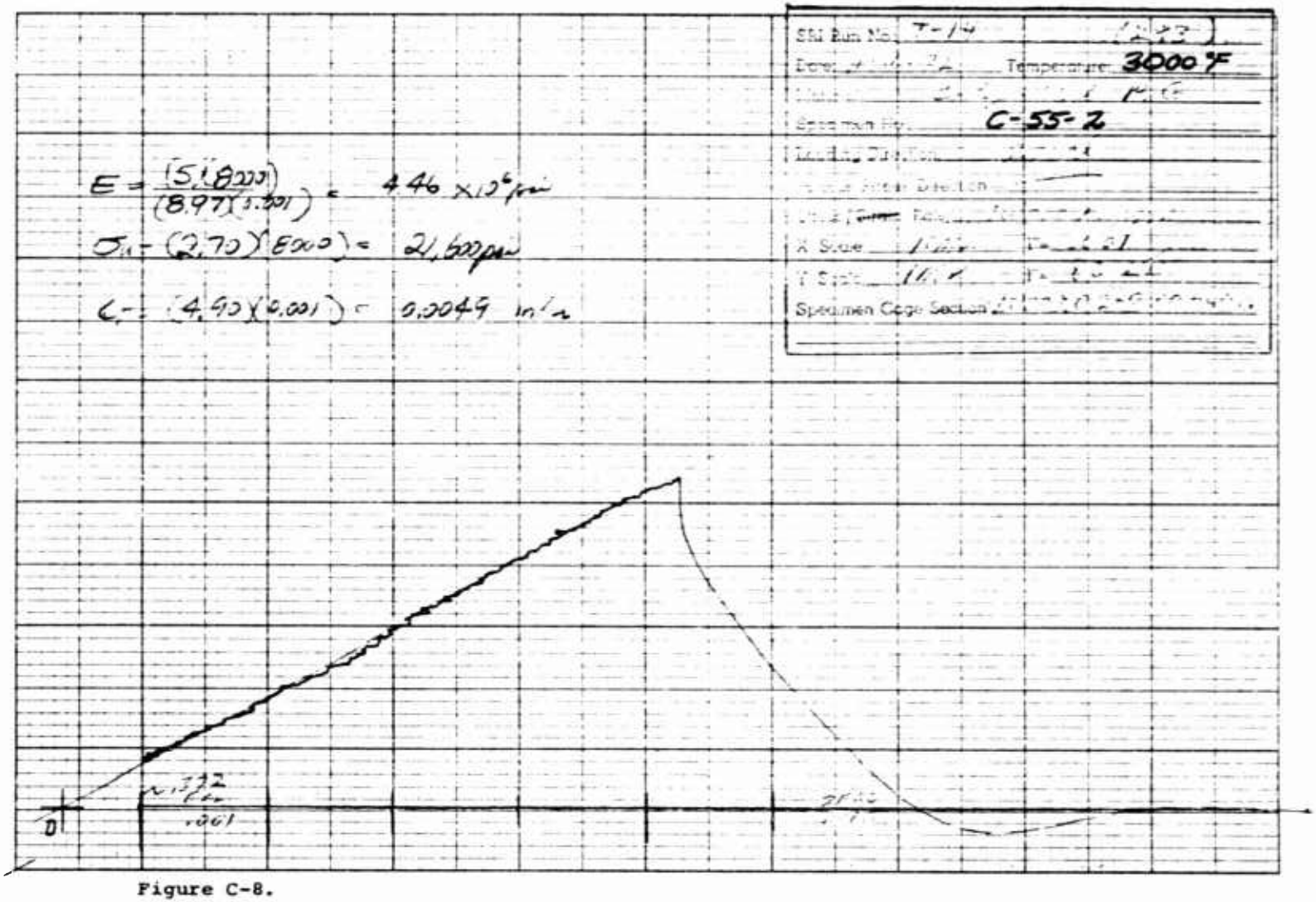

Figure C-8.

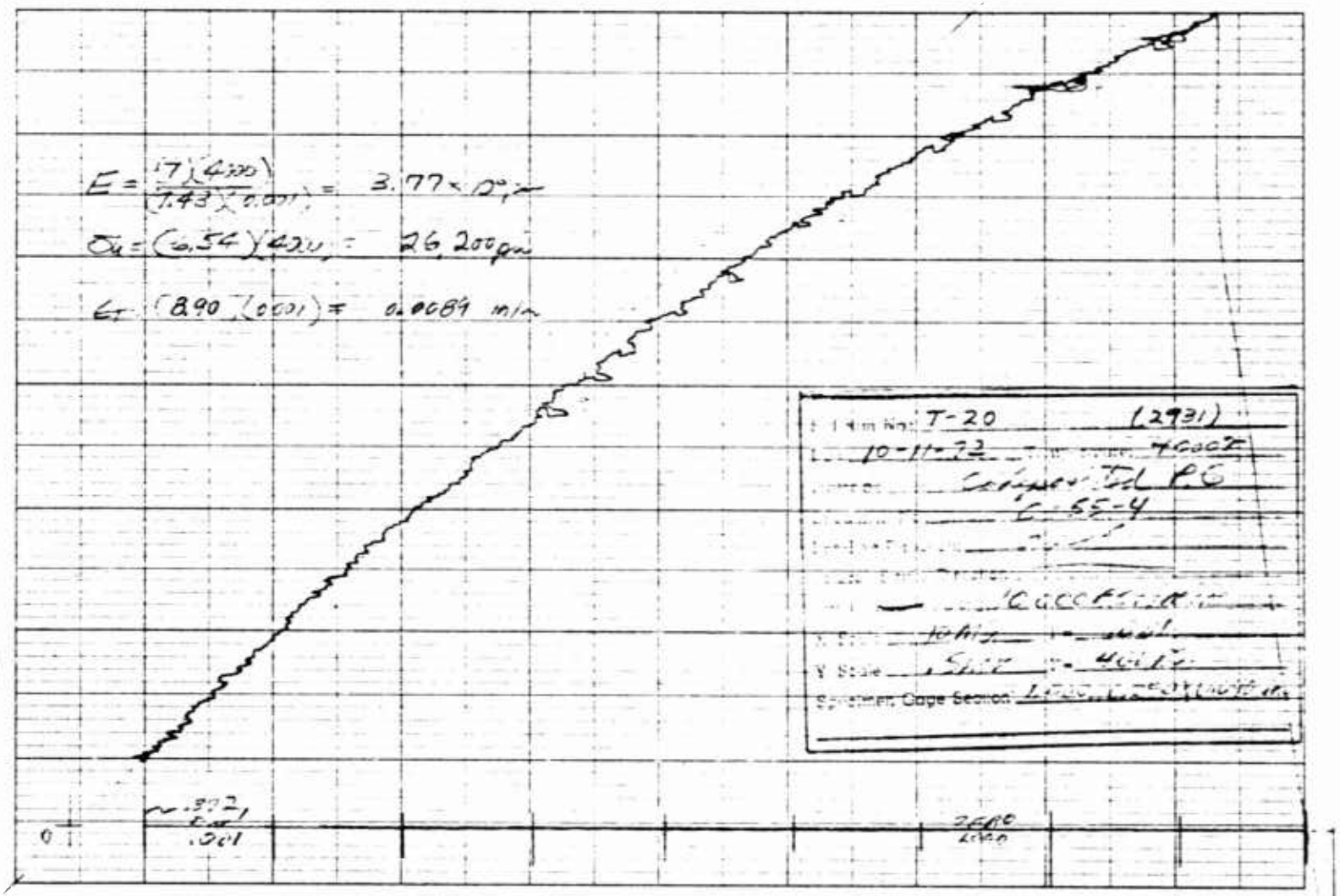

Figure C-9.

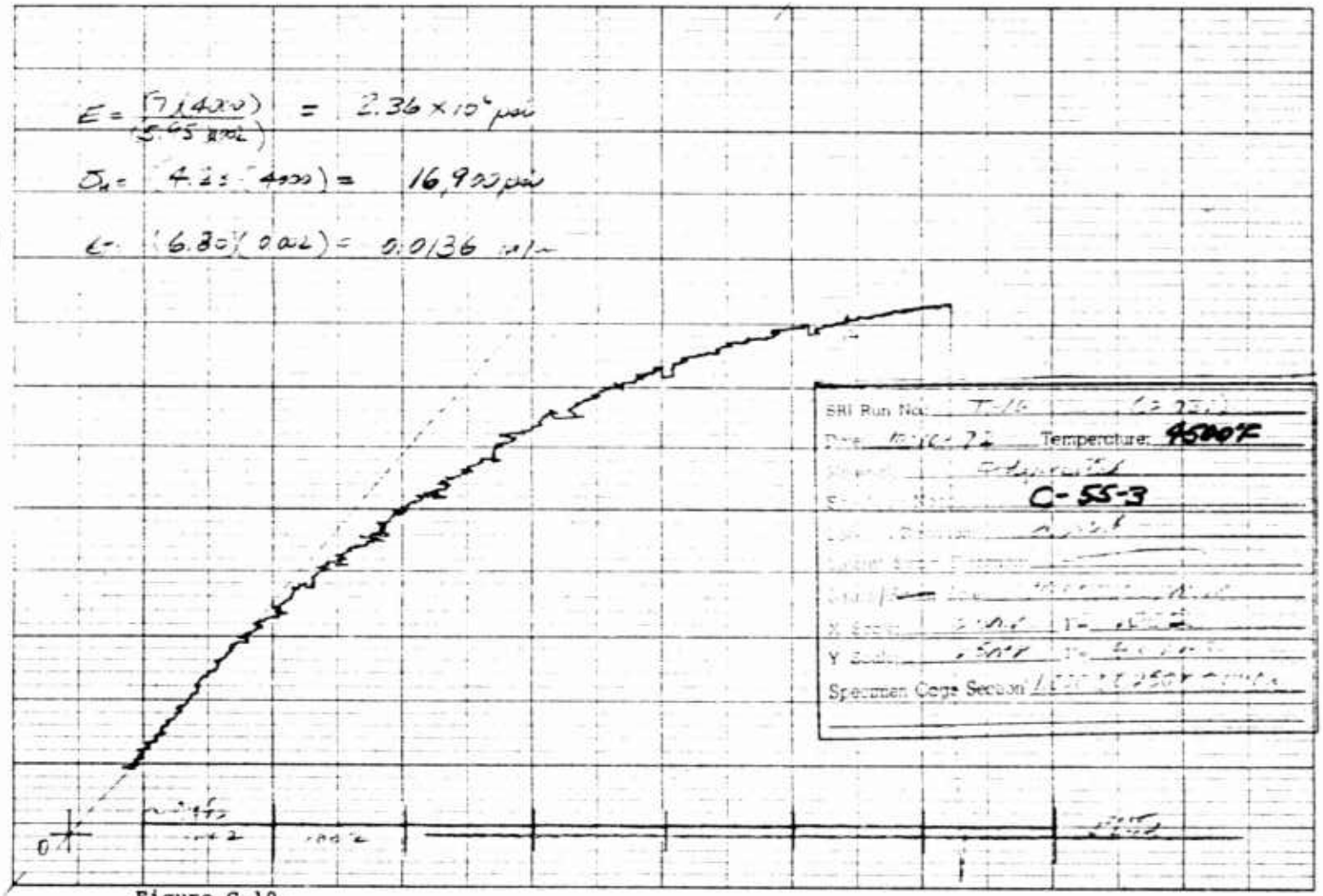

Figure C-10.

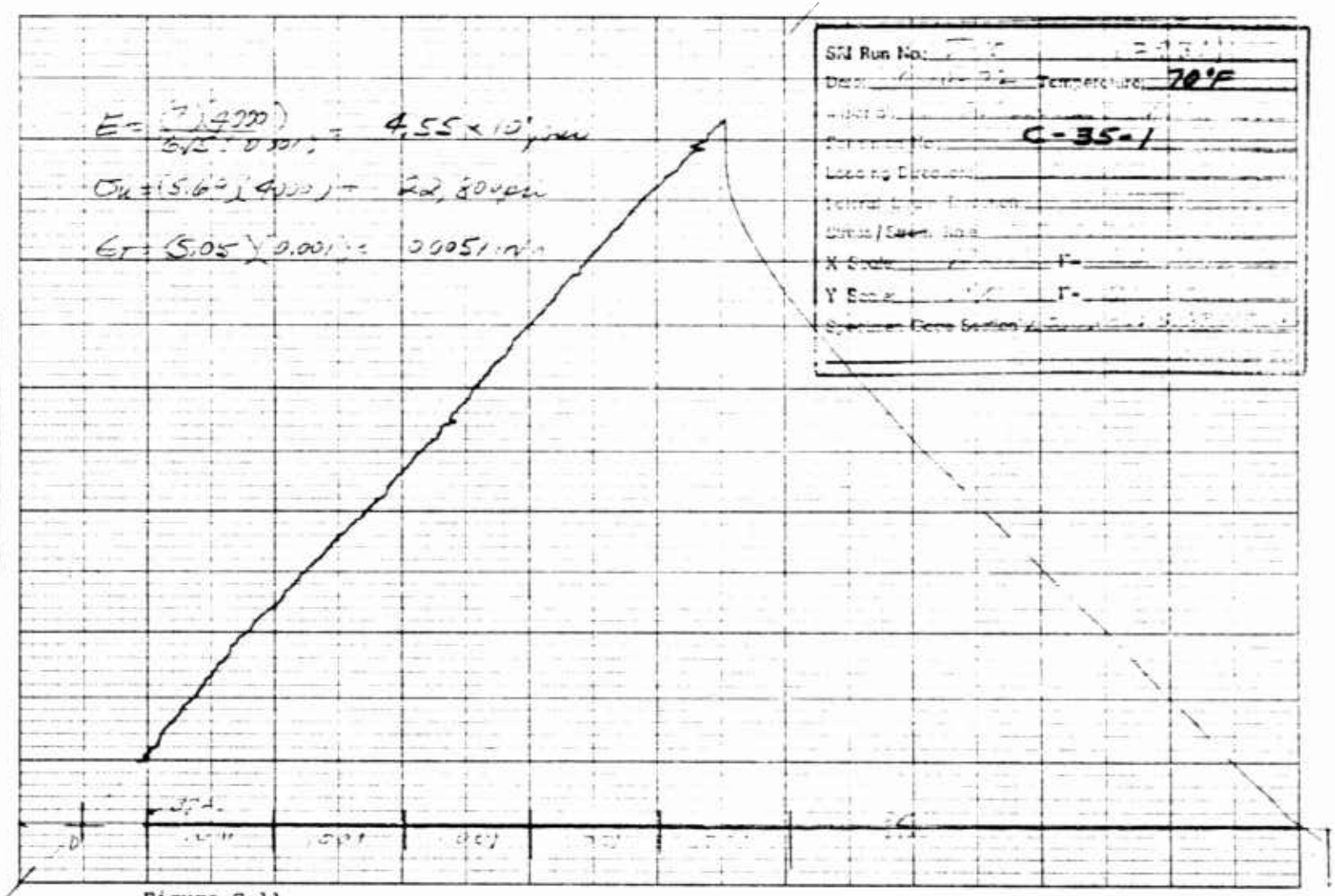

Figure C-11.

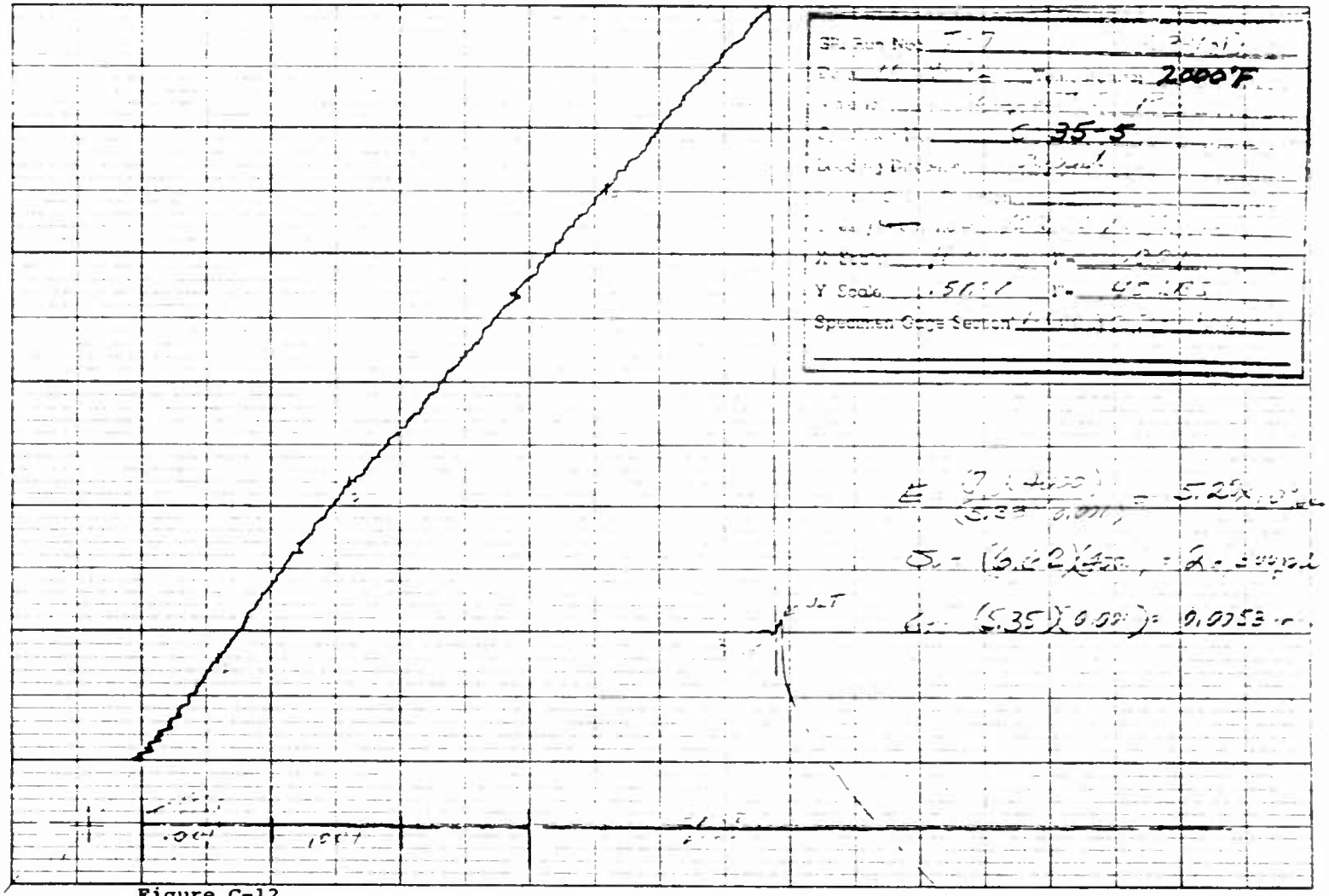

Figure C-12.

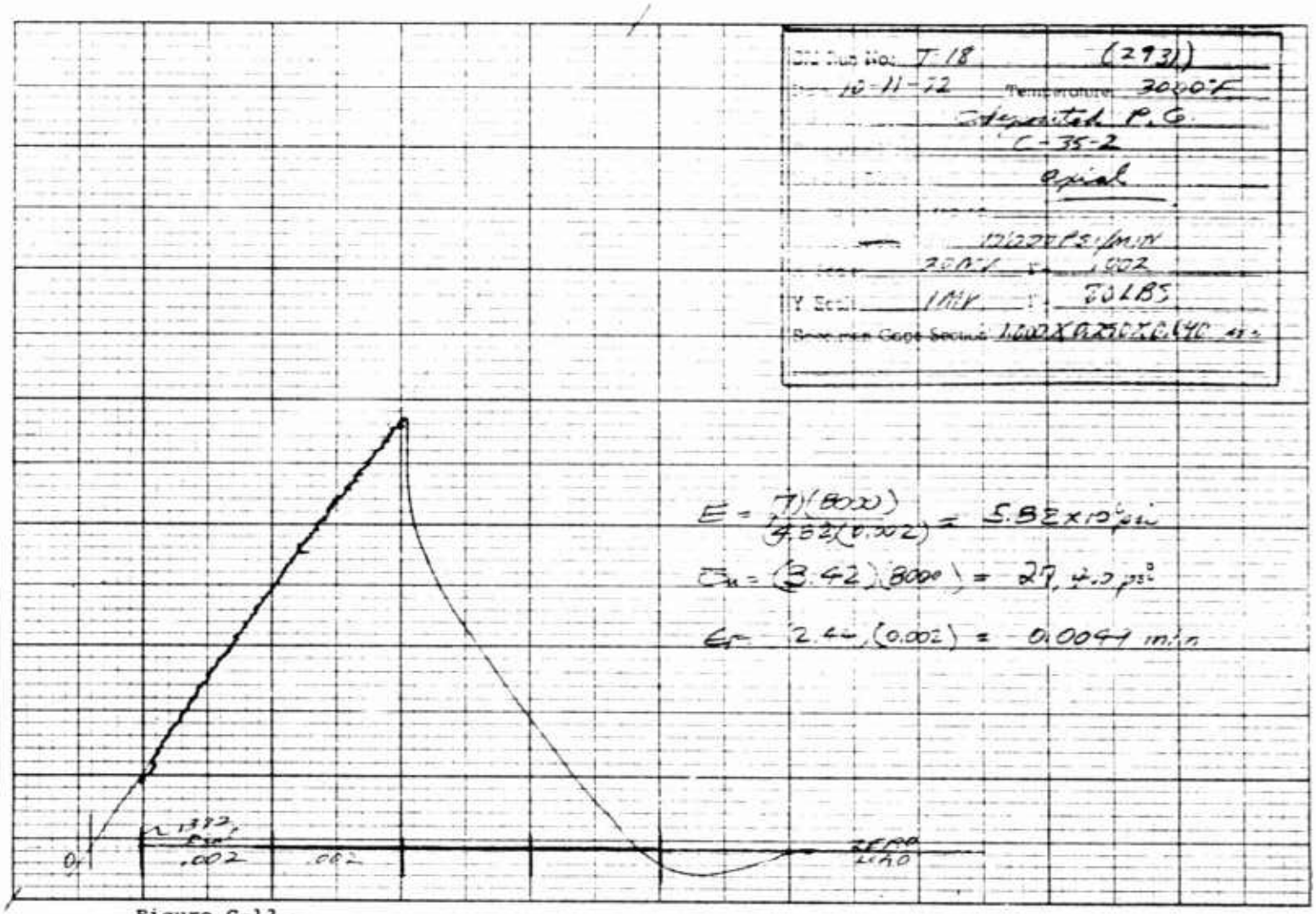

Figure C-13.

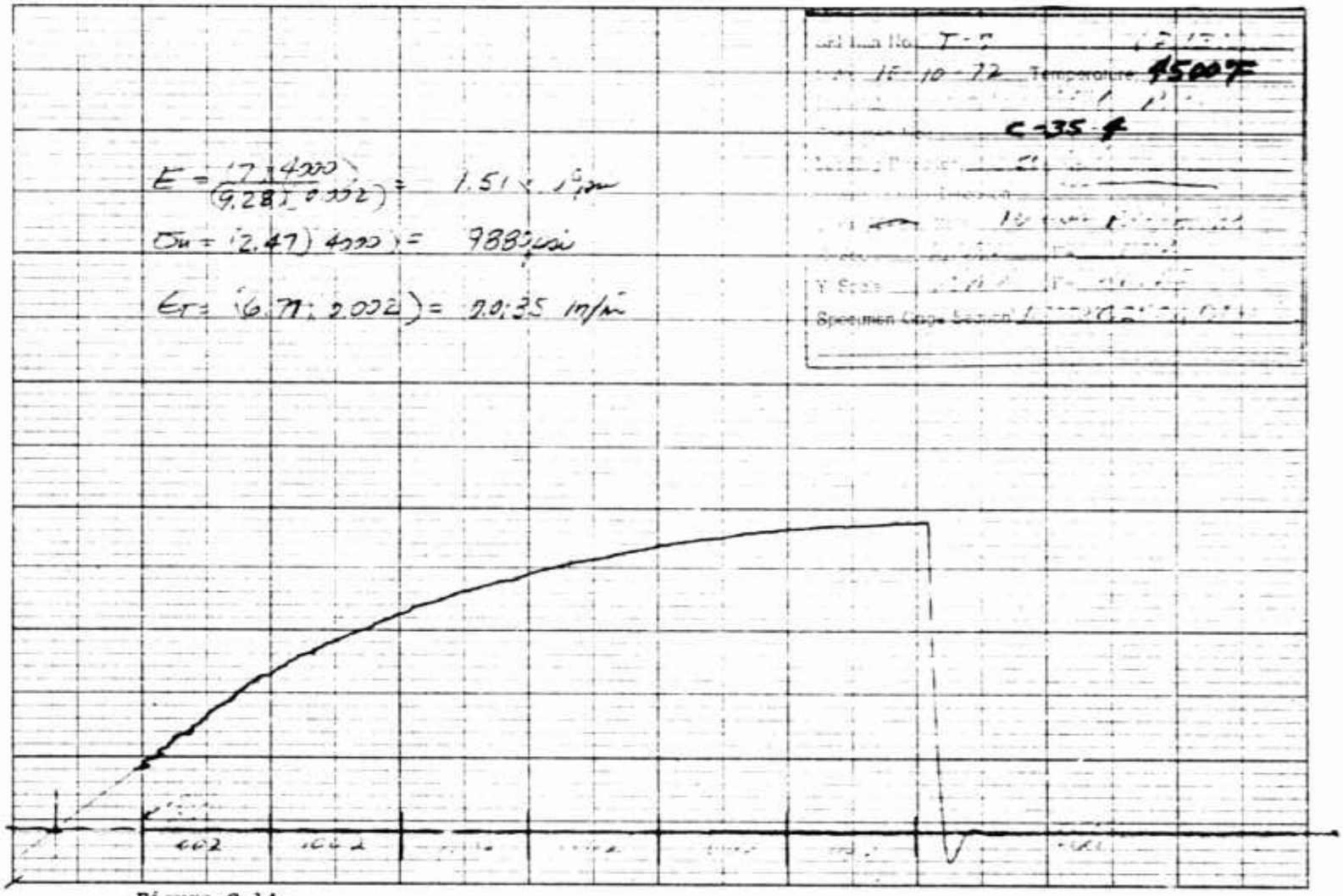
Temperature 1500F
C-35-4
E = (7.4000) / (9.28)(0.002) = 1.51 x 10^6 psi
σu = (2.47)(4000) = 9880 psi
εf = (6.77 / 2.002) = 20.35 in/in

Figure C-14.

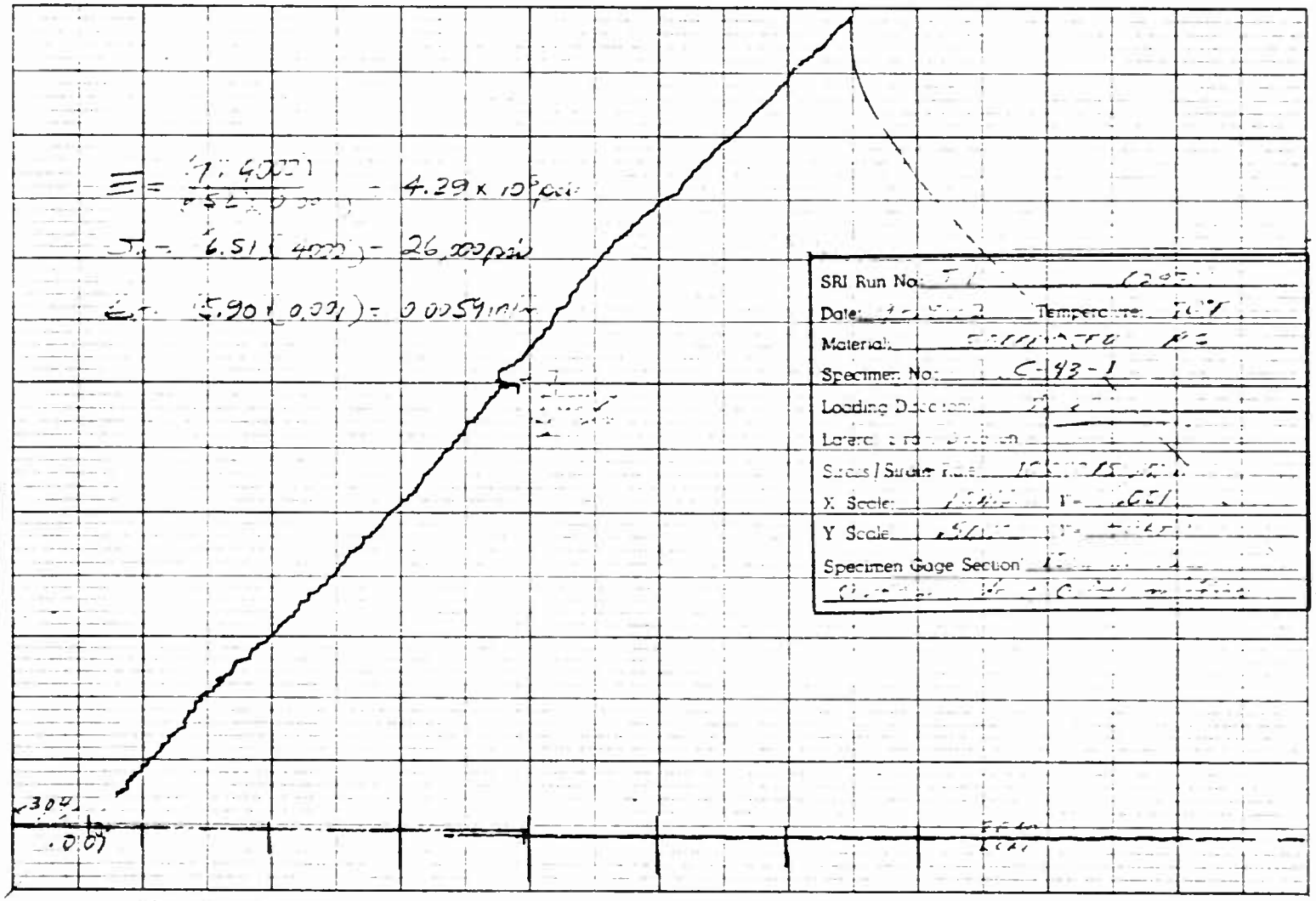

Figure C-15.

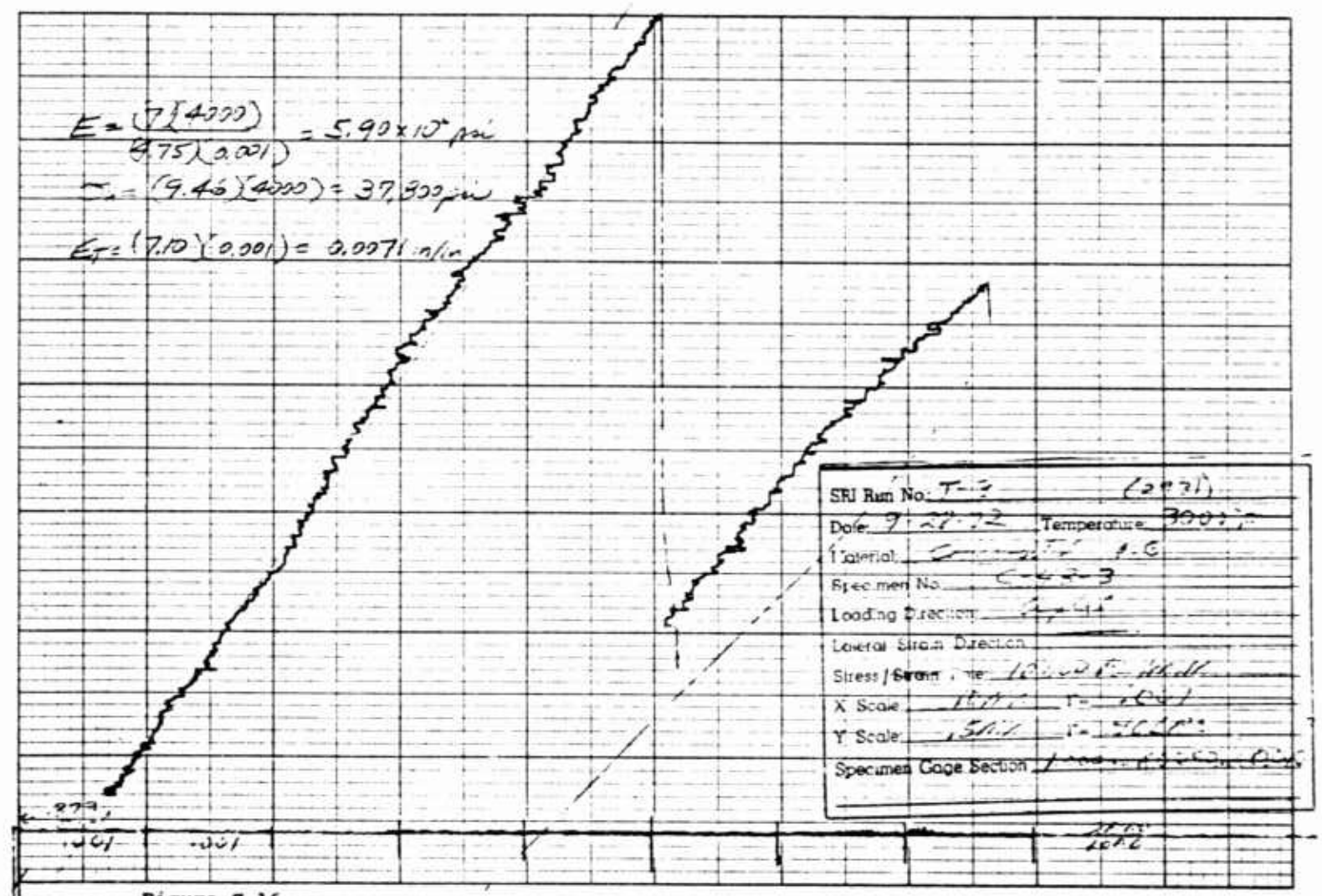

Figure C-16.

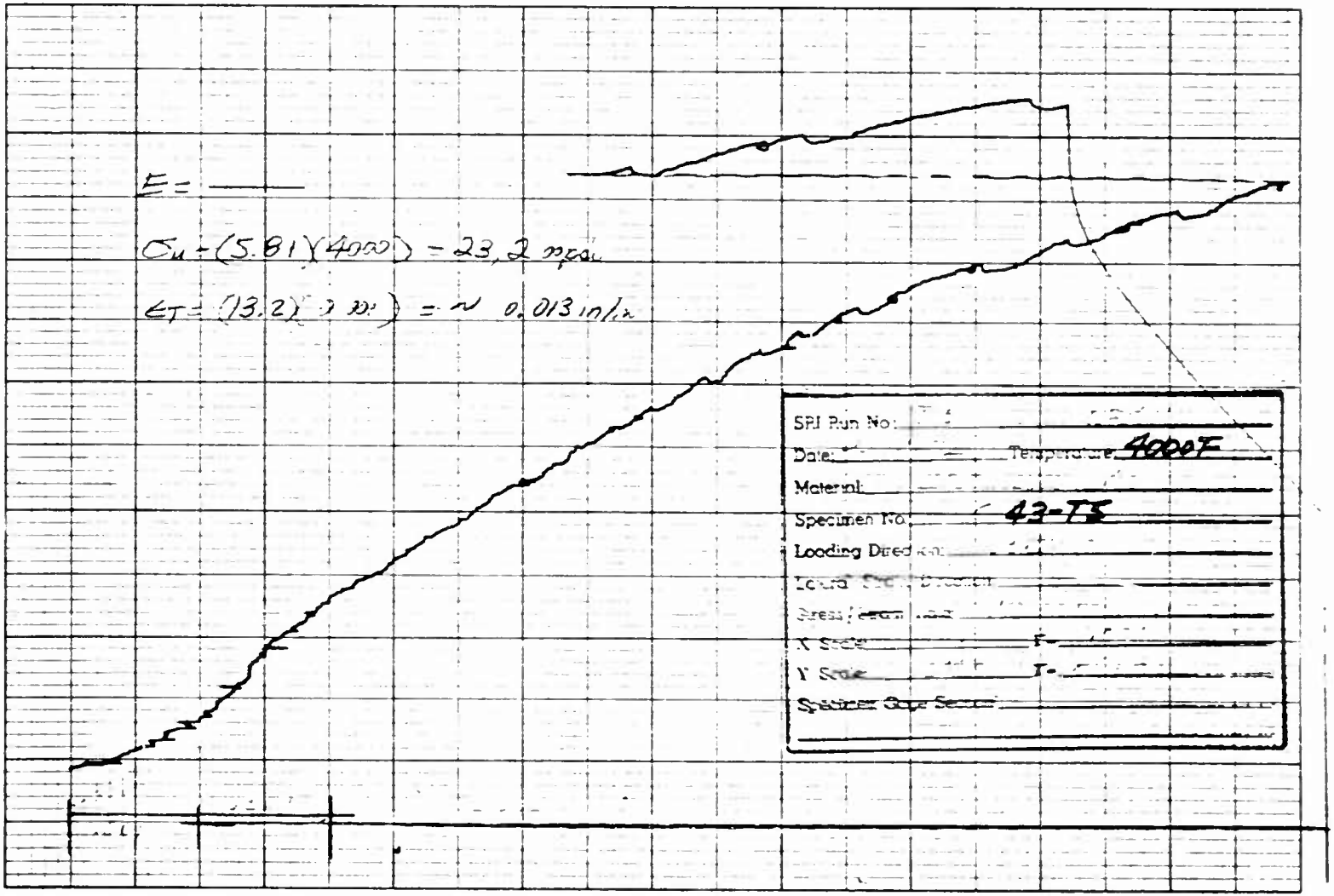

Figure C-17.

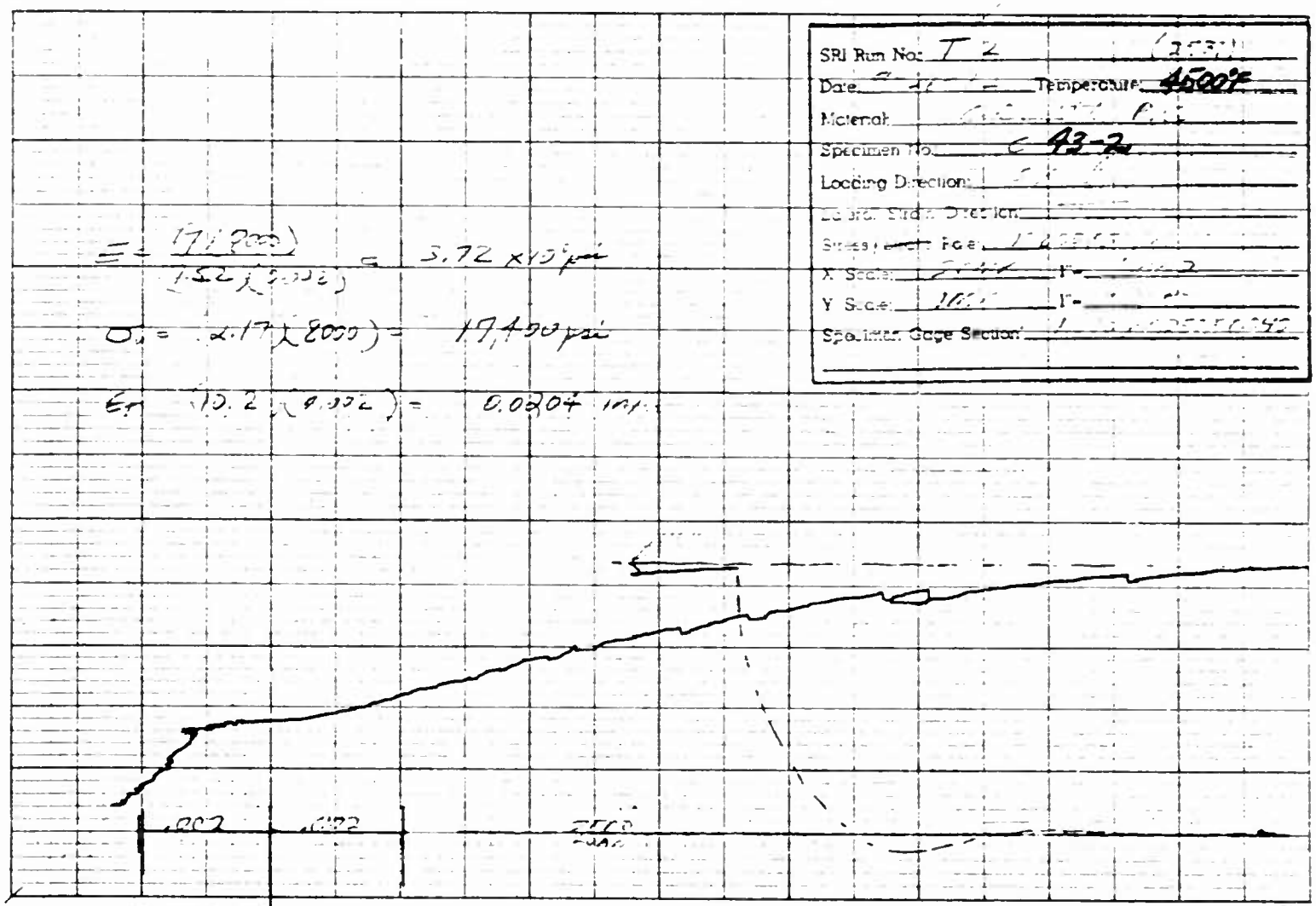
SRI Run No.: T 2
Date:
Temperature: 4500°F
Material:
Specimen No.: C 43-2
Loading Direction:
Load Stress Direction:
Stress/Load Rate:
X Scale:
Y Scale:
Specimen Gage Section:
E = (17,800) / (1.52)(.002) = 5.72 x 10^6 psi
σ_u = (2.17)(8000) = 17,400 psi
ε_f = (10.2)(.002) = 0.0204 in/in
.002
.002

Figure C-18.

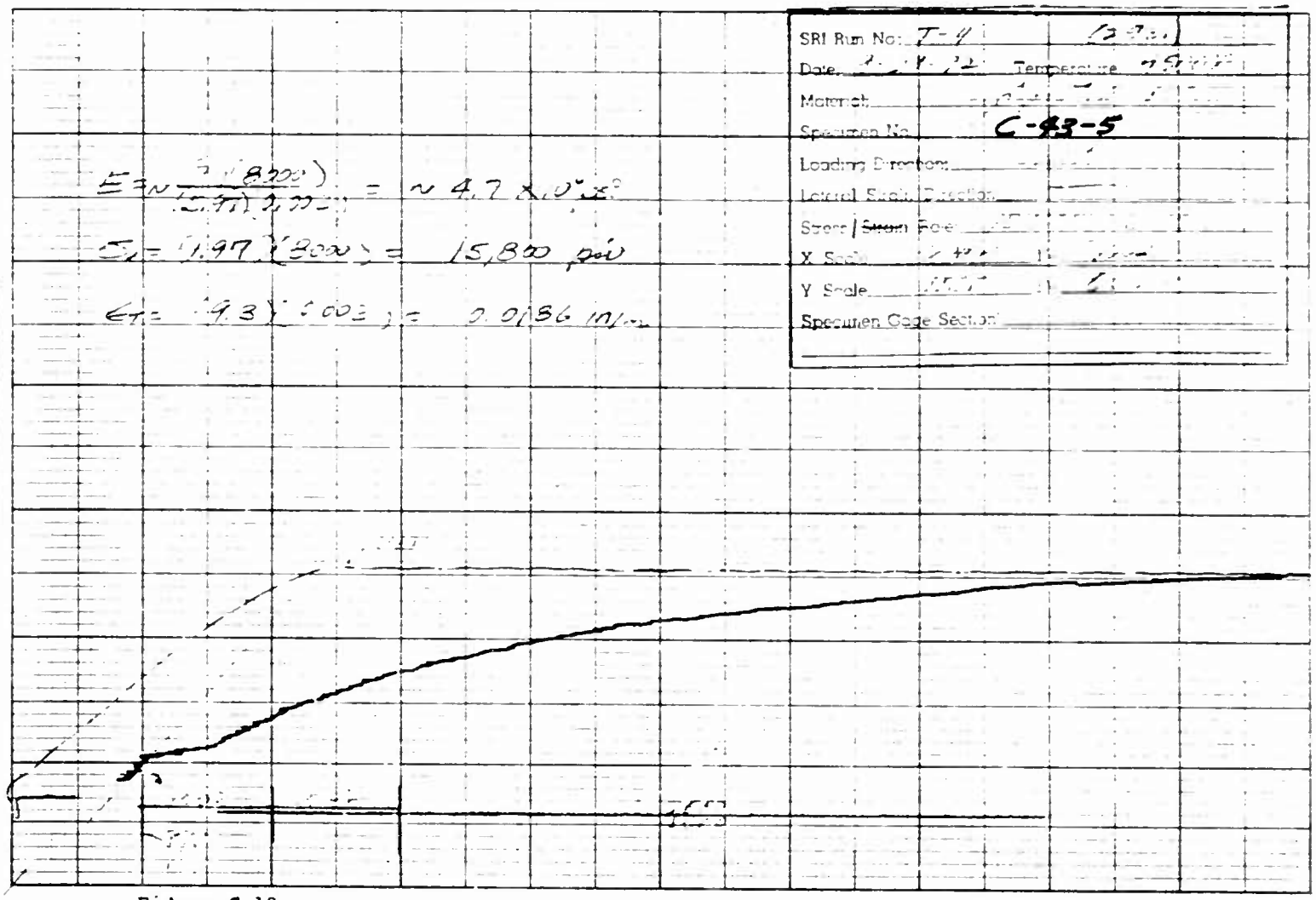

Figure C-19.

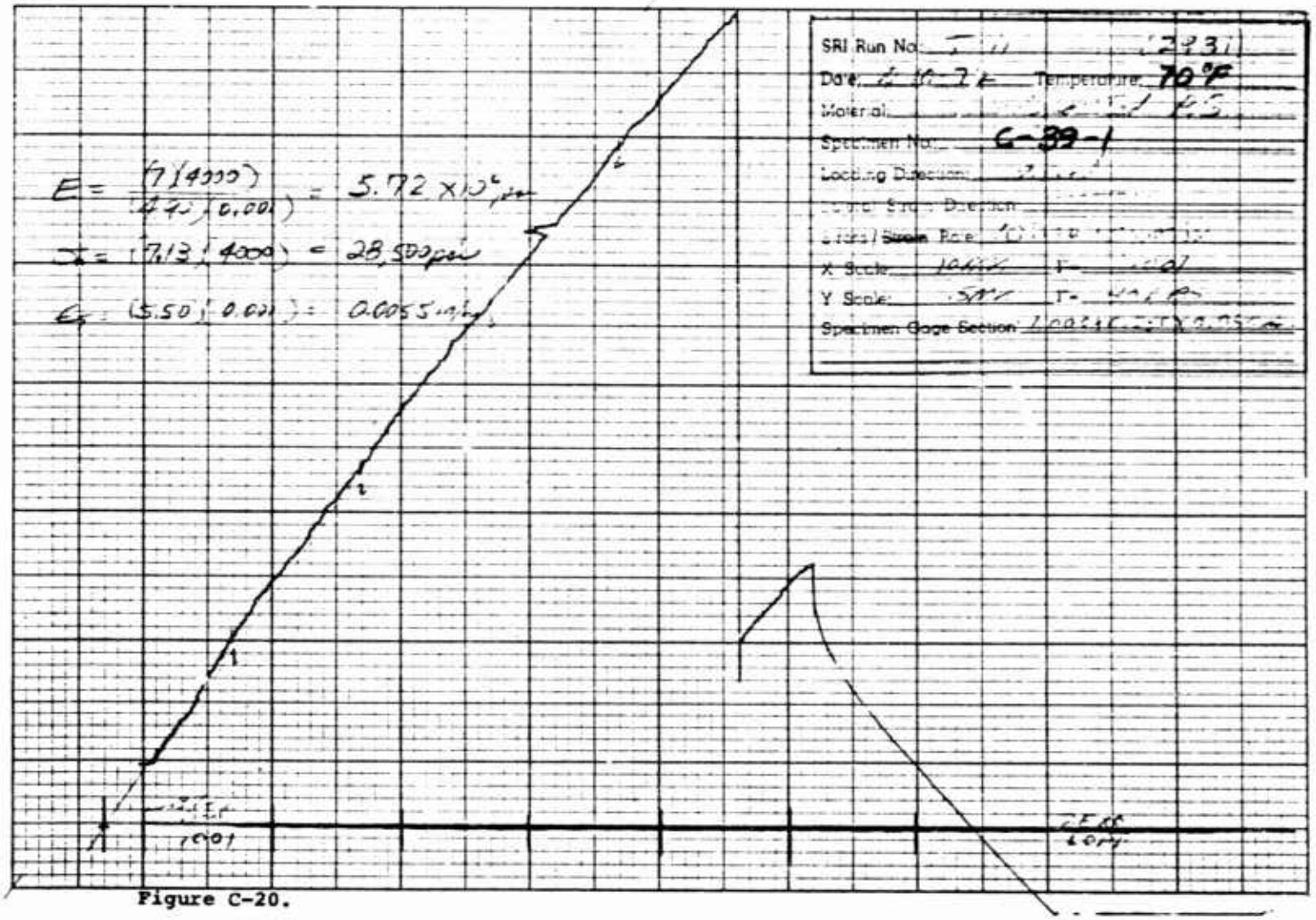
SRI Run No.
Date
Temperature 70°F
Material
Specimen No. G-39-1
Loading Direction
Load/Strain Rate
X Scale
Y Scale
Specimen Gage Section
E = (7)(4000) / (44)(0.001) = 5.72 x 10^6 psi
σ = (7.13)(4000) = 28,500 psi
ε = (5.50)(0.001) = 0.0055 in/in

Figure C-20.

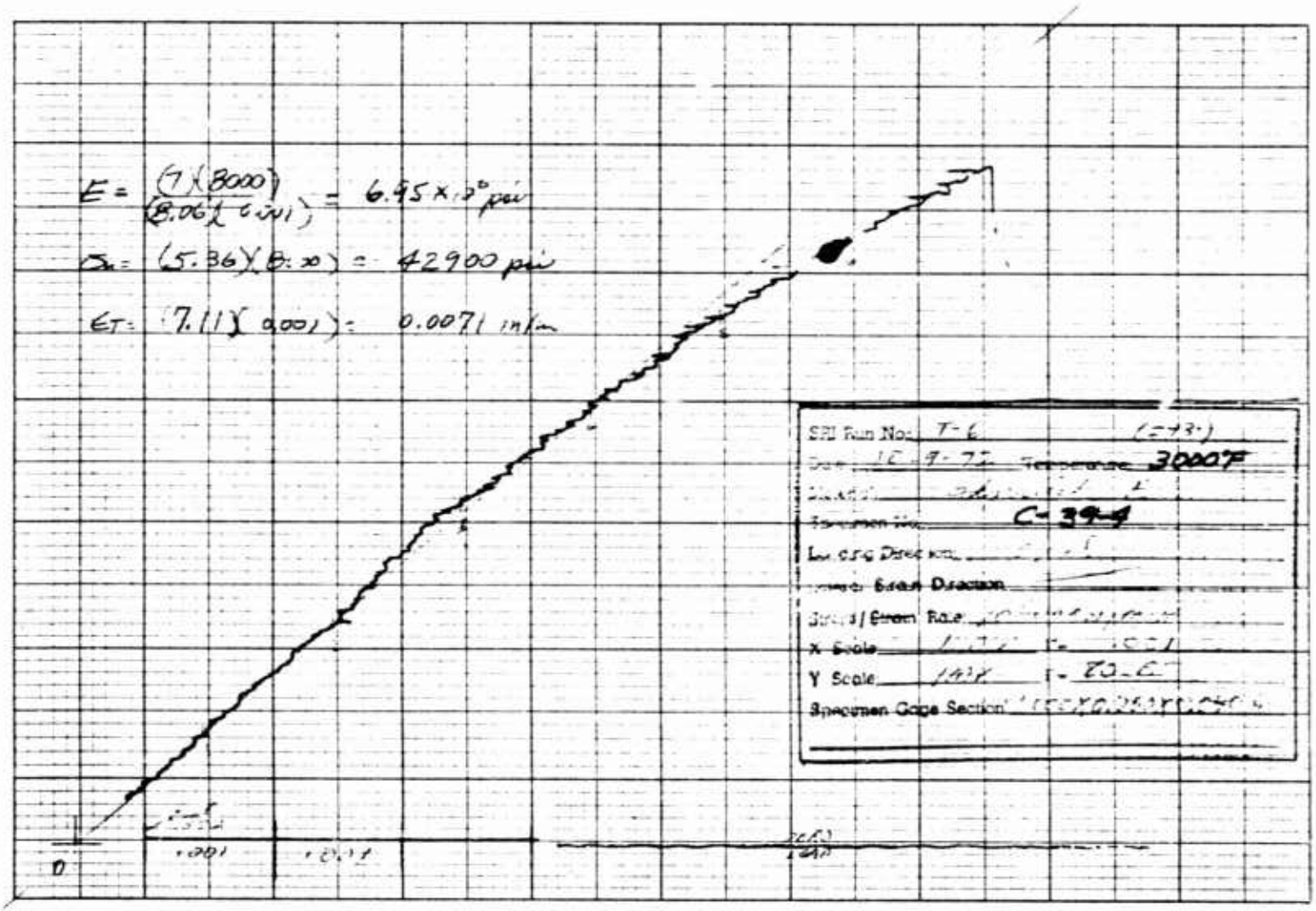

Figure C-21.

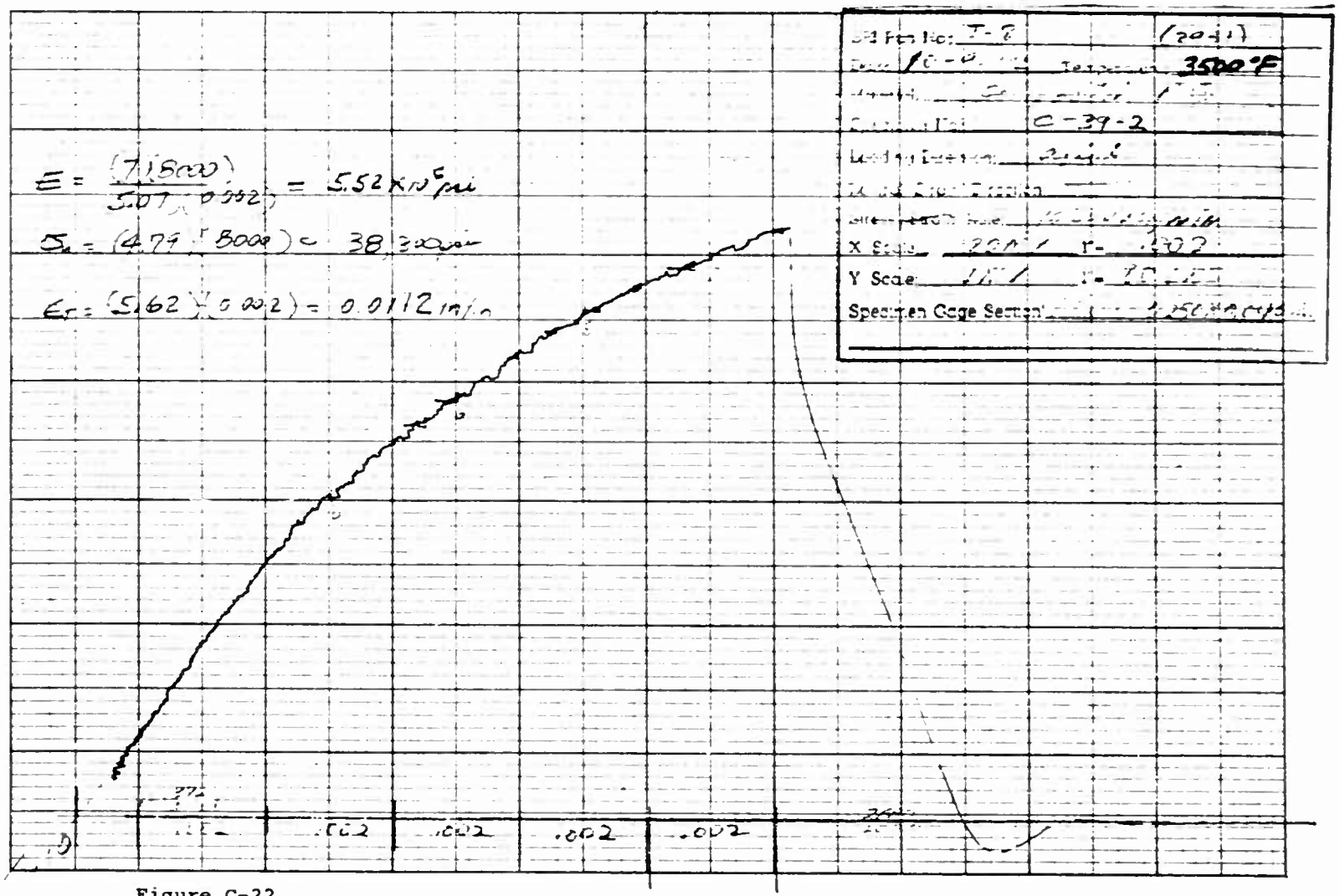

Figure C-22.

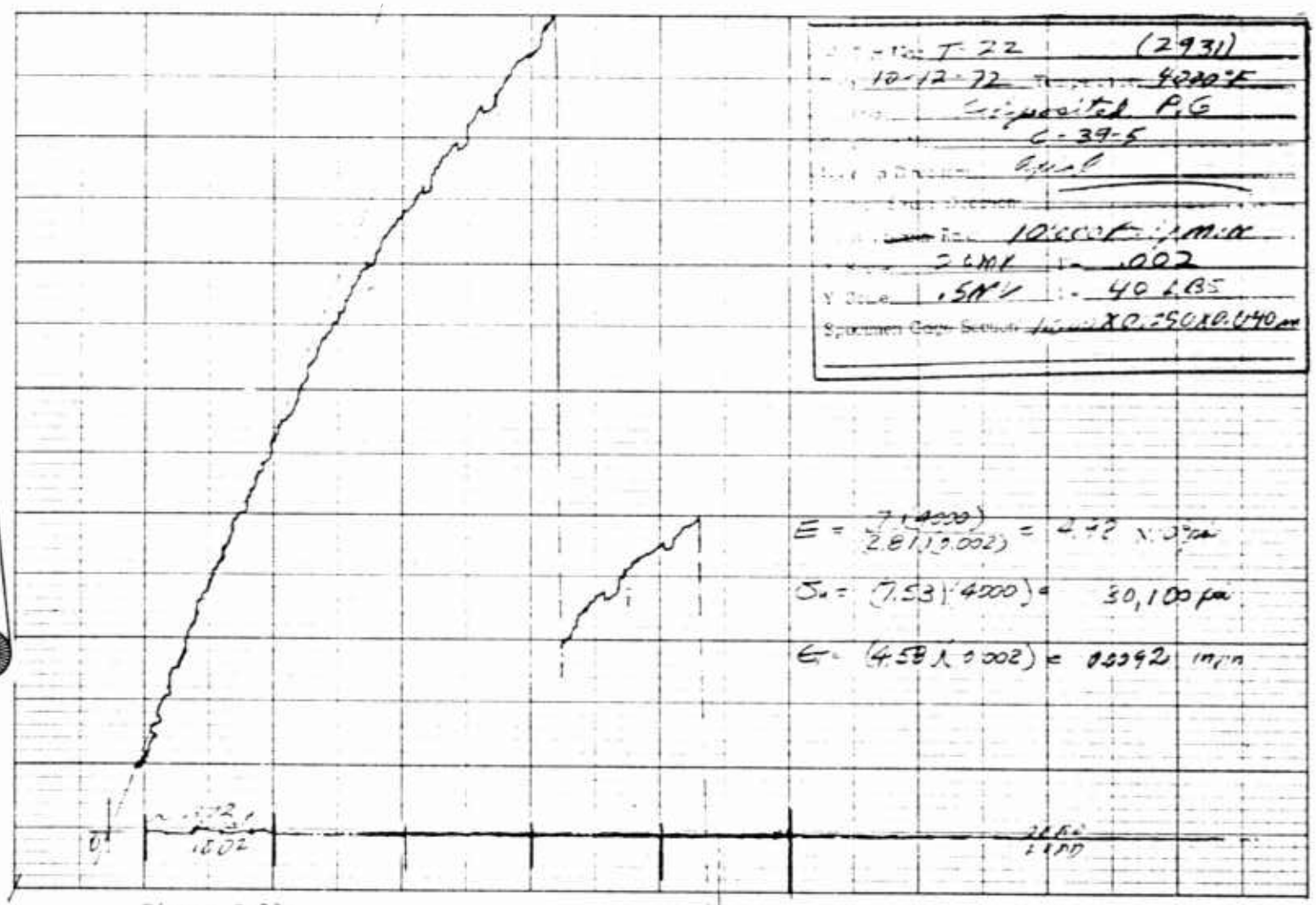

Figure C-23.

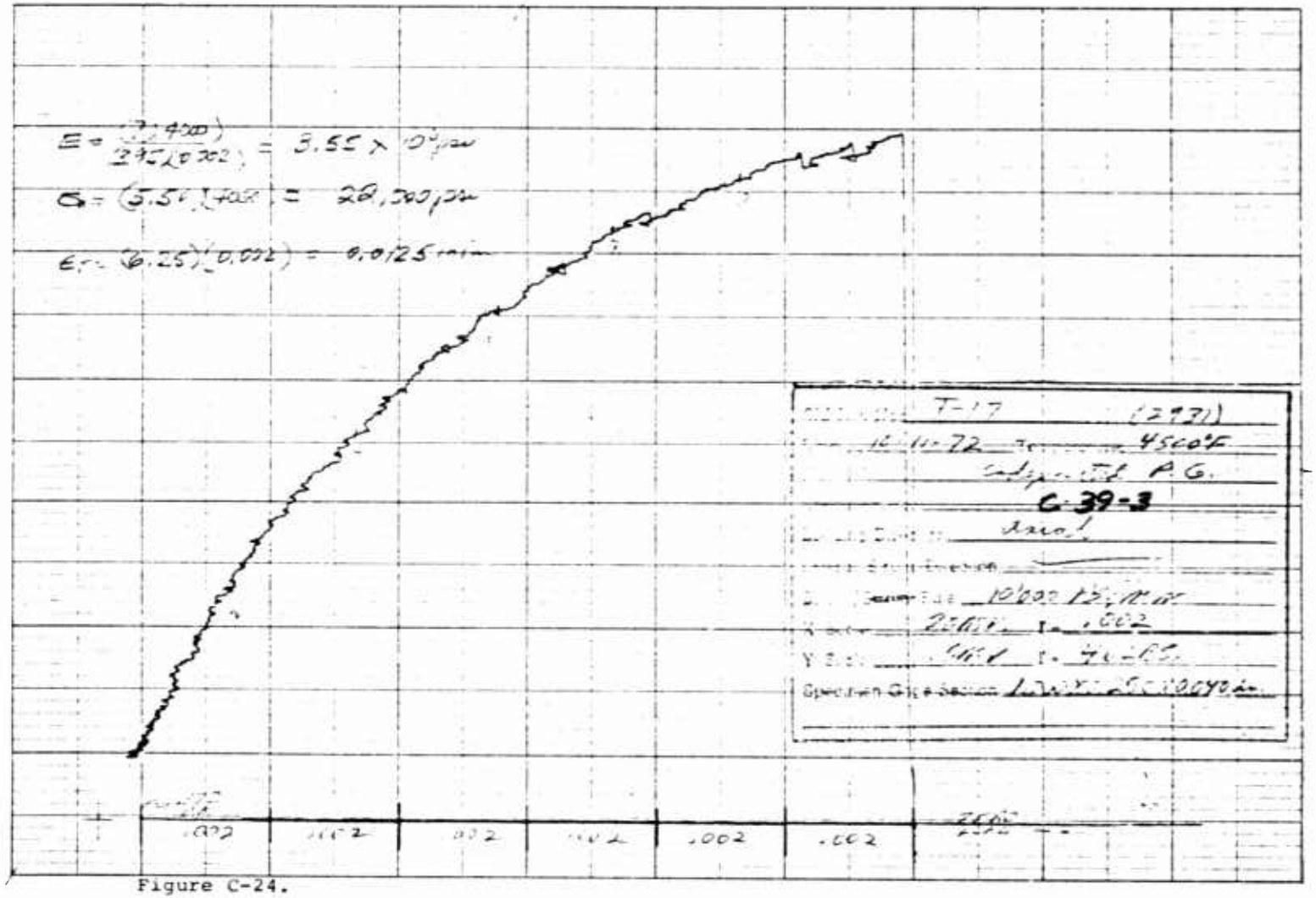

Figure C-24.

APPENDIX D

COMPRESSIVE STRESS-STRAIN CURVES FOR PG AND CODEPOSITED SiC/PG IN THE AB DIRECTION

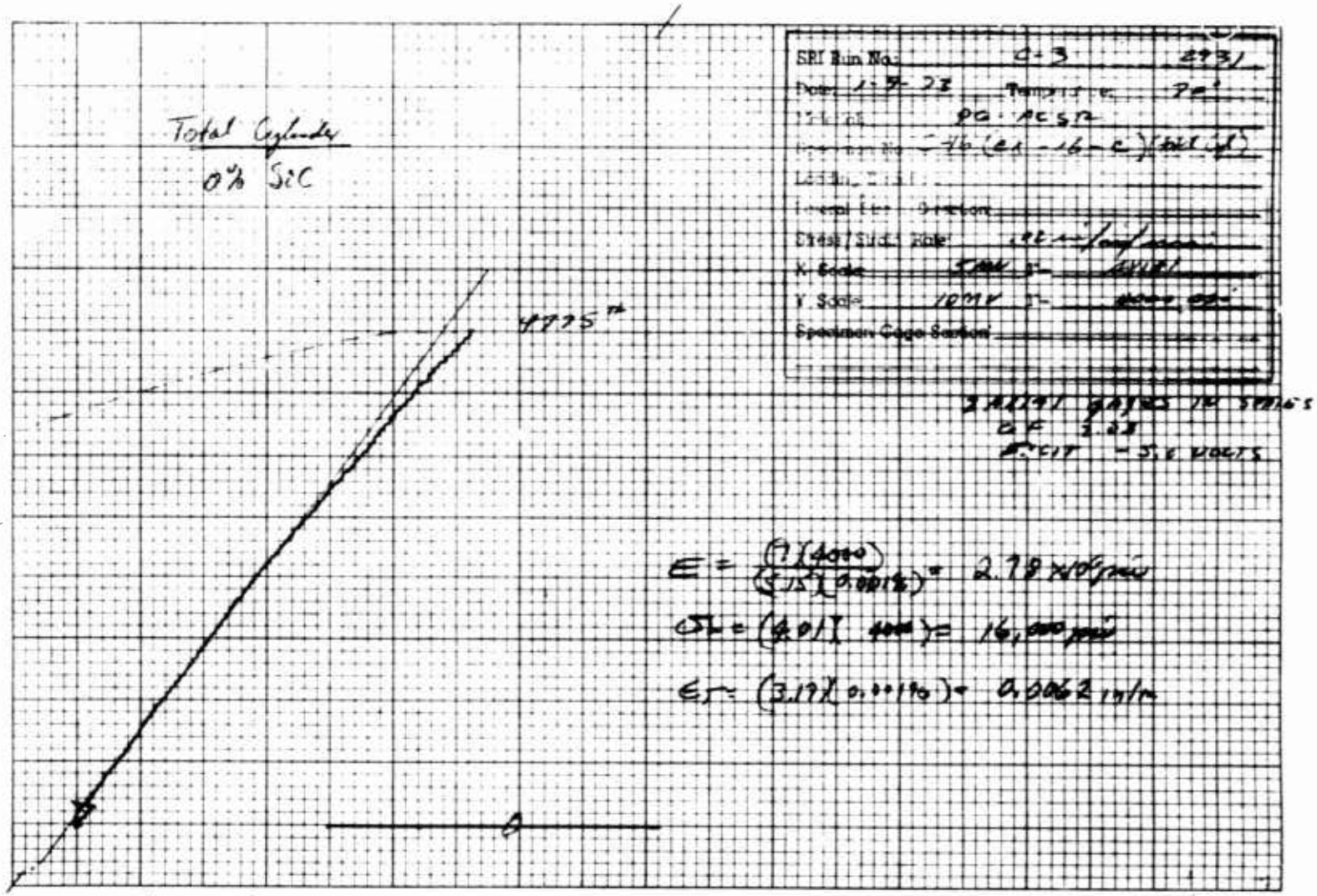

Figure D-1.

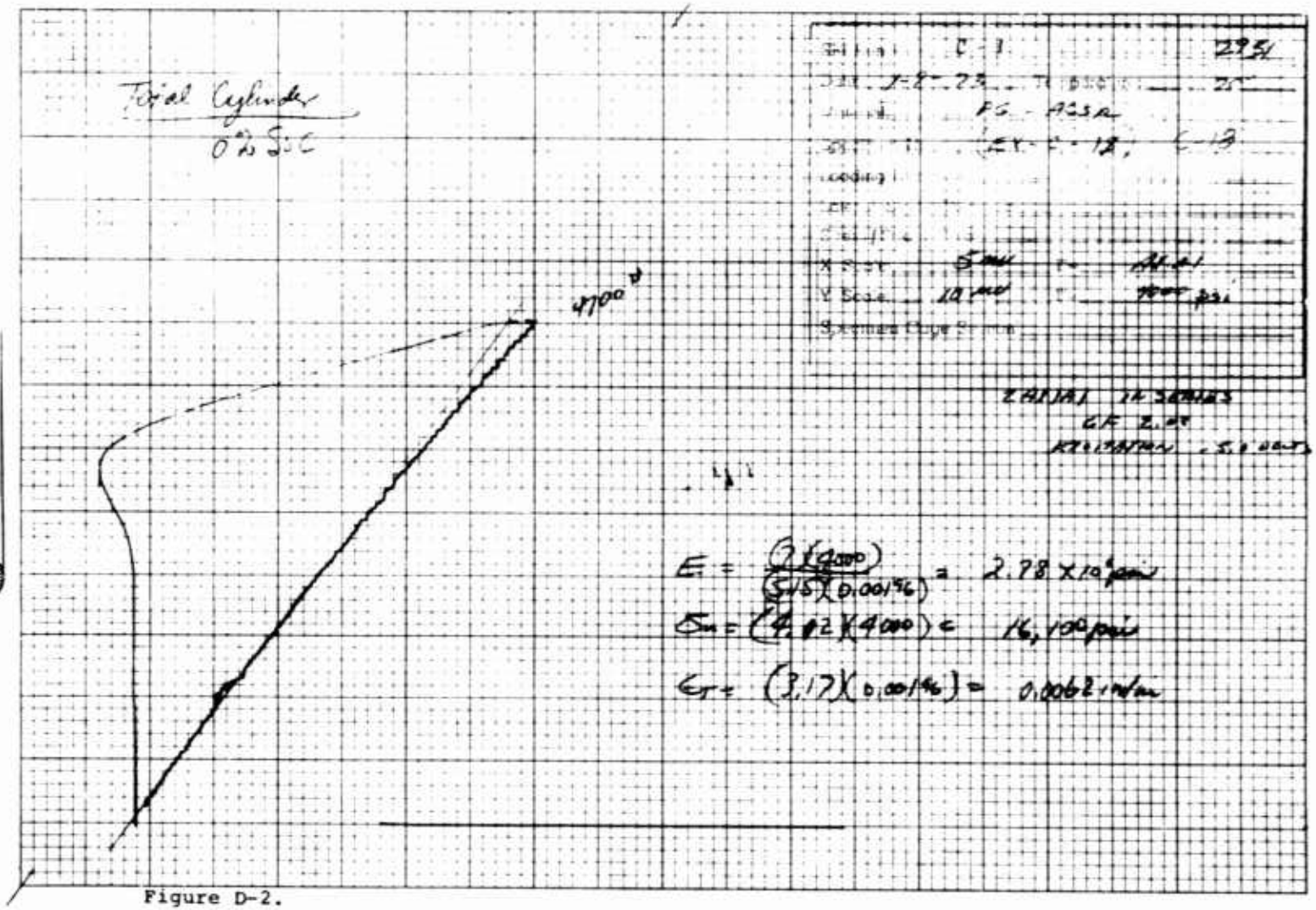

Figure D-2.

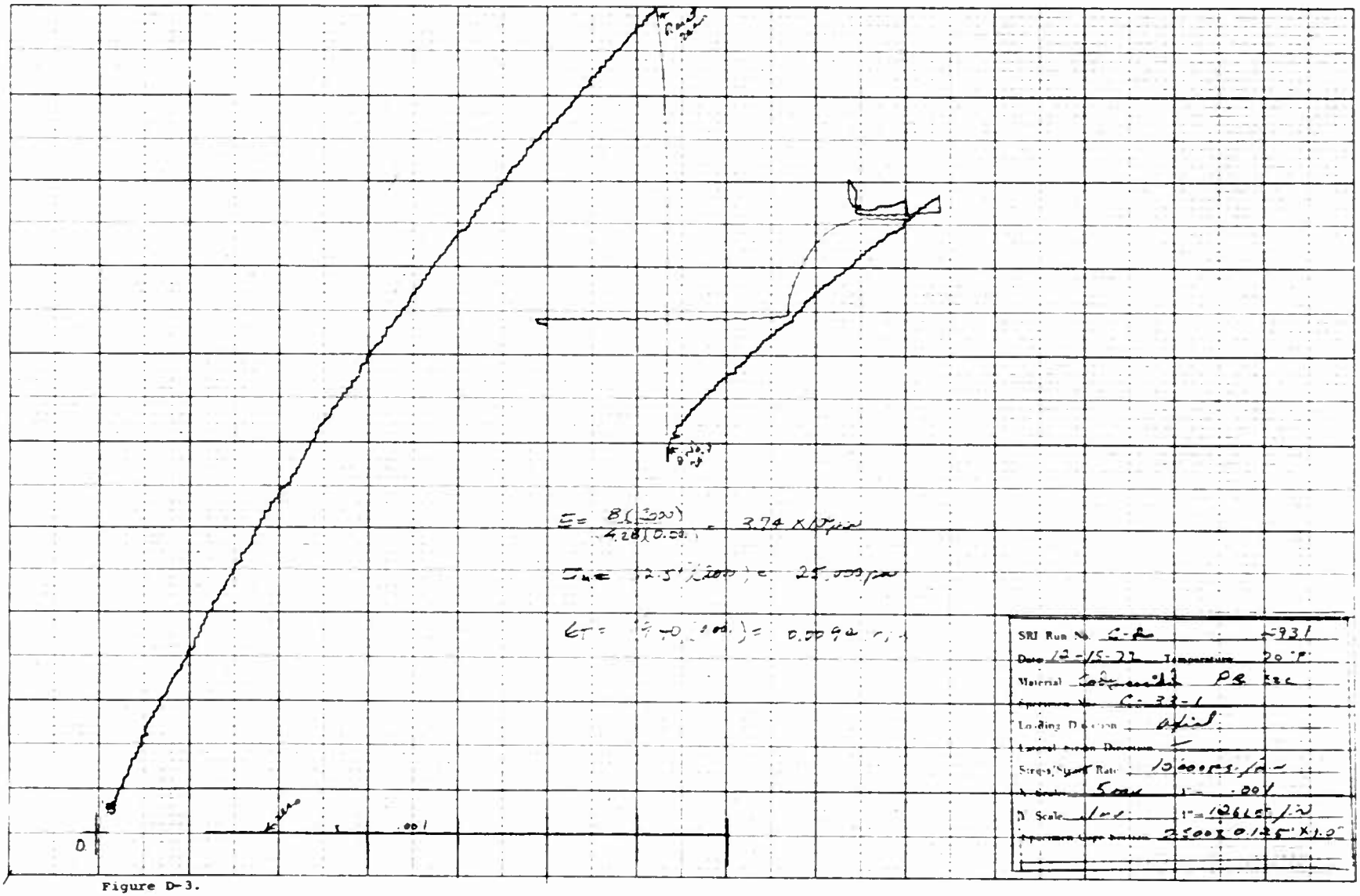

Figure D-3.

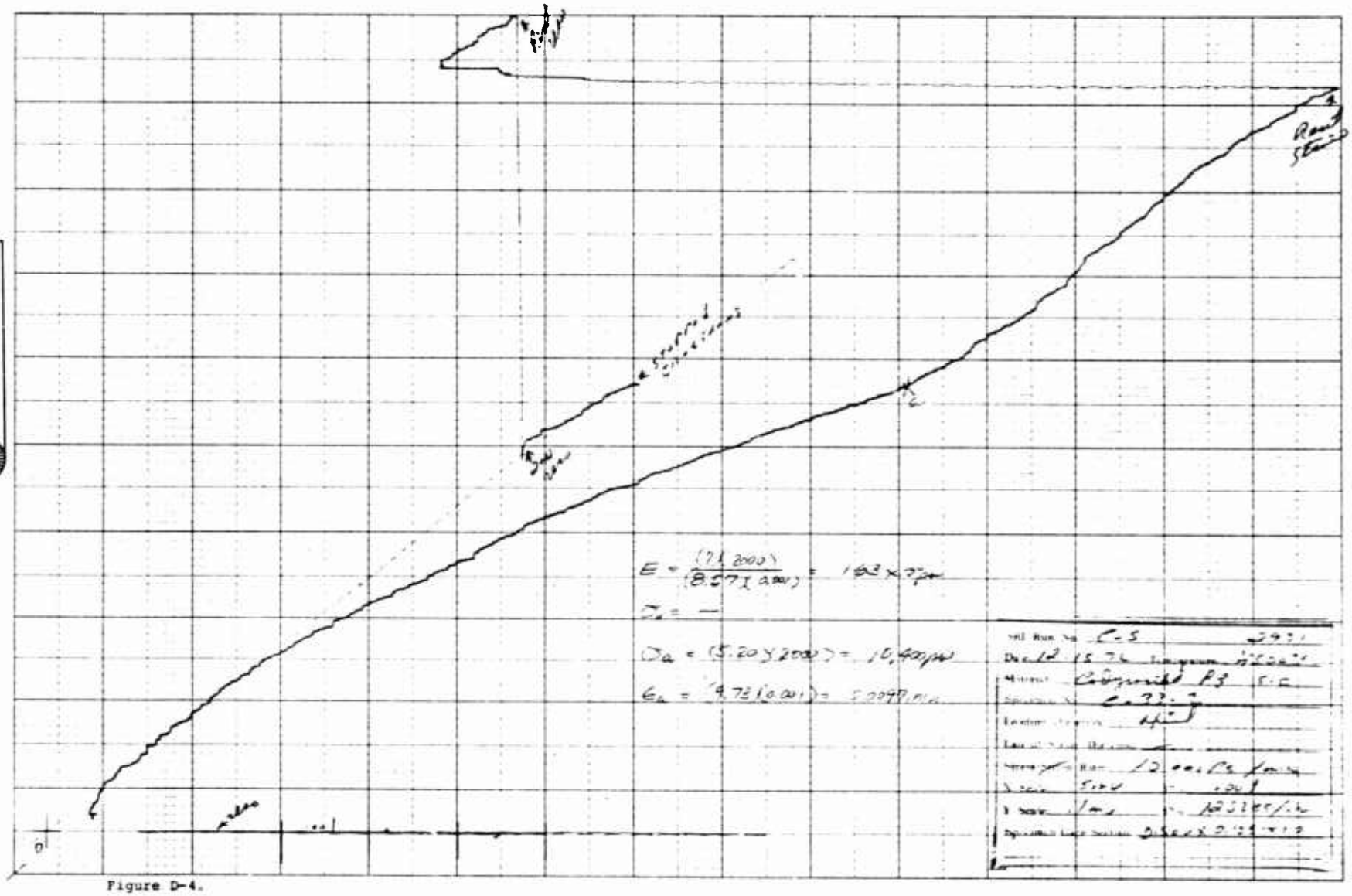

Figure D-4.

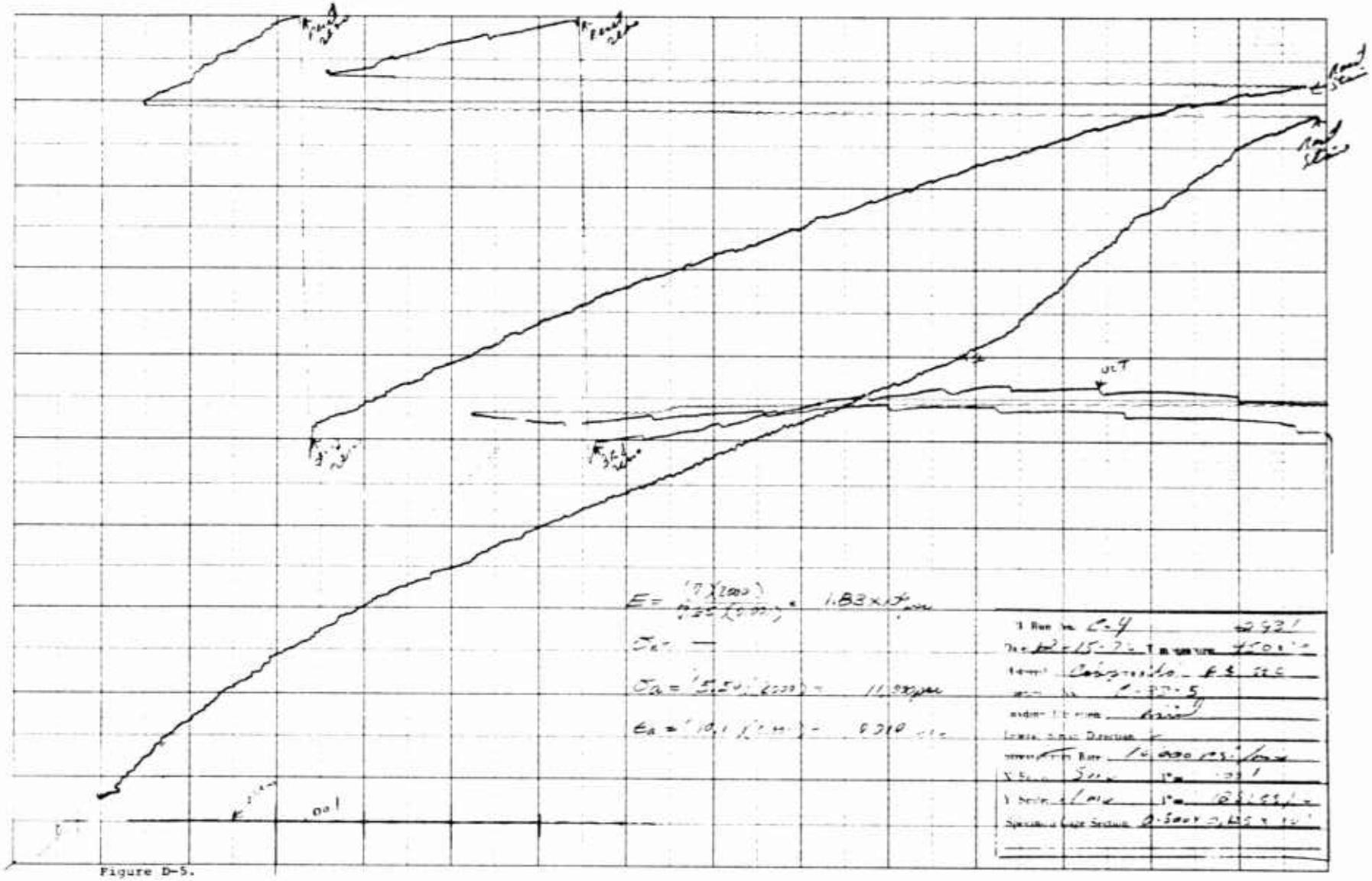

Figure D-5.

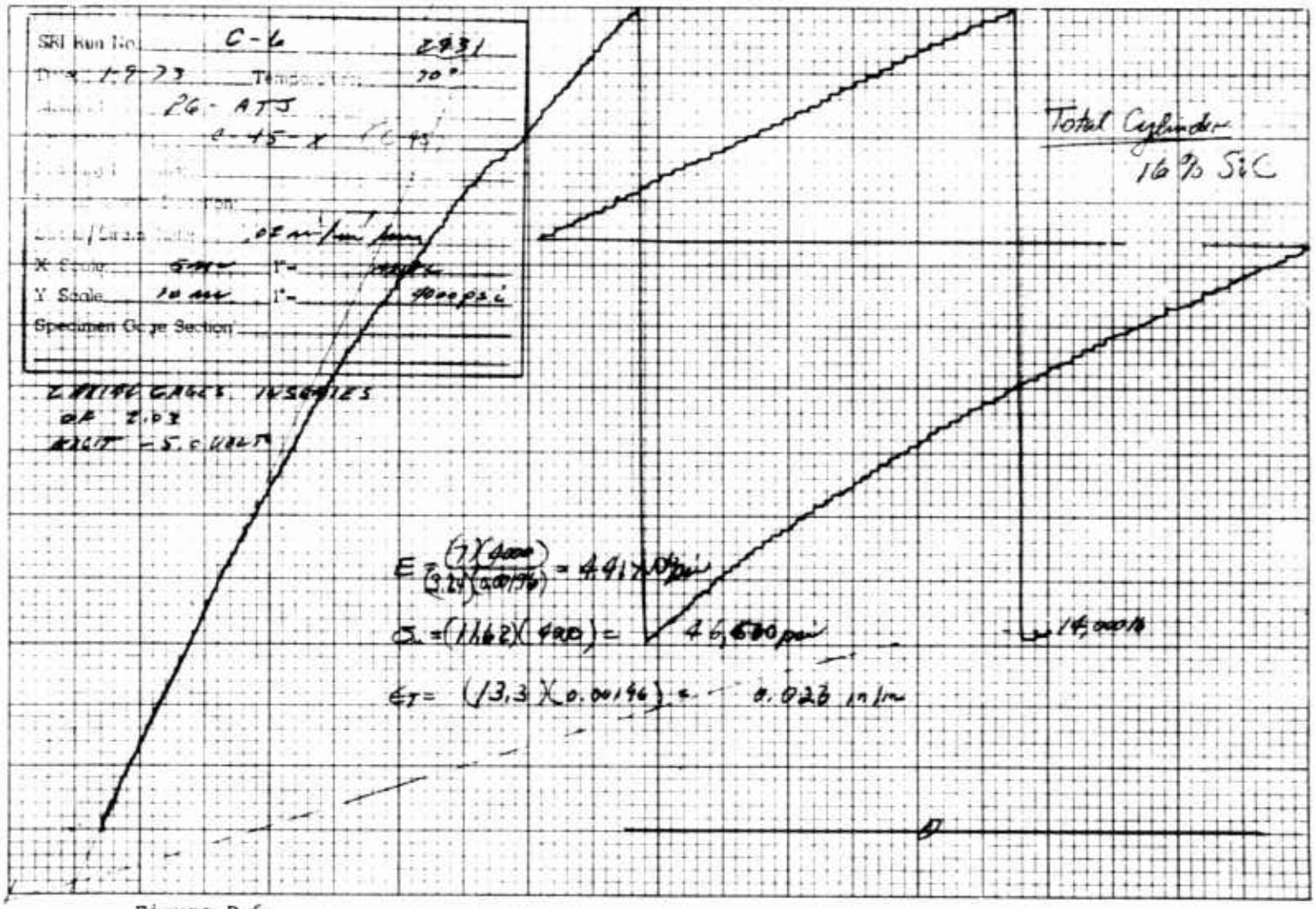
SRI Run No. C-6
2931
Temperature 70°
26 - ATJ
Total Cylinder
16% SiC
X Scale 5 mm 1" =
Y Scale 10 mm 1" = 4000 psi
Specimen Gage Section
E = (7)(4000) / (0.24)(0.0176) = 4.91 x 10^6 psi
σ = (11.62)(4000) = 46,480 psi
14,000 lb
ε_T = (13.3)(0.00146) = 0.020 in/in

Figure D-6.

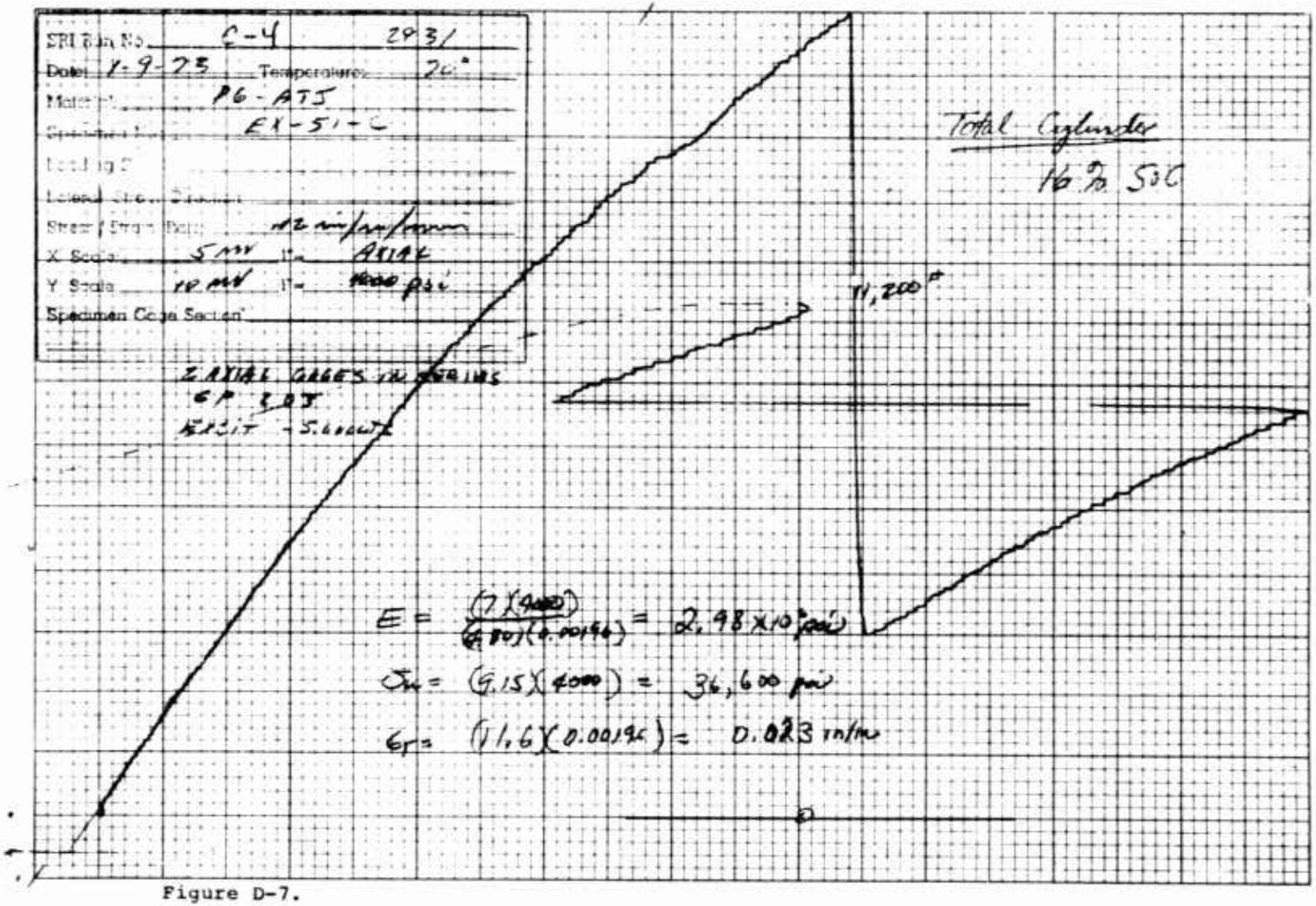
SRI Run No. C-4 2931
Date 1-9-73 Temperature 70°
Material P6-AT5
Specimen EX-51-C
Strain Point .02 in/in/mm
X Scale 5 mm = AXIAL
Y Scale 10 mm = 1000 psi
Specimen Cross Section
Total Cylinder
16 ft. 50C
11,200#
E = (7)(4000) / (6.80)(0.00196) = 2.98 x 10^6 psi
σu = (6.15)(4000) = 36,600 psi
εf = (11.6)(0.00196) = 0.023 in/in

Figure D-7.

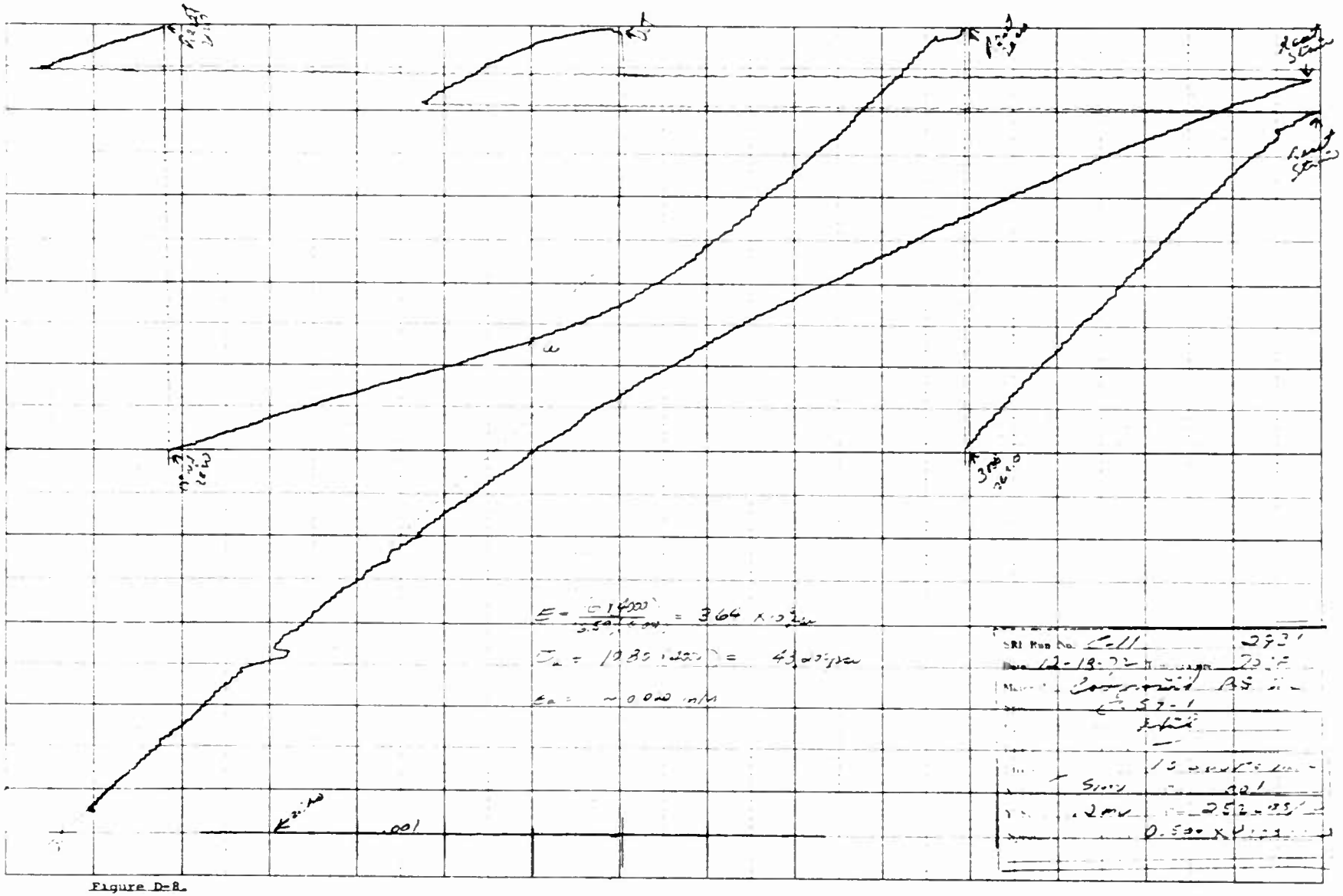

Figure D-8.

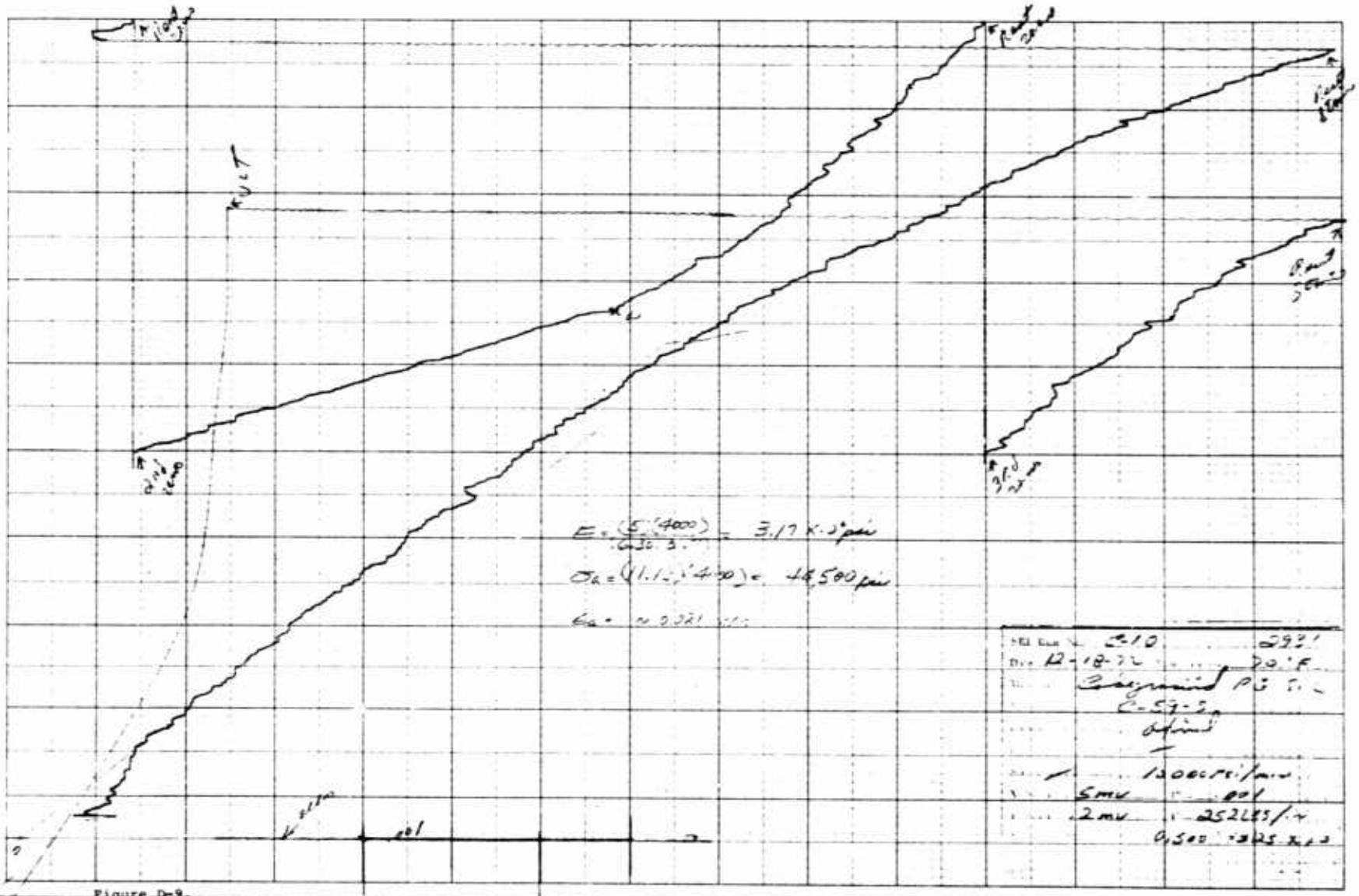

Figure D-9.

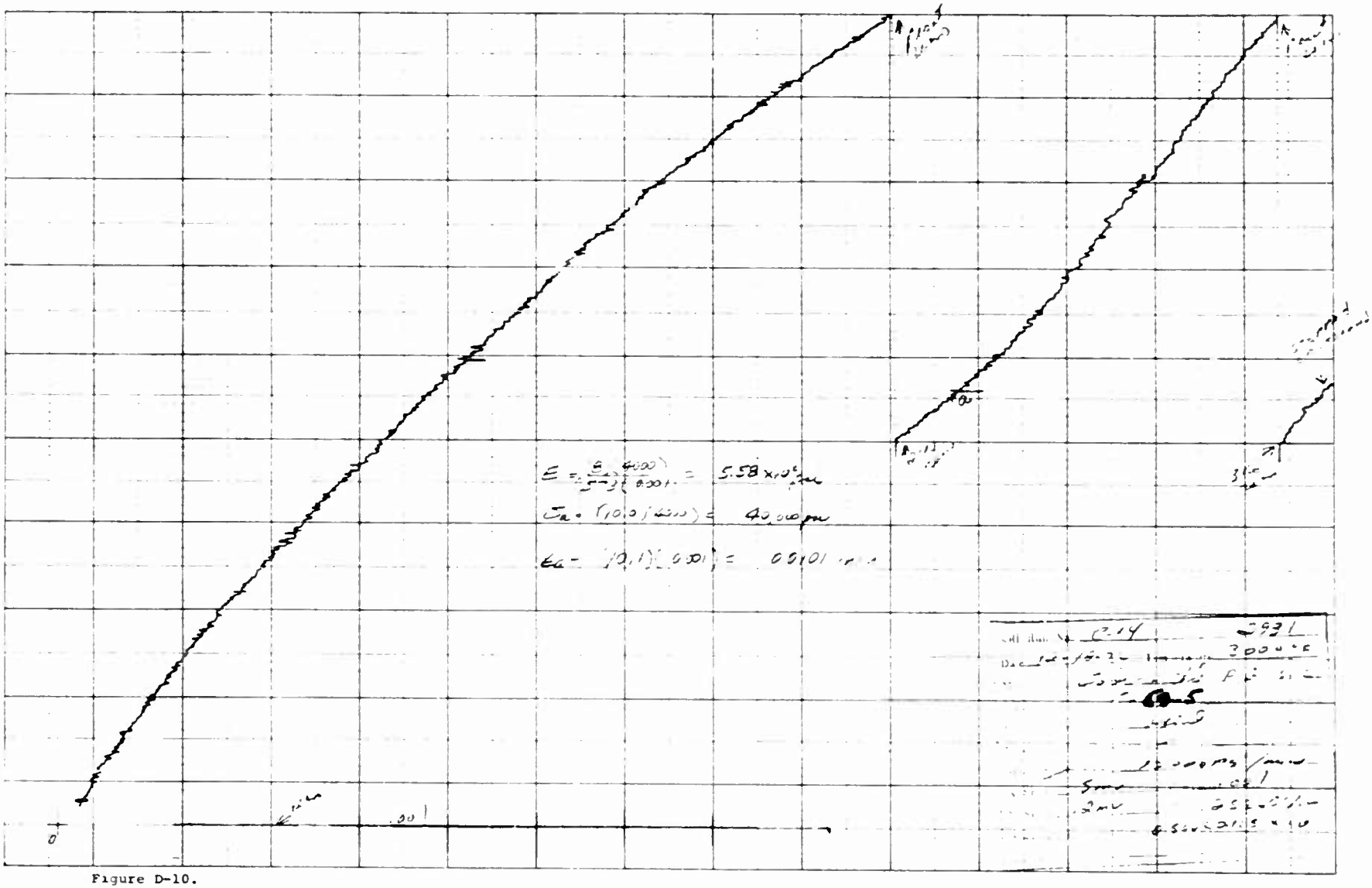

Figure D-10.

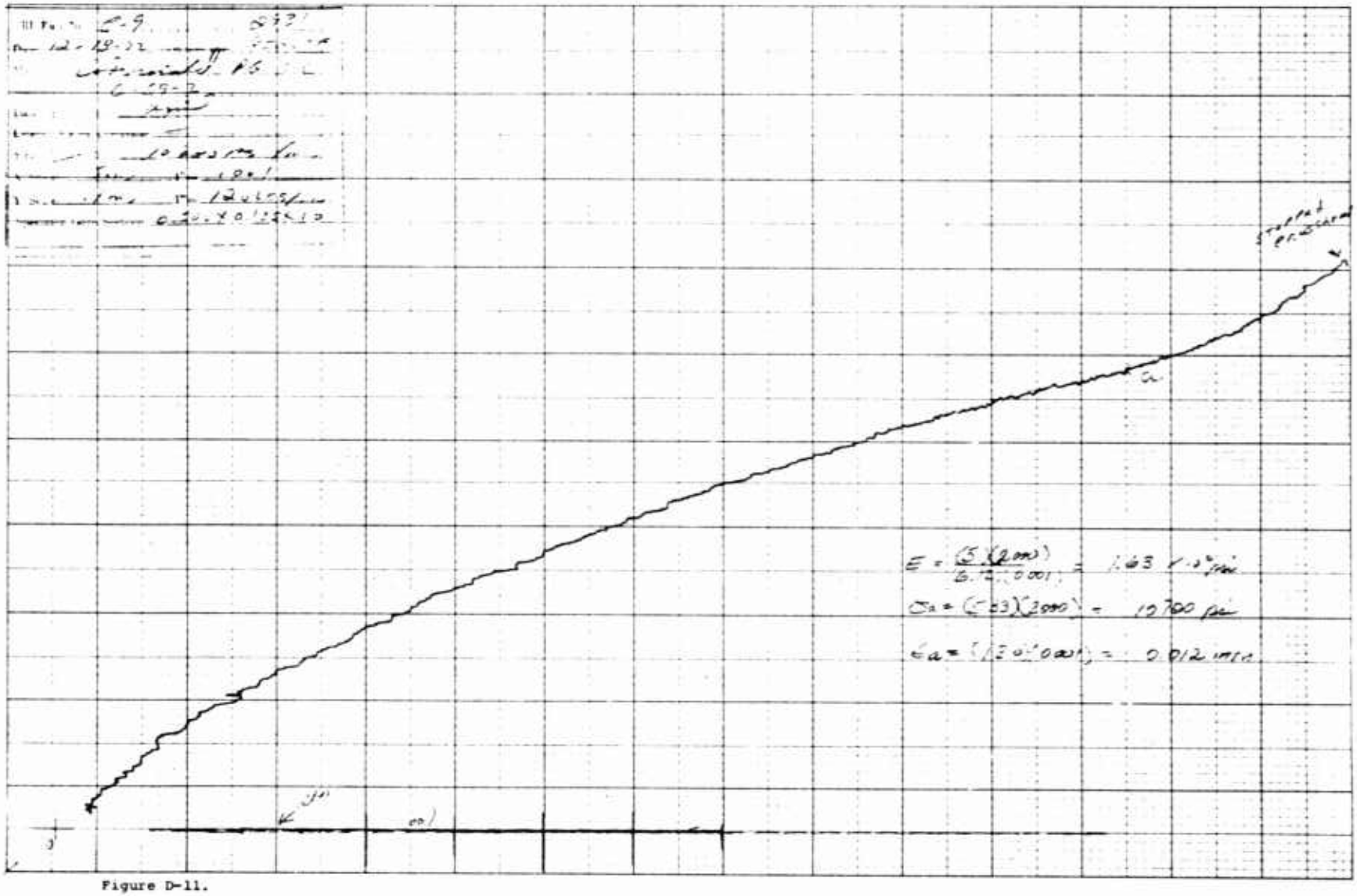
E = (5)(2000) / (6.12)(0.001) = 1.63 x 10^6 psi
σa = (5.33)(2000) = 10700 psi
εa = (1.63 x 10^6)(0.001) = 0.012 in/in

Figure D-11.

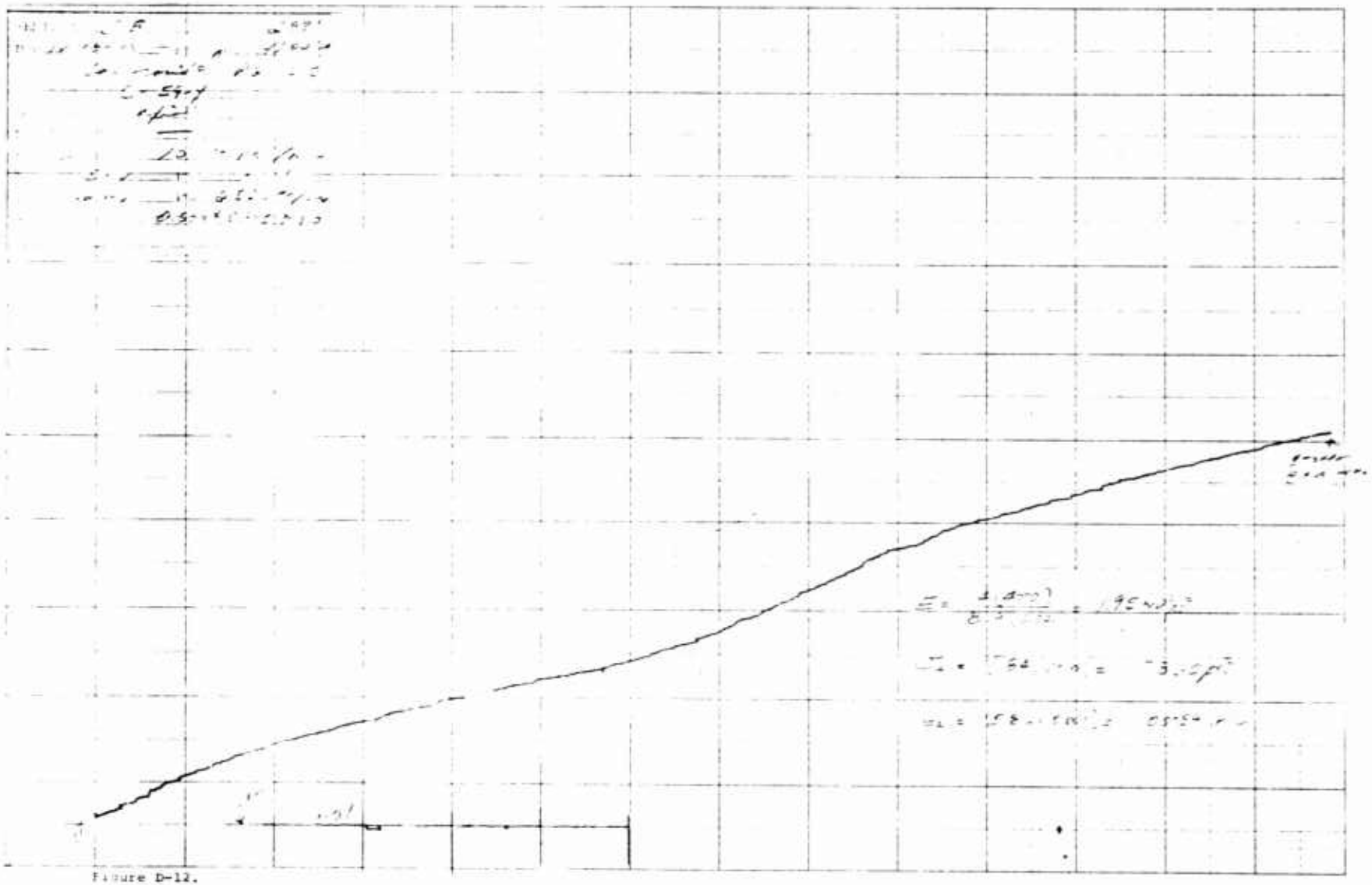

Figure D-12.

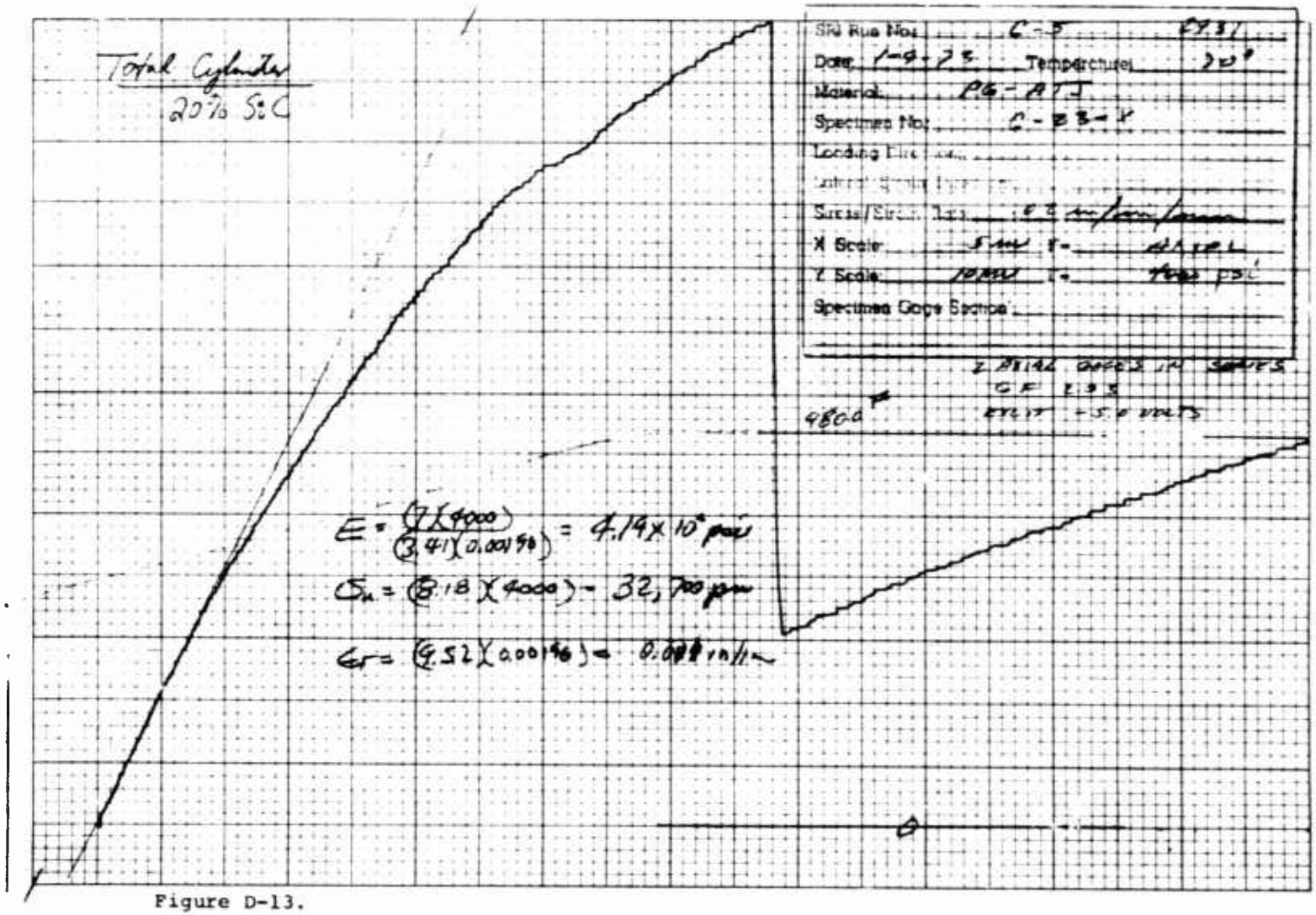

Figure D-13.

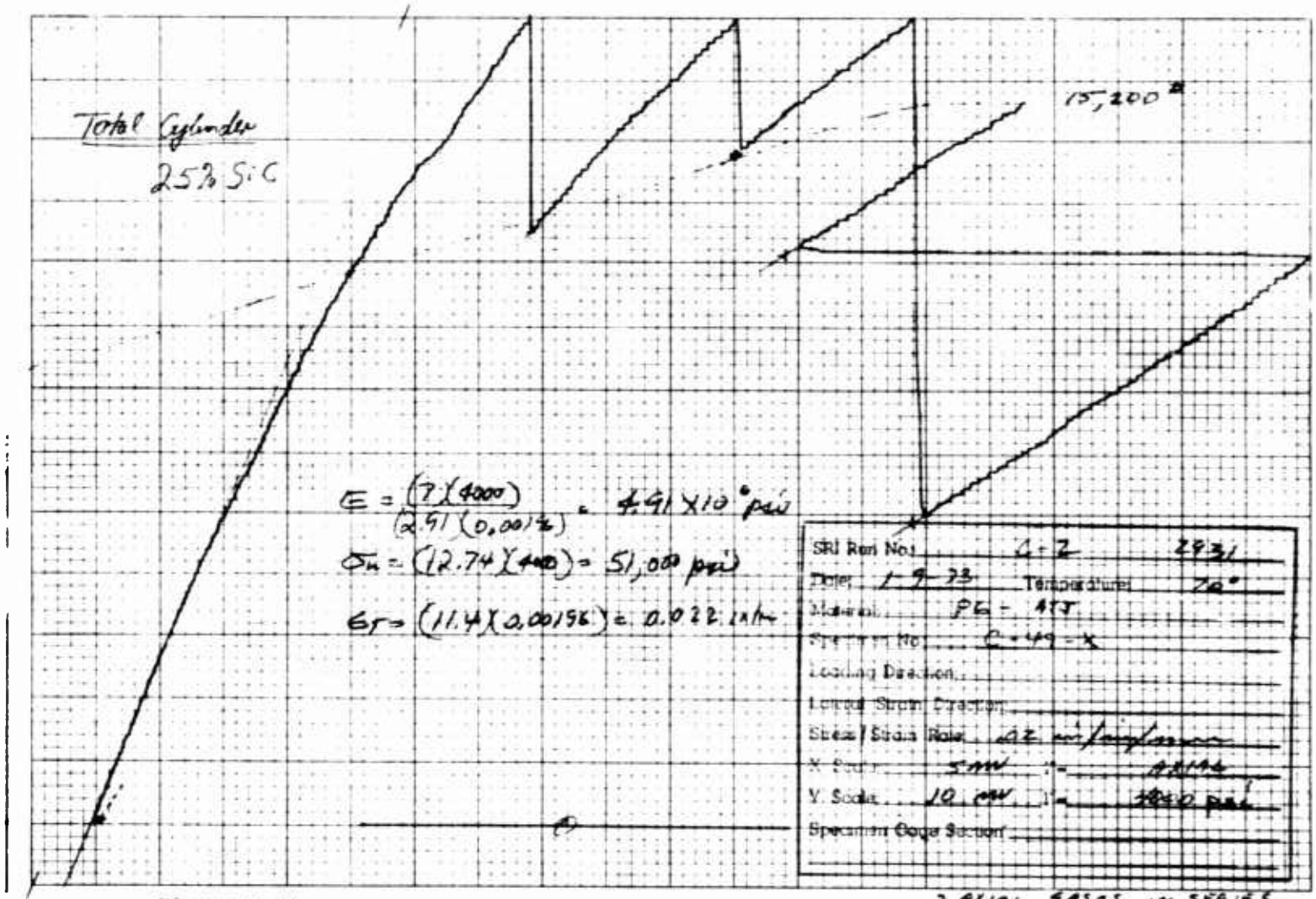

Figure D-14.

2 AXIAL GAGES IN SERIES
GF -2.02
EXCITATION 5.0 VOLTS

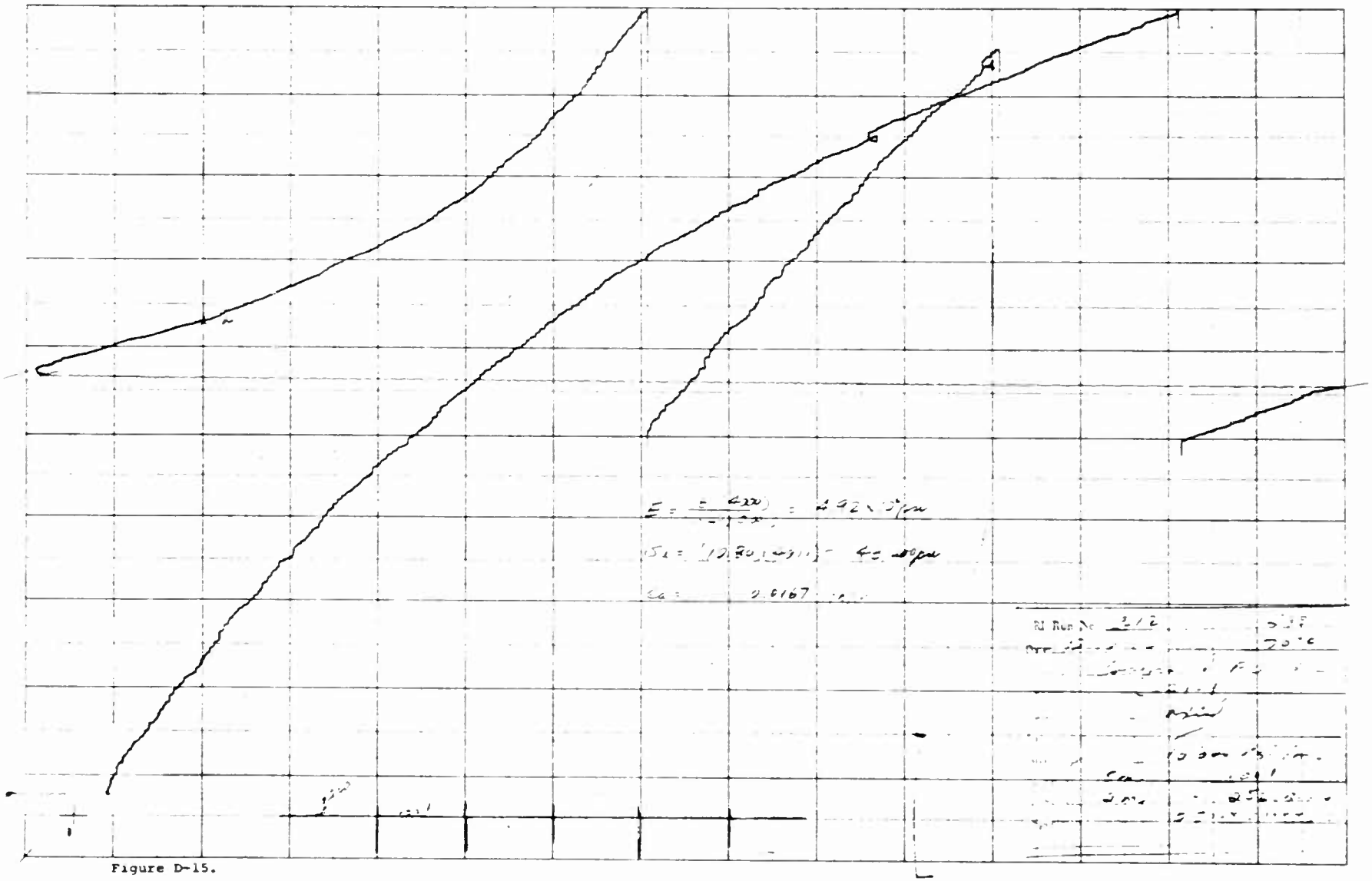

Figure D-15.

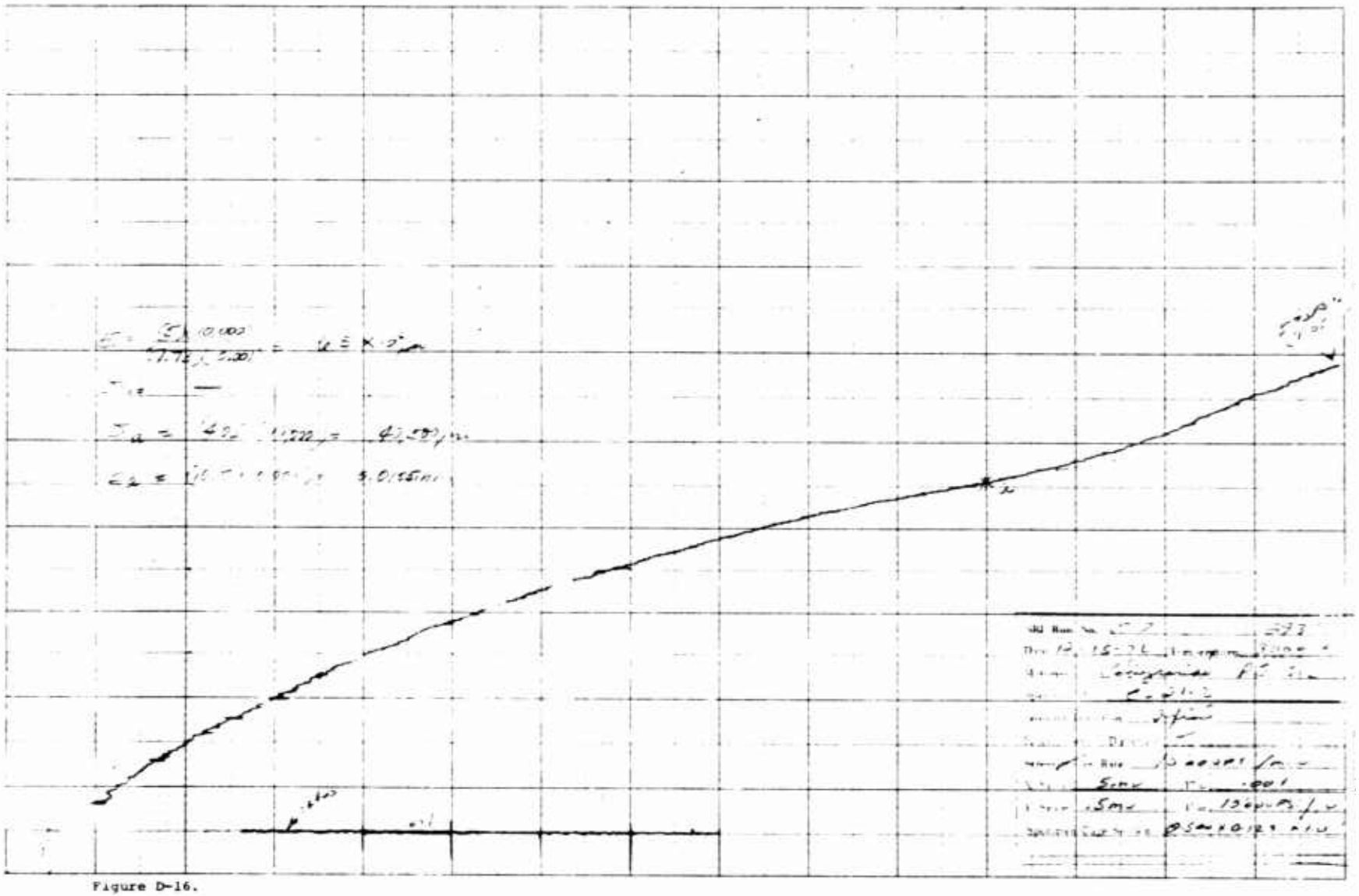

Figure D-16.

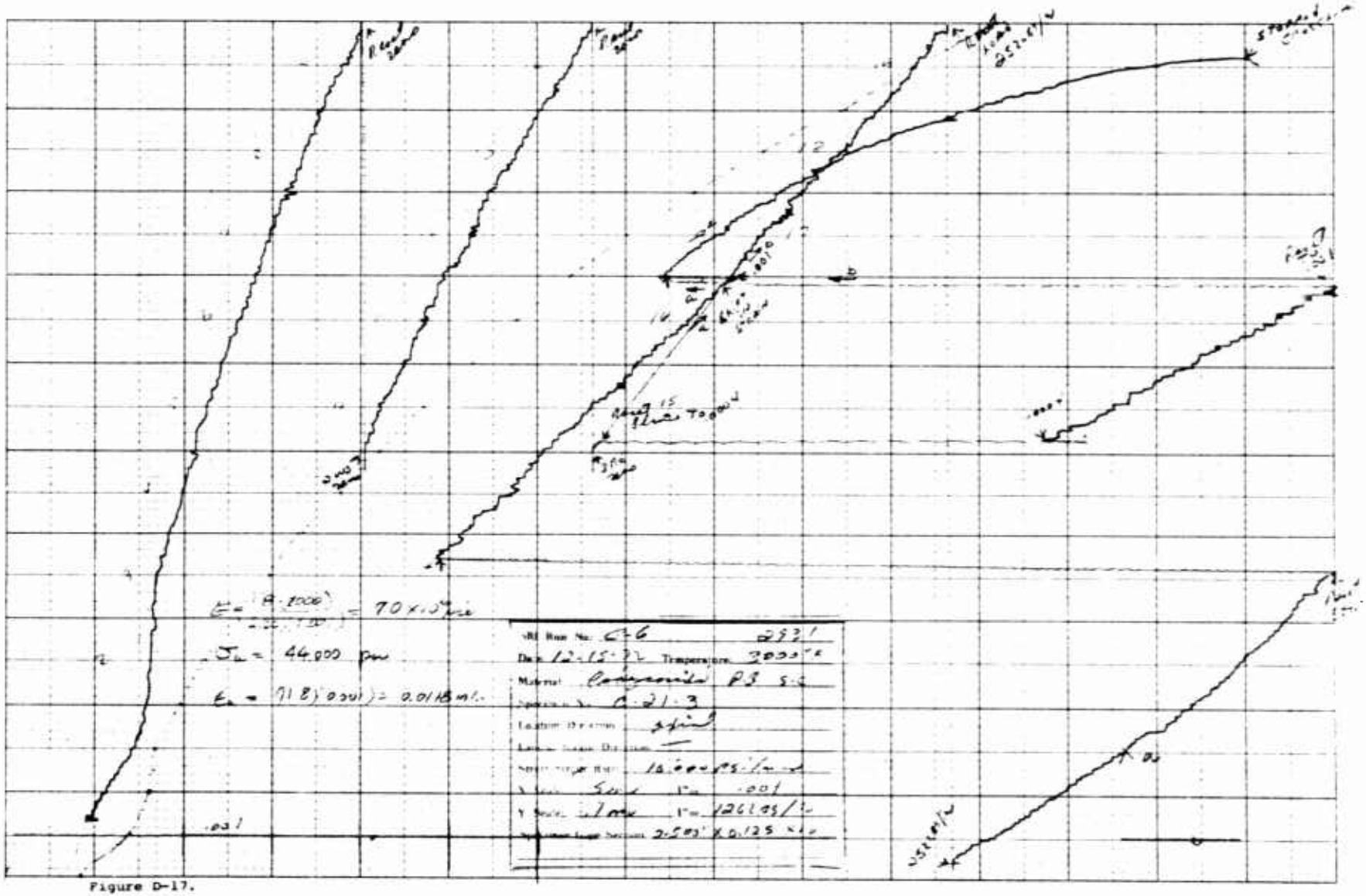

Figure D-17.

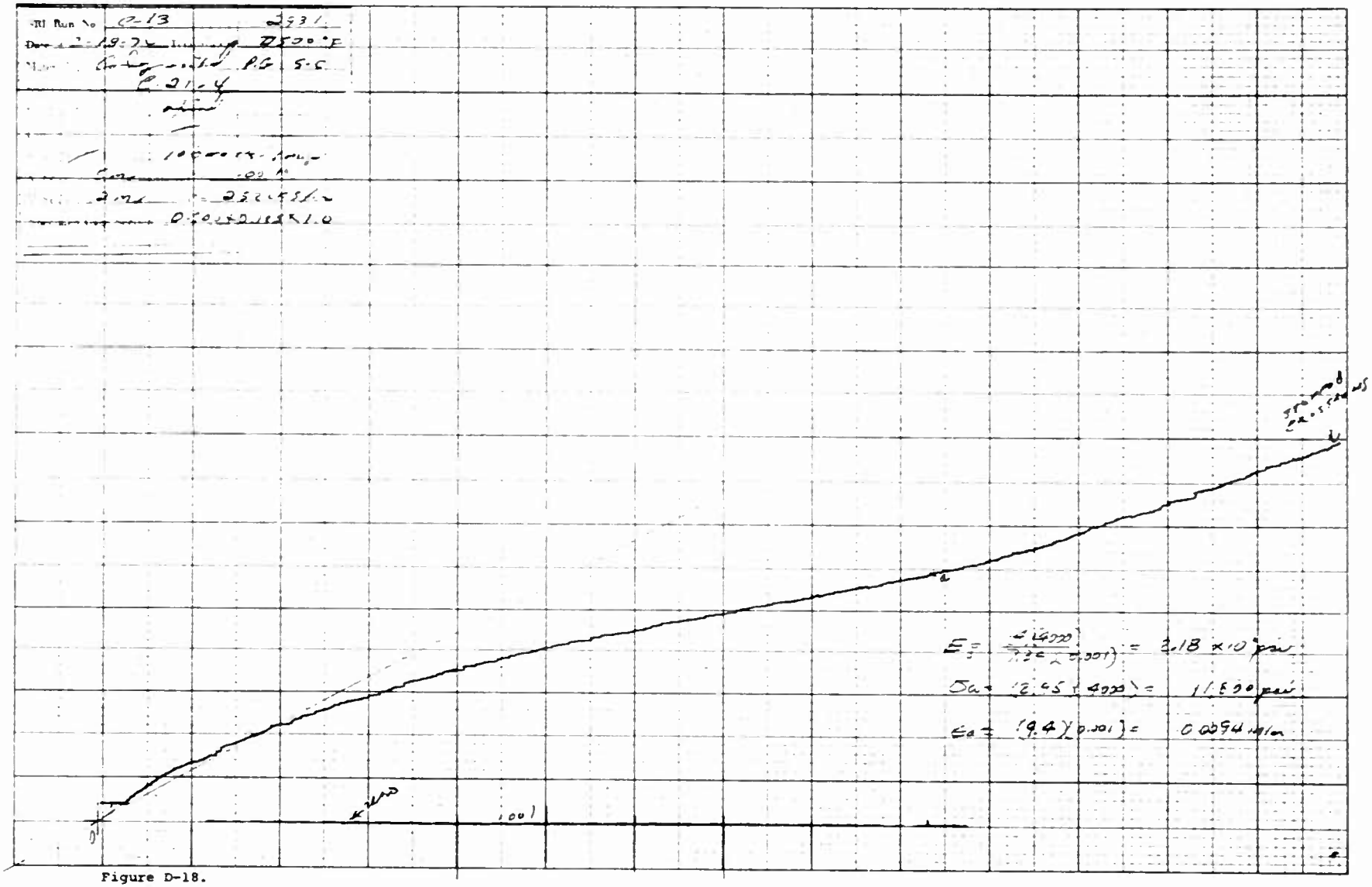

Figure D-18.

APPENDIX III

FLEXURAL STRENGTH AND ELASTIC MODULUS OF PG/SiC

III-1

Flexural strengths and elastic moduli were determined at room temperature using 1-inch radius cylindrical and plate stock that had been fabricated for the SoRI thermal property characterization program. The third cylindrical exit piece for ab direction thermal properties determination at SoRI and 1 of the 4 plate pieces for c directionthermal properties at SoRI were selected to give a range of SiC contents. Arc segments taken from rings which were in turn taken from the cylinders were broken with the substrate side in tension in the specially constructed fixture shown in Figures III-1 and III-2. Flat plate specimens were similarly broken. The fixture consists of an aluminum cylindrical shell with a steel base that fits inside of it. The steel base has two parallel 0.125-inch radius steel pins 1-inch apart built into it. The third steel pin is built into a steel plunger as shown. Specimens are then broken in 3-point loadings. A steel ball transmits the load from the cross-head platen to the plunger. The ball ensures good alignment provided the sides of the specimen are square and parallel. The fixture eliminates the need for perfectly aligned stationary and movable fixturing. The specimen is simply placed in the fixture which is then placed on the anvil of the tensile machine and the cross-head is moved downward at a rate of 0.2 in/min. The load and the deflection are plotted automatically on a strip-chart recorder. A model Tinius-Olsen tensile machine was used for this testing. The broken specimens were assayed for SiC content by ashing.

The following formulae were used to calculate the flexural strengths and elastic moduli:

$$S = \frac{1.5\ell}{bh^2}$$

and

$$E = \frac{P\ell^3}{4ybt^3}$$

where

S = strength, psi

E = elastic modulus, psi

P = loads, lb

ℓ = span length, in. = 1

b = specimen width, in.

h = specimen height, in.

t = deflection, in.

Use of the elastic modulus was based on the elastic modulus being the same in tension as it is compression. This turned out to be a reasonably good assumption as the data in Tables 2 and 4 of Appendix II show. A small

Figure III-1. Flexural Test Fixture.

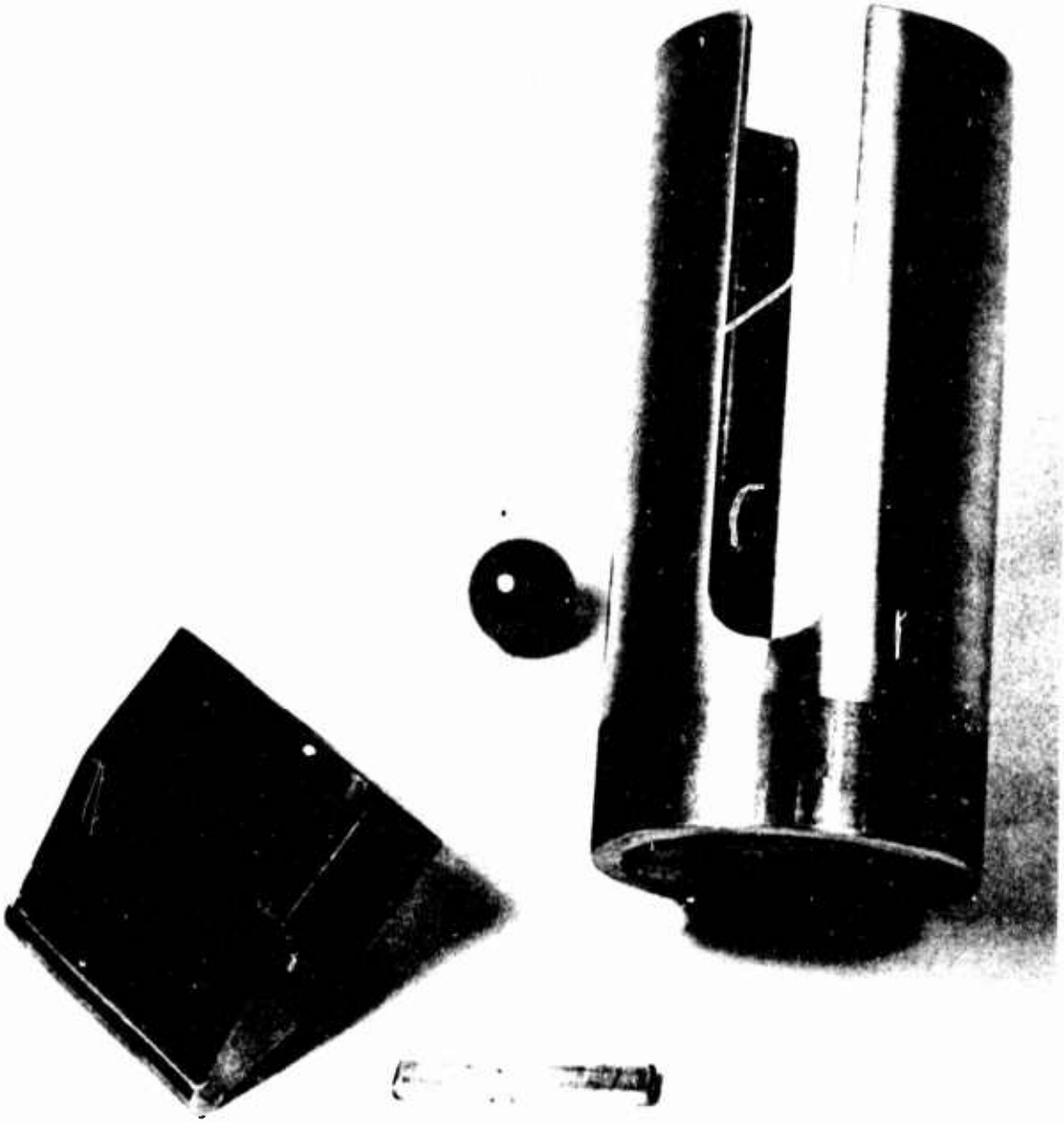

Figure III-2. Flexural Test Fixture Exploded.

236

correction was applied for the 1-inch radius arc specimens. This correction was a function of radius, r, to thickness, t, ratio as follows:

r/t	Percent Error (S)	Percent Error (E)
1	35.0	
2	17.0	
3	10.9	
4	9.2	
10	3.2	

The r/t for these specimens was on the order of 10. The results are shown in Table III-1.

The height measurement, h, was made on the fractured specimen, at the break, using an optical method. The minimum height was used for these specimens, which, by their nature, are somewhat rough, as deposited.

The microstructure was mostly Code 20 which contains a fine even dispersion of SiC, with diameters ranging from 0.9 to 2.6μ and and L/D of 3 or more, in a strain-line-free pyrographite matrix. The needles coarsened and tended to segregate in the SiC grain boundaries at the higher SiC concentrations. It is suspected that the SiC contents may be somewhat on the low side, particularly at the higher concentrations, since the ashing technique at Atlantic Research has been shown to be somewhat in error.

Table III-1. Flexural Strength Data — PG/SiC, "ab" Direction.

LOG RUN NO.	% SiC BY ASHING	b	h	P	t	FLEXURAL STRENGTH (Ksi)	MODULUS OF ELASTICITY (Msi)
CYLINDERS							
162-32 ENTR.	13.0	0.255	0.150	133.5	–	37.0	–
162-33 EXIT	11.8	0.244	0.145	116.5	0.0110	35.7	3.61
		0.248	0.165	90.3	0.0080	21.3	2.52
162-45 EXIT B	21.3	0.247	0.135	102.9	0.0080	35.7	5.30
		0.247	0.130	95.0	0.0075	35.7	5.85
162-7 EXIT	19.0	0.265	0.075	30.2	–	31.2	–
162-11 ENTR.	24.2	0.240	0.135	103.7	–	37.1	–
162-39 EXIT	18.4	0.237	0.105	51.1	0.0105	30.5	4.45
		0.237	0.110	51.1	0.0095	27.7	4.25
162-44 ENTR.	31.5	0.251	0.145	104.0	–	31.1	–
162-12 EXIT	34.7	0.255	0.060	23.5	0.0155	39.5	6.85
		0.240	0.060	22.0	0.0140	39.2	7.45
162-39 ENTR.	27.8	0.250	0.150	106.0	–	29.7	–
162-12 ENTR.	27.4	0.240	0.085	35.4	–	30.6	–
162.44 EXIT A	42.5	0.245	0.100	62.7	0.0072	39.7	8.82
		0.245	0.100	59.7	0.0070	40.1	8.73
PLATE							
162-26	19.2					28.1	–
162-28	16.9					34.0	–
162-35	11.6					23.1	–